MAN-MACHINE DYNAMICS IN THE STABILIZATION OF SINGLE-TRACK VEHICLES

by

David Jeffrey Eaton

A dissertation submitted in partial fulfillment
of the requirements for the degree of
Doctor of Philosophy
(Mechanical Engineering)
in The University of Michigan
1973

Doctoral Committee:

Associate Professor Leonard Segel, Chairman
Professor Glenn V. Edmonson
Associate Professor Francis E. Fisher
Professor Robert M. Howe
Professor Richard W. Pew
Professor Joseph E. Shigley

ACKNOWLEDGMENTS

The author wishes to thank each committee member for his encouragement and guidance, especially Mr. Leonard Segel, chairman, and Dr. Richard Pew.

The support of the Highway Safety Research Institute is gratefully acknowledged. Special thanks are due to Mr. John Campbell and Mr. Joseph Boissonneault for their assistance in preparing test equipment, to Mr. Douglas Brown for his help with the tire tests, and to Mrs. Jeannette Nafe for her excellent typing of the manuscript.

The author is indebted to Honda Motor Company for its valuable assistance in the form of partial financial support, the donation of two motorcycles, and technical information.

Appreciation is expressed to Mr. Rodney Wingrove, NASA Ames Research Center, and Dr. David Weir, Systems Technology, Inc., for their helpful comments.

Finally, the author wishes to thank his wife, Constance, for her endless patience and encouragement.

TABLE OF CONTENTS

TABLE OF CONTENTS (Continued)

LIST OF TABLES

LIST OF ILLUSTRATIONS

CHAPTER 1

CHAPTER 2

CHAPTER 3

LIST OF ILLUSTRATIONS (Continued)

CHAPTER 4

CHAPTER 5

CHAPTER 6

LIST OF ILLUSTRATIONS (Continued)

LIST OF ILLUSTRATIONS (Continued)

THE UNIVERSITY OF MICHIGAN LIBRARIES

LIST OF ILLUSTRATIONS (Continued)

THE UNIVERSITY OF MICHIGAN LIBRARIES

LIST OF APPENDICES

1. LITERATURE REVIEW AND THE SCOPE OF THE DISSERTATION

1.1 THE SINGLE-TRACK VEHICLE

The bicycle and motorcycle represent a unique form of road vehicle. Not only does the single-track vehicle depend upon forward motion for roll stability, but, depending upon vehicle design, the load carried, and the actual operating speed, stability often requires both forward motion and rider control. Also, because its roll angle is unconstrained and the ratio of rider mass to vehicle mass is high relative to other forms of ground transportation, the single-track vehicle is sensitive to motions of the rider with respect to his seat; thus, the rider can control the vehicle both by the handlebars and by his own body movements.

These and other dynamic peculiarities of the single-track vehicle have their advantages and disadvantages. On the negative side, the accident rate for motorcycles (which mingle more with traffic and operate at higher speeds than bicycles) appears to be greater than that for automobiles. Although the small size of the motorcycle makes it relatively invisible to the automobile driver and thus is probably the main reason for its greater accident rate, a poorly designed motorcycle can be dangerous by itself. For example, motorcycles and even bicycles have been observed to exhibit

THE UNIVERSITY OF MICHIGAN LIBRARIES

dangerous oscillatory instabilities, the frequencies of which are sufficiently high that they cannot be controlled by the rider.

On the positive side, motorcycles and bicycles are enjoyed by many as a pleasant form of recreation and an inexpensive means of transportation. Their use in the United States has greatly increased in recent years, and they seem likely to remain important in this country as well as others in the future. A better understanding of single-track vehicle dynamics can lead to vehicles having more desirable handling properties, thus making them more pleasant to operate for a large number of riders.

In addition to possibly improving the safety and roadability of motorcycles and bicycles, an understanding of their dynamic behavior is an interesting academic study and provides information which may be of use in such fields as vehicle dynamics and manual control.

The research described herein is a mostly experimental expansion of previous theoretical research efforts. Thus, a discussion of the objectives and scope of the dissertation is best presented with respect to the existing literature, which is outlined in the next section.

THE UNIVERSITY OF MICHIGAN LIBRARIES

1.2 REVIEW OF THE LITERATURE

In the past, the uncontrolled single-track vehicle, i.e., having rigid rider whose hands are off the handlebars, has received considerably more attention than the vehicle as a man-machine system. From a theoretical point of view, it was found as early as 1899 (Whipple [1]), using bicycle equations which included wheel gyroscopic moments, that the dynamic behavior of the vehicle was a function of its forward speed. For the particular bicycle analyzed by Whipple, only in one narrow range of speed, 10.4-12.2 mph, was the vehicle stable without rider control.

Other equations of motion for a bicycle were derived by Pearsall [2] in 1922, who included the geometric effect of tire thickness. His analysis included a test for stability, which test was the basis of design considerations to improve stability. Work by Manning [3] was similar to Pearsall's, showing the derivation of equations of motion for a riderless bicycle with thin tires making point contact with the ground. In their textbook on dynamics, Timoshenko and Young [4] derive similar bicycle equations, but with the additional assumption of negligible gyroscopic moments.

One of the best known analyses was performed by Döhring [5], who modified bicycle equations of motion to apply to a motorcycle, found the eigenvalues of the resulting equations, using physical quantities obtained from existing motorcycles, and compared his theoretical results with experiments he had previously performed [6]. It is interesting to note that Döhring, like Whipple, theoretically found several speed ranges, each of which was characterized by a particular dynamic behavior, although the speeds are considerably higher for motorcycles than for bicycles. At the upper end of the speed range, according to Döhring's results, the roll motion is slightly unstable, the angle of lean increasing very slowly, but requiring a correction from the driver. At low speeds, an instability exists in the form of an increasing oscillation. Döhring found an intermediate speed range in which the motorcycle is inherently stable, requiring no assistance from the rider.

With the aid of a digital computer, Collins [7] performed a stability analysis of a single-track vehicle using approximations and techniques similar to those of Döhring. Singh and Goel [8] applied Döhring's equations, with steering damper added, to the Indian scooter "Rajdoot," for comparison with the Italian scooter, "Vespa," previously analyzed by Döhring.

All of the above analyses did not allow the tires to sideslip. An attempt to include tire mechanics in motorcycle equations of motion was made by Singh [9] in 1964. However, his assumption that front and rear tire slip angles are proportional to the steering angle, while possibly giving reasonably accurate results, is questionable and introduces unknown parameters. While Singh performed some road tests in addition to his stability analysis, quantitative comparison between theory and experiment was not possible, since different vehicles were involved.

Other analyses included tire mechanics in the manner conventionally used in the study of automobiles. Fu [10] wrote equations for the steady turning situation, which equations were linearized in steering and tire slip angles and included some air resistance effects. Fu also performed some experimental work on steady turning. A more general set of linear equations with tire sideslip was prepared by Kondo [11, 12].

A large amount of theoretical and experimental work on bicycles has been performed at Calspan Corporation (formerly Cornell Aeronautical Laboratory, Inc.). Unfortunately, the study is of a contractual nature and few publications [13] have been released. This work involves a six-degree-of-freedom nonlinear bicycle model and has dealt with rider control in terms of steering torque and body lean.

It is believed that the theoretical analyses by Sharp [14] represent the most complete published to date. Sharp's equations of motion are based on assumptions like those made by Kondo, with the additional consideration of the fact that the lateral force response to a step input of slip angle is not a step but rather builds up to a steady-state value. This side force lag can be significant in high frequency shimmy motions (Pacejka [15]). Weir [16] also independently derived the equations of Sharp, but without the lateral force lag consideration.

In addition to studying the single-track vehicle by means of motion equations, several researchers have approached the problem experimentally. Experimental work on the roll stability of the uncontrolled motorcycle was performed by Kondo, et al. [17], Kageyama, et al. [18], and Kondo [11], although the results were not quantitatively related to any theoretical predictions.

A few others also discussed the motorcycle, both controlled and uncontrolled, from a "basic physics" or intuitive point of view. The most well-known work is probably that of Wilson-Jones [19], who was one of the first to consider tire mechanics and the effect of the rider in his discussion. He also included some experimental work, which explored the effects of altering steering geometry, and included measurements of tire slip angles and handlebar torques. Also presented was an interesting discussion of the process of entering and leaving a turn. A similar report, although less extensive, was written about the same time (1951) by Muhlfeld [20]. Although Bower [21] performed some mathematical work, unfortunately restricted to the unrealistic situation of a vehicle with a vertical steering head, he did present an interesting, though mostly subjective, description of the behavior of the machine under various conditions, such as steady turning and skidding. Another "basic physics" approach was taken by Jones [22], who carried out a series of experiments with bicycles having altered steering geometries and made some calculations with respect to steering geometries in general, in an attempt to identify basic mechanisms of stability.

Results of two other types of studies which do not fit into the above categories have also been published. Döhring [23] discussed the causes and cures of front wheel oscillation about the steering axis of high-speed motorcycles with the aid of a simple one-degree-of-freedom analysis, in which the interaction between front and rear frames was neglected and front wheel side force due to tire slip angle was treated as being approximately proportional to the steering angle. Unfortunately, Döhring considered only a tire having "instant response"; that is, no lag of the tire force behind the slip angle. Detailed analyses of the steering geometry of the single-track vehicle have also been performed (Sakai [24], Ellis and Hayhoe [25]).

Although much can be learned from qualitative discussions and "basic physics" arguments, it is believed that, because of the complexity of the system, a complete understanding of the dynamics of the single-track vehicle can only be achieved through a mathematical model of reasonable accuracy, especially if quantitative results are desired. From a review of the literature, the work of Sharp emerges as the most definitive to date.

In Sharp's analysis, the uncontrolled motorcycle is considered to possess four degrees of freedom: lateral translation, yawing, rolling, and steering of the front fork assembly. The equations are linearized, and modal roots are found, using data from an existing motorcycle, for four versions of his analysis: complete model; complete model, but with "instant response" of tire side force; model with no tire sideslip; and complete model with steer angle no longer being a degree of freedom (the so-called "fixed control" case). The effects of changing motorcycle parametric data were also studied. For the complete model, three modes dominate: the "wobble" mode, a high frequency oscillation of the steering assembly (usually about six-nine cycles/second, the mode studied by Döhring [23]); the "weave" mode, an oscillatory mode of lower frequency involving the entire vehicle; and the "capsize" mode, a non-oscillatory motion of the entire vehicle. (See Figures 1.1 and 1.2.) For the

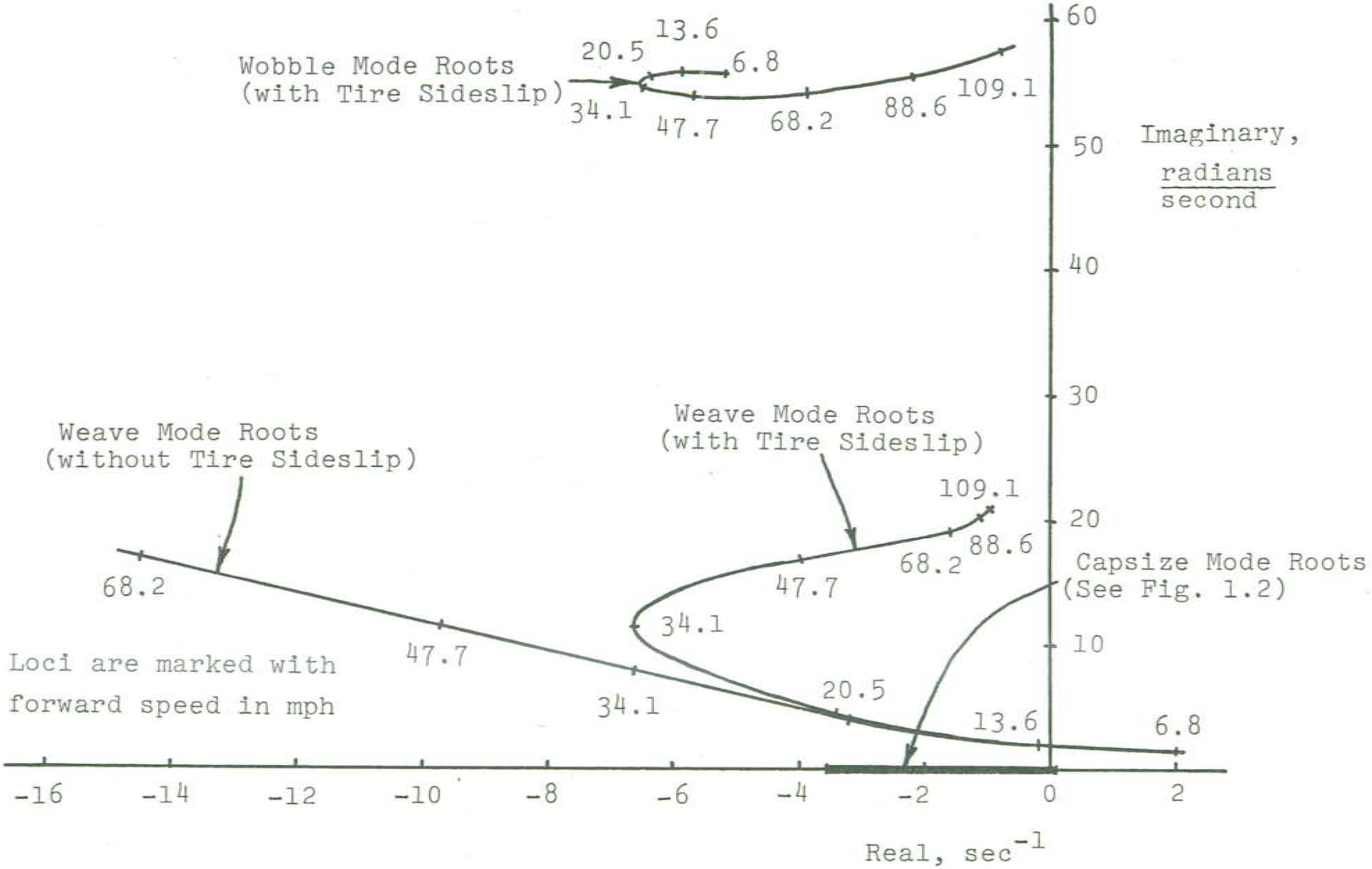

Figure 1.1 Root loci for BSA motorcycle (roots taken from Reference [14]).

THE UNIVERSITY OF MICHIGAN LIBRARIES

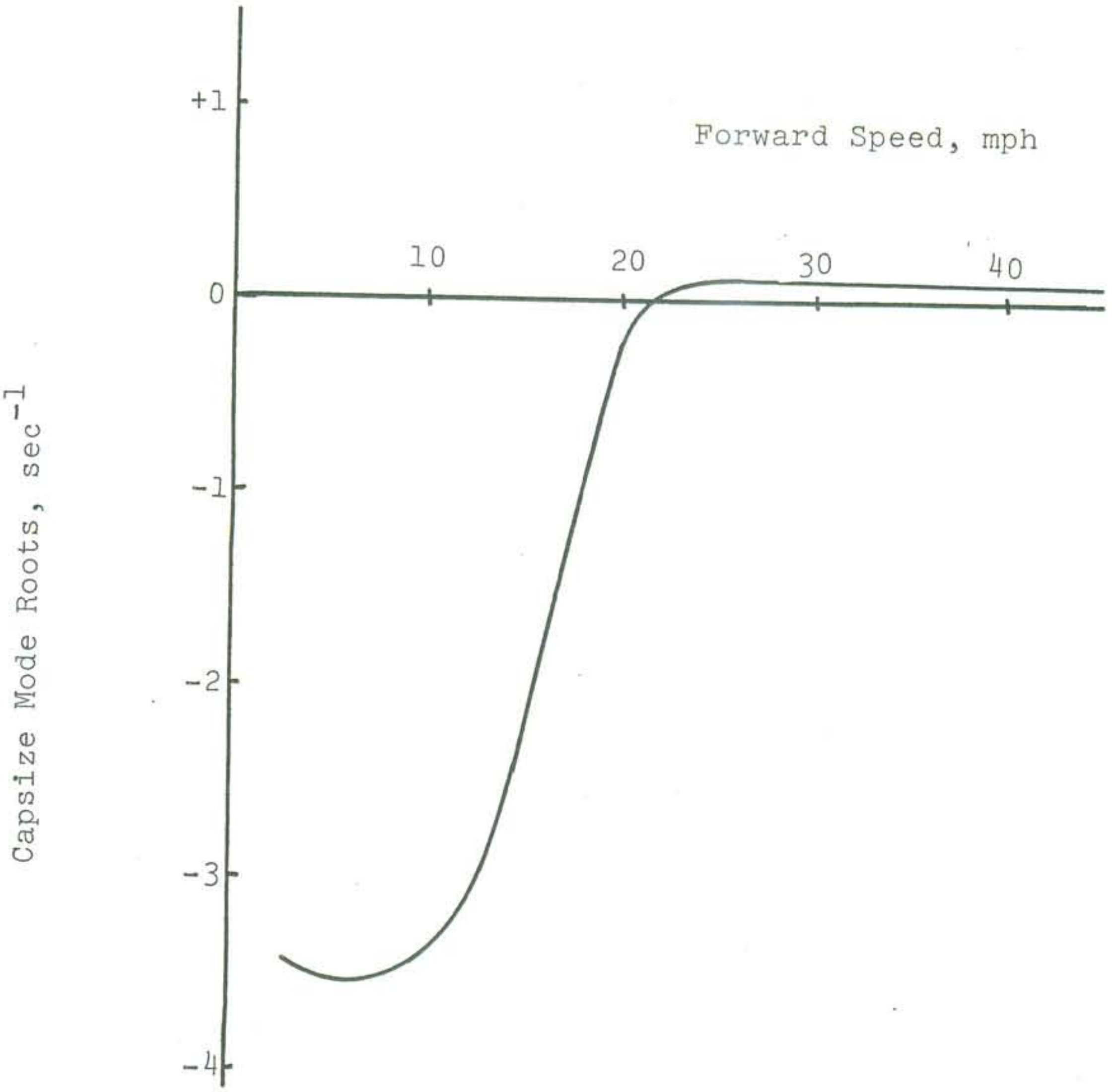

Figure 1.2 Capsize mode roots for BSA motorcycle (a portion of Figure 5, Reference [14]).

motorcycle studied by Sharp, low speeds are characterized by an unstable weave mode oscillation, while for medium speeds (about 20-30 mph) there is a range of complete stability. For higher speeds, the capsize mode becomes slightly unstable, with the possibility of wobble or weave instabilities at very high speeds. Omission of the tire sideslip freedom from the equations of motion, resulting in a vehicle model like those of Collins [7] and Döhring [5], eliminated the wobble mode entirely and greatly changed the weave mode for moderate and high speeds (see Figure 1.1). Omission of the lag in the development of tire lateral force from the equations that account for the sideslip degree of freedom increased the damping of the wobble mode, particularly at low speeds.

While the lag in the development of tire lateral force is often omitted from analyses of automobile dynamics, it is important in the case of the single-track vehicle. Sharp represented this lag in a very simple manner, i.e.,

$$\frac{\sigma}{u} \frac{dF_y}{dt} + F_y = - C_\alpha \alpha , \qquad (1.1)$$

where F_y = tire lateral force, u = forward speed, C_α = tire lateral stiffness, α = tire slip angle, t = time, and σ is the effective tire "relaxation length". The origins and limitations of Equation (1.1) are discussed in Chapter 3 of this dissertation.

While it is important to know how physical changes in the design of a single-track vehicle affect its dynamics in the uncontrolled situation, it is at least as important to know what dynamic properties are desirable from the point of view of the rider. For example, while several researchers have made design recommendations for improving stability, it is not obvious that their implementation is desirable in all situations (as long as existing instabilities can be easily controlled), since a very stable motorcycle or bicycle would tend to be difficult to maneuver.

Recently, some interest has been shown in studying the rider and single-track vehicle as a system. Such studies have made use of existing man-machine technology, much of which has been developed in connection with the control of aircraft. A common approach used in the study of man-machine systems is the quasilinear method [26, 27], wherein the human operator is represented in a closed-loop control system by a linear transfer function $Y_p(j\omega)$ and a random noise source or "remnant" (Fig. 1.3[1]). The dynamics of the machine being controlled are represented by $Y_c(j\omega)$. A reasonably general form of $Y_p(j\omega)$ which has been found to fit many closed-loop control situations is given by

---

[1] Figure 1.3 shows a compensatory tracking task (operator perceives error signal only), as opposed to a pursuit task (operator perceives both command and error).

THE UNIVERSITY OF MICHIGAN LIBRARIES

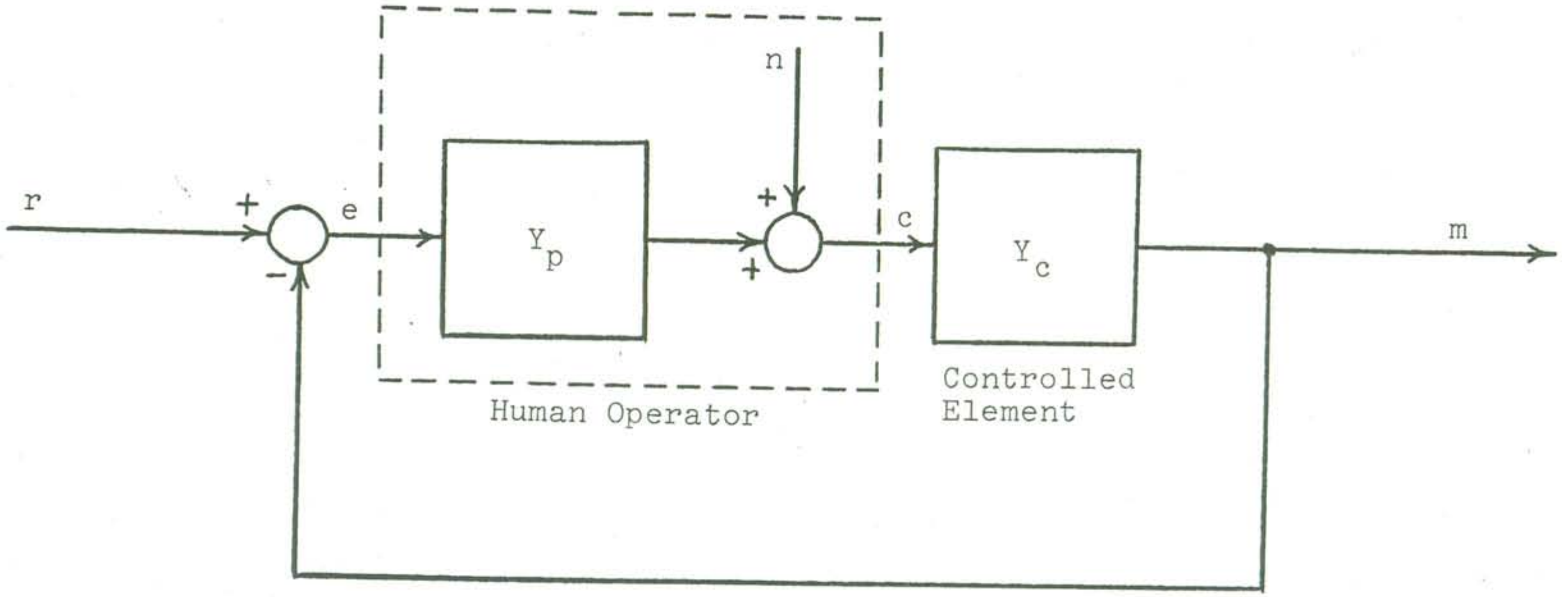

Symbols- r: command signal
e: error perceived by operator
n: operator's "remnant"
c: operator's output
m: system output
Y_p, Y_c: linear transfer functions

Figure 1.3 Basic compensatory manual control system.

THE UNIVERSITY OF MICHIGAN LIBRARIES

$$Y_p(j\omega) = \frac{Ke^{-j\tau\omega}(T_L j\omega+1)}{(T_I j\omega+1)(T_N j\omega+1)} ,$$

where the constants K, τ, T_L, T_I, and T_N are functions of $Y_c(j\omega)$ and the input r, as well as many "operator-centered" and "environmental" factors, such as motivation, level of fatigue, ambient temperature, etc. Note that the time delay, τ, always appears in the operator transfer function, $Y_p(j\omega)$, because real operators require a finite time to react to a stimulus.

Many manual control studies have been concerned with measuring $Y_p(j\omega)$ experimentally. These studies have shown that a surprisingly large amount of data collected in manual control experiments can be fit by a simple model, viz.,

$$Y_p(j\omega)Y_c(j\omega) \doteq \frac{\omega_c \, e^{-\tau_e j\omega}}{j\omega} , \qquad (1.2)$$

for ω near ω_c (the "crossover" frequency, at which $|Y_p(j\omega)Y_c(j\omega)| = 1$). Equation (1.2) is known as the "crossover model" [28] and has proved useful in theoretical manual control studies, e.g., McRuer and Weir [29].

By far, the most complete analysis of the man-motorcycle system presently available was that performed recently by Weir [16], with the aid of the crossover model. In this study, a number of possible closed-loop systems, having the form of that diagrammed in Figure 1.3, are first investigated.

The inputs to the rider are considered to be, for example, roll angle, yaw angle or lateral position, and the possible rider outputs are steering torque and upper body lean angle. For each possible system, the rider transfer function was chosen to be a gain plus time delay, while the vehicle dynamics were defined by the equations and parametric data published by Sharp.

The loop closures judged by Weir to be "good" control systems were refined and used to create the overall representation of the man-cycle system diagrammed in Figure 1.4. Weir also investigated the effects of changing forward speed and the design parameters of the motorcycle. A number of conclusions relating to vehicle design and operation were presented. It should be noted that the conclusions of Weir and Sharp are dependent upon the level of validity of their motorcycle equations of motion, which served as the basis for their findings.

Manual control studies using a bicycle simulator have been performed by Van Lunteren, et al. [30, 31, 32, 33, 34]. While this work represents a pioneering effort in obtaining rider transfer functions experimentally, these transfer functions were obtained while the operator was performing a control task that may have been considerably different from the task of stabilizing a real bicycle, because the simulator did not have forward motion, and the simulator dynamics were

THE UNIVERSITY OF MICHIGAN LIBRARIES

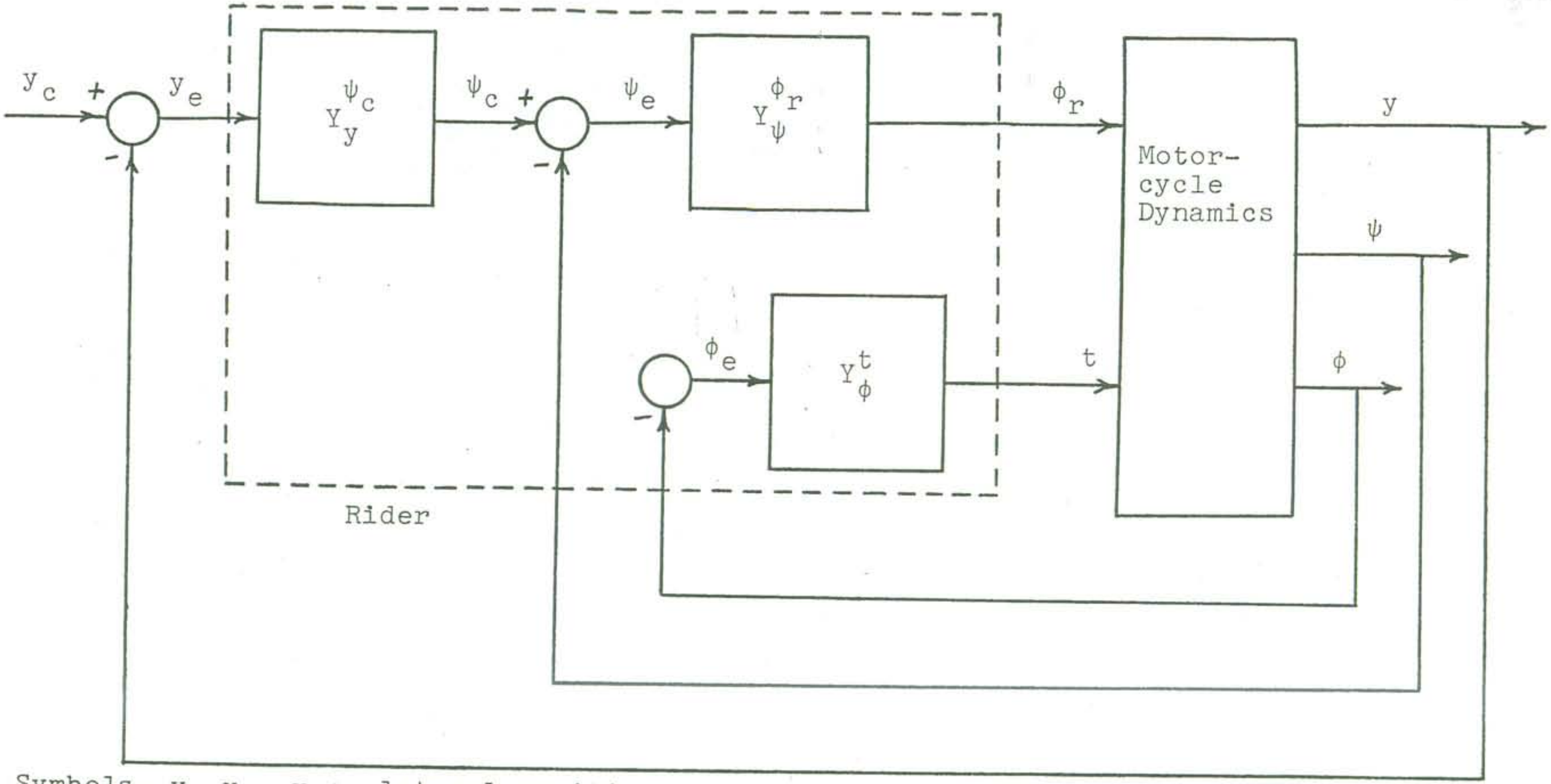

Symbols- y, y_c, y_e: lateral position

ψ, ψ_c, ψ_e: heading angle

ϕ, ϕ_e : roll angle

ϕ_r: rider body lean angle

t : rider-applied steering torque

$Y_y^{\psi_c}$, $Y_\psi^{\phi_r}$, Y_ϕ^t: linear transfer functions

Figure 1.4 Man-motorcycle system proposed by Weir (Figure 19, Reference [16]).

THE UNIVERSITY OF MICHIGAN LIBRARIES

based upon the differential equations of Whipple, equations that were not subjected to experimental verification. Furthermore, Van Lunteren, et al., assumed the rider's control outputs to be body lean and steering angle, rather than body lean and steering torque. For motorcycles, steering-torque control is more likely than position control, due to the greatly increased instability of the capsize mode when the steering degree of freedom is omitted [14, 16]. It is likely that torque control is also superior to position control in the case of the bicycle, although this superiority is not firmly established.

It should be pointed out that Van Lunteren's major interest was the manner in which the performance of the human operator would be influenced by various factors such as the use of drugs, etc. He was not concerned with the dynamics of the bicycle. The bicycle stabilization task was chosen because the system is familiar to most people, thus ensuring that the test subject could be representative of a large population rather than a select skilled group, and because the frequently unstable bicycle forces the subject to pay close attention to his control task.

Another bicycle simulator has recently been developed in Japan, as described by Hattori, et al. [35]. The simulator is not as realistic as the machine of Van Lunteren, since the test subject applies nearly vertical forces to

THE UNIVERSITY OF MICHIGAN LIBRARIES

the handlebars, no body movement is measured, and the experiments performed involve only a transient response to an initial imposed lean, rather than a continuous control task.

At the Massachusetts Institute of Technology, a vehicle was designed and built to test the feasibility of using an automatic device to control the rolling of a narrow track vehicle [36]. However, this work is not closely related to the stabilization of the single-track vehicle, since it involved a three-wheeled converted motorcycle in which rolling was induced by mechanically tilting the rear wheels and vehicle frame.

1.3 OBJECTIVES AND EXTENT OF THE DISSERTATION

This dissertation is intended to improve the understanding of the dynamics of the single-track vehicle by expanding upon previous research. In particular, the major objective has been to provide experimental information to relate to the theoretical work of Sharp and Weir. Chapters 2 and 3 deal with the uncontrolled motorcycle, that is, a vehicle in which the rider remains rigid with his hands off the handlebars. Chapters 4-6 discuss the man and motorcycle as elements of a closed-loop control system.

Chapter 2 presents a theoretical study of the effects of adding the self-aligning torques and overturning moments created by tire sideslip and inclination to Sharp's analysis and also examines the influence of the lateral force and aligning torque deriving from the instantaneous curvature of the path of the tire contact patch. By means of an analog computer simulation, a comparison is made between viscous and coulomb friction steering dampers. Parametric data for these analytic and simulation studies were obtained from measurements made on an actual motorcycle with the rider seated on the vehicle.

Chapter 3 describes road experiments in which the measured motorcycle was subjected to two disturbances. For each experiment, the transient response of the motorcycle was recorded and compared to the response predicted by the applicable equations of motion.

After the degree to which the equations of motion were valid was ascertained, the man-motorcycle closed-loop system was studied. The particular rider control task researched was the stabilization of the vehicle roll angle by means of rider-applied steering torque. The objective was one of identifying the linear transfer function that correlates the rider's steering torque output with the vehicle roll angle, using data obtained in constant speed road tests, which were approximately one minute in duration.

In Chapter 4, the man-machine system is analyzed to determine what constraints must be placed upon the rider's transfer function, in the interest of good system characteristics, especially stability.

THE UNIVERSITY OF MICHIGAN LIBRARIES

The roll stabilization experiments themselves are discussed in Chapter 5. In this experimental study, most of the excitation of the system was found to be the rider's remnant. Hence, although cross-spectral methods could be used to identify the transfer function that represents the motorcycle or "controlled element", it was necessary to use the method of Wingrove and Edwards [37, 38, 39, 40] to identify the rider's transfer function.

Chapter 6 presents the results of the roll stabilization experiments. Conclusions reached on the basis of the described research are summarized in Chapter 7.

THE UNIVERSITY OF MICHIGAN LIBRARIES

2. THEORETICAL STUDIES OF THE UNCONTROLLED MOTORCYCLE

2.1 EQUATIONS OF MOTION

During the early stages of the research described in this dissertation, equations of motion were derived that are nearly identical to those recently published by R. S. Sharp [14]. Sharp's analysis of the dynamics of the linearized single-track vehicle, which analysis has thus been substantiated by two independent efforts, the present work and that of Weir [16], serves as the theoretical basis of this dissertation. The reader is directed to Reference [14] for a derivation of Sharp's equations. Appendix A presents the equations after a change in notation and coordinate systems has been made, and after some additions to the theory (mostly tire mechanics considerations omitted by Sharp) have been included.

It should be pointed out that the following assumptions were made in the process of deriving the equations that are presented in Appendix A:

1. Vehicle and rider are comprised of five rigid bodies linked together: engine (with transverse axis), rear wheel, rear frame and rider, front frame, and front wheel.
2. The roll angle, ϕ, and front-frame steer angle, δ, are sufficiently small that the sines of these angles may be approximated by the angles

THE UNIVERSITY OF MICHIGAN LIBRARIES

in radians with the cosines of these angles set equal to unity.

3. Small disturbance motions prevail, permitting the equations to be linearized (except for coulomb friction in the steering head) by neglecting products of the variables v (lateral velocity), ϕ, ψ (heading angle), and δ, and their derivatives.

4. For $\delta=0$, both rider and vehicle are symmetrical with respect to the XZ plane as defined by the axis system placed in the vehicle (Appendix A).

5. Forward velocity, u, is approximately constant, and the rates of spin of the wheels and engine are proportional to forward velocity.

6. The road is flat and level. Rotational motions about the Y axis (pitching) are negligible.

7. The wheels are rigid and make point contact with the road. Tire forces and moments may be approximated as linear functions of slip and inclination angles and instantaneous path curvature. Rolling resistance moments and tire tractive force are considered negligible.

8. Aerodynamic forces and moments are neglected, including their influence on the distribution of the loading on the front and rear tires, which vertical loading influences the cornering and inclination stiffnesses of the two tires.

2.2 SOLUTION METHODS

The equations presented in Appendix A were solved both by digital and analog computation methods. Digital computation was employed to find the roots of the characteristic equation yielded by this dynamic system, as well as to determine (with the aid of the Laplace transformation) the time response of motion variables to a limited set of forcing functions, such as step and impulse functions. Thus the program was limited to analyzing and predicting the behavior of the <u>linear</u> single-track vehicle, that is, coulomb friction in the steering head could not be accommodated ($C_\delta = 0$).

Analog computation was employed to analyze the effects of coulomb friction and to investigate a much broader range of inputs and system modifications. Analog studies showed that the level of coulomb friction present in the steering head of the test vehicle (which has no damper in the steering mechanism) has a negligible effect on the motion of the vehicle. Consequently, the digital program proved to be a valuable tool in that it was very inexpensive to run since no integrations are required.

The digital program was developed first and, as written, requires that the front and rear tire relaxation lengths, σ_f and σ_r, be equal. Analog computer studies have shown, however, that the lag in side-force buildup on the

THE UNIVERSITY OF MICHIGAN LIBRARIES

rear tire has a negligible effect on the response of the system. Hence, in digital computations, the relaxation length of the rear tire was assumed to be equal to that of the front tire. These parameters and all remaining coefficients in the equations of motion were determined from measurements made on a 1971 Honda CL 175, which served as the test vehicle in this study. Appendices C and D present a discussion of the measurement techniques that were employed and a listing of the resulting parameter data, respectively.

In order to identify the various natural modes of motion, the terminology introduced by Sharp [14] will be retained. The "wobble" mode refers to the natural mode that is predominantly characterized by an oscillatory motion of the front frame assembly. The "weave" and "capsize" modes refer, respectively, to an oscillatory and non-oscillatory motion of the entire vehicle. It should be noted that Sharp's calculations were restricted to a determination of the roots of the characteristic equation. Substitution of his motorcycle parameter data into the calculation procedure developed in this study produced roots that were identical to those reported in Reference [14].

THE UNIVERSITY OF MICHIGAN LIBRARIES

2.3 TIRE MODEL STUDIES

It should be noted that single-track vehicles depend entirely upon forces and moments produced at the tire-road interface for not only directional control, but also roll stabilization. Thus, the degree to which these forces and moments are realistically described in a dynamic analysis has a strong bearing on the accuracy of that analysis. For this reason, an investigation was made to determine the need for representing the mechanics of the pneumatic tire more completely than had been done by Sharp [14]. In particular, his equations of motion were modified to include tire aligning torques and overturning moments resulting from slip and inclination angles as well as lateral force and aligning torque due to instantaneous curvature of path of the tire contact patch. (See Appendix A.)

As is discussed in Reference [41], a pneumatic tire, constrained to roll in a straight path with zero slip angle and its center plane inclined with respect to the vertical, develops forces and moments at the tire-road interface (e.g., "camber thrust"). If the path of the tire is curved, the tire distorts to conform to the shape of the path, with these distortions causing both a lateral force and an aligning torque. For example, a tire having no slip or inclination angle, but constrained to move along a curved path, is subjected to (1) a lateral force from the road pushing the tire away from the instantaneous center of the path and (2) an aligning torque opposing the direction of the turn. Lateral force and aligning torques arising from path curvature are referred to in the remainder of this dissertation as "path curvature effects."

Whereas the overturning moment, namely, the moment caused by the lateral shift in the effective centroid of the vertical pressure distribution, is a negligible quantity on a two-track vehicle, it is readily seen that this lateral shift is significant on a single-track vehicle. The importance of this lateral shift in the vertical load, together with the other effects noted above, was produced with six different representations of the pneumatic tire. These six tire models are identified below:

1. Side forces caused by slip and inclination angle; no moments other than aligning torque as a function of slip angle; no path curvature effects.
2. Same as "1", with path curvature effects added.
3. Same as "1", with aligning and overturning moment dependence on inclination angle added.
4. Same as "3", with path curvature effects added (thus constituting the most complete tire model).

5. Same as "1", with aligning torque dependence on inclination angle added.

6. Same as "1", with overturning moment dependence on inclination angle added.

The modal roots, yielded by each of these six tire models, have been plotted in Figures 2.1, 2.2, and 2.3 as a function of forward speed. Only the wobble, weave, and capsize mode roots are plotted since the remaining modes of motion are judged to be physically insignificant, either because they are heavily damped or they cannot be excited to amplitudes comparable to the amplitudes achieved in the wobble, weave, and capsize modes. In making these calculations, it was assumed that the transmission gear would be selected in accordance with the following schedule:

First gear, $0 < u < 10$ mph
Second gear, $10 \leq u < 15$ mph
Third gear, $15 \leq u < 20$ mph
Fourth gear, $20 \leq u < 25$ mph
Fifth gear, $u \geq 25$ mph

Although the top speed of the test vehicle is approximately 80 mph, modal roots have been calculated for speeds up to 100 mph in order to locate the speed at which the wobble mode becomes unstable.

THE UNIVERSITY OF MICHIGAN LIBRARIES

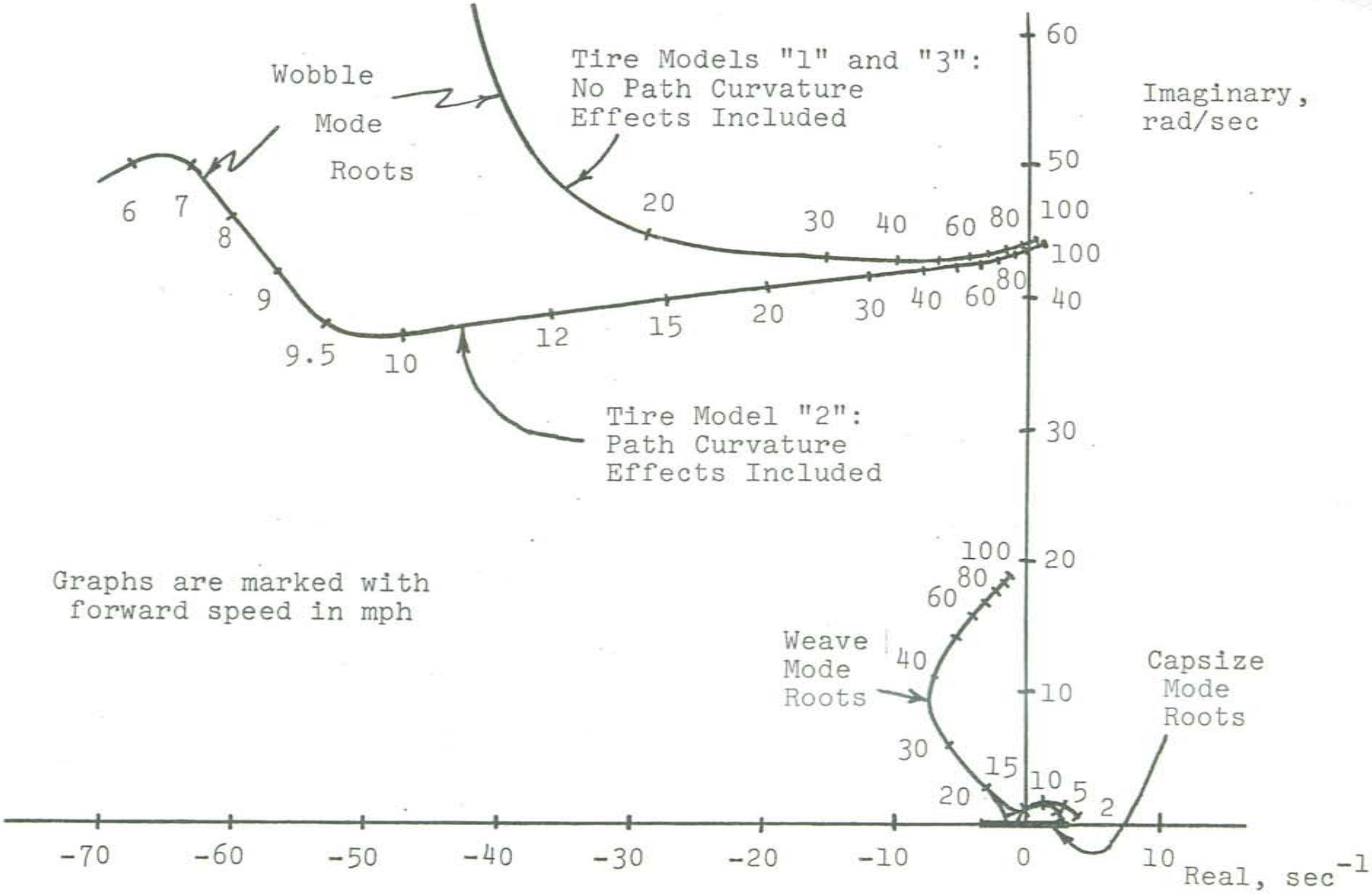

Figure 2.1 Root loci.

THE UNIVERSITY OF MICHIGAN LIBRARIES

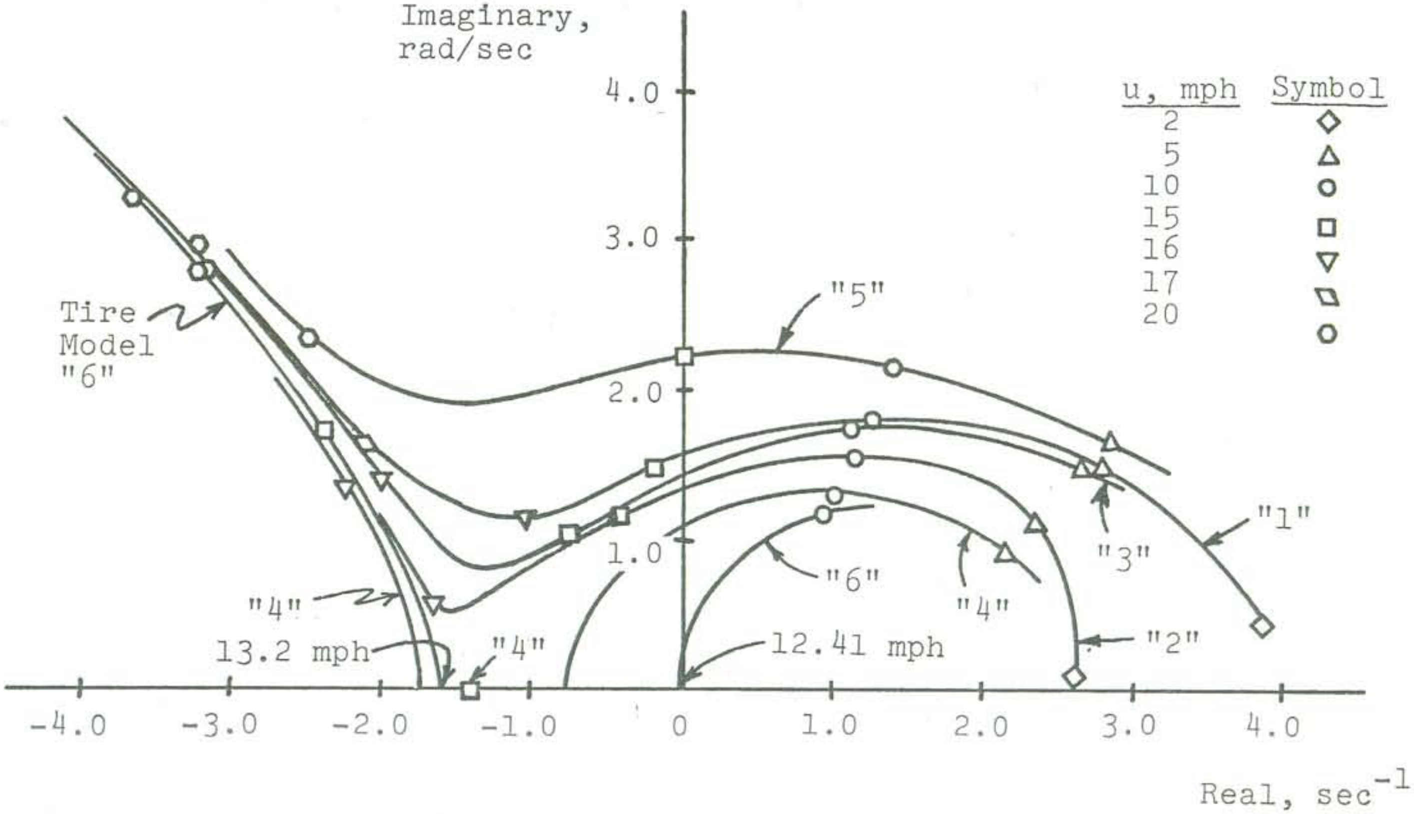

Figure 2.2 Weave mode roots, low forward speed.

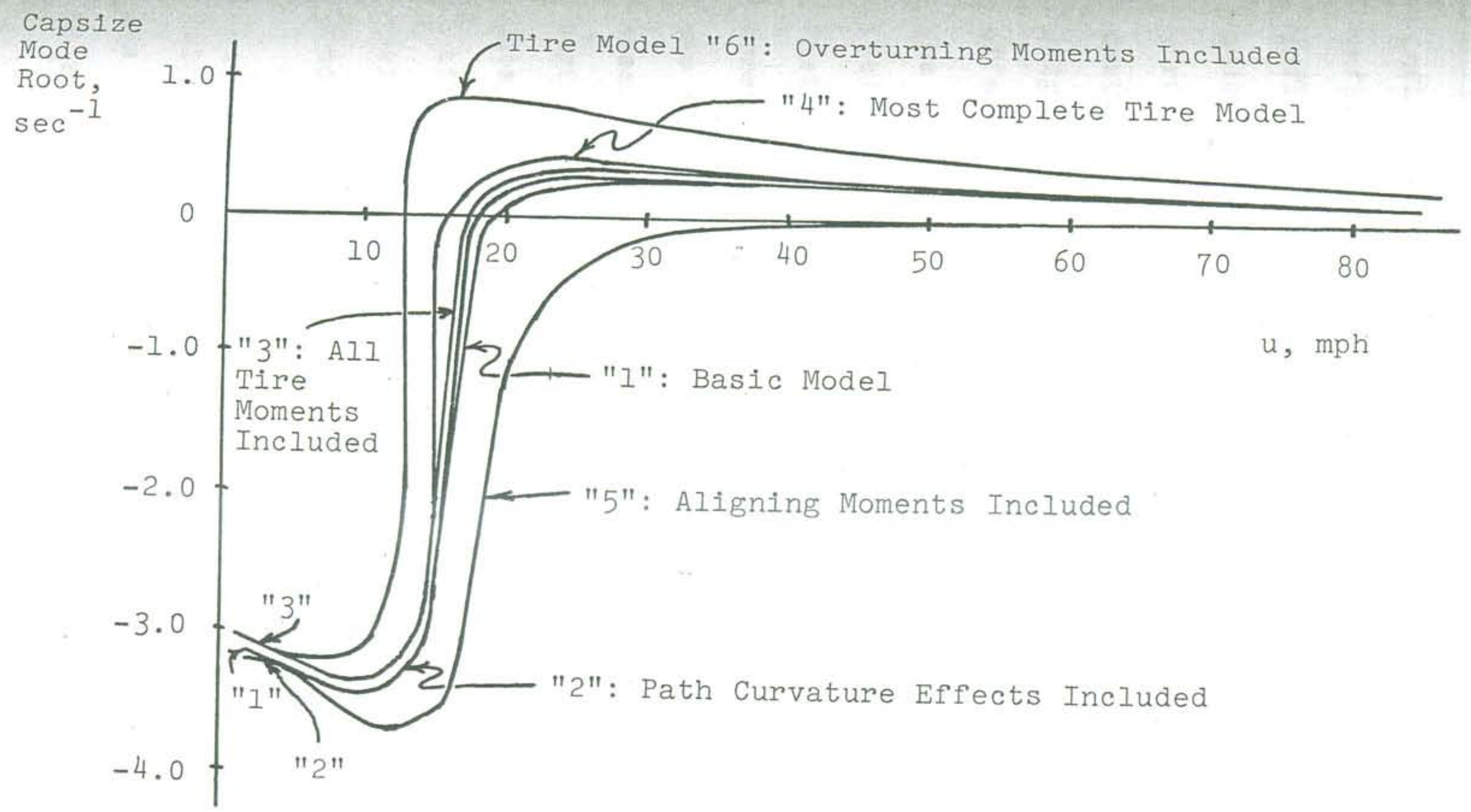

Figure 2.3 Capsize mode roots.

THE UNIVERSITY OF MICHIGAN LIBRARIES

An examination of the root loci plotted in Figures 2.1, 2.2, and 2.3 shows that (1) path-curvature effects primarily influence the wobble mode, (2) tire moments have an important influence on the capsize mode, and (3) the weave mode is influenced by the choice of a tire model only when speeds are below 20 mph. In particular, it is noted that the overturning moment due to inclination of the tire tends to destabilize the capsize mode (see Fig. 2.3) whereas the aligning torque caused by inclination angle has the opposite effect. Examination of the equations of motion shows that the overturning moment and aligning torque produced by inclination angle tend to counterbalance each other since their major influence on the vehicle system derives from the moments that are created about the steering axis. When these two tire moments are transformed into moments about the steering axis, they are seen to be of approximately equal magnitude but opposite sign. Without the existence of tire data and the equations of motion that have been derived for a single-track vehicle, such as a motorcycle, it is not obvious how these two properties of the tire combine to produce the effect noted.

Although not demonstrated in these root loci plots, calculations have shown that reduced inclination stiffness has approximately the same effect on the capsize mode as an increased overturning moment, namely, to cause the capsize

THE UNIVERSITY OF MICHIGAN LIBRARIES

mode to become unstable at lower values of forward speed. It is clear that a tire of different construction than was used in this study, e.g., a radial ply tire with a higher cornering stiffness and a lower inclination stiffness, would have a marked influence on the modal roots of the motorcycle under consideration.

As noted earlier, the choice of a tire model influences the roots calculated for the weave mode only at low speeds (see Fig. 2.2). Aligning moments arising from inclination angles tend to increase the weave mode frequency in the 12-17 mph speed range, while overturning moments due to inclination angle and path curvature effects move the locus in the opposite direction, i.e., toward the real axis.

Two extreme examples of this frequency reduction result from the use of models "4" and "6", which cause the complex roots to break into two real roots for narrow ranges of speed, about 14.9 to 15.2 mph for model "4" and 12.4 to 13.2 mph for model "6". For these speed ranges, the weave mode, defined to be oscillatory, is replaced by three capsize modes. Thus, if the capsize mode is expressed as a function of speed, this function is continuous but multiple-valued for speeds at which the weave mode does not exist (see Fig. 2.3).

THE UNIVERSITY OF MICHIGAN LIBRARIES

2.4 STEERING DAMPING STUDIES

By means of analog computer simulation, it was found that the small amount of coulomb friction present in the steering head of the test vehicle had negligible effect on the calculated motion of the cycle. Nevertheless, coulomb friction is a nonlinear effect deemed worthy of study. Accordingly, the analog computer was utilized to compare viscous versus dry friction steering dampers. In this study, it was assumed that the test machine could be fitted with these dampers.

Figures 2.4 and 2.5 show simulated transient responses of the test motorcycle, with a forward speed of 42.5 mph, subjected to a mathematical impulse of torque applied to the handlebars about the steering axis, with a few different levels of coulomb and viscous friction present in the steering head. These responses show the superiority of the viscous damper in two ways. First, it is seen that while the viscous damper hardly influences the rolling motion at all (at 42.5 mph), the dry friction damper introduces increased roll instability. The exact response in the coulomb friction case is a function of the ratio of magnitude of the disturbance to the friction level, but it is seen that eventually the vehicle falls more quickly with a coulomb friction damper.

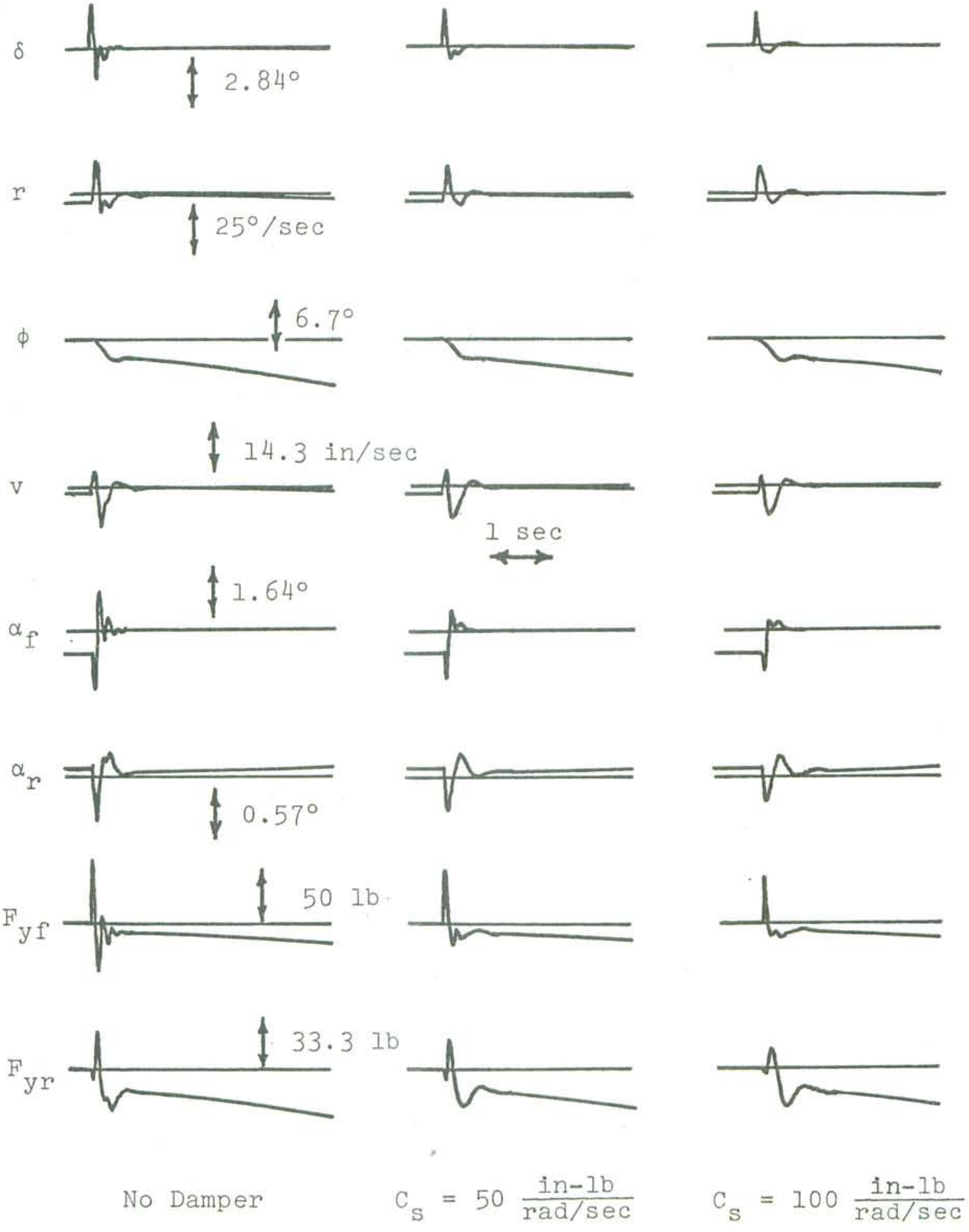

Figure 2.4

Effects of viscous steering damper on the transient response of the uncontrolled motorcycle; u=42.5 mph.

THE UNIVERSITY OF MICHIGAN LIBRARIES

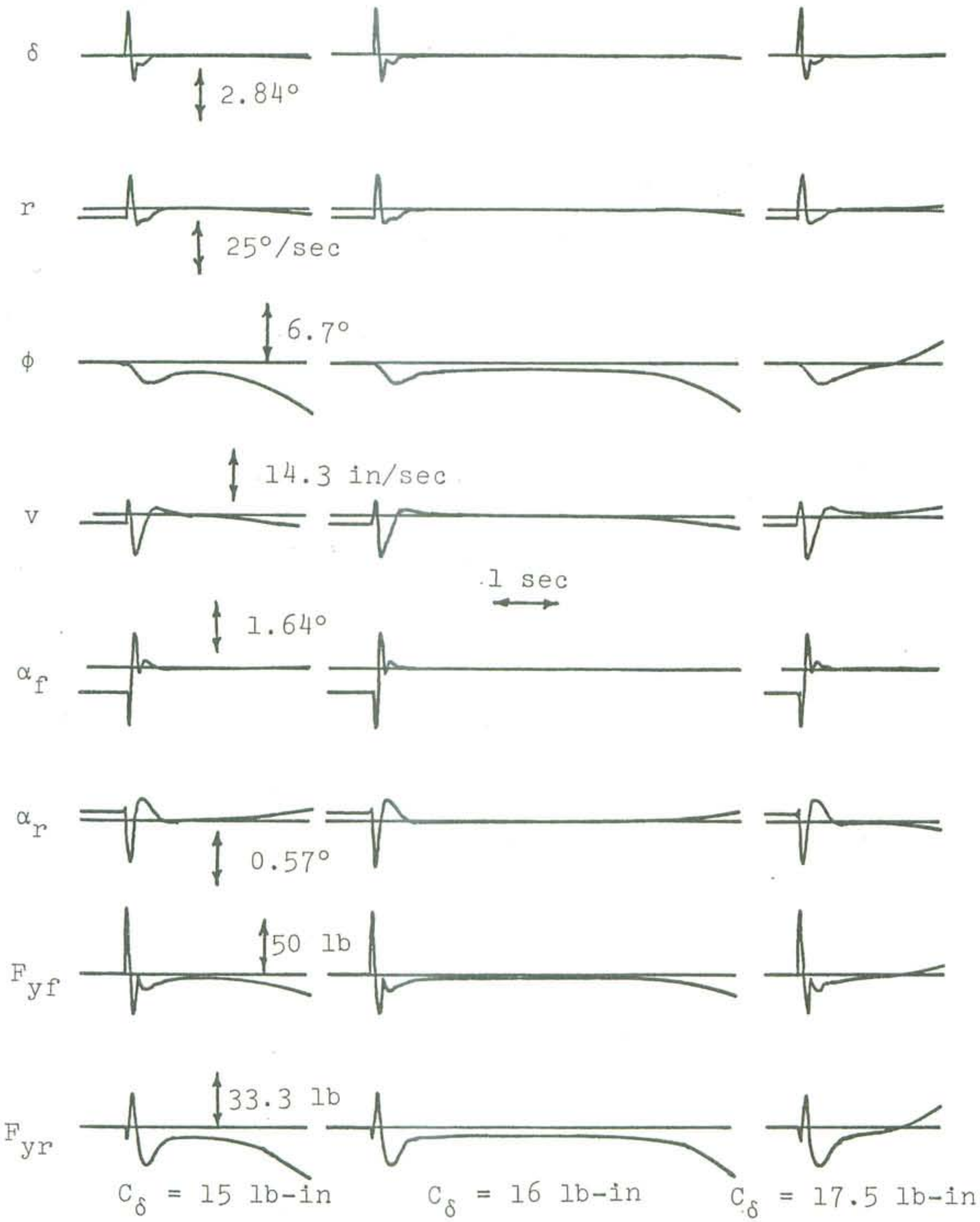

Figure 2.5

Effects of coulomb friction steering damper on the transient response of the uncontrolled motorcycle; u=42.5 mph.

THE UNIVERSITY OF MICHIGAN LIBRARIES

A second, perhaps more important, consideration is that coulomb friction dampers, being nonlinear, have different effects for different levels of disturbance. This fact indicates that a rider, encountering small disturbances, may set his damper to a level which could not handle large disturbances, should they occur. Also, if the damper's maximum capability is reduced by, say, oil or water contamination, it may not be possible to adjust the damper tightly enough.

THE UNIVERSITY OF MICHIGAN LIBRARIES

3. EXPERIMENTAL STUDIES OF THE TRANSIENT RESPONSE OF THE UNCONTROLLED MOTORCYCLE

3.1 DESCRIPTION OF EXPERIMENTS

A major objective of this study was to compare the motion predicted by solutions of the motorcycle equations of motion with experimental data. To make this comparison, the test vehicle was instrumented and road tests were performed. During these road tests, the motorcycle was ridden at a constant forward speed, with the rider's hands off the handlebars, and his upper body prevented from leaning relative to the motorcycle by a rigid brace. The motorcycle was disturbed in such a manner that the disturbance could be simulated by the analog computer, thus allowing a comparison between the simulation and experimental data.

The test vehicle was instrumented to measure steering angle (δ), roll angle (ϕ), and yaw rate (r). A third wheel located at the end of a 27 1/2-inch pivoted bar was used to sense roll angle. (A soft model-aircraft tire was mounted on this wheel and proved to be very satisfactory for absorbing road roughness.) The angular displacement of the steering head and of the roll-sensing bar were both measured with rotary potentiometers that were geared up to increase their sensitivity, the effects of backlash proving to be negligible. Yaw velocity was measured with a rate gyro.

THE UNIVERSITY OF MICHIGAN LIBRARIES

The outputs from these transducers were recorded on a multi-channel strip chart recorder. Both the recorder and the power supply for the potentiometers and the gyro motor were carried in an automobile that operated alongside the motorcycle during a test. Figure 3.1 shows the physical configuration employed in conducting the road tests—the beam supporting the wires between the vehicles, the rider restraining brace, and the third wheel arrangement.

Although straightforward in theory, in practice it proved to be difficult to directly compare the transient response of the motorcycle given various forcing functions, to the response predicted by the mathematical analysis. Forcing functions or disturbances were selected by considering both the information desired and practical limitations. An ideal set of forcing functions would excite each mode of motion independently while being workable from a physical standpoint.

In practice, it was possible to excite the various modes independently of each other to a very limited degree. The wobble mode, being nearly uncoupled from the other modes, especially at higher speeds, and being stable, was the easiest to excite and detect, primarily because of its oscillatory nature. The weave mode and the capsize mode were not so easily observed. The difficulty in identifying and observing these latter two modes derived from a number of factors.

THE UNIVERSITY OF MICHIGAN LIBRARIES

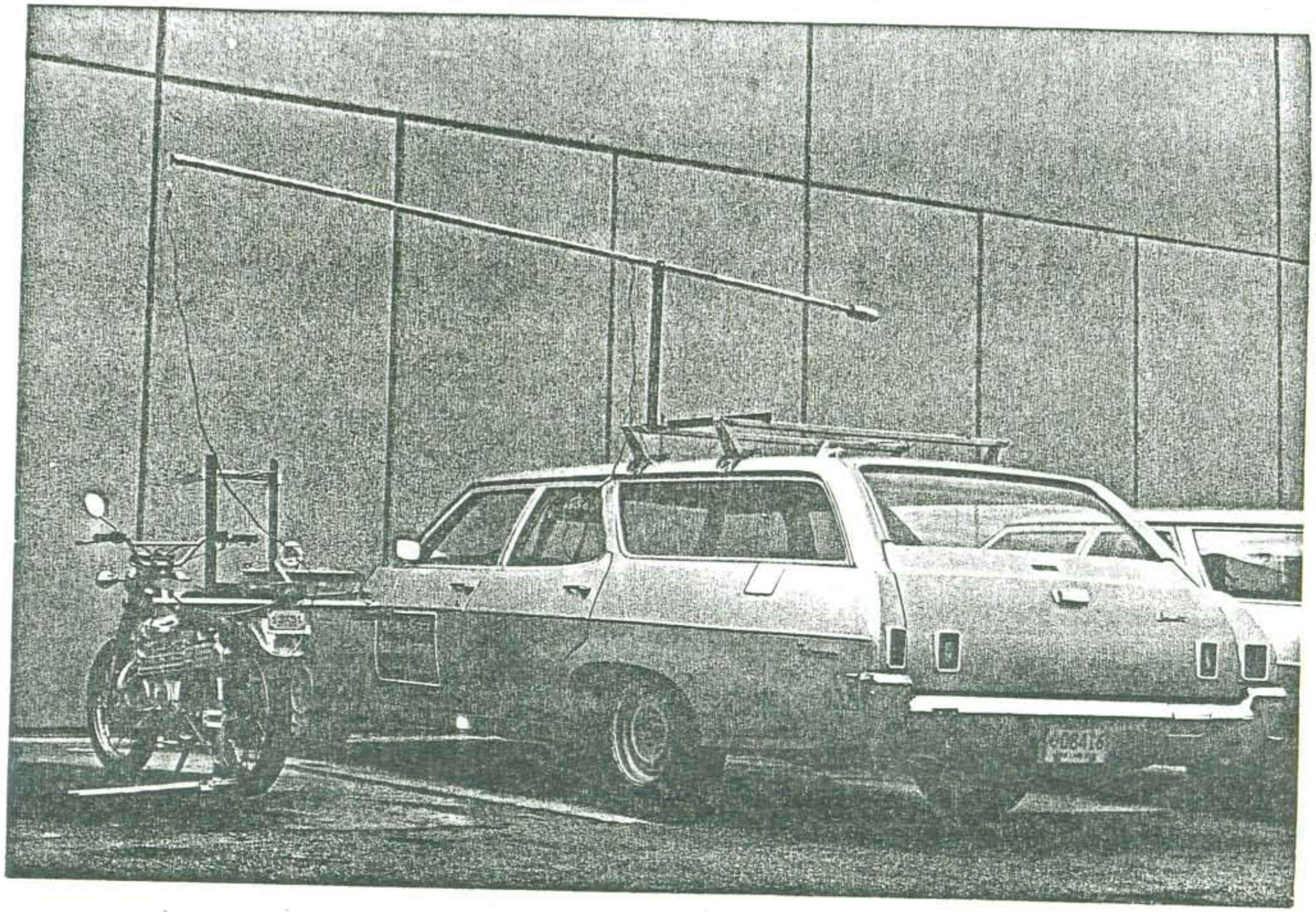

Figure 3.1 Test motorcycle and instrumentation car.

THE UNIVERSITY OF MICHIGAN LIBRARIES

First, testing was limited to a top speed of about *45 mph*, due to safety considerations. Thus, for moderate to high test speeds, the damping ratio of the weave mode was approximately 0.7, eliminating a visible oscillation. In general, at low speeds, a weave mode oscillation existed, but the negative damping was so large that for any disturbance, which necessarily had to be significantly larger than the random disturbances produced by wind forces and road irregularities, the first peak was very small, while the second peak, if it existed at all, was very large, far outside the linear range of motion.

As was the case for the weave mode, the capsize mode could only be observed directly when it became unstable. These instabilities made the vehicle tests difficult to perform and limited the duration of each run to a few seconds. Irrespective of the existence of stability or instability, run length was also limited by the length of the instrumentation cable, unless the motorcycle heading direction before the disturbance was such that after the disturbance, the new heading direction was the same as the accompanying car.

It is clear that the dynamics of the single-track vehicle are such that each of its natural modes of motion cannot be excited and observed independently. Hence, to test the theory it is necessary to compare the theoretical predictions and experimental measurements of responses to a well-defined set of forcing functions.

THE UNIVERSITY OF MICHIGAN LIBRARIES

Two types of forcing functions were employed in the road tests. The first, aimed at exciting the wobble mode, consisted of a pulse of torque about the steering axis. This disturbance was effected on the road by the rider striking one side of the handlebars as briefly as possible with the palm of his hand and allowing the system to move unrestricted until it was necessary to take control. This input can be approximated mathematically as an impulse of steering torque, although of unknown magnitude, since steering torques were not measured experimentally.

The second forcing function consisted of a step function of torque applied about the roll (x) axis to excite the weave and capsize modes. To produce this input in the road tests, a weight was attached to each side of the motorcycle at a distance of 18 inches from the vehicle center plane. One weight was bolted in place; the other could be dropped by means of a pull wire, a microswitch recording the instant of release. (See Fig. 3.1.) The magnitudes of the torques applied by dropping these weights were ±108 lb-in (six-pound weights) and ±216 lb-in (twelve-pound weights). A positive t_ϕ (positive torque) corresponded to dropping a weight from the left side of the vehicle. Note that in addition to producing a roll torque when the weight was dropped, the fixed weight also changed the parameters of the vehicle (e.g., moments of inertia, front wheel load, etc.) to a slight extent.

These changes were estimated by treating the added weight as a point mass. On calculating the new parameters, it was found that changes in tire properties resulting from modified vertical loads on the front and rear wheels were extremely small and could be neglected.

It should be emphasized that the mathematical functions used to represent the physical inputs are approximations. It is not physically possible to apply a pure impulse of steering torque (infinite torque for infinitesimal time). Also, the step input of roll torque does not actually remain constant on the road, but changes as the vehicle rolls, due to a shortened moment arm. The amount of this variation, which depends on the position of the fixed weight relative to the vehicle XYZ axes as well as the roll angle, was found to be less than 3 1/2% for a roll angle of 10°, an angle larger than the roll angles encountered during the road tests. Thus, assuming a constant torque input appears to be valid for the small disturbance motion of interest here.

In practice, it was found that longer runs and consequently more information could be obtained by combining the steer displacement and roll moment inputs. Specifically, the rider would bring the vehicle as nearly as possible to "zero initial conditions" (i.e., v, r, ϕ, δ, and their time derivatives are equal to zero) and drop one weight. After a time interval, a, he would apply a steering pulse in the direction tending to correct the fall induced by dropping the weight.

THE UNIVERSITY OF MICHIGAN LIBRARIES

3.2 DISCUSSION OF RESULTS

To compare theoretical results with experimental data, the response of the motorcycle to a step moment about the roll axis, applied at time t=0, followed by an impulse of torque applied to the front frame assembly about the steering axis, was simulated by the equations of motion derived by Sharp, with these equations being modified to include the aligning torques due to slip angle. Thus, the equations of motion used in the simulation correspond to model number "1", as defined in Section 2.3. The use of this model appears adequate, since it was found (by studying the vehicle responses to the step roll moment and the steering-torque impulse with the aid of the digital computer) that the addition of tire overturning moments and aligning torques due to tire inclination or the addition of path curvature effects (models "2", "3" or "4", Section 2.3) did not significantly influence the simulated responses. For example, the changes in damping of the wobble mode brought about by path curvature effects were not noticeable in the response curves, since at high speeds the effect was small, and at low speeds the wobble mode as predicted by the model not including path curvature effects was heavily damped, and the addition of path curvature considerations merely increased this damping. As a result, very little low speed wobble oscillation was predicted using a tire model with or

THE UNIVERSITY OF MICHIGAN LIBRARIES

without path curvature effects. Further, it was found that a tire model including overturning moments due to inclination angles influenced the theoretical vehicle transient response in a manner opposite that of a model including aligning torques due to inclination angle. Taken together, the effects of these two moments approximately cancelled, as was the case with their influence on the weave and capsize mode roots. Simulation exercises that included coulomb friction in the steering head (as estimated to exist on the test vehicle) showed that these frictional effects were negligible. Accordingly, coulomb friction was omitted in the simulations conducted to correspond with test conditions.

Figures 3.2-3.5 show the transient response of the motorcycle as obtained from experimental data and as simulated, for forward speeds of 10.5, 20.0, 28.2, and 42.5 mph. The high frequency wobble oscillation can be seen in all of the measured time histories, except roll angle (ϕ). The weave mode, with its heavy damping, is not visible in either the experimental or simulated results. The presence of the capsize mode is best observed in the data obtained at the two highest speeds, where it is seen that all of the dependent variables, most notably roll angle, are slowly diverging in the absence of any steering control.

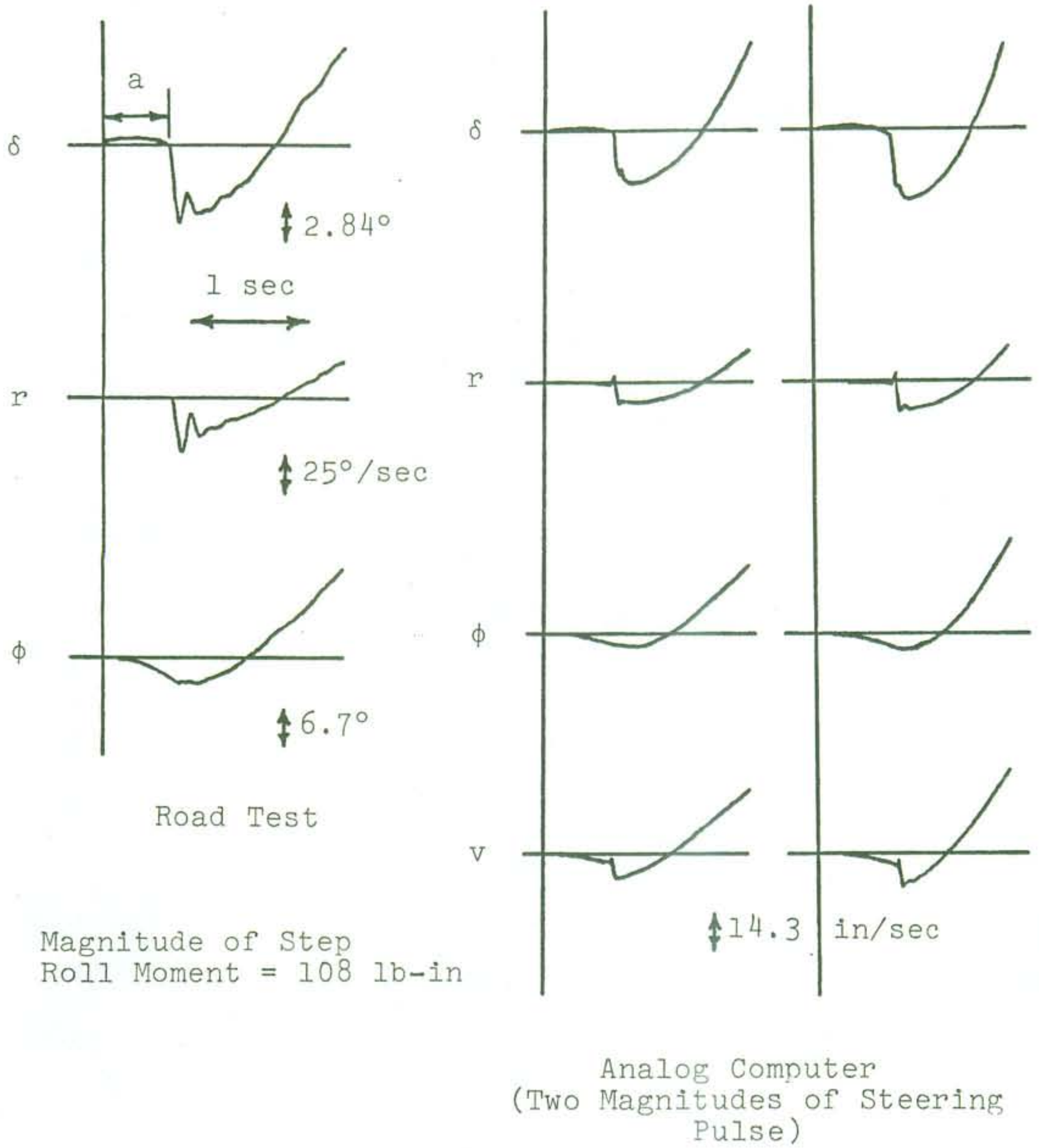

Road Test

Magnitude of Step
Roll Moment = 108 lb-in

Analog Computer
(Two Magnitudes of Steering
Pulse)

Figure 3.2

Comparison of experimental and theoretical responses of the uncontrolled motorcycle; u=10.5 mph, second gear.

THE UNIVERSITY OF MICHIGAN LIBRARIES

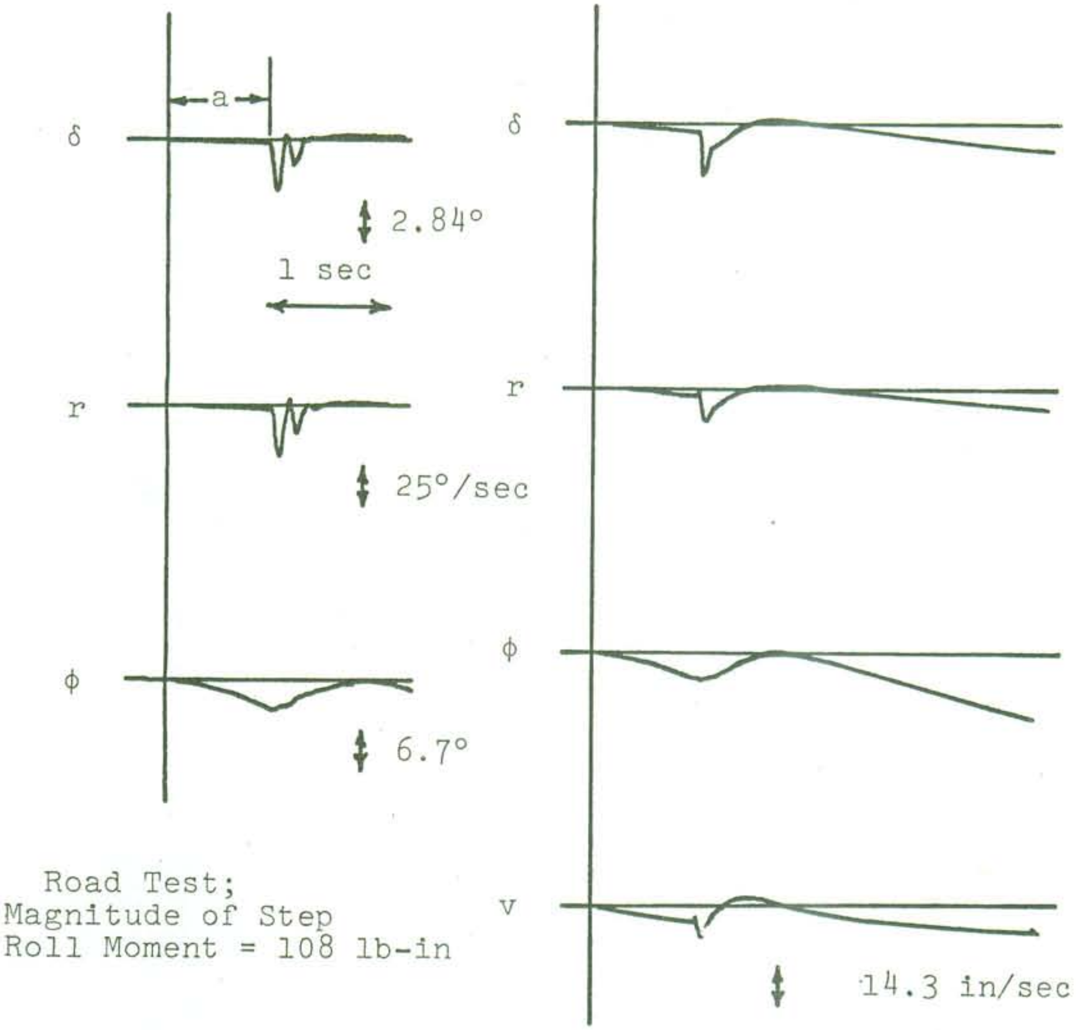

Road Test;
Magnitude of Step
Roll Moment = 108 lb-in

Analog Computer

Figure 3.3

Comparison of experimental and theoretical responses of the uncontrolled motorcycle; u=20.0 mph, second gear.

THE UNIVERSITY OF MICHIGAN LIBRARIES

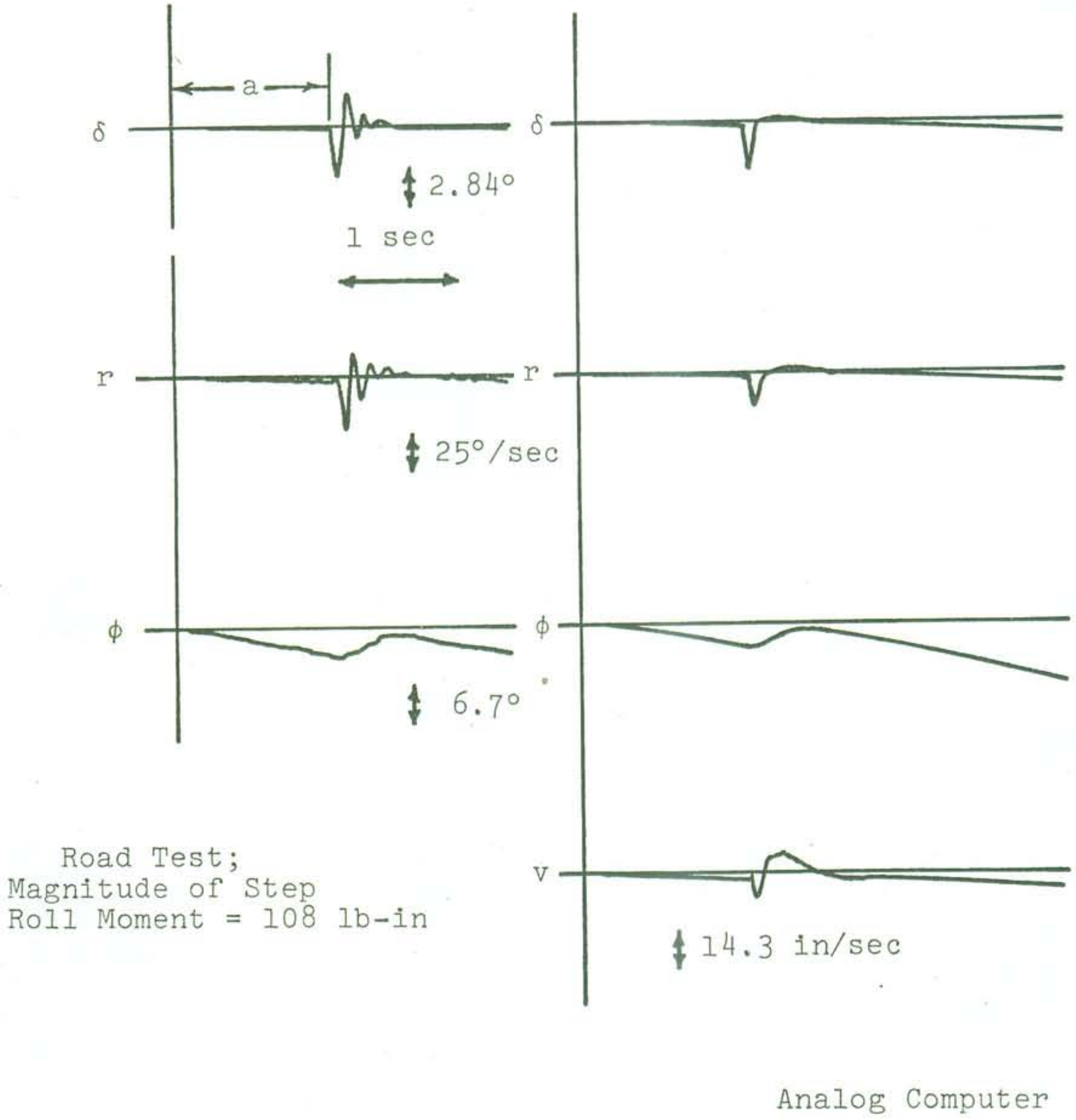

Figure 3.4

Comparison of experimental and theoretical responses of the uncontrolled motorcycle; u=28.2 mph, third gear.

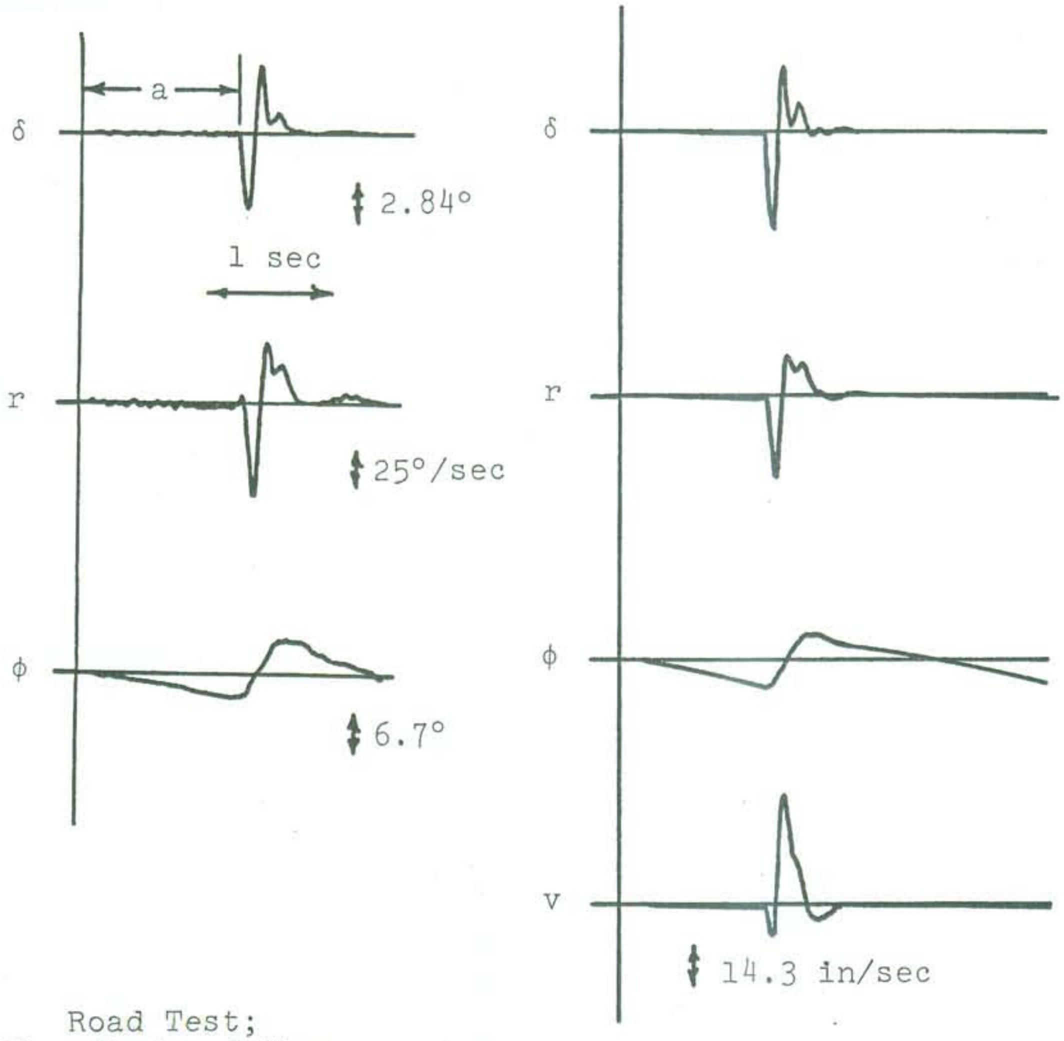

Road Test;
Magnitude of Step
Roll Moment = 216 lb-in

Analog Computer

Figure 3.5

Comparison of experimental and theoretical responses of the uncontrolled motorcycle; u=42.5 mph, fifth gear.

THE UNIVERSITY OF MICHIGAN LIBRARIES

Many tests were made, and the variability between tests was small. The experimental results shown in Figures 3.2-3.5 are representative of the body of data that were obtained.

Figures 3.2 through 3.5 show that the high frequency wobble mode is accurately predicted by theory in the neighborhood of 40 mph, with the simulation becoming a poorer prediction of wobble behavior as forward speed decreases. Specifically, the oscillation of the actual steering assembly has less damping than that predicted by theory. In fact, the wobble mode was observed experimentally to have nearly constant damping and frequency throughout the speed range, even at zero speed.

The simulation of the vehicle response to a step moment about the roll axis also becomes less realistic as speed decreases. For speeds less than about 15 mph, the experimental data clearly indicate that the real vehicle rolls more quickly in response to a step roll torque than does the simulated vehicle, while for higher speeds, the agreement between theory and experiment is very good with respect to the response to a step roll moment. Also, for the higher speeds, the agreement is very good with respect to the roll response (as opposed to high frequency wobble response) produced by a pulse of steering torque.

THE UNIVERSITY OF MICHIGAN LIBRARIES

In addition to conducting tests in which quantitative data were obtained, a number of qualitative experiments were performed, during which the motorcycle was ridden "hands off", with no disturbance applied and the rider's body restrained by the brace. During these runs, several observations about the dynamics of the vehicle were made. Specifically, the following points were noted in these qualitative experiments.

1. The test vehicle seemed to be unstable at all speeds, thus failing to confirm the range of complete stability (about 13-17 mph) predicted by the theory, using tire model "1". Other tire models, except model "6", also predicted a stable speed range.

2. No low frequency weave oscillation could be excited on the road, in spite of the undamped oscillations at low speed predicted by the theory, using every tire model except possibly "6". For the motorcycle to sustain such an oscillation, it was necessary for the front system to "automatically" steer into a fall (induced by a non-zero roll angle), thus providing a lateral force at the tires tending to right the vehicle. During the test runs, it was observed that the "automatic" steering did exist, but that it was not fast enough to provide a sufficient correction. Hence, instead of oscillating, the vehicle roll angle exhibited an exponential divergence in one direction.

THE UNIVERSITY OF MICHIGAN LIBRARIES

3. The instability of the vehicle became less severe as speed increased. Apparently, the magnitude of the unstable capsize root was decreasing with increasing speed, as would be expected from the theoretical results. (See Fig. 2.3, Capsize mode roots.)

The absence of any speed range for complete stability or any undamped weave oscillation would indicate that perhaps tire model "6", lateral forces from slip and inclination angles, aligning moments from slip angles, and overturning moments from inclination angles, is the most realistic tire model, while model "5", lateral forces and aligning moments from slip and inclination angles, is the least realistic. However, the simulated response of the motorcycle, using model "6" (this simulation is not shown here), indicated a capsize mode that was much too unstable, as compared with the experimental data. There is no evidence that any of the tire models are more realistic than model "1" (lateral forces from slip and inclination angles, and aligning moments from slip angles).

The remainder of this chapter is devoted to discussing the possible reasons for the differences that were observed on comparing experimental data with the computer simulation. These discussions are given below, beginning with hypotheses that were rejected, and ending with the most probable explanations for the noted discrepancies.

THE UNIVERSITY OF MICHIGAN LIBRARIES

1. In simulating the steering torque disturbance, a mathematical impulse function was employed for speeds less than about 35 mph. At higher speeds (e.g., 42.5 mph, Fig. 3.5), the experimental time histories, as compared with the simulation, indicated that a torque of constant magnitude, lasting less than a quarter-cycle of steering wobble oscillation, would result in a better simulation. The inadequacy of the impulsive torque at higher speeds is consistent with the experimental observation that the steering assembly of the real vehicle, which was approaching complete stability as speed increased, was strongly self-centering. Hence, disturbing the steering assembly significantly with an impulsive torque would require an impractically large magnitude of torque, and the rider was forced to "spread" the torque over a longer period of time.

The fact that both the impulsive and "truncated-step" simulated steering torques are not exactly the same as the real disturbances (which were not measured) is not a likely explanation of the excessive damping of the simulated wobble mode, simply because the theoretical wobble mode was seen to be too heavily damped to permit oscillatory motion, regardless of excitation.

(It should be noted that in simulating the steering disturbance, the level of applied torque was adjusted until the best experimental correlation was obtained. Since the

THE UNIVERSITY OF MICHIGAN LIBRARIES

accuracy of the simulation with respect to experiment was the poorest at low speed, there was no "best" level of steering torque impulse in simulating the motorcycle at a forward speed on the order of 10 mph. Hence, Figure 3.2 shows two simulations, corresponding to two levels of steering torque impulse.)

2. Flexibility of the front wheel is not a likely explanation of the low speed wobble oscillation. This oscillation was observed closely at zero speed, and no deformation of the wheel could be noted. Rather, it was noted that tire flexibility was providing the necessary restoring torque.

Also, free-play in the front wheel bearings would cause a delay in the transmission of front tire forces and moments to the fork assembly. Such a delay could reduce the damping of the wobble mode. However, no wheel bearing play could be found to exist in the test vehicle.

3. During the road experiments, the values of the roll angle, steer angle, and yaw rate at time t=0 were not exactly as assumed in the simulation. (In most cases, these initial conditions were assumed to be zero.) Nevertheless, it is believed that the difference between the actual and assumed initial conditions was too small to account for the discrepancies under discussion, because the experiments were found to be readily repeatable. Tests performed at

the same speed agreed with each other to a much higher degree than the low speed tests agreed with the simulation. This repeatability could not have been obtained if initial conditions had been varying significantly from one test to another. (Note: for the 20 mph experiment, Fig. 3.3, a small initial roll velocity was estimated from the data, since the slope of the roll angle curve at time t=0 is not zero. This nonzero initial condition was included in the simulation.)

4. It is possible, but not very likely, that the motorcycle traveling at low forward speed can only be correctly simulated with nonlinear equations of motion. Although nonlinearities of the steering geometry and sliding of the front tire contact patch upon application of the sharp steering excitation may need to be taken into account, they are probably insignificant because

a. the range of the motion variables is approximately the same at low speed as at high speed, where accurate simulation is obtained,

b. calculated slip angles (using analog simulation) arising from the simulated application of a sharp steering pulse are very small, and

c. after the application of a steering pulse, the amplitudes of the calculated slip angles decay very rapidly, thus making it extremely unlikely

THE UNIVERSITY OF MICHIGAN LIBRARIES

that a sliding condition could exist
throughout a large portion of a wobble
oscillation.

5. The test motorcycle, with rider, was not symmetrical with respect to its X-Z plane (the plane of the rear wheel, passing through the center of the rear tire contact patch), as was assumed in the derivation of the equations of motion. The actual vehicle center of mass, with the rider seated such that his plane of symmetry coincided with the plane of symmetry of the seat, was approximately 0.5 inch to the left of the X-Z plane. The rider could move the overall center of mass to the right by shifting his hips to the right, relative to the motorcycle seat. (His upper body was constrained by the brace, while he held his knees firmly against the fuel tank to keep his legs from moving.) The lateral shift of the rider's hips required to bring the total center of mass into the X-Z plane was determined by trial and error, while the motorcycle was being ridden. If the overall vehicle center of mass was not close to the X-Z plane, the motorcycle would drift from the straight-ahead direction when the handlebars were released. The rider would then shift his position accordingly. No data was taken until the drifting of the motorcycle was imperceptible. Since perfect adjustment of the center of mass position was not possible, there is probably a small amount of bias in the experimental data. Experiments in which a positive step of roll torque was applied

THE UNIVERSITY OF MICHIGAN LIBRARIES

to the vehicle (rather than the negative steps shown in Figures 3.2-3.5) indicate that there may have been a slight bias to the left; that is, given a magnitude of a step roll torque, the vehicle tended to roll more quickly in response to that torque when the sign of the torque was negative than when it was positive. Thus, the lack of vehicle symmetry appears to have accounted for a small part, but by no means all, of the difference between the measured roll response to a step roll torque and that predicted by the simulation.

6. In the derivation of the equations of motion, it was assumed that the motorcycle and rider are comprised of several rigid bodies. Several components of the man-machine system deviated from this assumption, especially the rider and the gasoline in the fuel tank.

Oscillations of the gasoline in the fuel tank are judged to be an unlikely source of low speed steering oscillations because (1) the tank was kept filled to minimize the chance of any oscillations, and (2) the frequency of fuel oscillations was observed to be considerably below the wobble mode frequency. Compliance of the rider's body did not appear to be a cause of the differences observed between the wobble behavior of the motorcycle and the wobble response predicted by theory, since a wobble oscillation could easily be induced in the motorcycle at very low speeds, without the rider

THE UNIVERSITY OF MICHIGAN LIBRARIES

seated on the vehicle, whereas the theory did not predict an oscillation under these conditions. (Moments of inertia, etc., were measured for the motorcycle without rider, as well as with rider.)

In spite of his restraining brace, it is possible that the rider unconsciously exercised a small amount of body control, which would influence the measured roll response to a step roll moment. It is likely that this body control occurred to a greater extent at low rather than high speeds, because (1) the vehicle tended to be more unstable at low speeds than high speeds, and (2) it was more difficult to correct the roll instability at low speeds by means of steering control. Both of these conditions tended to pressure the rider into taking some premature control action, i.e., body control. In riding the motorcycle "hands off", it was noted that body lean tended to oppose roll angle—that is, if the motorcycle started to roll to the left, the rider would tend to lean to the right. Thus, if the rider was making unconscious corrections to a negative step of roll torque, he would be leaning to the right. In that case, to keep the total vehicle center of gravity position unchanged, the motorcycle would roll further in the negative direction. Since the third wheel measured the lean of the motorcycle only (not the position of the combined rider-motorcycle center of gravity), it would indicate a faster roll than it would have if the rider had remained rigid.

THE UNIVERSITY OF MICHIGAN LIBRARIES

The hypothesis that body movements performed unconsciously by the rider have influenced the low frequency response of the vehicle is a possible but not the most likely explanation of differences between theory and experiment. There are a few shortcomings to this hypothesis. First, care was taken to notice such movements if possible. Next, at 20 mph, the experimental roll response to a step roll torque appeared to diverge slightly faster than the simulated response, in the manner of 10 mph experiments, but, at 20 mph, the rider was under much less pressure to make a body movement correction. Finally, and most significantly, in the absence of disturbances, the rider was unable to sustain a roll oscillation, even while making body movements (within the constraint of the rigid brace) intended to reinforce such an oscillation.

7. Regardless of whether or not the rider was in fact influencing the roll response of the motorcycle to a step input of roll torque, it is very unlikely that he influenced the wobble mode, either actively or passively. Rather, it is felt that the reason the wobble mode is poorly predicted by the simulation is that none of the tire models investigated adequately represented the dynamic response of the tire lateral force and aligning torque to time varying values of slip angle. A finding in support of this hypothesis consists of the observation that the lightly damped wobble mode

THE UNIVERSITY OF MICHIGAN LIBRARIES

can be obtained in the simulation by artificially adjusting the relaxation length of the front tire. Unfortunately, no single relaxation length was found to give valid results for all speeds.

The greatest advantage of the method in which tire dynamic effects have been included in the motorcycle equations (see Eq. (1.1)) is the ease with which tire dynamics may be incorporated into the vehicle equations of motion, and also the ease with which the resulting equations may be solved. It should be recognized, however, that tire dynamics models exist which have been found to predict transient lateral forces and aligning moments in a more realistic manner than the "point-contact" model of Equation (1.1). These more complete models are usually based on "string theory" [42, 43], in which the differential equations governing the lateral deformation of the tire tread are the same as equations governing the motion of a stretched string with an elastic lateral restraint. The tire dynamics model of Equation (1.1) can be derived from a string theory model by allowing the tire contact length, 2ℓ, to become zero (hence the name, "point-contact" model).

While it is difficult to incorporate a string theory model with finite contact length into the motorcycle equations of motion, it can be shown that such an incorporation promises at least a more realistic theoretical prediction

THE UNIVERSITY OF MICHIGAN LIBRARIES

of the wobble mode, i.e., reduced damping at low speeds. To show this, consider a tire and wheel constrained such that the wheel plane remains vertical and the hub center moves with constant velocity (speed = u). Define the yaw angle, ψ, of the wheel plane to be zero when the wheel plane is aligned with the velocity vector of the hub center, and further require the yaw angle to vary sinusoidally with a frequency of Ω radians/second, i.e.,

$$\psi = \psi_o \sin \Omega t \ .$$

If path curvature considerations are ignored, the slip angle, α, is the negative of ψ. Consider the lateral force response of the tire to the yaw angle input. Based on a one-dimensional string model, hereafter termed the "finite-contact" model, the sinusoidal lateral force output is expected to lag the yaw angle by the phase angle [42],

$$\phi_s = \tan^{-1}\left(\frac{-\sin \frac{2\ell\Omega}{u}}{\cos \frac{2\ell\Omega}{u} + 1}\right) + \tan^{-1}\left(-\frac{\sigma_s\Omega}{u}\right), \qquad (3.1)$$

where σ_s is the relaxation length associated with the finite-contact model. In the case of the point-contact model, the force lags the yaw angle by the phase angle [42],

THE UNIVERSITY OF MICHIGAN LIBRARIES

$$\phi_p = \tan^{-1} -\left(\frac{\sigma_p \Omega}{u}\right) , \qquad (3.2)$$

where σ_p is the relaxation length associated with the point-contact model.

The string model and the point-contact model also predict different lateral force (F_y) responses to a step change in slip angle. For the finite-contact model, this response is [41]

$$\frac{F_y(x)}{F_{yss}} = \begin{cases} \dfrac{(\ell + \sigma_s)x - x^2/4}{(\ell + \sigma_s)^2} , & 0 < x < 2\ell \\[2ex] 1 - \dfrac{\sigma_s^2 \, e^{-(x-2\ell)/\sigma_s}}{(\ell + \sigma_s)^2} , & x > 2\ell , \end{cases} \qquad (3.3)$$

where x is the distance rolled by the tire, and F_{yss} is the steady-state level of lateral force. For the point-contact model, Equation (3.3) reduces to

$$\frac{F_y(x)}{F_{yss}} = 1 - e^{-\sigma_p/x} . \qquad (3.4)$$

For a given tire, the lateral force response to a step slip angle can be measured, and the values of σ_s and σ_p can

THE UNIVERSITY OF MICHIGAN LIBRARIES

be estimated by fitting Equations (3.3) and (3.4) to the experimental data. In Appendix C, the value of $\sigma_p \equiv \sigma_f$ is obtained in this manner (Fig. C.10). The value of the tire contact length, 2ℓ, was estimated to be about 4-5 inches for the front tire of the test motorcycle. Fitting Equation (3.3) to the data of Figure C.10, with $2\ell = 5$ inches, yields $\sigma_s = 1.15$ inches. From Appendix D, the value of $\sigma_p = \sigma_f$ is found to be 2.1 inches.

The phase lag of the lateral force behind the yaw angle can now be estimated from Equations (3.1) and (3.2) for the front tire of the test motorcycle. The wobble frequency of the test motorcycle was observed to remain essentially constant with forward speed, at a value of about 45 radians/second. Thus, in Equations (3.1) and (3.2), $\Omega = 45$ radians/second. Both ϕ_s and ϕ_p are functions of Ω/u, which quantity is termed the "reduced frequency" (Ω_r). Table 3.1 displays values of ϕ_s and ϕ_p for u = 10, 30 and 45 mph. The corresponding (approximate) values of Ω_r are also shown.

Notice in Table 3.1 that the lateral force output of the tire, as predicted by the finite-contact model, lags considerably more behind the yaw angle (and consequently the negative of the slip angle) than the force output as predicted by the point-contact model, especially at the lower speeds, where the simulation of the wobble mode based on the

THE UNIVERSITY OF MICHIGAN LIBRARIES

TABLE 3.1

COMPARISON OF FINITE-CONTACT AND POINT-CONTACT TIRE MODELS

u, mph	Ω_r, rad/ft	ϕ_s, degrees	ϕ_p, degrees
45	0.66	-12	-7
30	1	-18	-10
10	3	-52	-28

motorcycle equations of motion was found to be the poorest. Thus, it is reasonable to expect that the finite-contact model, if incorporated into the motorcycle equations of motion, would result in an improved simulation of, at least, the wobble mode.

Use of the finite-contact tire model in the motorcycle equations might also improve the accuracy of the predicted roll response to a step input of roll torque. Solutions to the present motorcycle equations have indicated that if the value of σ_f is adjusted artificially to give a good prediction of the wobble mode at 10 mph, for example, no improvement in the roll response to the step input of roll torque results. However, the effects of the finite-contact tire model are not the same as the effects of adjusting the value of σ_f. For example, the lateral force response of the tire to a sinusoidal slip angle input, as predicted by the

THE UNIVERSITY OF MICHIGAN LIBRARIES

point-contact model, does not depend on whether the slip angle is induced by pure yawing, as discussed in connection with Table 3.1, or by pure lateral translation, whereas the finite-contact model does distinguish between these two types of inputs.

Some intuitive reasoning suggests a manner in which the finite-contact area of the real tire might influence the roll stability of the uncontrolled motorcycle at low forward speeds. The existence of roll stability and weave oscillations apparently depends upon the ability of the front fork assembly to steer in the direction of an impending fall. If the motorcycle is stationary and is given a small roll angle, the steering assembly cannot rotate significantly, because the friction between the tire and the road produces a moment acting on the steering assembly to oppose such a rotation. Thus, forward motion of the vehicle is needed to allow the front fork assembly to steer. However, if the forward speed is sufficiently low, friction at the tire-road interface still interferes with the steering of the front fork assembly. This interference may explain the inaccurate simulation of the vehicle response to a step input of roll torque, and the observations that the real vehicle could not sustain an undamped weave oscillation or did not have a speed range of complete stability.

THE UNIVERSITY OF MICHIGAN LIBRARIES

In summary, it appears that an improved static and dynamic representation of the pneumatic tire is required to adequately account for the dynamic behavior that is exhibited by the motorcycle at low forward speeds of travel.

THE UNIVERSITY OF MICHIGAN LIBRARIES

4. THE MAN-MOTORCYCLE SYSTEM

4.1 MODELING THE MAN-MOTORCYCLE SYSTEM

Chapters 2 and 3 have dealt with the uncontrolled motorcycle. In the remainder of the dissertation, this restriction is relaxed, and the rider is allowed to control the vehicle by applying a steering torque to the handlebars. The man and motorcycle are assumed to interact in the form of the closed-loop control system diagrammed in Figure 4.1. In this model of the system, the rider, desiring to maintain a roll angle of zero, perceives an error signal equal to the negative of the actual roll angle ($\phi(t)$). He makes a correction in the form of a steering torque which is related to the error by the linear transfer function $Y_p(j\omega)$. His total steering-torque output ($t_\delta(t)$) is the sum of the torque correlated with the error plus an additive noise or "remnant" ($n(t)$). The motorcycle dynamics are represented by the linear transfer function, $Y_c(j\omega)$. Disturbances caused by cross winds and road irregularities are included in $i(t)$.

In this study, attention has been restricted to the roll stabilization task performed by the rider as the vehicle travels on a straight level road. The path following task is not being considered. Using analytical methods, Weir [16] has shown that the best closed-loop control system representing the stabilization task is the one shown in Figure 4.1, and that rider-body lean is more useful for path-following control.

THE UNIVERSITY OF MICHIGAN LIBRARIES

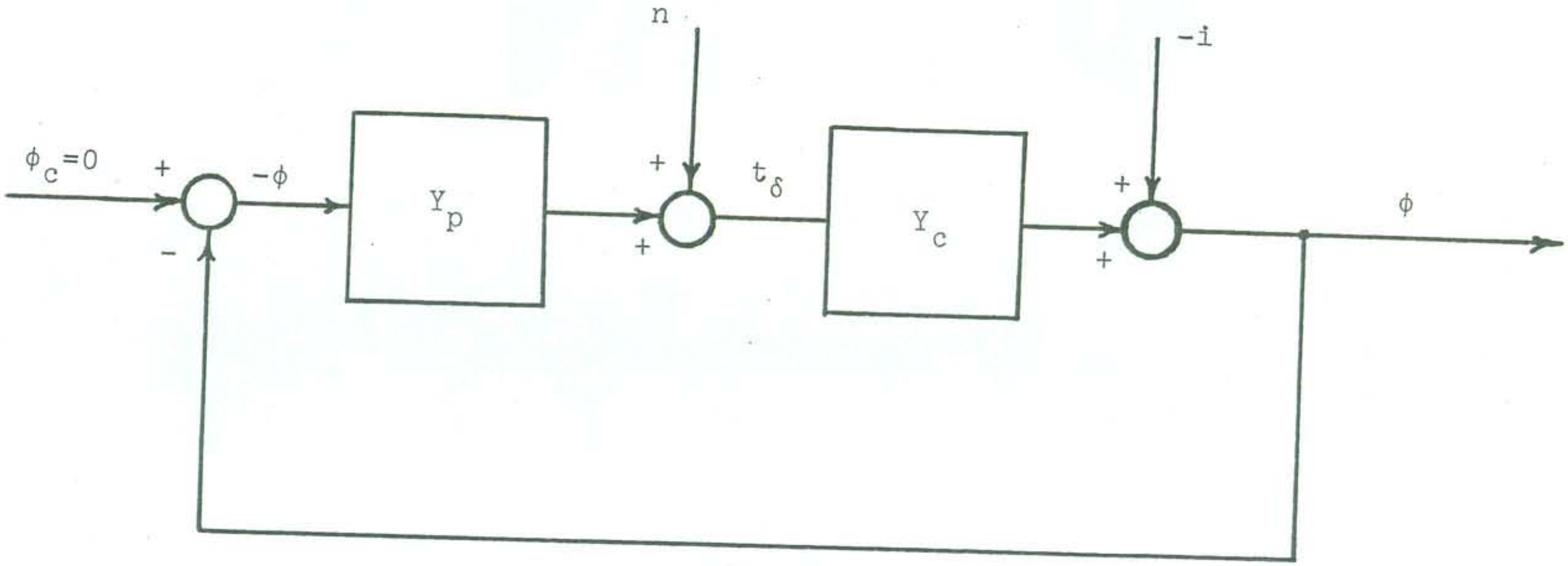

Figure 4.1 Block diagram of the man-motorcycle system.

THE UNIVERSITY OF MICHIGAN LIBRARIES

By restricting the study to straight-path operations, the rider's chief activity is one of stabilization. Because stabilization can be accomplished most effectively with the use of steering torque, body lean would be expected to be small. In fact, in the qualitative experiments performed in this study with the rider's body braced, it was found that, except for very low speeds, the motorcycle could be controlled on curved and straight roads just as easily as when body lean was permitted. Apparently in situations of "easy" operation, control by body lean is optional, and there is probably much more variation in control techniques with time and between different riders when body lean is allowed. In order to simplify the problem and reduce the variability in the experimental findings, body-lean control, although very interesting and important in many situations[1], was purposely eliminated as being beyond the scope of this dissertation.

In modeling the stabilization task of the rider in operating the vehicle on a straight road, the remnant, n(t), consists of all the steering torque output of the rider that is not related to the roll angle by the linear transfer function, $-Y_p(j\omega)$. The remnant contains (1) rider output

---

[1] Body lean control is probably the most important for low speed operation and "difficult" path following maneuvers. For example, the author has observed that riding a bicycle along a very narrow path seems to require significant body control.

which is nonlinearly related to the roll angle, (2) path correction steering torques not linearly related to the roll angle (such as corrections needed due to the real road not being perfectly straight, obstacle or bump avoidance, etc.), (3) miscellaneous steering torques, voluntary or involuntary (such as direct mechanical transmission of road shocks through the rider's arms to the handlebars, although road shocks are high frequency phenomena), and (4) any time variation in $Y_p(j\omega)$.

4.2 THE CONTROLLED ELEMENT (Y_c)

In modeling the man-motorcycle system, the motorcycle transfer function, $Y_c(j\omega)$, with steering torque as input and roll angle as output, was calculated from the motorcycle equations of motion. (This calculation is described in Appendix A.)

The transfer function of the controlled element was calculated at forward speeds of 15, 30 and 45 mph, using parameter data corresponding to the Honda test motorcycle as instrumented for the man-motorcycle experiments. (The additional instrumentation—a steering-torque measuring bar—was estimated to have negligible effect on the calculation of $Y_c(j\omega)$.) The results of these calculations, shown in Table 4.1 (analytical expressions) and Figure 4.2 (Bode

THE UNIVERSITY OF MICHIGAN LIBRARIES

TABLE 4.1 CONTROLLED ELEMENT TRANSFER FUNCTION FOR THREE FORWARD SPEEDS

u, mph	Theoretical $Y_c(j\omega)$
15	$\frac{-.00121(j\omega+21.2)(j\omega+68.5)(j\omega+125.0\pm j0.545)(j\omega+54.1\pm j46.0)(j\omega+43.4\pm j186.5)}{(j\omega+3.04)(j\omega+0.349\pm j1.438)(j\omega+41.0)(j\omega+125.0\pm j1.221)(j\omega+42.5\pm j64.1)(j\omega+60.1\pm j63.1)}$
30	$\frac{-.00121(j\omega+175.3)(j\omega+221.4)(j\omega+246.6)(j\omega+253.0)(j\omega+13.7\pm j26.8)(j\omega+73.0\pm j159.5)}{(j\omega-0.274)(j\omega+6.13\pm j5.74)(j\omega+214\pm j5.26)(j\omega+15.5\pm j43.1)(j\omega+251\pm j6.71)(j\omega + 26.7)}$
45	$\frac{-.00121(j\omega+8.76\pm j27.8)(j\omega+312)(j\omega+361)(j\omega+378)(j\omega+83.6\pm j136.7)(j\omega+368)}{(j\omega-0.232)(j\omega+13.06)(j\omega+6.64\pm j12.93)(j\omega+392)(j\omega+339)(j\omega+363\pm j21.1)(j\omega+8.44\pm j43.1)}$

THE UNIVERSITY OF MICHIGAN LIBRARIES

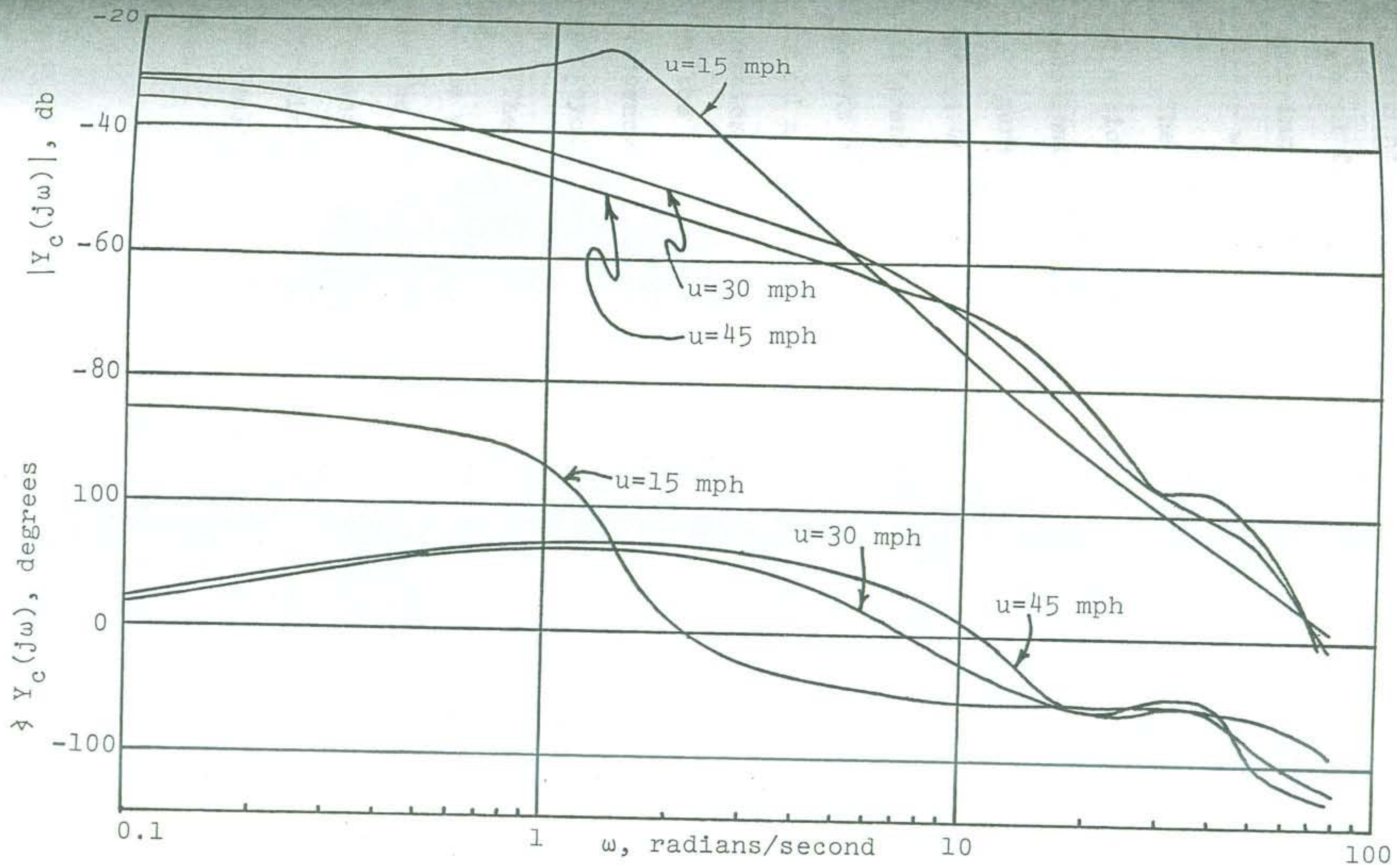

Figure 4.2 Controlled element; u=15, 30 and 45 mph.

THE UNIVERSITY OF MICHIGAN LIBRARIES

diagrams), were obtained from the motorcycle equations of motion having the simplest tire model studied, namely, tire lateral forces due to slip and inclination angles, and aligning moments arising from slip angles only. No steering damper was included, since the test vehicle did not have one.

The motorcycle, as described by the derived equations of motion, is stable at 15 mph, whereas it exhibits a capsize-mode instability at speeds of 30 and 45 mph. The Bode diagrams in Figure 4.2 show that the vehicle transfer function at 30 and 45 mph is nearly the same, but is considerably different from the transfer function describing the controlled element at 15 mph. Frequencies less than about 10 radians/second are controllable by the rider, and for these frequencies low-speed operation is dominated by the weave mode and the (stable) capsize mode, while for higher speeds, the frequency and damping of the weave mode increases and the motorcycle is dominated by the unstable capsize mode.

The domination of the dynamics of the controlled element by the weave and capsize modes provides some intuitive feel for the behavior of the motorcycle. For example, at low frequencies, and at 15 mph, the controlled element behaves approximately as a third order system, while, at 30 and 45 mph, the cycle can be approximated by a first order system of the form

THE UNIVERSITY OF MICHIGAN LIBRARIES

$$Y_c(j\omega) \doteq \frac{K_c}{T_c j\omega - 1} \qquad (4.1)$$

Figure 4.3 shows such an approximation for the 30 mph case, with $K_c = -.0262$ radian/lb-in, and $\frac{1}{T_c} = .274$ radians/second (the capsize mode root). A more accurate approximation of $Y_c(j\omega)$ at 30 mph would require an additional second-order factor corresponding to the weave mode.

From the preceding discussion, it is seen that the theoretical transfer function of the controlled element, while speed dependent, has two basic forms for speeds at which real motorcycles normally operate. (At speeds higher than 45 mph, the transfer function of the controlled element has the same form that it has at 30 and 45 mph.) Research in man-machine systems (e.g., [28]) indicates that the form of the human operator's transfer function is strongly dependent upon the form of the transfer function of the controlled element. Thus, conclusions reached by studying the man-motorcycle system at one speed can probably be generalized to other speeds at which the transfer function of the controlled element has the same form.

4.3 THEORETICAL REQUIREMENTS FOR STABILITY OF THE MAN-MOTORCYCLE SYSTEM

Man-machine systems in which the controlled element has the form given in Equation (4.1) have been studied by a number of investigators [28, 45, 46, 47]. Both McRuer [28] and Jex [45] have shown that the preferred form of the operator's

THE UNIVERSITY OF MICHIGAN LIBRARIES

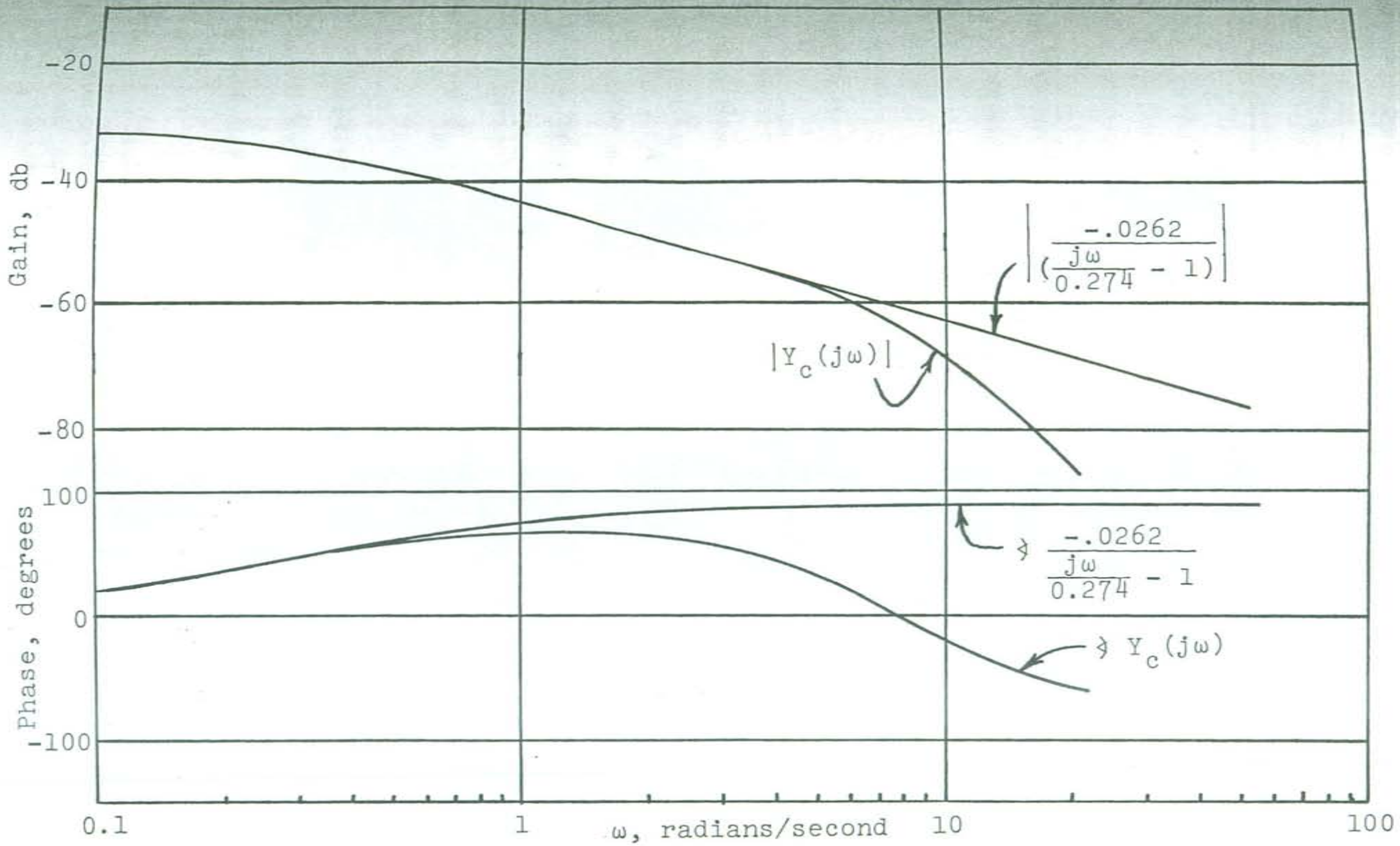

Figure 4.3 Controlled element transfer function, u=30 mph, and its approximation by a first order transfer function.

THE UNIVERSITY OF MICHIGAN LIBRARIES

transfer function, $Y_p(j\omega)$, is simply a constant gain, K_p, and pure time delay[1], τ_p, i.e., $Y_p(j\omega) = K_p e^{-\tau_p j\omega}$.

The stability of the closed-loop system having the open-loop transfer function (Laplace transform notation),

$$Y_p(s)Y_c(s) = \frac{K_p K_c \; e^{-\tau_p s}}{T_c s - 1} , \qquad (4.2)$$

can be determined by the application of the Nyquist criterion, which states that

$$Z = N + P , \qquad (4.3)$$

where Z is the number of zeroes of the closed-loop characteristic function $(1 + Y_p(s)Y_c(s))$ located in the right half of the complex plane, P is the number of poles of $Y_p(s)Y_c(s)$ in the right half of the complex plane, and N is the number of clockwise encirclements of the -1 point by the Nyquist map of $Y_p(s)Y_c(s)$, or the number of clockwise encirclements of the $-1/(K_pK_c)$ point by the Nyquist map of $Y_p(s)Y_c(s)/(K_pK_c)$. A Nyquist plot of $Y_p(s)Y_c(s)/(K_pK_c)$ is shown in Figure 4.4. For $Y_p(s)Y_c(s)$ as defined in Equation (4.2), P = 1. If stability of the closed-loop system is to be achieved (Z = 0), N must be -1. From Figure 4.4, it is seen that there is one counterclockwise

---

[1] It is shown in [28] and [45] that lead and lag equalization as part of the operator's transfer function did not significantly improve the closed-loop system performance.

encirclement of the $-1/(K_pK_c)$ point by the $Y_p(s)Y_c(s)/(K_pK_c)$ map $(N = -1)$ if $1 < K_pK_c < a$, where a, defined in Figure 4.4, depends upon T_c and τ_p. For $K_pK_c < 1$, there are no encirclements of the $-1/(K_pK_c)$ point $(N = 0)$. For $K_pK_c > a$, there is one clockwise encirclement of the $-1/(K_pK_c)$ point $(N = +1)$. Hence, only for $1 \leq K_pK_c \leq a$ is the closed-loop system stable.

Most of the remainder of the dissertation is concerned with rider-cycle behavior at 30 mph, at which speed the controlled element transfer function, $Y_c(j\omega)$, has a form similar to the form discussed in the preceding paragraph. Because of this similarity, it is reasonable to expect the motorcycle rider's transfer function also to be a gain and time delay.

A Nyquist plot of

$$Y_p(s)Y_c(s) = -K_pe^{-\tau_ps}Y_c(s), \qquad (4.4)$$

is shown in Figure 4.5. In this figure, $Y_c(s)$ is the theoretical transfer function of the controlled element for 30 mph, τ_p was chosen to be 0.3 second, and K_p = 100 lb-in/radian. (Note that a negative sign is required in Equation (4.4) so that the $Y_p(s)Y_c(s)$ map can encircle the -1 point.) An application of the Nyquist criterion in the same manner as before gives the following range of values for K_p producing closed-loop stability:

THE UNIVERSITY OF MICHIGAN LIBRARIES

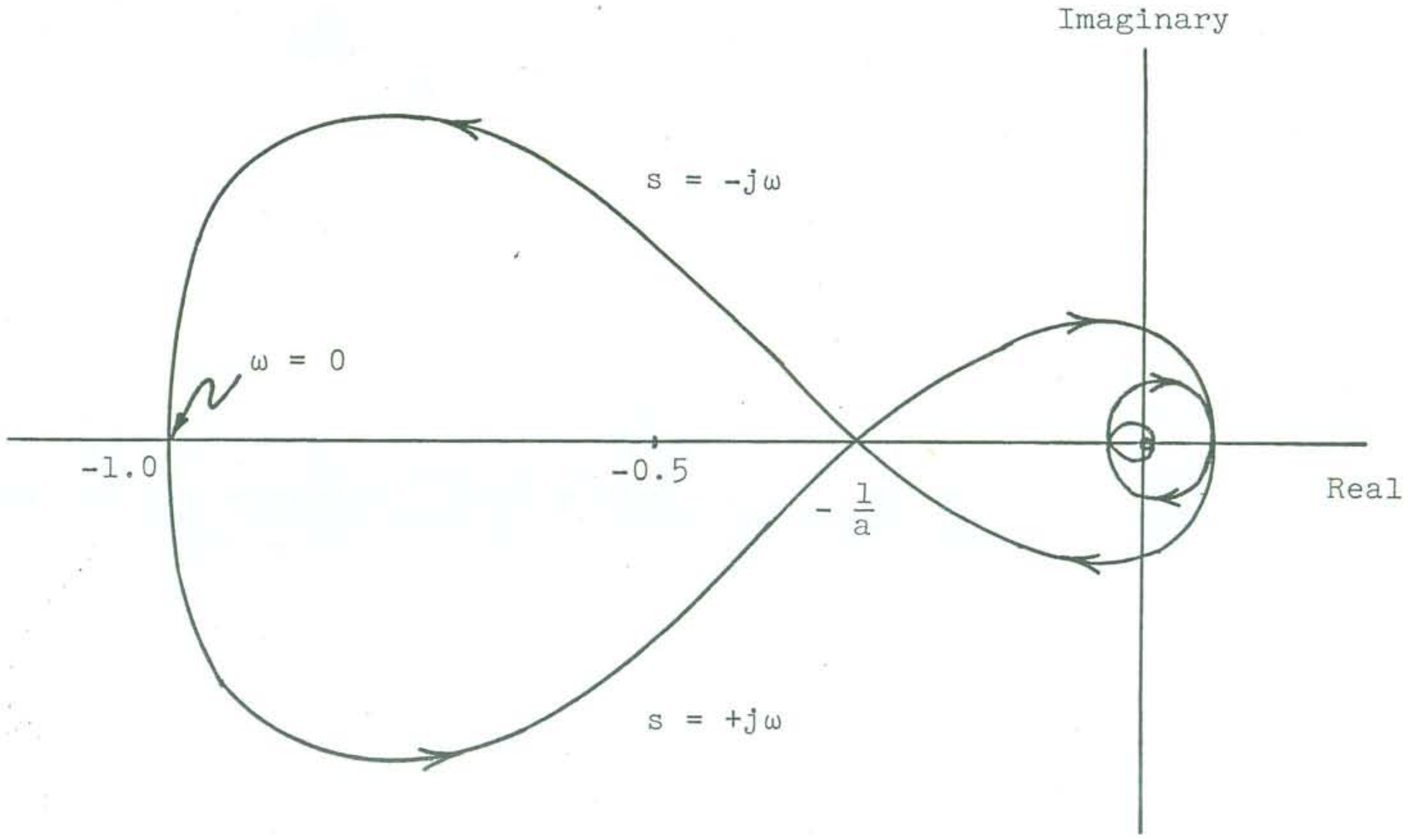

Figure 4.4 General Nyquist plot of $\frac{e^{-\tau_p s}}{T_c s - 1}$.

THE UNIVERSITY OF MICHIGAN LIBRARIES

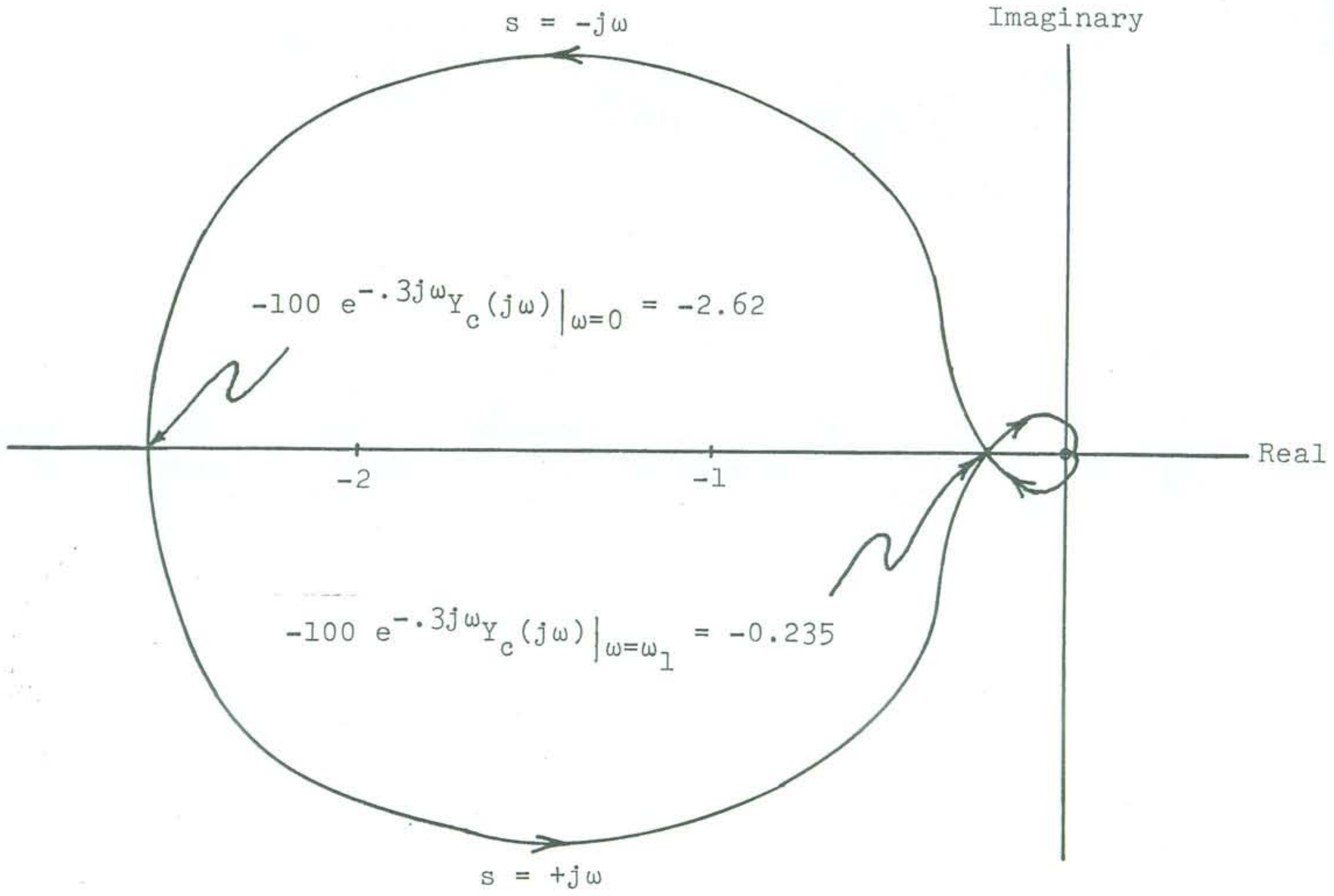

Figure 4.5 Nyquist plot of $-100e^{-.3s}Y_c(s)$, 30 mph.

THE UNIVERSITY OF MICHIGAN LIBRARIES

$$38.2 \leq K_p \leq 425 \text{ lb-in/radian.}$$

These results, in the form of Nyquist plots, can be replotted as a Bode diagram, $-Y_p(j\omega)Y_c(j\omega) = K_p e^{-\tau_p j\omega} Y_c(j\omega)$, where $Y_c(j\omega)$ is again the theoretical transfer function of the controlled element at 30 mph; e.g., see Figure 4.6, for which $K_p = 1$ lb-in/radian, and $\tau_p = 0.3$ second. For stability, the minimum value of K_p is defined by

$$(K_p)_{min}|Y_c(j\omega)|_{\omega=0} = 1,$$

while the maximum value of K_p is determined by

$$(K_p)_{max}|Y_c(j\omega)|_{\omega=\omega_1} = 1 ,$$

where ω_1 is the frequency (other than zero) for which $\measuredangle(-K_p e^{-\tau_p j\omega} Y_c(j\omega)) = -180°$, or $\measuredangle(K_p e^{-\tau_p j\omega} Y_c(j\omega)) = 0$.

THE UNIVERSITY OF MICHIGAN LIBRARIES

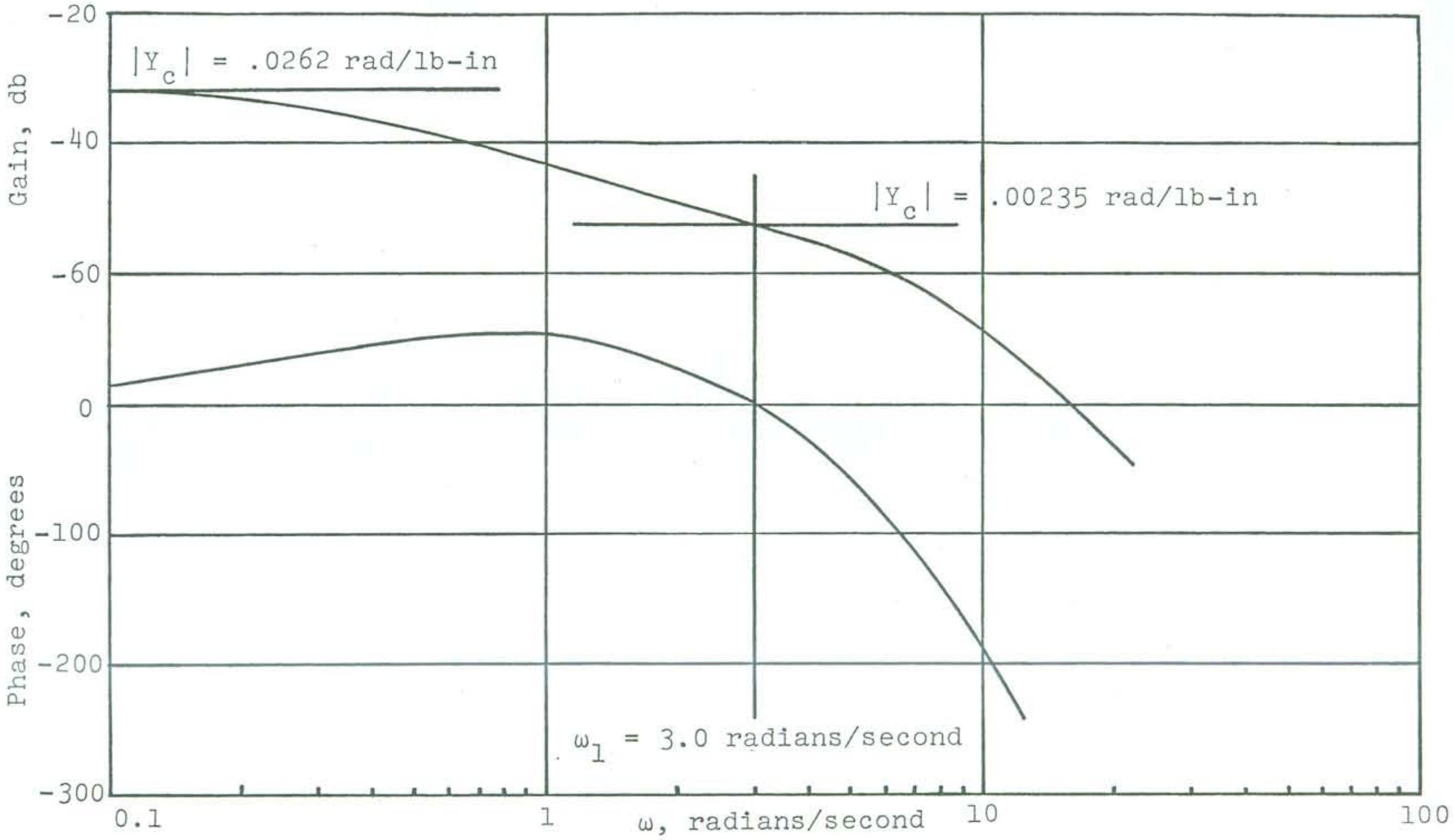

Figure 4.6 Bode diagram of $+e^{-.3j\omega}Y_c(j\omega)$, u=30 mph.

THE UNIVERSITY OF MICHIGAN LIBRARIES

5. ROLL-STABILIZATION EXPERIMENTS

5.1 *OBJECTIVE* AND DESCRIPTION OF EXPERIMENTS

The major objective of the manual control portion of the investigation described in this dissertation has been to identify a transfer function representation of the rider's task in stabilizing the vehicle. Experiments providing the necessary data have been performed using the test vehicle described in Chapter 3, with three test subjects, denoted Riders A, B, and C.

The test motorcycle was instrumented as follows. Roll angle and steer angle were measured as described in Chapter 3 (third wheel and geared rotary potentiometers). Yaw rate was not recorded, but the rate gyro was positioned to measure roll rate. To record steering torques applied by the rider, the rider steered one-handed[1] with a torque bar (1/8" x 1" cross-section) attached to the handlebars (Fig. 5.1). This bar was designed to measure the component of applied force[2] parallel to the plane of the front wheel and

---

[1] Throttle control was relocated to the rear frame to replace the usual hand grip control on the handlebars. The effect of this unusual control arrangement upon the generality of the results is not known, but it is felt that any such effects were small and, at least, considerably smaller than they would have been if the rider had been using position control rather than torque control.

[2] Force was measured rather than moment directly to allow the sensitivity of the measuring bar to be adjusted by changing its position relative to the handlebars.

THE UNIVERSITY OF MICHIGAN LIBRARIES

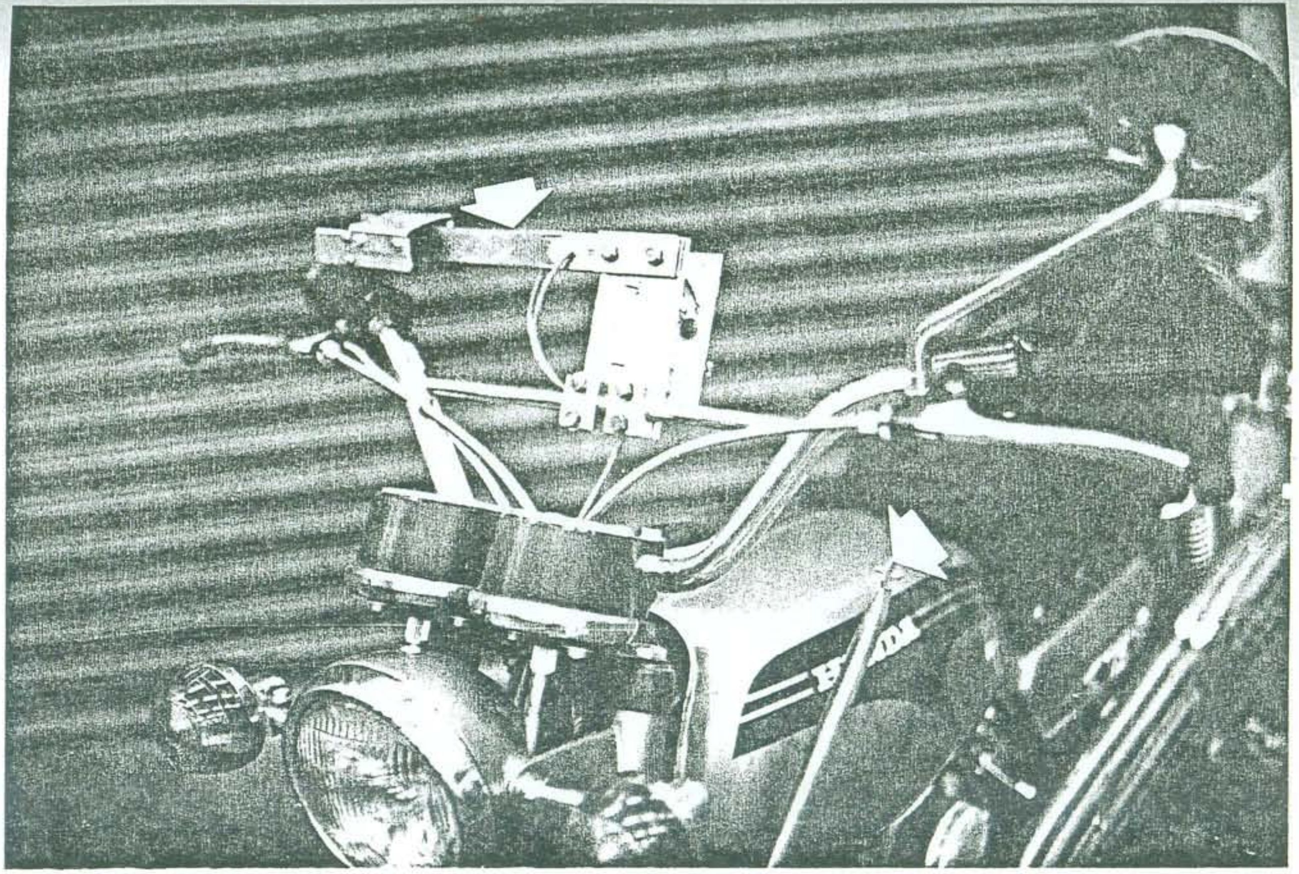

Figure 5.1 Steering torque bar and throttle control (arrows).

THE UNIVERSITY OF MICHIGAN LIBRARIES

perpendicular to the steering axis. Strain gages (with temperature compensation) were attached to the 1" wide faces of the bar, which faces were parallel to the steering axis. The handle held by the rider was attached to the bar in such a manner that the rider could not apply moments to the bar, except about the axis parallel to the wheel plane and perpendicular to the steering axis. Due to the position of the strain gages and the bar itself, the gages were insensitive to moments about this axis and to force components along the longitudinal axis of the bar or parallel to the steering axis. Hence, the desired force was directly measured, and the steering torque was the product of that force and the distance from the front wheel center plane to the free end of the torque bar. Output from the four transducers, roll and steering-angle potentiometers, rate gyro and steering-torque bar, was recorded on analog magnetic tape. Power supplies and recording equipment were carried in an accompanying automobile in the manner described in Chapter 3. Appendix E presents a schematic of the instrumentation.

After the runs were made with each test subject, the analog records were filtered with a first-order filter having a break frequency of five radians/second, converted to digital form and stored on digital magnetic tape.

In each experiment, the motorcycle and accompanying automobile operated at constant forward speed over a section of essentially straight and reasonably smooth road, about

THE UNIVERSITY OF MICHIGAN LIBRARIES

one-half mile in length. Riders A, B, and C operated the cycle at a speed of 30 mph for about 50-60 seconds per trial (test run), and about a dozen trials per rider were performed. In addition, a few trials, lasting 65 seconds, were made with Rider A at 15 mph.

The vehicle parameter data were measured with Rider A on the motorcycle. To minimize the changes in these parameters due to different-sized riders, it was desirable to find other riders approximately the same size as Rider A. It was also desired to find experienced riders. Riders B and C fit these characteristics, except that Rider B is a few inches taller than Rider A, and Rider C is about 10 pounds heavier, while several inches shorter than Rider A. Changes in $Y_c(j\omega)$ due to rider size differences were found to be negligible (Chapter 6).

5.2 METHODS OF INTERPRETING DATA

Given records of the random input, x(t), and output, y(t), for a linear system whose (unknown) transfer function is $G(j\omega)$, it is possible to estimate $G(j\omega)$ by several methods. Two of these methods have been used in this study.

One method used herein is the cross-spectral method, in which $G(j\omega)$ is estimated by

$$\hat{G}(j\omega) = \frac{\hat{S}_{xy}(\omega)}{\hat{S}_{xx}(\omega)} ,$$

THE UNIVERSITY OF MICHIGAN LIBRARIES

where $\hat{S}_{xy}(\omega)$ is the estimated cross-spectrum between x(t) and y(t), and $\hat{S}_{xx}(\omega)$ is the estimated power spectrum of x(t).

The second method is termed the impulse response method, and consists of estimating the impulse response function $g(\tau)$ (the inverse Fourier transform of $G(j\omega)$) directly from the data and finding its Fourier transform. The input x(t) and output y(t) of the system are related by the convolution integral

$$y(t) = \int_{0}^{\infty} g(\tau)\ x(t-\tau)d\tau. \tag{5.1a}$$

For data which has been digitized, that is, sampled at a time interval h, Equation (5.1a) may be approximated by

$$y(kh) \doteq h \sum_{m=1}^{M} g[(m-1)h]\ x\ [(k-m+1)h],\ k=k_o,k_o+1,\ldots K. \tag{5.1b}$$

The discrete form of $g(\tau)$ is then estimated by a standard linear regression technique. Appendix F gives a more thorough description of the cross-spectral and impulse response methods, including an outline of the computer implementation of these methods.

THE UNIVERSITY OF MICHIGAN LIBRARIES

Before the analysis techniques were applied to actual road test data, they were checked out by using them to identify known systems. Data was first generated by driving an analog computer circuit with a low frequency random noise generator and digitizing the resulting signals. Cross-spectral analysis was used to identify a few transfer functions, such as an integration and a first-order Padé approximation to a pure time delay,

$$e^{-\tau j\omega} \doteq - \frac{(j\omega-2/\tau)}{(j\omega+2/\tau)} \quad .$$

While these identifications were successful, it was found more convenient to use artificial data generated entirely digitally, since it was then easier and less costly to prepare and change the data. Also, with solely digital data, the pure time delay could be created exactly, rather than with a Padé approximation. A more complete discussion of using both analysis methods to identify known transfer functions is given in Appendix G.

Consider next the closed-loop system shown in Figure 5.2, which system is of the same form as the one used to model the man-motorcycle system (Fig. 4.1). In the system of Figure 5.2, the transfer function belonging to the rider or operator is G(jω). In most, if not all, practical test situations, the output of G(jω) (that is, x(t)) is not known; only c(t) is measured. If the disturbance, i(t), is known, x(t) is not needed to identify G(jω), which can then be estimated as

THE UNIVERSITY OF MICHIGAN LIBRARIES

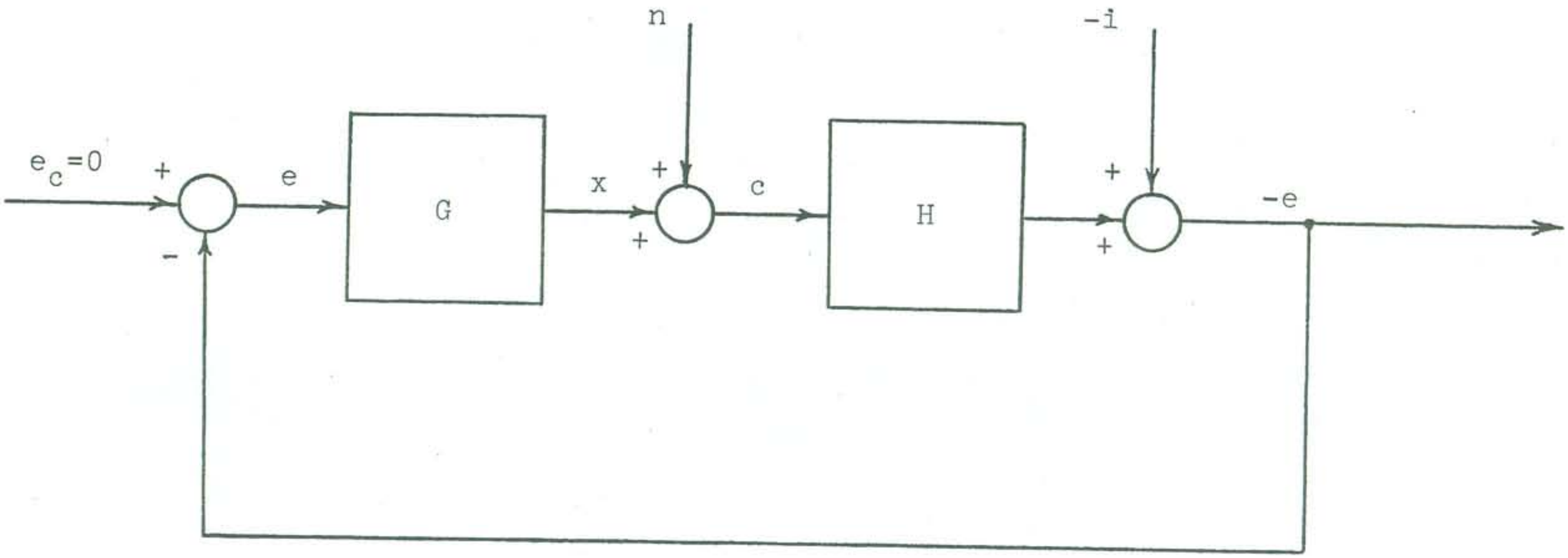

Figure 5.2 Block diagram of a typical manual control system.

THE UNIVERSITY OF MICHIGAN LIBRARIES

$$G(j\omega) = \frac{\hat{S}_{ic}(\omega)}{\hat{S}_{ie}(\omega)} ,$$

where $\hat{S}_{ic}(\omega)$ and $\hat{S}_{ie}(\omega)$ are the estimates of the cross-spectra between i(t) and c(t), and i(t) and e(t), respectively. (See, e.g., Reference [26].)

Suppose now that i(t) is not known. In this case, it is necessary to estimate $G(j\omega)$ by an open-loop method; that is,

$$\hat{G}_m(j\omega) = \frac{\hat{S}_{ec}(\omega)}{\hat{S}_{ee}(\omega)} . \qquad (5.2)$$

It may be shown [37, 38] that even if there is no error in estimating $S_{ec}(\omega)$ and $S_{ee}(\omega)$ ($\hat{S}_{ec}(\omega) = S_{ec}(\omega)$, $\hat{S}_{ee}(\omega) = S_{ee}(\omega)$), there will be, in general, an error in identifying $G(j\omega)$, and, in fact,

$$\hat{G}_m(j\omega) = G(j\omega) + \frac{S_{en}(\omega)}{S_{ee}(\omega)} .$$

The term, $\frac{S_{en}(\omega)}{S_{ee}(\omega)}$, is the error in identification (termed "bias error") and is seen to arise from correlation between e(t) and n(t). This correlation, and hence the bias error, will be reduced if i(t) is much larger than n(t). On the other hand, if n(t) is substantial relative to i(t), the bias error will be large. If n(t) is much greater than i(t),

THE UNIVERSITY OF MICHIGAN LIBRARIES

the analysis will not identify $G(j\omega)$; rather, it will identify $- 1/H(j\omega)$ [37], and a method for reducing the bias error is needed.[1] A method for accomplishing this error reduction has been developed by Wingrove and Edwards [37, 38, 39, 40], and will be referred to subsequently as the time shifting or Wingrove-Edwards method.

The time shifting method is applied as follows. First, $e(t)$ is delayed in time relative to $c(t)$ by an amount λ. Next, the transfer function having $e(t-\lambda)$ as input and $c(t)$ as output is identified by a technique which is constrained to identify only physically realizable systems, such as the impulse response method[2], the transfer function estimate being denoted $\hat{G}_m(j\omega)$. Finally, the estimate of $G(j\omega)$, denoted $\hat{G}(j\omega)$, is calculated from

$$\hat{G}(j\omega) = e^{-\lambda j\omega}\, \hat{G}_m(j\omega) \quad . \tag{5.3}$$

THE UNIVERSITY OF MICHIGAN LIBRARIES

---

[1] In an experimental situation, if only $e(t)$ and $c(t)$ are being measured, it can be determined whether $n(t) >> i(t)$ or $i(t) >> n(t)$. In the former situation, application of Equation (5.2) will yield $-1/H(j\omega)$. In the latter case, $G(j\omega)$ can be identified. If $n(t)$ and $i(t)$ are approximately the same size, a transfer function "in between" $G(j\omega)$ and $-1/H(j\omega)$ will be identified.

[2] It will be shown that cross-spectral methods, which are not constrained to identify only physically realizable systems, cannot be used with the Wingrove-Edwards method.

The range of λ is $0 \leq \lambda \leq \tau_p$, where τ_p is the time delay in $G(j\omega)$. Theoretical work was performed by Wingrove and Edwards only for this range of λ. For $\lambda > \tau_p$, the estimate in Equation (5.3) becomes less accurate, for the following reason. Let $G'(j\omega)$ be defined by

$$G'(j\omega) = e^{+\tau_p j\omega} G(j\omega).$$

The transfer function having $e(t-\lambda)$ as input and $c(t)$ as output is

$$G_\lambda(j\omega) = e^{\lambda j\omega} G(j\omega) = e^{(\lambda-\tau_p)j\omega} G'(j\omega) \tag{5.4}$$

From Equation (5.4), it is seen that if $\lambda > \tau_p$, $G_\lambda(j\omega)$ is not physically realizable. Hence, $G_\lambda(j\omega)$ cannot be accurately identified by a method which is constrained to identify a physically realizable system. The estimate of $G_\lambda(j\omega)$ is $\hat{G}_m(j\omega)$. Thus, the estimate of $G(j\omega)$ in Equation (5.3) is expected to decrease in accuracy when $\lambda > \tau_p$.

It can be shown [37] that if there exists a lag $\tau_o \leq \tau_p$ such that the autocorrelation function $r_{nn}(\tau)$ of the remnant $n(t)$ is zero for $\tau \geq \tau_o$, then the estimate for $G(j\omega)$ in Equation (5.3) will have zero bias error when $\tau_o \leq \lambda \leq \tau_p$.

THE UNIVERSITY OF MICHIGAN LIBRARIES

In a practical situation, however, $r_{nn}(\tau)$ will not in general be zero for τ greater than some τ_o, in which case it can be shown [37] that the bias error in identifying $G(j\omega)$ by Equation (5.3) is a minimum when $\lambda = \tau_p$. If $r_{nn}(\tau)$ is small for all values of $\tau > \tau_p$, the bias error will also be small. The closer $r_{nn}(\tau)$ is to a mathematical impulse function, or, equivalently, the nearer $n(t)$ is to being "white" noise, the greater will be the accuracy in identifying $G(j\omega)$.

When dealing with experimental data, the value of τ_p is known only approximately and is, in fact, one of the pieces of information desired from the data. Knowledge of τ_p is also important in the identification of $G(j\omega)$, since it is necessary to select $\lambda = \tau_p$ in order to minimize the bias error.

The value of τ_p is determined as follows [38]. For each value of λ, $G(j\omega)$ is estimated by Equation (5.3). A transfer function of the form,

$$\hat{G}''(j\omega) = e^{-\hat{\tau}_p j\omega} \hat{G}'(j\omega),$$

is fitted to a Bode plot of $\hat{G}(j\omega)$. This process is repeated with a new value of λ until the estimated time delay $\hat{\tau}_p$ is equal to λ, in which case $\hat{\tau}_p = \lambda$ is the estimated value of τ_p.

THE UNIVERSITY OF MICHIGAN LIBRARIES

With reference to Figure 5.2, the remnant is defined by

$$n(t) = c(t) - x(t)$$

or, from Equation (5.1),

$$n(t) = c(t) - \int_{o}^{\infty} g(\tau)\ e\ (t-\tau)d\tau \qquad (5.5)$$

The normalized mean squared error (NMSE) is defined by

$$\text{NMSE} = \frac{\int_{o}^{T} n^2(t)dt}{\int_{o}^{T} c^2(t)dt},\ T = \text{data record length}, \qquad (5.6)$$

and is a measure of the remnant content of the operator's output. When test data are being analyzed, the remnant and the NMSE may be estimated, after the impulse response function $g(\tau)$ has been estimated, from discrete forms of Equations (5.5) and (5.6), as discussed in Appendices F and G. A large estimated NMSE does not necessarily mean that the transfer function $G(j\omega)$ has been poorly identified; rather, it means that a large portion of the operator's output is not linearly related to his error signal. Another measure of the remnant content of the operator's output is the linear coherence, ρ^2 [40], defined by

$$\rho^2 = 1 - \text{NMSE}\big|_{\lambda=\tau_p}.$$

THE UNIVERSITY OF MICHIGAN LIBRARIES

As mentioned earlier, application of the time-shifting method requires that after delaying e(t), the procedure used to calculate $\hat{G}_m(j\omega)$ must be constrained to identify only physically realizable systems. Such a constraint is inherent in the impulse response method, but not the cross-spectral method.

As an illustrative example of the results of attempting to use the cross-spectral method in conjunction with the time-shifting method, the system shown in Figure 5.2 was analyzed with the following assumptions being made:

$$G(j\omega) = e^{-.4j\omega}$$

and

$$H(j\omega) = \frac{1}{j\omega}.$$

The data required for analysis was prepared artificially on a digital computer, as described in Appendix G. In creating the data, it was assumed that $i(t) = 0$; thus, the system was excited only by the remnant, $n(t)$, the situation in which the bias error is greatest. The auto-correlation function of $n(t)$ (shown in Appendix G) was less than .01 for $\tau > 0.4$ second. Thus, it was possible to identify $G(j\omega)$ with the time-shifting and impulse response methods combined (Fig. G.6, Appendix G). If, however, the cross-spectral method is combined with the time shifting

THE UNIVERSITY OF MICHIGAN LIBRARIES

method, it is only possible to identify $-1/H(j\omega) = -j\omega$. Figure 5.3 shows estimates $\hat{G}_m(j\omega)$ for $\lambda = 0, 0.1, 0.2, 0.3$, and 0.4 second, using cross-spectral analysis. For each λ,

$$\hat{G}_m(j\omega) = -e^{\lambda j\omega}/H(j\omega) = -j\omega\ e^{\lambda j\omega} \tag{5.7}$$

while the actual value of $G_\lambda(j\omega)$ is, from Equation (5.4),

$$G_\lambda(j\omega) = e^{(\lambda-\tau_p)j\omega} .$$

From Equations (5.3) and (5.7), the estimate of $G(j\omega)$ is

$$\hat{G}(j\omega) = -1/H(j\omega) = -j\omega ,$$

regardless of the value of λ.

The reason the cross-spectral method did not identify $G(j\omega)$ is that it is capable of identifying the non-realizable transfer function in Equation (5.7), which transfer function represents a higher degree of correlation between $e(t-\lambda)$ and $c(t)$ than does $G_\lambda(j\omega)$. The impulse response method, however, cannot identify the function in Equation (5.7), and thus is forced to identify $G_\lambda(j\omega)$, even though $G_\lambda(j\omega)$ represents a considerably weaker correlation between $e(t-\lambda)$ and $c(t)$ than does $-e^{\lambda j\omega}/H(j\omega)$.

THE UNIVERSITY OF MICHIGAN LIBRARIES

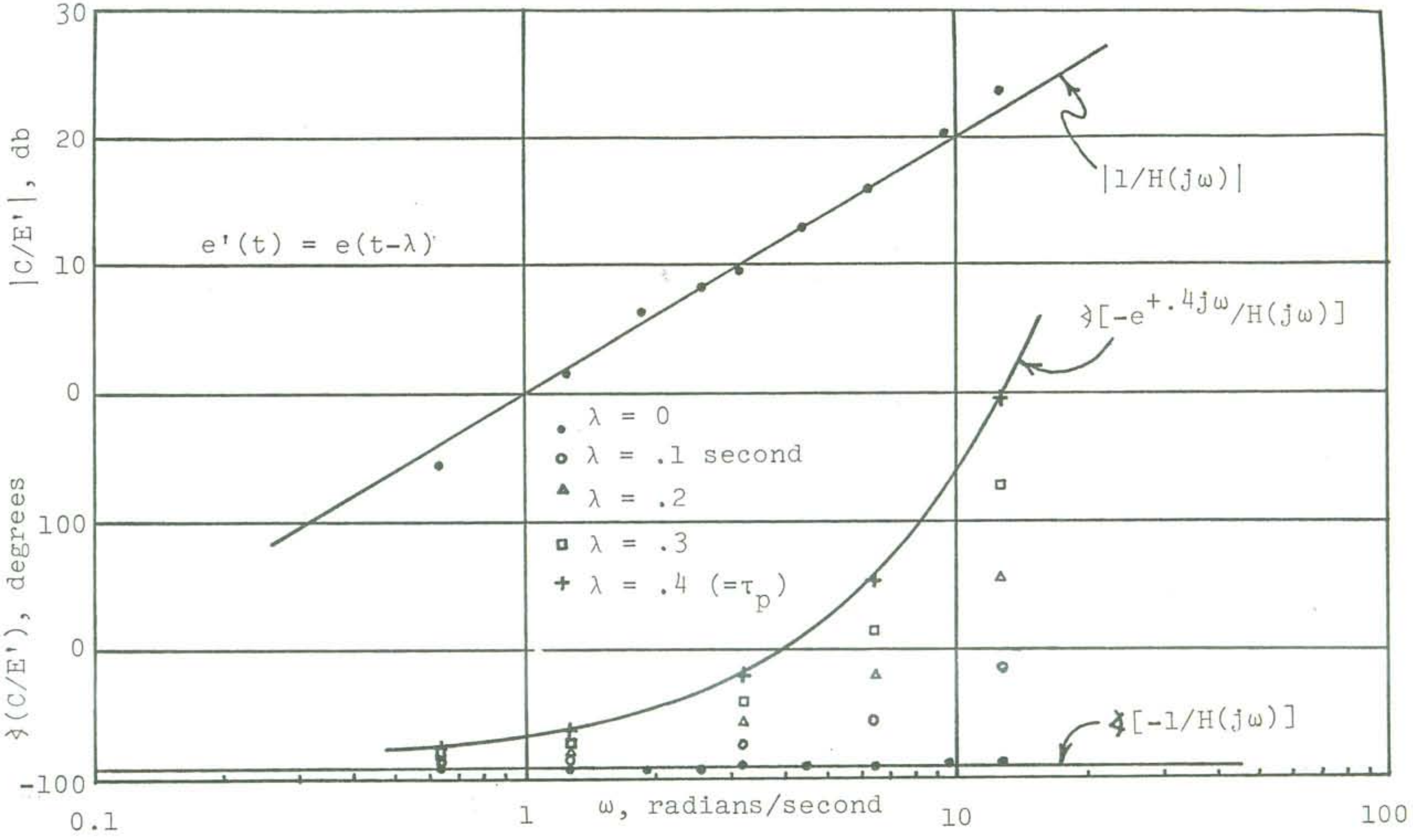

Figure 5.3 Combination of the Wingrove-Edwards and cross-spectral analysis methods.

THE UNIVERSITY OF MICHIGAN LIBRARIES

Since the impulse response and time shifting methods are not nearly as well documented in the literature as the cross-spectral method, some studies with prepared artificial data were carried out (Appendix G) to aid in interpreting Bode diagrams of $\hat{Y}_p(j\omega)$, the estimate of $Y_p(j\omega)$. Most of the rules set forth below are derived from the results of these analyses, using both artificial data and road test data.

1. Because the impulse-response function is estimated for a finite time interval, (M-1)h (M is defined in Eq. 5.1b), systems having an impulse response function which does not decay with time can be difficult to identify. This difficulty is illustrated in Appendix G for the case of an integrator, the impulse response function of which is a step function. Identification of an integrator at low frequencies, where the error is greatest, is sensitive to truncation number, M. Such a sensitivity is probably a good indicator that an unknown impulse response function is constant or growing unbounded with time.

2. When $\hat{Y}_p(j\omega)$ is heavily biased ($r_{nn}(\tau)$ is not close to zero for $\tau \geq \tau_p$), $|\hat{Y}_p(j\omega)|$ tends toward $|1/Y_c(j\omega)|$ at the upper and lower ends of the frequency range (near 1 and 10 radians/second, respectively).

3. When $Y_p(j\omega)$ is of the form, $Y_p(j\omega) = -K_p e^{-\tau_p j\omega}$, and $\hat{Y}_p(j\omega)$ is biased,

$$|\hat{Y}_p(j\omega)| < K_p ,$$

THE UNIVERSITY OF MICHIGAN LIBRARIES

and

$$\measuredangle(\hat{Y}_p(j\omega)) < -\tau_p\omega.$$

4. When $\hat{Y}_p(j\omega)$ is biased, the frequency bandwidth of the estimated remnant, $\hat{n}(t)$, decreases with increasing λ, but is always greater than the bandwidth of the actual remnant n(t).

5. A typical graph of the NMSE against λ is shown in Figure 5.4. When $\hat{Y}_p(j\omega)$ is strongly biased, however, the NMSE often increases monotonically with increasing λ and does not exhibit a local minimum at $\lambda=\tau_p$.

6. Instabilities in $\hat{Y}_p(j\omega)$, evidenced by oscillations in the Bode diagrams, indicate that $Y_p(j\omega)$ is difficult to identify, either because it is not physically realizable, its impulse response function cannot be truncated, the estimate is biased by n(t) or possibly because there is little power in the records at the frequencies at which the instabilities occur.

7. When a transfer function being identified by the impulse response method is of such a form that accurate identification is possible, the effect of the truncation number, M, is apparently similar to the effect of the number of lags, L (Appendix F), in a spectral analysis. That is, increasing M tends to increase the variance of the estimator, as evidenced by increased oscillations in the Bode diagrams. Probably, an increase in M would also improve the ability of

THE UNIVERSITY OF MICHIGAN LIBRARIES

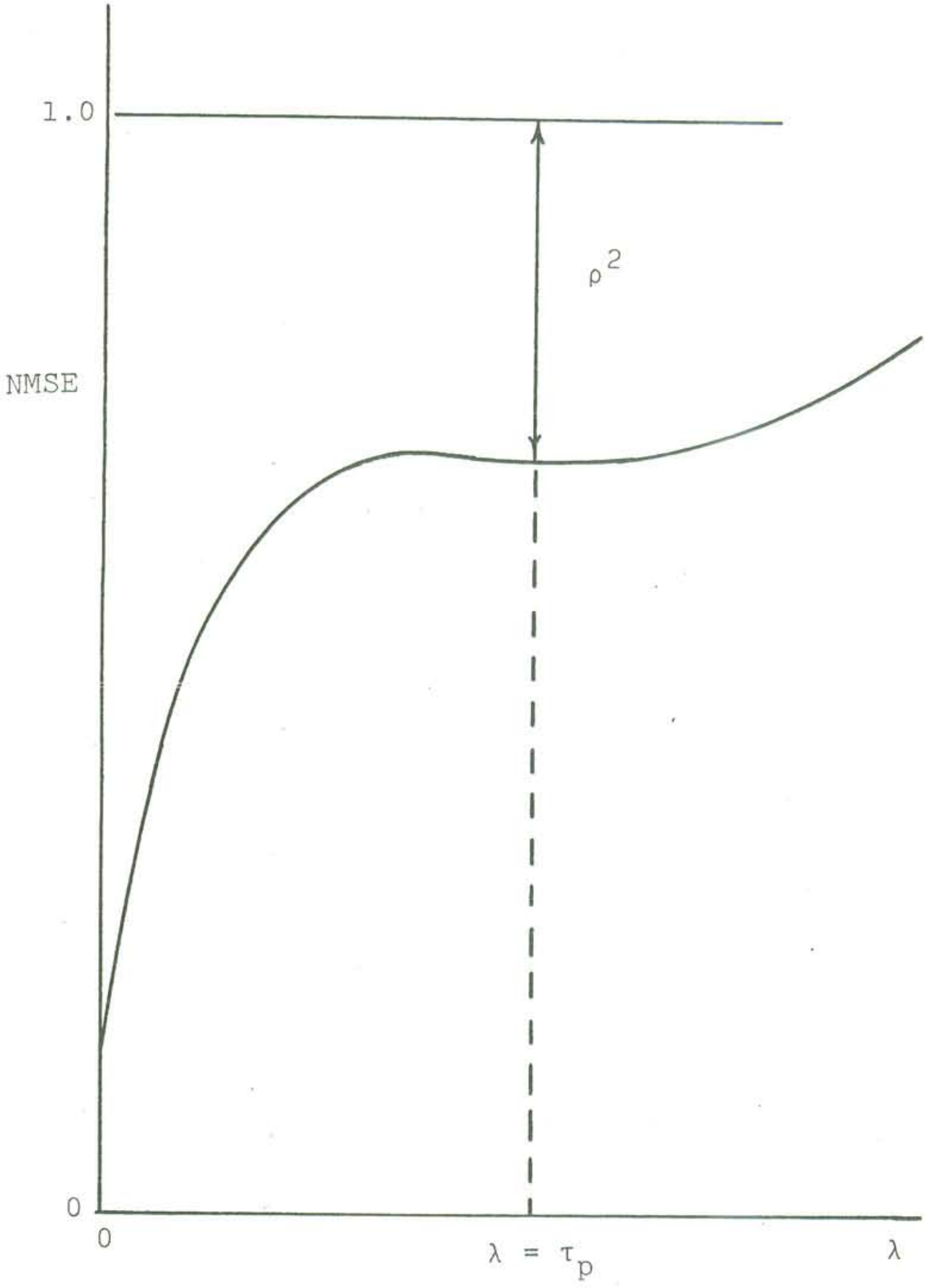

Figure 5.4 Typical variation of the NMSE with λ.

THE UNIVERSITY OF MICHIGAN LIBRARIES

the impulse response method to pick out details in the transfer function.

8. In any situation involving identification with the impulse response method [44],

$$\lim_{\omega \to 0} \frac{d|\hat{G}(j\omega)|}{d\omega} = 0 , \qquad (5.8)$$

and

$$\lim_{\omega \to 0} \sphericalangle(\hat{G}(j\omega)) = 0, \text{ or } \pm 180^{o} , \qquad (5.9)$$

where $\hat{G}(j\omega)$ is the estimate of the unknown transfer function. When roll rate is used to identify $Y_p(j\omega)$, $\hat{Y}_p(j\omega) = j\omega\hat{Y}'_p(j\omega)$, where $\hat{Y}'_p(j\omega)$ is the estimate of the transfer function the input of which is roll rate and the output is steering torque, and from Equations (5.8) and (5.9),

$$\lim_{\omega \to 0} \frac{d|\hat{Y}_p(j\omega)|}{d\omega} = \hat{Y}'_p(j0),$$

and

$$\lim_{\omega \to 0} \sphericalangle \hat{Y}_p(j\omega) = \pm 90^{o}.$$

9. The accuracy of $Y_p(j\omega)$ for frequencies at which the power of the records being processed is small is questionable. Unlike cross-spectral analysis, it is possible for the impulse response method to extrapolate accurately beyond these frequencies. However, this extrapolation is only possible if (1) the estimate of the

THE UNIVERSITY OF MICHIGAN LIBRARIES

impulse response function is accurate before Fourier transformation, and (2) the transfer function being identified does not have details which occur outside of the bandwidths of the records being analyzed (e.g., a high frequency lead or lag). In practice, it cannot be determined whether either of these two conditions are met. Hence, estimates of $Y_p(j\omega)$ outside the bandwidths of the records may be incorrect.

THE UNIVERSITY OF MICHIGAN LIBRARIES

6. RESULTS OF THE ROLL-STABILIZATION EXPERIMENTS

6.1 DESCRIPTION OF THE DATA

A total of fifteen trials were performed with Rider A (the author). These trials took place on two days about four months apart. In the first session, experiments began with a 30 mph test, followed by a 15 mph test, followed by a 30 mph test, etc., until eleven (total) were recorded, with three trials at each speed being suitable for analysis. The remaining nine were selected from a group of ten (all at 30 mph) performed on the second day.

On a single day, a total of thirteen trials were carried out with Rider B, with twelve of these being suitable for analysis. Similarly, on a single day, twelve trials were recorded with Rider C, eleven trials being suitable for analysis. Both riders were instructed to ride at a constant 30 mph while minimizing body movements with the aid of the brace attached to the motorcycle. A few practice runs were made before recording was begun.

Table 6.1 displays the rms levels and approximate maxima of the time histories that were recorded.

While the greatest emphasis has been placed upon 30 mph tests, the three trials at 15 mph provide some interesting comparisons with the 30 mph data. The most predominant

THE UNIVERSITY OF MICHIGAN LIBRARIES

TABLE 6.1

DATA DESCRIPTION, ROLL-STABILIZATION EXPERIMENTS

	Day of session	1	1	2	3	4
	Speed, mph	15	30	30	30	30
	Number of trials	3	3	9	12	11
	Rider	A	A	A	B	C
Average rms levels	Steering angle, deg.	.535	.151	.114	.067	.111
	Steering torque, lb-in	5.70	7.29	6.28	3.68	6.41
	Roll angle, deg.	1.16	1.55	1.30	1.10 (1st 5 tests)	1.29 (7 tests)
	Roll rate, deg/sec	2.70	3.03	2.66	1.28	2.22
Approximate maximum values	Steering angle, deg.	3	0.5	0.5	0.5	0.5
	Steering torque, lb-in	30	30	30	25	30
	Roll angle, deg.	4	4	4	4	5
	Roll rate, deg/sec	15	15	15	8	15

THE UNIVERSITY OF MICHIGAN LIBRARIES

difference is the dependence of the level of steering displacement upon motorcycle speed. From Table 6.1 it is seen that the steering displacements were about 3.5-5 times as great at 15 mph than at 30 mph. (For the 30 mph tests, the actual steering displacements may have been slightly higher than measured, since the steering potentiometer mechanism, which was not designed to measure such small angles, did possess some hysteresis arising from shaft clearance and the free play of the floating wiper within the potentiometer.)

While the steering displacements were found to be much smaller at 30 mph than at 15 mph, steering-torque levels were nearly speed independent, at least for the speeds tested, the torques being only about 20% lower for the lower speeds (Table 6.1). Additional experiments in which the motorcycle was steered by means of a torque wrench attached to the handlebars indicated that, during normal "casual" riding, maximum torque levels also did not vary significantly for speeds higher than 30 mph (approximately 45 mph being the highest speed investigated). For a given steering deflection, however, considerably more torque is required at moderate and high speeds than at low speeds.

The very low steering displacements which have been observed to occur during normal operation at moderate and high speeds are consistent with statements made in References [14] and [16], namely, that torque control of the motorcycle

THE UNIVERSITY OF MICHIGAN LIBRARIES

roll angle is preferable to steering-angle control. These statements were based upon the severe instability of the cycle yielded by a fixed-control analysis, the poor performance of a theoretical closed-loop man-machine system with steering-angle control, and the small steering angles involved. At low speeds, although the steering angles are larger and the equations of motion are of lesser validity, torque control is probably still preferable. However, the basis for asserting the superiority of torque control is considerably more subjective at low speeds than at moderate and high speeds.

Reference to Table 6.1 shows that roll angles and roll rate levels were also nearly speed independent for the speeds tested. Surprisingly, the roll angles are seen to be a little smaller at a low speed than at a moderate speed.

Spectral analysis of the time histories of steering torque and roll rate yielded a dominant frequency, as characterized by a peak in the power spectrum. This dominant frequency ranged from about 1.5 to 5.0 radians/second. The power spectrum of roll angle tended to be smoother, due to the filtering effect of Y_c. Typical power spectra are shown in Figure 6.1. Since the data were filtered prior to analysis with a first-order filter, having a break frequency of 5 radians/second, the estimated spectra include the effects of this filter.

THE UNIVERSITY OF MICHIGAN LIBRARIES

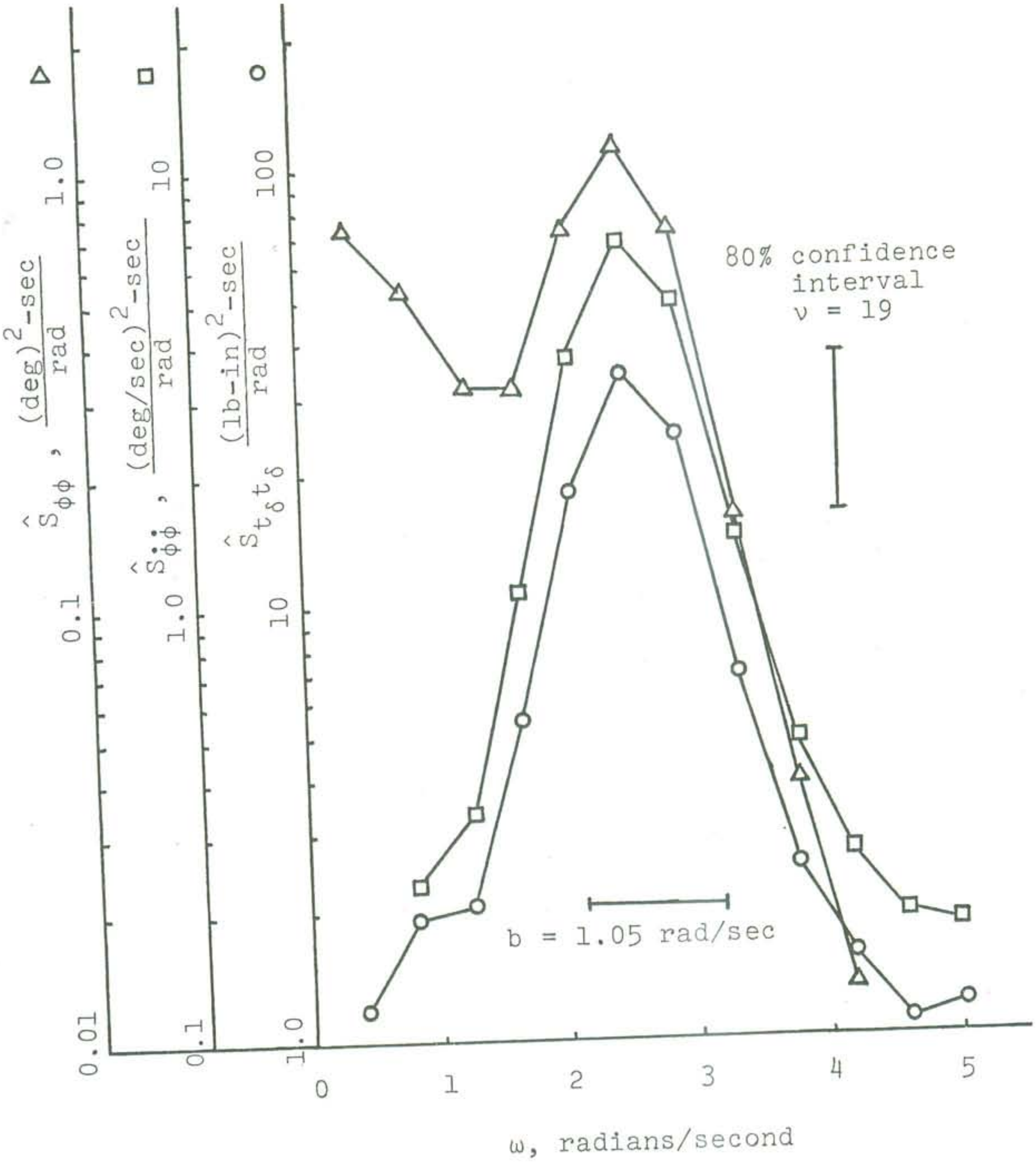

Figure 6.1a Estimated power spectra, 30 mph; Rider A, Day 1 (b = spectral window bandwidth; ν = degrees of freedom; see Appendix F).

THE UNIVERSITY OF MICHIGAN LIBRARIES

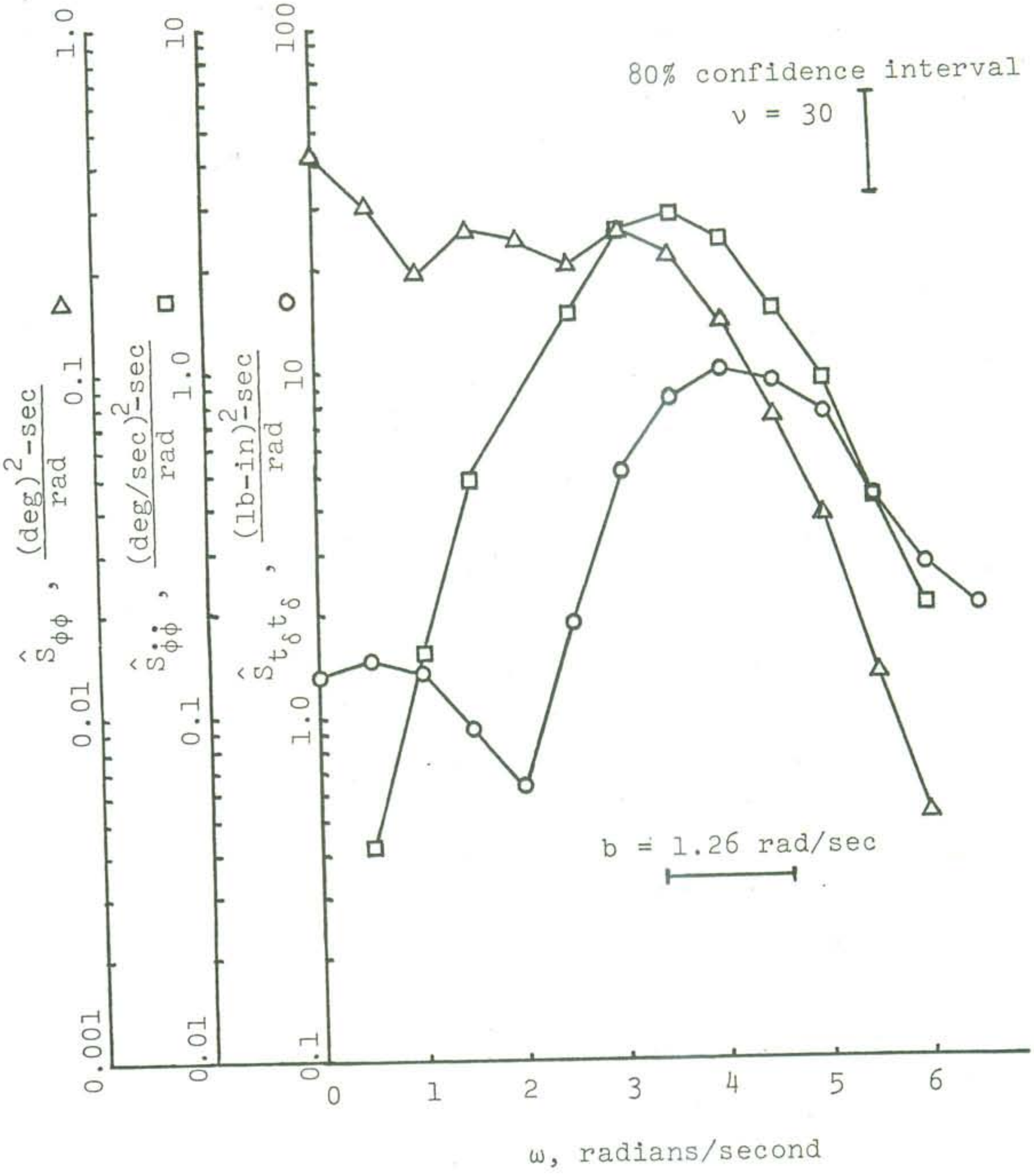

Figure 6.1b Estimated power spectra, 15 mph.

THE UNIVERSITY OF MICHIGAN LIBRARIES

6.2 IDENTIFICATION OF THE CONTROLLED ELEMENT

Figure 6.2 shows a typical result obtained by applying cross-spectral analysis to records of roll angle and steering torque. It can be seen that the result of this cross-spectral analysis is close to the transfer function of the controlled element, as calculated from the motorcycle equations of motion. (See Chapter 4.)

Recall that the motorcycle equations of motion have been shown in Chapter 3 to be a realistic descriptor of vehicle motions at low frequency. Thus, the fact that $Y_c(j\omega)$ can be fairly accurately identified by a cross-spectral analysis indicates that the rider's remnant, n(t), is a much larger source of excitation to the man-motorcycle system than is the road/wind disturbance, i(t). When the remnant is the primary disturbance to the system, identification of the controlled element is straightforward, while identification of the rider's transfer function requires the time-shifting method of Wingrove and Edwards.

Since the remnant is the primary disturbance, it is fortunate that the motorcycle represents an unstable system, since this instability forces the rider into continuous control activity. Were the motorcycle stable, the rider would be able to operate the vehicle for periods of time with no control activity, a situation that would make the identification of either $Y_c(j\omega)$ or $Y_p(j\omega)$ to be much more difficult than is actually the case.

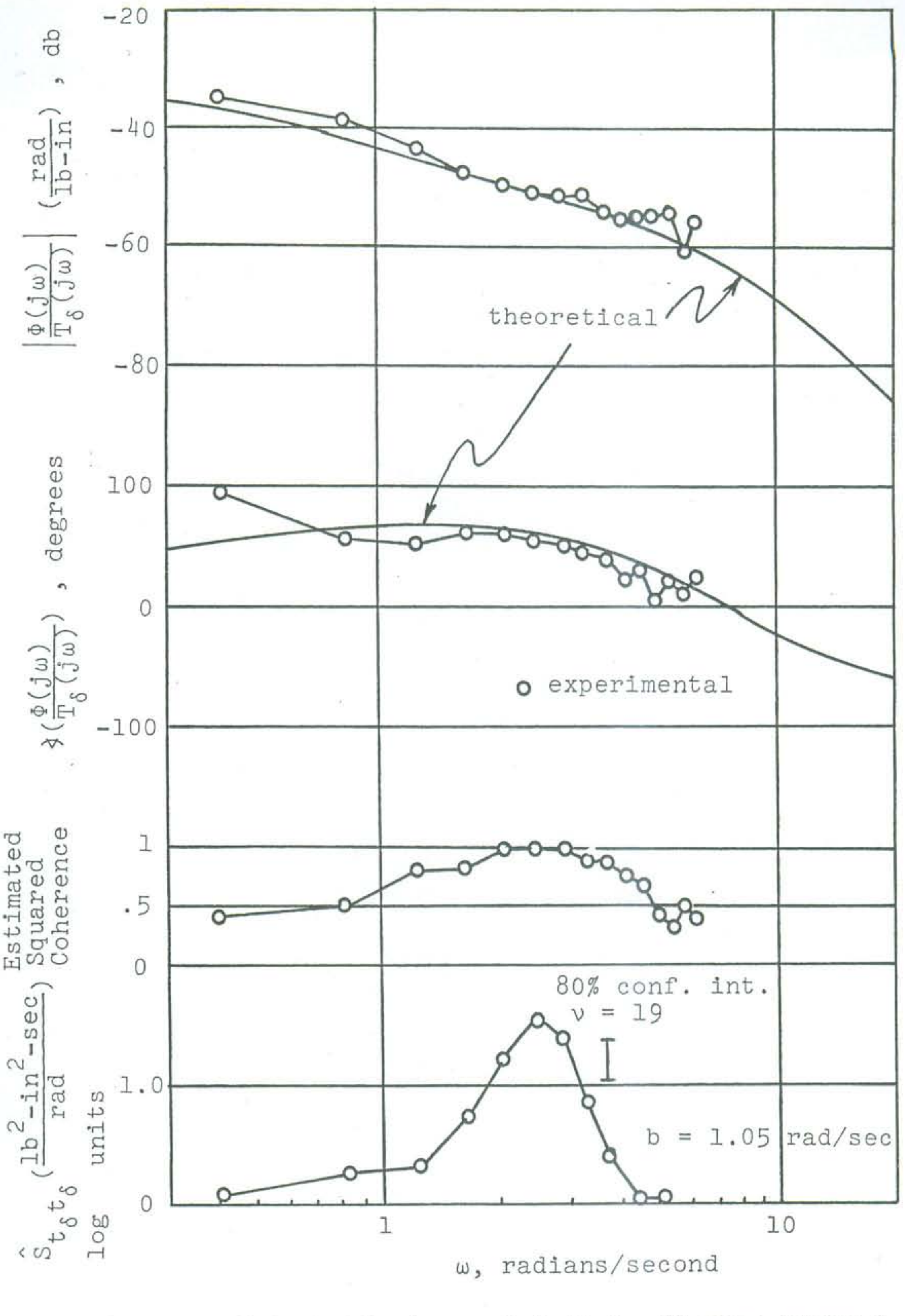

Figure 6.2 Estimation of $Y_c(j\omega)$, 30 mph; Rider A, Day 1. Calculated from records of roll angle and steering torque.

THE UNIVERSITY OF MICHIGAN LIBRARIES

The ability to identify the theoretical $Y_c(j\omega)$ from experimental data can also be interpreted as additional support for the motorcycle equations of motion, at least with respect to roll response to steering torque inputs, over a limited frequency range. (If the disturbance i(t) had been large relative to n(t), and the equations of motion had been a poor representation of the vehicle behavior, it is unlikely that any bias introduced into the identification of $Y_c(j\omega)$ by the presence of i(t) would have caused the identification to agree with the incorrect theoretical $Y_c(j\omega)$.) Note that, as a result of this cross-spectral analysis, nothing can be concluded about the wobble mode, whose representation was found to be unrealistic in the transient response experiments (Chapter 3), since the frequency of the wobble mode is far above the range included in the spectral analysis.

In Figure 6.2, the graph of estimated squared coherence indicates the degree to which the two time histories are related by a linear transfer function (a value of 1 indicating a perfect linear relationship) and shows that the best identification of $Y_c(j\omega)$ occurs in a fairly narrow range of frequency. This restriction in identification is due to the fact that most of the power in the time histories of ϕ and t_δ is also concentrated in a narrow frequency band.

THE UNIVERSITY OF MICHIGAN LIBRARIES

Good identification for frequencies at which there is little power of t_δ, ϕ, or both cannot be obtained with cross-spectral methods. It was found that higher levels of coherence and, usually, a wider "good identification" frequency range could be obtained by performing a cross-spectral analysis with roll rate and steering torque, since the power spectra of these quantities were much more closely aligned than were roll angle and steering torque (see Fig. 6.1).

A particularly accurate identification of $Y_c(j\omega)$ using $\dot{\phi}$ and t_δ in a cross-spectral analysis is shown in Figure 6.3. (For comparison, Figures 6.1a, 6.2, and 6.3 were prepared from the same experiment.) A correction factor of $1/j\omega$ has been applied after the cross-spectral analysis, since $Y_c(j\omega)$ relates steering torque to roll angle. Note the higher estimated squared coherence.

Figure 6.4 shows the identification of the controlled element for a vehicle speed of 15 mph. For frequencies of high estimated squared coherence, the agreement with the theoretical controlled element is very good. It is seen that for frequencies about 1-2 rad/sec, the agreement tends to worsen, although less certainty can be attached to the estimates at these frequencies, due to the low coherence. However, assuming that the remnant is again a much greater source of disturbance than wind and road irregularities, the estimates

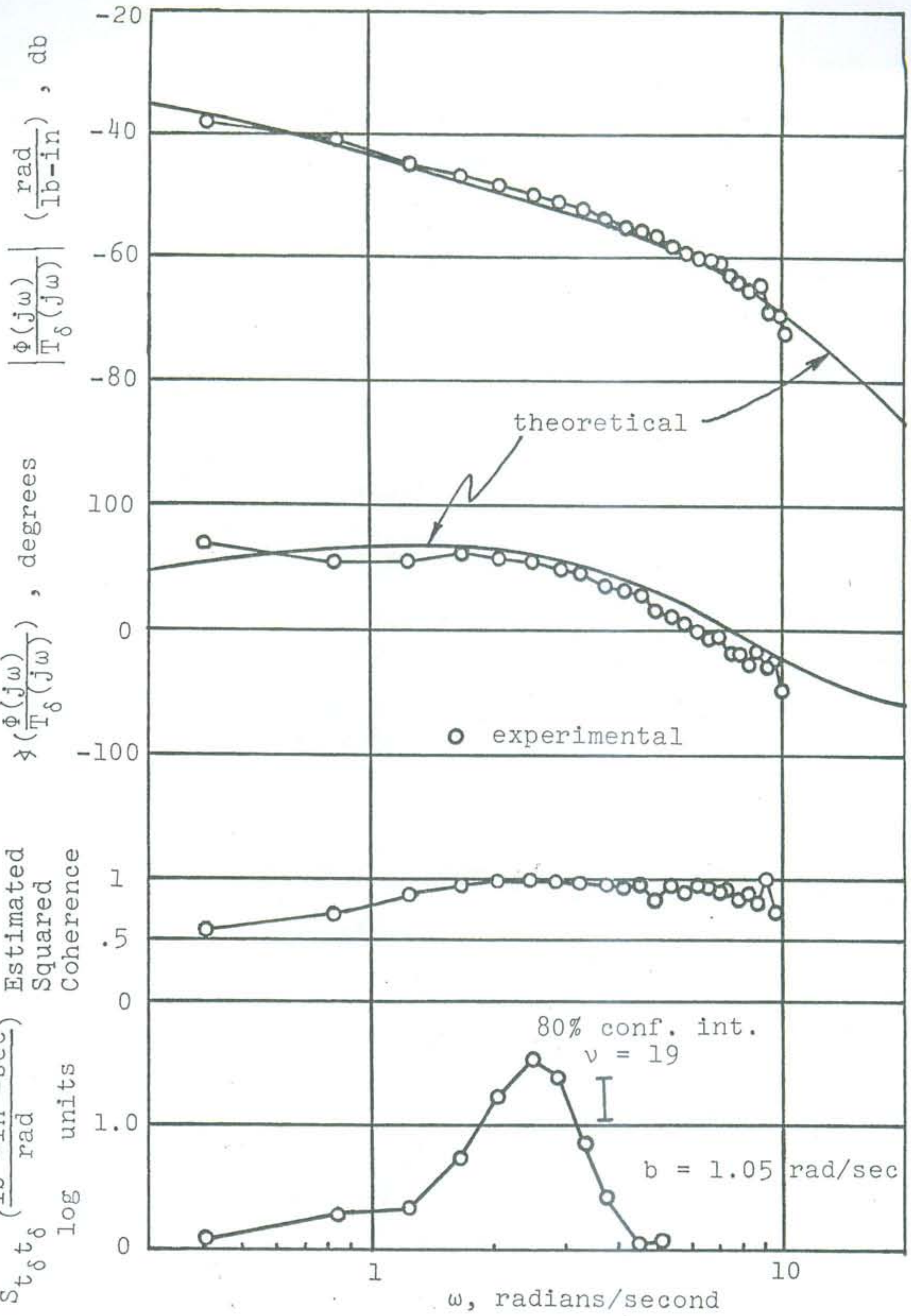

Figure 6.3 Estimation of $Y_c(j\omega)$, 30 mph; Rider A, Day 1. Calculated from records of roll rate and steering torque.

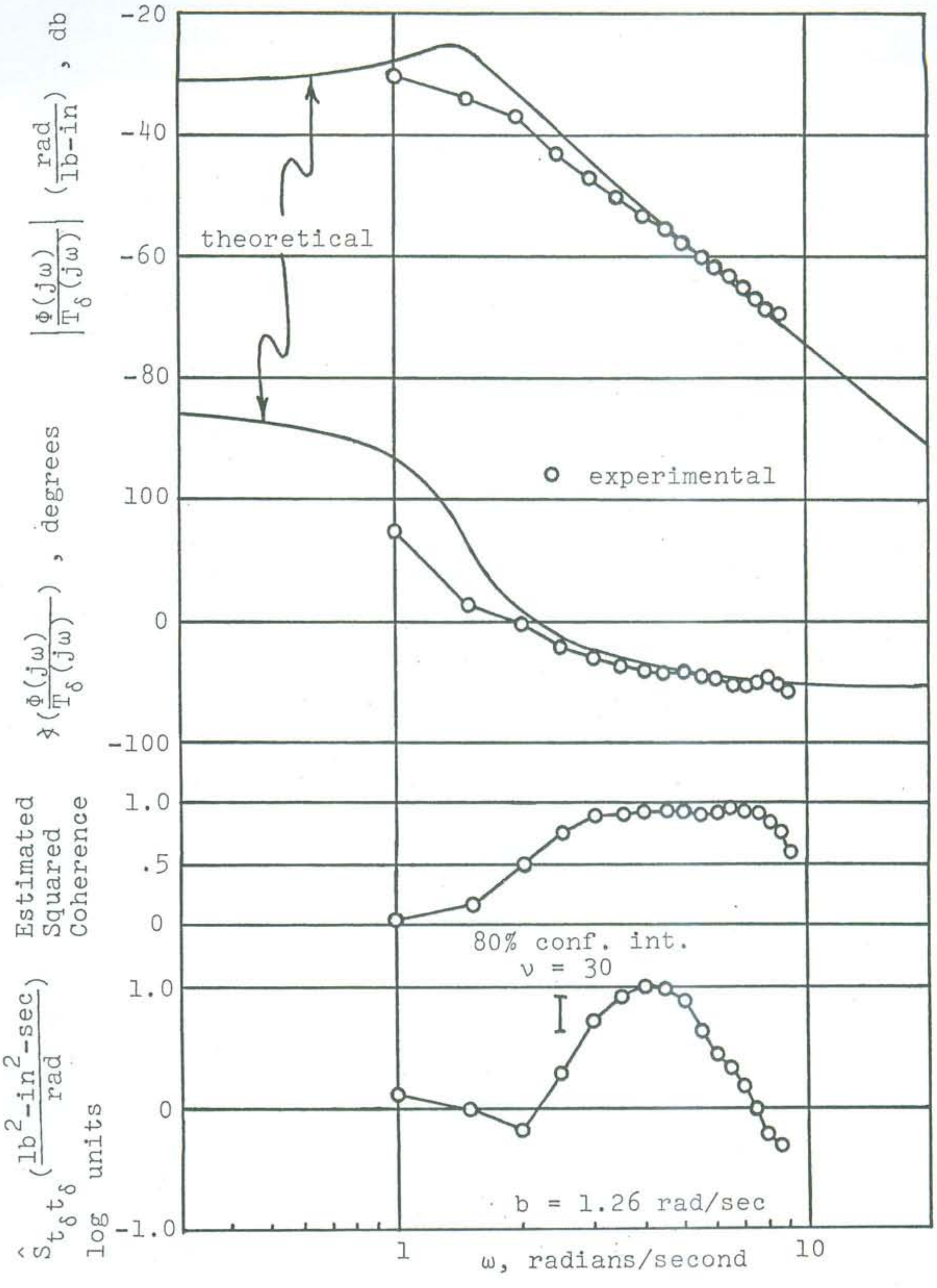

Figure 6.4 Estimation of $Y_c(j\omega)$, 15 mph. Calculated from records of roll rate and steering torque.

seem to indicate that the experimental controlled element amplitude is considerably less "peaked" than the theory predicts. That is, the weave mode of the real vehicle at low speed is apparently more heavily damped than is the theoretical weave mode, an observation which is consistent with the results of the uncontrolled motorcycle study (Chapter 3). It may also be observed from Figure 6.4 that the slope of the experimental $|Y_c(j\omega)|$, for $\omega > 2$ radians/second, is steeper than -40 db/decade, but not as steep as the theoretical -60 db/decade.

In spite of the size differences between the three riders, the controlled element, as identified experimentally, did not display a rider sensitivity. Figures 6.5 and 6.6 show identifications of the controlled element (30 mph), using cross-spectral analysis and records of Riders B and C, respectively, operating the test vehicle.

6.3 IDENTIFICATION OF THE RIDER'S TRANSFER FUNCTION

To identify the rider's transfer function using the time shifting method, one might work with either roll angle or roll rate. Before the data was taken, it was expected that the use of roll rate would be superior, because a small amount of friction present in the roll angle measuring apparatus caused the bar to bend very slightly when it was moved by the third wheel, creating a hysteresis effect.

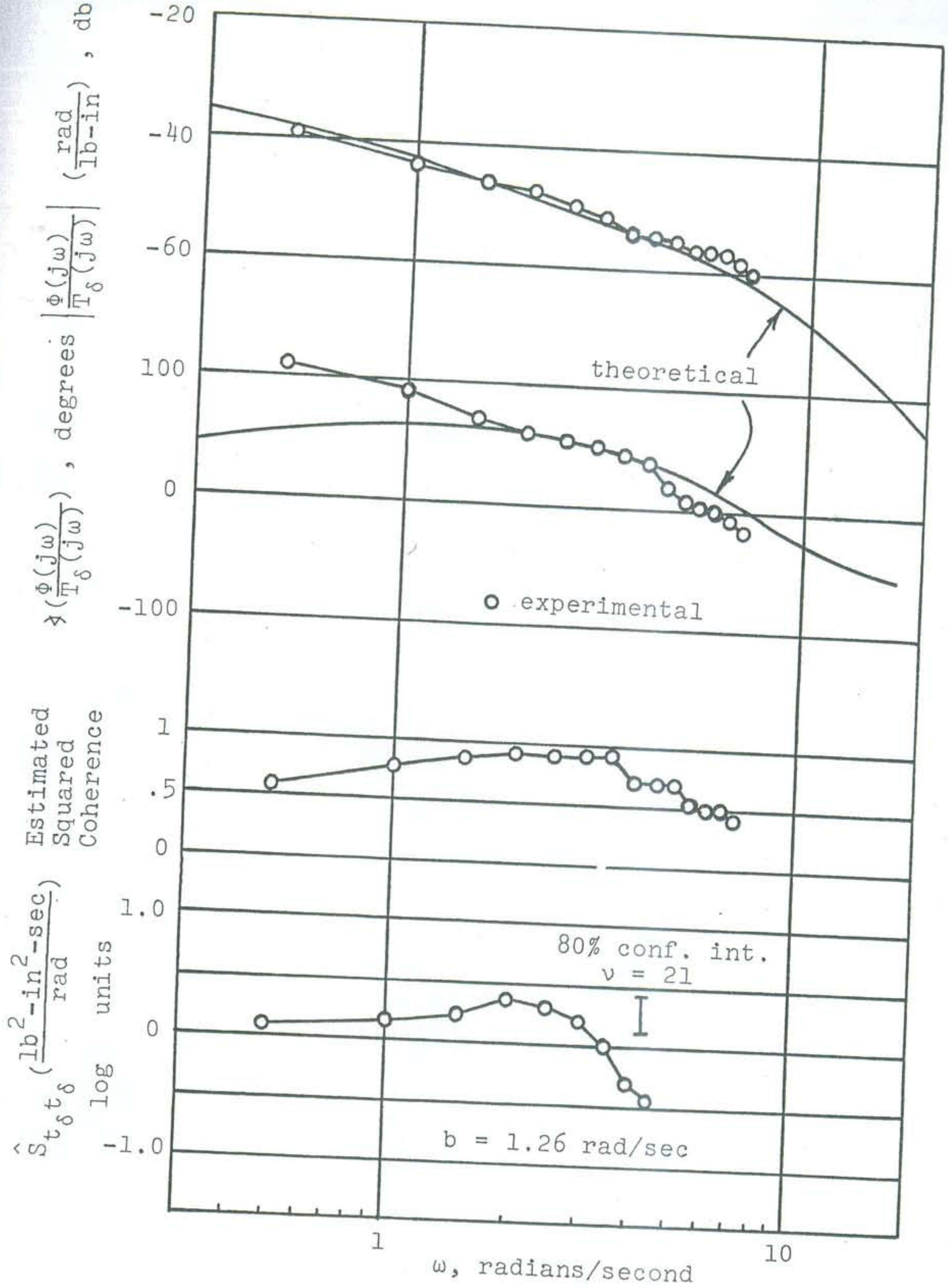

Figure 6.5 Estimation of $Y_c(j\omega)$, 30 mph; Rider B. Calculated from records of roll rate and steering torque.

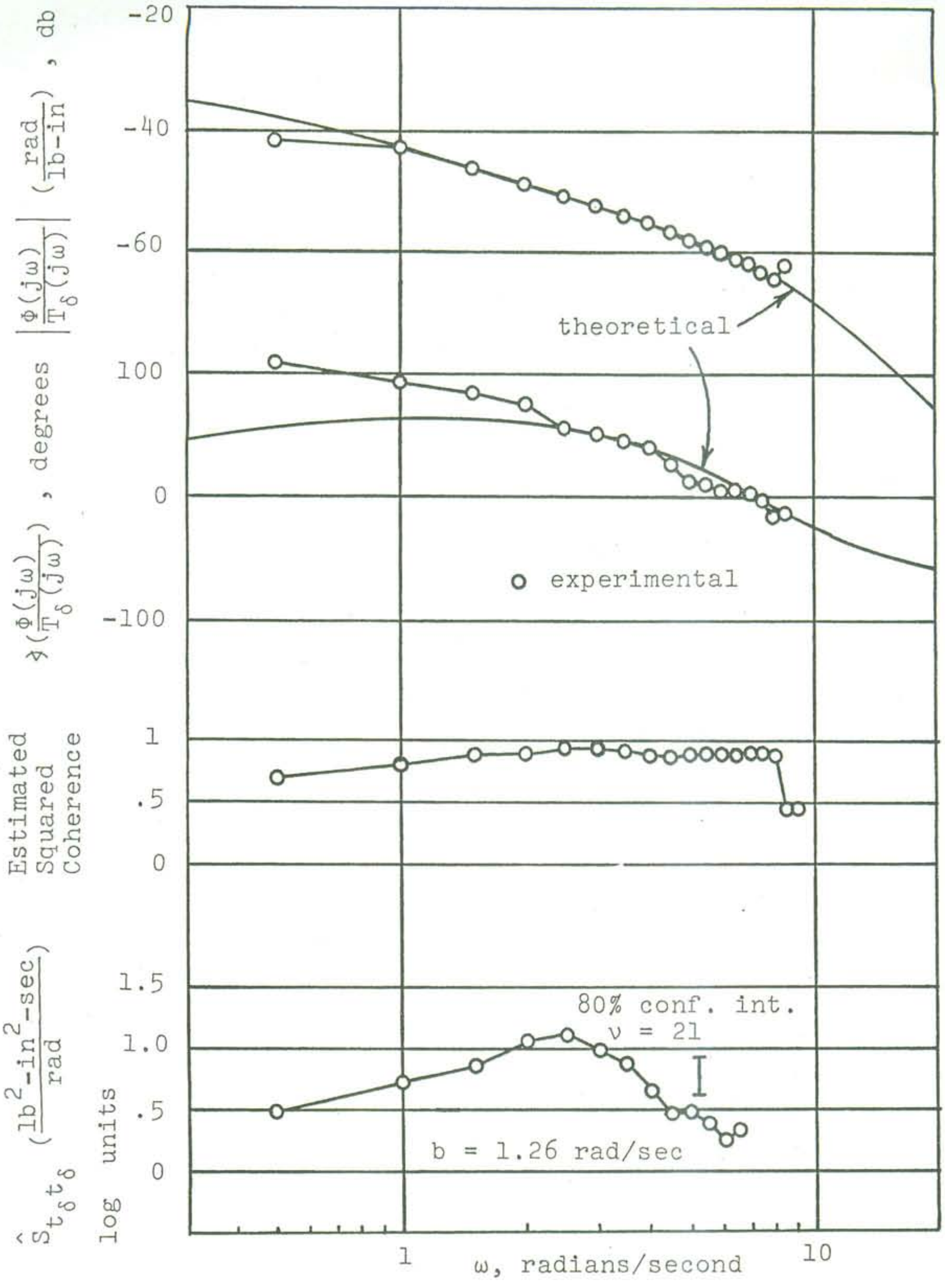

Figure 6.6 Estimation of $Y_c(j\omega)$, 30 mph; Rider C. Calculated from records of roll rate and steering torque.

However, subsequent analysis of the data has indicated that this bending is of negligible concern[1], and, for a number of reasons, it became apparent that the use of roll angle, when it was available[2], was superior to roll rate.

The main difficulty in identifying $Y_p(j\omega)$ from records of roll rate and steering torque is that, in most cases, $Y_p(j\omega)$ was found to have the form

$$Y_p(j\omega) = -K_p e^{-\tau_p j\omega} . \qquad (6.1)$$

Thus, the transfer function relating $\dot{\phi}$ to t_δ is

$$Y'_p(j\omega) = -K_p e^{-\tau_p j\omega}/j\omega \quad ,$$

which, as shown in Appendix G, cannot be accurately identified by the impulse response method.

---

[1] The results using roll angle agreed with results using roll rate. Possibly engine vibrations reduced the friction and consequently the bending; or, possibly the hysteresis, about 5% of the maximum roll angle, is negligible in these analyses.

[2] Unfortunately, the roll angle measuring device, being in a hostile environment near the road, was not as reliable as the other transducers. No roll angle data are available for the last half of the tests with Rider "B" or for four tests with Rider "C".

Furthermore, it was found that the transfer function $1/Y_c(j\omega)$ is difficult to identify with the impulse response method, while the transfer function $1/(j\omega Y_c(j\omega))$ can be identified with that method. As a result, with $\lambda=0$ and roll angle records being used in the identification, the impulse response method, which cannot identify $1/Y_c(j\omega)$, approximately identifies $-Y_p(j\omega)$. If $\lambda=0$ and roll rate records are employed, $1/Y_c(j\omega)$ is fairly accurately identified, after a correction factor of $j\omega$ is applied. When $\lambda = \tau_p$, the accuracy of both identifications of $-Y_p(j\omega)$ is, of course, improved, but in the practical case of a non-"white" remnant, the bias errors are probably better removed when roll angle is used, since the bias errors in using roll angle have already been removed to a large extent when $\lambda=0$.

In estimating $Y_p(j\omega)$, the experimental steering torque spectrum was found to be a very valuable tool, if used in conjunction with the experimental Bode diagrams of $-\hat{Y}_p(j\omega)$ resulting from the application of the time shifting and impulse response methods. In many cases, the Bode diagrams were only of sufficient accuracy to indicate the form of the transfer function, plus approximate values of the parameters of interest, such as K_p and τ_p. A more refined estimate of these parameters could then be obtained by a trial and error procedure: assuming a rider model, a theoretical steering torque spectrum could be calculated. The parameters of the rider model then could be adjusted until the shape of the theoretical spectrum matched that of the experimental spectrum.

The theoretical steering torque spectrum was found as follows. Given the man-motorcycle system of Figure 4.1, with $i(t) = 0$, simple closed-loop relationships [49] yield the following expression:

$$T_\delta(j\omega) = \left(\frac{1}{1 + Y_p(j\omega)Y_c(j\omega)}\right) N(j\omega) \ .$$

Hence [49], the steering torque spectrum, $S_{t_\delta t_\delta}(\omega)$, is related to the remnant spectrum, $S_{nn}(\omega)$ by the expression,

$$S_{t_\delta t_\delta}(\omega) = \left|\frac{1}{1 + Y_p(j\omega)Y_c(j\omega)}\right|^2 S_{nn}(\omega) \qquad (6.2)$$

Furthermore, the experimental records were filtered with a 5 radians/second first-order filter. Thus, the theoretical steering torque spectrum of Equation (6.2) was modified as follows:

$$[S_{t_\delta t_\delta}(\omega)]_{filt} = \left|\frac{1}{1 + Y_p(j\omega)Y_c(j\omega)}\right|^2 \left(\frac{25}{25 + \omega^2}\right) S_{nn}(\omega), \tag{6.3}$$

where $[S_{t_\delta t_\delta}(\omega)]_{filt}$ is the theoretical steering torque spectrum of the filtered steering torque record. To evaluate Equation (6.3), it was assumed that $S_{nn}(\omega)$ = constant (a "white" remnant), an assumption supported by the data (Section 6.6). The actual value of $S_{nn}(\omega)$ was not of concern since only the shape of $\log[S_{t_\delta t_\delta}(\omega)]_{filt}$ was matched to experimental spectra. For the values of ω involved, the theoretical and experimental controlled element were in close agreement for both 15 and 30 mph. Hence, for convenience, the theoretical $Y_c(j\omega)$ was used to evaluate Equation (6.3).

Estimated transfer functions are presented below for Riders A, B, and C.

6.4 RIDER A

Rider A was tested under three conditions: a speed of 15 mph, and a speed of 30 mph on two different days. For each condition, a different form of the transfer function, $Y_p(j\omega)$, was determined, although two of the three conditions included only three test runs each and thus are not as significant.

Figure 6.7 shows the Bode diagrams and steering torque spectra for two of the three 30-mph trials performed on Day 1; the results of the third trial are more similar to the results presented in Figure 6.7b than Figure 6.7a. The Bode diagrams indicate that a rider transfer function of the form

$$Y_p(j\omega) = - K_p \, e^{-\tau_p j\omega} \qquad (6.4)$$

is appropriate. Average values of $\hat{K}_p$ and $\hat{\tau}_p$ for these three tests were calculated, with the aid of the t_δ spectra, and were found to be 277 lb-in/radian and 0.30 second, respectively. Based on the theoretical computation of $Y_c(j\omega)$, the phase margin of the resulting man-motorcycle system was calculated for each $\hat{Y}_p(j\omega)$. The mean value of these three phase margins was found to be 28.3^o.

Figure 6.7 illustrates many of the observations made in Sections 5.2 and 6.3 about the interpretation of biased estimates of $Y_p(j\omega)$. Notice that $|-\hat{Y}_p(j\omega)|$ usually tends toward $|1/Y_c(j\omega)|$ at high and low frequencies, particularly when $\dot{\phi}$ has been employed in the analysis. Further, the Bode diagrams tend to indicate a lower K_p and higher τ_p than those values chosen with consideration given to the t_δ spectra. (This latter observation is considerably more evident in Figure 6.7a than Figure 6.7b.) Finally, the advantages of analyzing roll angle rather than roll rate are readily apparent. Both the level of instability in $\hat{Y}_p(j\omega)$ and the behavior of the estimates at low frequencies are much

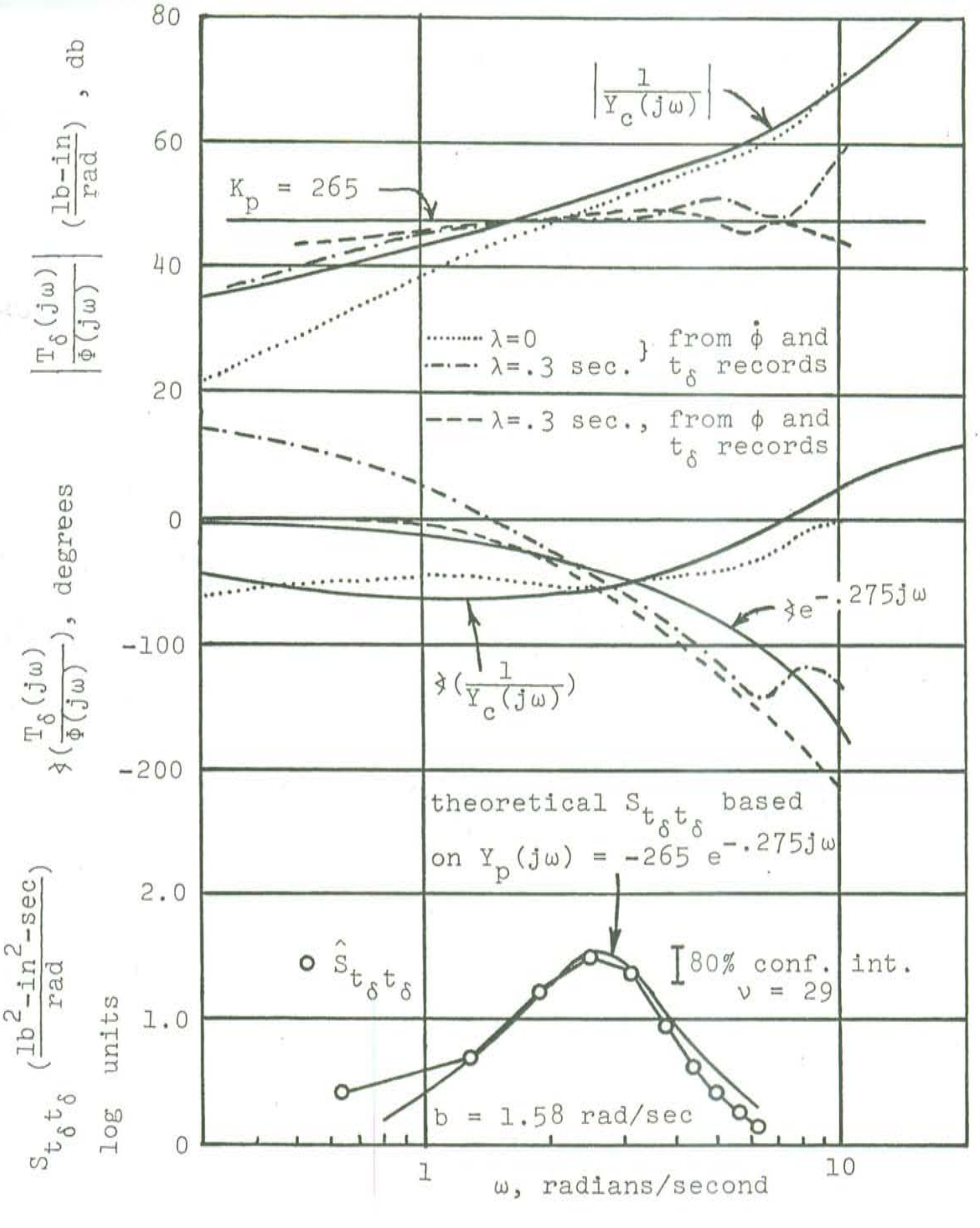

Figure 6.7a Estimation of $Y_p(j\omega)$, 30 mph; Rider A, Day 1.

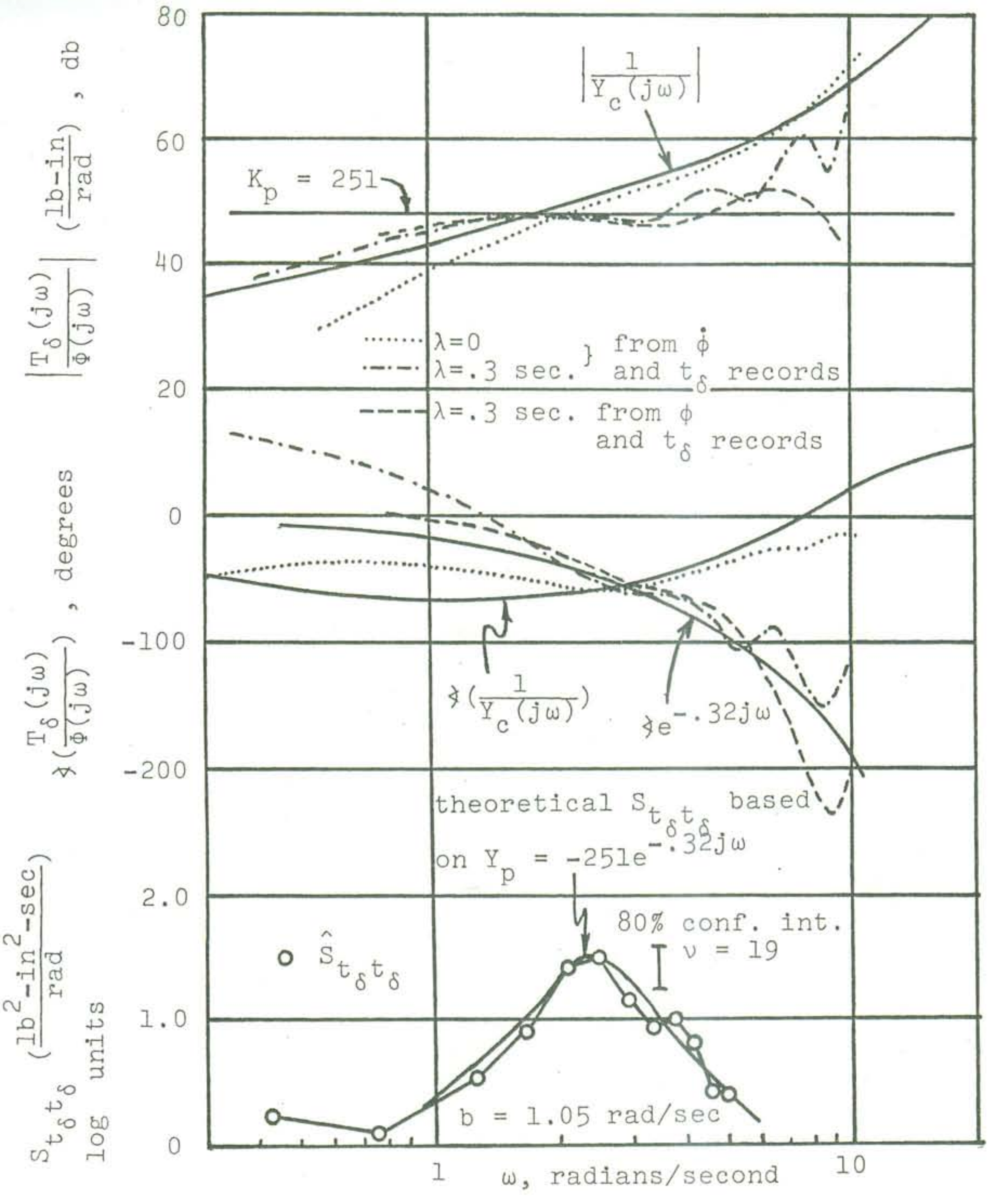

Figure 6.7b Estimation of $Y_p(j\omega)$, 30 mph; Rider A, Day 1.

improved when roll angle is employed. The transfer function estimates when ϕ is used and $\lambda=0$ are not shown but were found to be closer to the rider transfer function than $1/Y_c(j\omega)$. With $\dot{\phi}$, however, the estimates for $\lambda=0$ are seen to be close to $1/Y_c(j\omega)$.

As seen from Figure 6.7, the dominant frequencies in the t_δ power spectra were about 2.5 radians/second. When Rider A was tested on the second day, the dominant frequencies were considerably higher, ranging from about three to nearly five radians/second. If a transfer function of the form of Equation (6.4) is assumed to represent the rider, nearly all of the test data are "explained" by the assumed model, when K_p = 200-320 lb-in/radian and τ_p = 0.14-0.21 second. However, one trial, in which the dominant frequency in the steering torque spectrum was 4.8 radians/second, could not be fitted with a transfer function consisting of a constant gain and time delay, since the value of τ_p that would be required is unrealistically small, about 0.1 second. Also, difficulty was experienced in matching the t_δ spectrum for this test. In this case, it was found necessary to include a lead factor in the rider's transfer function, which then had the form,

$$Y_p(j\omega) = - K_p e^{-\tau_p j\omega} (T_\ell j\omega + 1). \qquad (6.5)$$

The strong indication of lead found in one test suggests that the behavior of Rider A during all trials on the second day might be described by the transfer function of Equation (6.5). However, it was found that nearly equally good fits to most of the Bode diagrams of $\hat{Y}_p(j\omega)$ and the t_δ spectra could be obtained with either the transfer function of Equation (6.4) or Equation (6.5). That is, the data did not strongly indicate one form or the other in many cases.

Thus, for a given trial, after a value of K_p had been selected, it was possible to choose an infinite number of pairs of T_ℓ and τ_p that would give a good fit to the Bode plots of $\hat{Y}_p(j\omega)$ and the t_δ spectra. However, the experiments conducted with other riders and on the first day with with Rider A indicated an average value of τ_p that was consistently close to 0.3 second. Manual control research indicates that the human operator's time delay is less variable between different trials and different subjects than are quantities like K_p and T_ℓ. Thus, it is likely that the value of τ_p for the trials with Rider A on the second day should also be close to 0.3 second. In order that $\hat{Y}_p(j\omega)$ for each trial involving Rider A on the second test day could be represented by analytical expressions, the value of τ_p was arbitrarily fixed at 0.30 second, and K_p and T_ℓ were adjusted to fit the data.

Figure 6.8 shows two examples of $\hat{Y}_p(j\omega)$ Bode diagrams and t_δ spectra. (The first example is the trial in which the data could only be interpreted with a rider transfer function analysis, at least for the frequency range in which the values of the power spectra of the time histories being analyzed are sufficiently large. As would be expected from the results of the uncontrolled motorcycle experiments, agreement between $\hat{Y}_c(j\omega)$, as estimated from cross-spectral analyses of experimental data, and $Y_c(j\omega)$, as calculated from the motorcycle equations of motion, is better at 30 mph than at 15 mph.

2. The time shifting method [37] can be used to identify $Y_p(j\omega)$, the transfer function of the rider in the roll-stabilization task. There were varying degrees of bias present in $\hat{Y}_p(j\omega)$, and the steering torque power spectra obtained in the experiments were helpful in interpreting Bode diagrams of $\hat{Y}_p(j\omega)$.

3. At 30 mph, the rider transfer function, $Y_p(j\omega)$, was found to be a constant gain and time delay, with the optional inclusion of lead equalization having a break frequency in neighborhood of 5-10 radians/sec. Time delays were about 0.3 second for all the tests, and gains were about -150 to -350 lb-in/radian.

4. Only three test runs were performed at 15 mph, but the results indicated that a combination of rate control and lead equalization (break frequency, 5-10 radians/second) was required on the part of the rider. Here the time delays were about 0.25-0.35 second, and the gains were about -60 to -90 lb-in/radian.

5. The experimental results agree with the crossover model, which has been used to study theoretically the man-motorcycle system [16]. Varying amounts of lead and/or rate control in $Y_p(j\omega)$ are needed to establish or extend a $|Y_p(j\omega)Y_c(j\omega)|$ slope of -20 db/decade near the crossover frequency (ω_c). At 30 mph, lead is optional, since the weave mode damped natural frequency is much greater than ω_c, but as speed decreases, the damped natural frequency of the weave mode also decreases, requiring lead and rate control.

6. Much of the rider's steering torque output was remnant. The power spectrum of n(t) was found to have about the same shape as that of "white" noise passed through the same filter that was applied to the original analog records. Hence, n(t) appears to be "white", at least relative to the analog data filter used (break frequency: 5 radians/second).

7. System phase margins of about 30-50° and gain margins of about 4-11 db were implied by the estimated rider transfer functions. At this level of stability, power spectra of steering torque and roll rate exhibited a pronounced peak at a dominant frequency. The value of this frequency varied from about 1.5 to 5.0 radians/second (including the effects of the filter applied to the data).

8. Body lean control was not studied here. Although Weir [16] has determined theoretically that body lean is more suitable for path following control than roll stabilization, riding the motorcycle with the upper body braced has indicated that body control is by no means necessary in normal maneuvers at speeds greater than about 15 mph. Hence, body control is optional and its use is probably determined by the "style" of the individual rider.

It would, however, be interesting to conduct roll-stabilization experiments in which body lean is the only means of control available to the rider.

REFERENCES

1. Whipple, F. J. W., "The Stability of the Motion of a Bicycle", Quarterly Journal of Pure and Applied Math., Vol. 30, No. 120, 1899, p. 312-348.

2. Pearsall, R. H., "The Stability of the Bicycle", Proc. Inst. Automobile Eng., Vol. XVII, 1922, p. 395.

3. Manning, J. R., "The Dynamical Stability of Bicycles", Department of Scientific and Industrial Research, Road Research Laboratory, Note No. RN/1605/JRM, July, 1951.

4. Timoshenko and Young, Advanced Dynamics, McGraw-Hill, New York, 1948, p. 239.

5. Döhring, E., "Stability of Single-Track Vehicles", Forschung, Vol. 21, No. 2, 1955, p. 50-62 (translated by J. Lotsof, March, 1957).

6. Döhring, E., "Die Stabilitāt von Einspurfahrzeugen", Automob. techn. z., Bd. 56, 1954, s. 68-72.

7. Collins, Robert Neil, "A Mathematical Analysis of the Stability of Two-Wheeled Vehicles", Ph.D. Thesis, University of Wisconsin, 1963.

8. Singh, D. V., and Goel, V. K., "Stability of Rajdoot Scooter", Paper #710273, SAE Automotive Engineering Congress, January, 1971.

9. Singh, Digvijai V., "Advanced Concepts of the Stability of Two-Wheeled Vehicles--Application of Mathematical Analysis to Actual Vehicles", Ph.D. Thesis, University of Wisconsin, 1964.

10. Fu, Hiroyasu, "Fundamental Characteristics of Single-Track Vehicles in Steady Turning", Bulletin of JSME, Vol. 9, No. 34, 1965, p. 284-293.

11. Kondo, M., "Dynamics of Single-Track Vehicles", Foundation Bicycle Tech. Research, Japan, 1962.

12. Kondo, M., Nagaoka, A., and Yoshimura, F., "Theoretical Study on the Running Stability of the Two-Wheelers", Transactions of the SAE Japan, Vol. 17, No. 1, 1963, p. 8.

13. Rice, Roy S. and Roland, R. Douglas Jr., "An Evaluation of the Performance and Handling Qualities of Bicycles", Cornell Aeronautical Laboratory, Technical Report No. VJ-2888-K, April, 1970.

14. Sharp, R. S., "The Stability and Control of Motorcycles", Journal Mechanical Engineering Science, Vol. 13, No. 5, 1971.

15. Pacejka, H. B., "Analysis of the Shimmy Phenomenon", Proc. Institution of Mech. Engrs., Vol. 180 (Pt. 2A), 1965-66, p. 251.

16. Weir, David H., "Motorcycle Handling Dynamics and Rider Control and the Effect of Design Configuration on Response and Performance", Ph.D. thesis, University of California (L. A.), 1972.

17. Kondo, M., et al., "Experimental Study on the Stability and Control of Single-Track Vehicles", Journal of the JSME, Vol. 58, No. 442, 1955, p. 827-833.

18. Kageyama, K., Fu, H., and Kosa, F., "Experimental Study on the Standing Stability of the Motorcycle", Bulletin of JSME, Vol. 5, No. 17, 1962, p. 202-209.

19. Wilson-Jones, R. A., "Steering and Stability of Single-Track Vehicles", Proceedings of the Inst. of Mechanical Engineers, Automobile Division, London, 1951-52.

20. Muhlfeld, A., "Die Lenkung des Kraftrades", Automob. techn. z., Vol. 53, No. 10, 1951, p. 249-252.

21. Bower, George S., "Steering and Stability of Single-Track Vehicles", The Automobile Engineer, Vol. V, 1915, p. 280-283.

22. Jones, David E. H., "The Stability of the Bicycle", Physics Today, April, 1970, p. 34-40.

23. Döhring, E., "Steering Wobble in Single-Track Vehicles", Automob. techn. z., Vol. 58, No. 10, 1957, p. 282-286 (MIRA Translation No. 62167).

24. Sakai, Hideo, "Cornering Properties of Motorcycle Tires", Journal SAE of Japan, Vol. 21, No. 11, 1967, p. 1115-1121.

25. Ellis, J. R. and Hayhoe, G. F., "The Steering Geometry of a Single-Track Vehicle", Second International Conference on Vehicle Mechanics, University of Paris, September 6-9, 1971.

26. McRuer, Duane T., and Krendel, Ezra S., "Dynamic Response of Human Operators", Wright Air Development Center, Report 56-524, October, 1957.

27. Graham, D. and McRuer, D. T., Analysis of Nonlinear Control Systems, J. Wiley and Sons, 1961.

28. McRuer, D. T., Graham, D., Krendel, E., and Reisener, W., Jr., "Human Pilot Dynamics in Compensatory Systems", AFFDL-TR-65-15, July, 1965.

29. McRuer, D. T., and Weir, D. H., "Theory of Manual Vehicular Control", Ergonomics, Vol. 12, No. 4, 1969, p. 599-633.

30. Van Lunteren, A., and Stassen, H. G., Annual Report of the Man-Machine Systems Group, Laboratory for Measurement and Control, Dept. of Mech. Eng., Delft University of Technology, 1970.

31. Van Lunteren, A., and Stassen, H. G., "On the Influence of Drugs on the Behavior of a Bicycle Rider", 6th Annual Conference on Manual Control, Wright-Patterson AFB, Ohio, 1970.

32. Van Lunteren, A., and Stassen, H. G., "Investigations on the Characteristics of a Human Operator Stabilizing a Bicycle Model", Intern. Symp. on Ergonomics in Machine Design, Prague, 1967.

33. Van Lunteren, A., and Stassen, H. G., "On-Line Parameter Estimation of the Human Transfer in a Man-Bicycle System", IVth IFAC Congress, Warsaw, 1969, paper 70.3.

34. Van Lunteren, A., and Stassen, H. G., "On the Variance of the Bicycle Rider's Behavior", 6th Annual Conference on Manual Control, Wright Patterson AFB, Ohio, 1970.

35. Hattori, Kawase, Haga, Ogishima, "Response of the Human Body to Disturbance and its Simulation in Riding a Bicycle, No. 2", Bicycle Research Laboratory, Japan, 1969.

36. Li, Y.T., Meiry, J. L., and Roeseler, W. G., "An Active Roll Mode Suspension System for Ground Vehicles", Journal of Basic Engineering, June, 1968, p. 167-174.

37. Wingrove, Rodney C., and Edwards, Frederick G., "Measurement of Pilot Describing Functions From Flight Test Data With an Example From Gemini X",

4th Annual NASA-University Conference on Manual Control, The University of Michigan, March, 1968.

38. Wingrove, Rodney C., and Edwards, Frederick G., "A Technique for Identifying Pilot Describing Functions From Routine Flight-Test Records", NASA TN D-5127, May, 1969.

39. Wingrove, Rodney C., "Comparison of Methods for Identifying Pilot Describing Functions From Closed-Loop Operating Records", NASA TN D-6235, March, 1971.

40. Edwards, Frederick G., "Determination of Pilot and Vehicle Describing Functions From the Gemini-10 Mission", NASA TN D-6803, May, 1972.

41. Clark, Samuel K., Editor, Mechanics of Pneumatic Tires, U. S. National Bureau of Standards Monograph 122, U. S. Government Printing Office, 1971.

42. Clark, S. K., Dodge, R. N., and Nybakken, G. H., "An Evaluation of String Theory for the Prediction of Dynamic Tire Properties Using Scale Model Aircraft Tires", NASA CR-2058, June, 1972.

43. Segel, Leonard, "Force and Moment Response of Pneumatic Tires to Lateral Motion Inputs", Transactions ASME, J. Engr. for Industry, Av-2, 1965.

44. Taylor, L. W., Jr., "A Comparison of Human Response Modeling in the Time and Frequency Domains", Third Annual NASA-University Conference on Manual Control, University of Southern California, L. A., March 1-3, 1967.

45. Jex, H. R., McDonnell, J. D., and Phatak, A. V., "A 'Critical' Tracking Task for Manual Control Research", IEEE Trans. Human Factors in Electronics, Vol. HFE-7, Dec., 1966, p. 138-144.

46. Jex, H. R., McDonnell, J. D., and Phatak, A. V., "A 'Critical' Tracking Task for Man-Machine Research Related to the Operator's Effective Time Delay: Part I. Theory and Experiments With a First-Order Divergent Controlled Element", NASA CR-616, November, 1966.

47. Jex, H. R., "Two Applications of A Critical-Instability Task on Secondary Work Load Research", Communications, IEEE Trans. Human Factors in Electronics, Dec., 1967, p. 279-282.

48. Raven, F. H., Automatic Control Engineering, McGraw-Hill Book Company, New York, 1968.

49. Davenport, W. B., and Root, W. L., An Introduction to the Theory of Random Signals and Noise, McGraw-Hill Book Company, New York, 1958.

50. Lipson, C., and Sheth, N. J., Statistical Design and Analysis of Engineering Experiments (to be published by McGraw-Hill Book Company, New York).

51. "Vehicle Dynamics Terminology", SAE J670a, Handbook Supplement, December, 1965.

52. Shigley, J. E., Simulation of Mechanical Systems, McGraw-Hill Book Co., New York, 1967.

53. Dixon, W. J., Editor, Biomedical Computer Programs, University of California Press, Berkeley and Los Angeles, 1967.

54. Bendat, J. S., and Piersol, A. G., Measurement and Analysis of Random Data, John Wiley and Sons, Inc., New York, 1966.

55. Jenkins, G. M., and Watts, D. G., Spectral Analysis and its Applications, Holden Day, Inc., San Franscisco, 1969.

56. Blackman, R. B., and Tukey, J. W., The Measurement of Power Spectra from the Point of View of Communications Engineering, Dover Publications, Inc., New York, 1958.

57. Sage, A. P., and Melsa, J. L., System Identification, Academic Press, Inc., New York, 1971.

58. Savant, C. J., Basic Feedback Control System Design, McGraw-Hill Book Company, New York, 1958.

APPENDIX A

MOTORCYCLE EQUATIONS OF MOTION

A.1 DEFINITION OF SYMBOLS

TABLE A.1

DEFINITION OF SYMBOLS

SYMBOL	DEFINITION
C_s	Coefficient of steering viscous damper.
$C_{\alpha f}$, $C_{\alpha r}$	Front and rear tire cornering stiffnesses, respectively.
C_δ	Magnitude of steering coulomb friction.
$C_{\gamma f}$, $C_{\gamma r}$	Front and rear tire inclination stiffnesses, respectively.
C_{Mxf}, C_{Mxr}	Front and rear tire overturning moment slip angle coefficients, respectively.
C_{Mzf}, C_{Mzr}	Front and rear tire aligning torque slip angle coefficients, respectively.
$C_{\gamma xf}$, $C_{\gamma xr}$	Front and rear tire overturning moment inclination angle coefficients, respectively.
$C_{\gamma zf}$, $C_{\gamma zr}$	Front and rear tire aligning torque inclination angle coefficients, respectively.
e, h_o, h_s, H, ℓ_f, ℓ_r, ℓ_s, ℓ''_s, L	Linear dimensions (See Figure A.1.).
F_{yf}, F_{yr}	Front and rear tire lateral forces, respectively.
g	Acceleration due to gravity.
I_{xt}, I_{zt}, I_{xzt}	Moments and product of inertia of entire vehicle, including rider, with respect to XYZ axes (Figure A.1).
$\overline{I}_{sx}$, $\overline{I}_{sz}$, $\overline{I}_{sxz}$	Moments and product of inertia of front system with respect to $X_fY_fZ_f$ axes.

TABLE A.1 (Continued)

SYMBOL	DEFINITION
$\overline{I}_{fy}$, $\overline{I}_{ry}$, $\overline{I}_{ey}$	Polar moments of inertia of front wheel, rear wheel, and engine, respectively.
M	Mass of rear frame, including wheel, engine, and rider.
m_s	Mass of front frame, including wheel.
M_{xf}, M_{xr}	Front and rear tire overturning moments, respectively.
M_{zf}, M_{zr}	Front and rear tire self-aligning moments, respectively.
R_f, R_r	Front and rear wheel rolling radii, respectively.
t	Time.
$t_\delta(t)$	External moment about the steering axis applied to the front frame assembly.
$t_\phi(t)$	External roll moment applied to the rear frame assembly.
W_f	Front tire vertical load.
u, v, w	Velocity of point O (Fig. A.1) with respect to XYZ axes.
XYZ	Right-handed axis system fixed in vehicle rear frame with origin at point O. See Figure A.1.
$X_fY_fZ_f$	Right-handed axis system fixed in vehicle front frame with origin at front frame center of mass. See Figure A.1.
α	Constant such that $\overline{I}_{ey}\alpha u$ = angular momentum of engine about its spin axis.
α_f, α_r	Front and rear tire slip angles, respectively [51].
δ	Steer angle of vehicle.
γ_f, γ_r	Front and rear wheel inclination angles, respectively [51].

TABLE A.1 (Continued)

SYMBOL	DEFINITION
ϕ	Roll angle of vehicle [51].
ψ	Yaw (heading) angle of vehicle [51].
$\dot{\psi}=r$	Yaw rate of vehicle.
σ	Steering head angle (Fig. A.1).
σ_f, σ_r	Front and rear tire relaxation lengths, respectively.

The following symbols allow the equations of motion to be written in a more concise form:

$m_t = m_s + M$ (total mass)

$$\left.\begin{aligned} L_t &= (m_s \ell_s - ML)/m_t \\ H_t &= (m_s h_s + MH)/m_t \end{aligned}\right\}$$ x and z coordinates of total vehicle center of gravity (XYZ axes)

$\beta = \cos\sigma$

$\gamma = \sin\sigma$

$K_f = 1/R_f$

$K_r = 1/R_r$

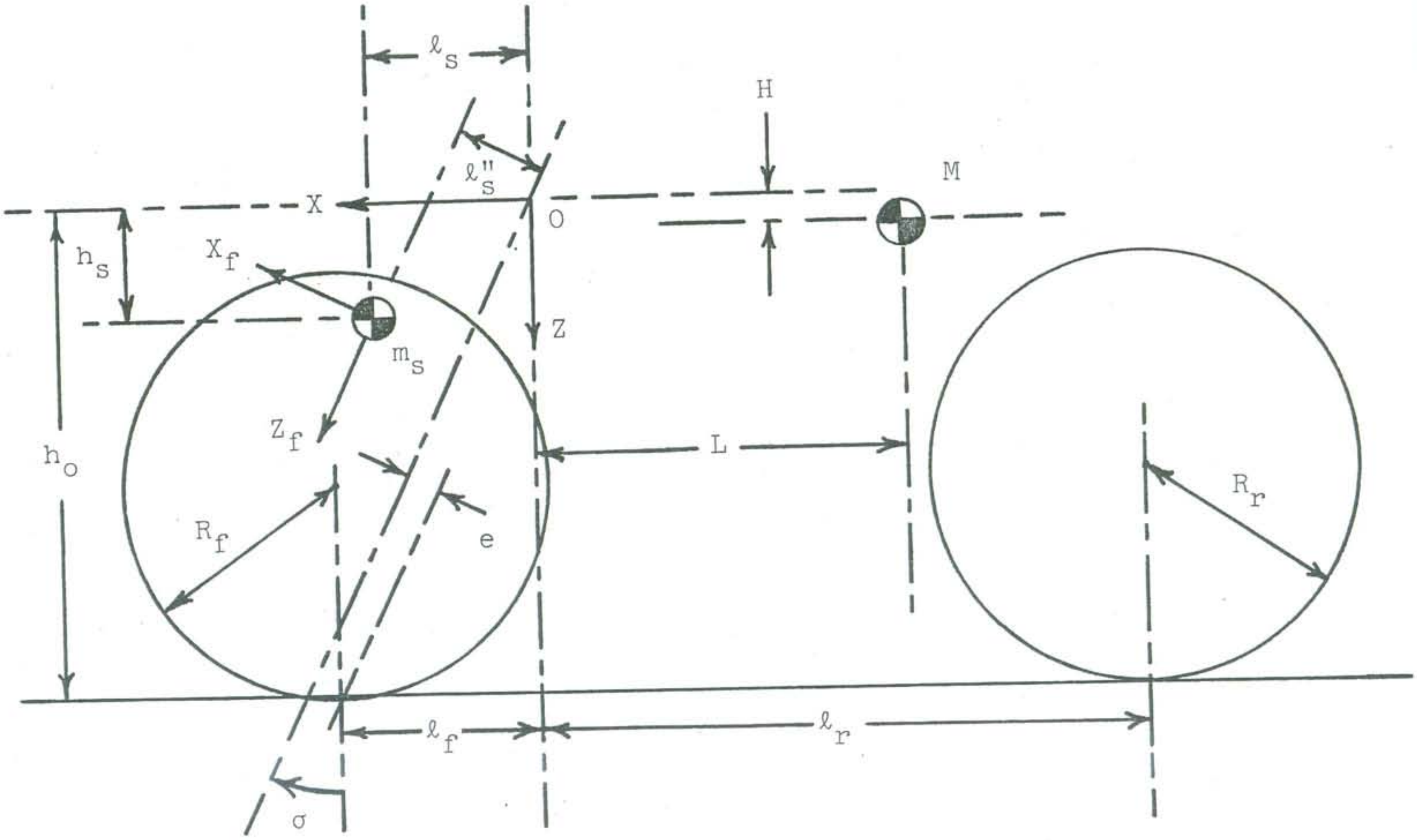

Figure A.1 Single-track vehicle: dimensions, masses and axis systems.

A.2 CONSTRUCTION OF A MORE COMPLETE TIRE MODEL

The equations of motion derived in Reference [14] have been rewritten to conform to the notation and axis systems of Figure A.1. Furthermore, the tire mechanics and steering coulomb friction considerations that are discussed in Chapter 2 have been added to Sharp's equations, and the resulting equations are presented at the end of this section. The methods of incorporating the tire mechanics and steering friction additions into the equations of motion are outlined below.

It is seen from the equations of motion that the first three equations (A.3, A.4, A.5) represent force and moment balances on the entire vehicle, the first being a force balance in the Y-direction, the second and third being moment balances about the Z and X axes, respectively. Equation (A.6) is a balance of moments acting on the front frame assembly about the steering axis. Thus, the tire overturning moments appear in the third and fourth equations, while the tire self-aligning torques appear in the second and fourth equations. Steering coulomb friction is an additional moment in the fourth equation.

Furthermore, lateral force and self-aligning torque are dependent on the instantaneous path curvature of the tire. For a linearized approximation, it may be shown that the instantaneous path curvature of a point p in a body moving in a plane with velocity components (u_p, v_p) relative to axes fixed in the body is given by (u_p = forward velocity = constant)

$$1/\rho = \dot{v}_p/u_p^2 + r_p/u_p, \qquad (A.1)$$

where r_p is the angular velocity of the body.

The linearized lateral velocities of the front and rear tires are

$$\begin{aligned} v_f &= v - e\dot{\delta} - h_o\dot{\phi} + \ell_f r \\ v_r &= v - h_o\dot{\phi} - \ell_r r \end{aligned} \qquad (A.2)$$

Thus, from Equations (A.1) and (A.2) the path curvatures for the front and rear tires are given by

$$1/\rho_f = (\dot{v} - e\ddot{\delta} - h_o\ddot{\phi} + \ell_f\dot{r})/u^2 + (r + \dot{\delta}\cos\sigma)/u$$

$$1/\rho_r = (\dot{v} - h_o\ddot{\phi} - \ell_r\dot{r})/u^2 + r/u$$

From Reference [41], approximate expressions for lateral *force and* aligning torque resulting from path curvature and tire inclination are

$$F_y = C_y(-1/\rho + \frac{\gamma}{r_o}) ,$$

$$M_z = C_z(-1/\rho + \frac{\gamma}{r_o}) ,$$

where r_o = tire rolling radius, and

γ = tire inclination angle.

This requires that

$$\left.\begin{aligned} C_{yf} &= R_f C_{\gamma f} \\ C_{zf} &= R_f C_{\gamma zf} \end{aligned}\right\} \text{front tire}$$

$$\left.\begin{aligned} C_{yr} &= R_r C_{\gamma r} \\ C_{zr} &= R_r C_{\gamma zr} \end{aligned}\right\} \text{rear tire}$$

The resulting equations of motion are given below:

$$m_t\dot{v} + m_t L_t \dot{r} - m_t H_t \ddot{\phi} + m_s \ell''_s \ddot{\delta} + m_t u\, r - F_{yf} - F_{yr} = 0 \quad (A.3)$$

$$m_t L_t \dot{v} + I_{zt}\dot{r} - I_{xzt}\ddot{\phi} + (\overline{I}_{sz}\beta + \overline{I}_{sxz}\gamma + m_s \ell_s \ell''_s)\ddot{\delta}$$

$$+ m_t L_t u\ r - (\overline{I}_{ry}K_r + \overline{I}_{fy}K_f + \overline{I}_{ey}\alpha)u\dot{\phi} - \overline{I}_{fy}\gamma K_f u\ \dot{\delta}$$

$$- F_{yf}\ \ell_f + F_{yr}\ \ell_r - M_{zf} - M_{zr} = 0 \qquad (A.4)$$

$$-m_t H_t \dot{v} - I_{xzt}\dot{r} + I_{xt}\ddot{\phi} + (\overline{I}_{sz}\gamma - \overline{I}_{sxz}\beta - m_s h_s \ell''_s)\ddot{\delta}$$

$$+ (\overline{I}_{ry}K_r + \overline{I}_{fy}K_f + \overline{I}_{ey}\alpha - m_t H_t)u\ r + \overline{I}_{fy}\beta K_f u\dot{\delta}$$

$$+ (H_t - h_o)m_t g\phi + (W_f e - m_s g\ell''_s)\delta + h_o(F_{yr} + F_{yf}) - M_{xr} - M_{xf} = t_\phi(t)$$

$$(A.5)$$

$$m_s \ell''_s v + (\overline{I}_{sz}\beta + \overline{I}_{sxz}\gamma + m_s \ell''_s \ell_s)\dot{r} + (\overline{I}_{sz}\gamma - \overline{I}_{sxz}\beta - m_s \ell''_s h_s)\ddot{\phi}$$

$$+ (I_{sz} + m_s \ell''^2_s)\ddot{\delta} + (\overline{I}_{fy}K_f\gamma + m_s \ell''_s)u\ r + C_s\dot{\delta}$$

$$+ (W_f e - m_s g\ell''_s) + (W_f e - m_s g\ell''_s)\gamma\delta + F_{yf}e - M_{zf}\beta - M_{xf}\gamma$$

$$+ C_\delta \mathrm{sgn}\dot{\delta} = t_\delta(t) \qquad (A.6)$$

$$\frac{\sigma_f}{u}\dot{F}_{yf} + F_{yf} = - C_{\alpha f}\alpha_f + C_{\gamma f}(- \frac{R_f}{\rho_f} + \gamma_f)$$

$$\frac{\sigma_r}{u}\dot{F}_{yr} + F_{yr} = - C_{\alpha r}\alpha_r + C_{\gamma r}(- \frac{R_r}{\rho_r} + \gamma_r)$$

$$\frac{\sigma_f}{u}\dot{M}_{xf} + M_{xf} = C_{Mxf}\alpha_f + C_{\gamma xf}\gamma_f$$

$$\frac{\sigma_r}{u}\dot{M}_{xr} + M_{xr} = C_{Mxr}\alpha_r + C_{\gamma xr}\gamma_r$$

$$\frac{\sigma_f}{u}\dot{M}_{zf} + M_{zf} = C_{Mzf}\alpha_f + C_{\gamma zf}(- \frac{R_f}{\rho_f} + \gamma_f)$$

$$\frac{\sigma_r}{u}\dot{M}_{zr} + M_{zr} = C_{Mzr}\alpha_r + C_{\gamma zr}(- \frac{R_r}{\rho_r} + \gamma_r)$$

$$\alpha_f = (v - e\dot{\delta} - h_o\dot{\phi} + \ell_f r)/u - \beta\delta$$

$$\alpha_r = (v - h_o\dot{\phi} - \ell_r r)/u$$

$$\gamma_f = \phi + \gamma\delta$$

$$\gamma_r = \phi$$

$$1/\rho_f = (\dot{v} - e\ddot{\delta} - h_o\ddot{\phi} + \ell_f\dot{r})/u^2 + (r + \beta\dot{\delta})/u$$

$$1/\rho_r = (\dot{v} - h_o\ddot{\phi} - \ell_r\dot{r})/u^2 + r/u$$

A.3 THEORETICAL TRANSFER FUNCTIONS

The motorcycle equations of motion (Eqs. (A.3)-(A.6)) may be written in vector-matrix form as follows:

$$A''\underline{x}(t) = \underline{B}'' , \qquad (A.7)$$

where the elements of the 4 x 4 matrix A" have the form

$$a''_{ij} = c''_{ij} \frac{d^2}{dt^2} + d''_{ij} \frac{d}{dt} + e''_{ij}$$

(c''_{ij}, d''_{ij}, e''_{ij} constants),

$$\underline{x}(t) = \begin{pmatrix} v(t) \\ r(t) \\ \phi(t) \\ \delta(t) \end{pmatrix} ,$$

and $\underline{B}''$ is of the form

$$\underline{B}'' = \begin{pmatrix} \dfrac{g_{11}}{\dfrac{\sigma_f}{u}\dfrac{d}{dt} + 1} + \dfrac{g_{12}}{\dfrac{\sigma_r}{u}\dfrac{d}{dt} + 1} \\ \dfrac{g_{21}}{\dfrac{\sigma_f}{u}\dfrac{d}{dt} + 1} + \dfrac{g_{22}}{\dfrac{\sigma_r}{u}\dfrac{d}{dt} + 1} \\ t_\phi(t) + \dfrac{g_{31}}{\dfrac{\sigma_f}{u}\dfrac{d}{dt} + 1} + \dfrac{g_{32}}{\dfrac{\sigma_r}{u}\dfrac{d}{dt} + 1} \\ t_\delta(t) + \dfrac{g_{41}}{\dfrac{\sigma_f}{u}\dfrac{d}{dt} + 1} + \dfrac{g_{42}}{\dfrac{\sigma_r}{u}\dfrac{d}{dt} + 1} \quad -C_\delta \operatorname{sgn} \dot{\delta} \end{pmatrix}$$

where each $g_{k\ell}$ is a linear combination of v, $\dot{v}$, r, $\dot{r}$, ϕ, $\dot{\phi}$, $\ddot{\phi}$, δ, $\dot{\delta}$, and $\ddot{\delta}$.

If $\sigma_f = \sigma_r$ and $C_\delta = 0$, Equation (A.7) may be written

$$A'\underline{x}(t) = \underline{B}' , \qquad (A.8)$$

where the elements of the 4 x 4 matrix A' have the form

$$a'_{ij} = c'_{ij}\frac{d^3}{dt^3} + d'_{ij}\frac{d^2}{dt^2} + e'_{ij}\frac{d}{dt} + f'_{ij}$$

(c'_{ij}, d'_{ij}, e'_{ij}, f'_{ij} constants), and

$$\underline{B}' = \begin{pmatrix} 0 & \\ 0 & \\ (\frac{\sigma_f}{u} \frac{d}{dt} + 1) & t_\phi(t) \\ (\frac{\sigma_f}{u} \frac{d}{dt} + 1) & t_\delta(t) \end{pmatrix}$$

Finally, with the assumption of zero values of v, r, ϕ, δ and their derivatives at t=0, subjecting Equation (A.8) to Laplace transformation yields

$$A \underline{X}(s) = \underline{B} , \qquad (A.9)$$

where the elements of A are

$$a_{ij} = c_{ij}s^3 + d_{ij}s^2 + e_{ij}s + f_{ij}$$

$$(c_{ij} = c'_{ij}, d_{ij} = d'_{ij}, e_{ij} = e'_{ij}, f_{ij} = f'_{ij}) ,$$

$$\underline{X}(s) = \begin{pmatrix} V(s) \\ R(s) \\ \Phi(s) \\ \Delta(s) \end{pmatrix}$$

(s = Laplace operator, V(s) = Laplace transform of v(t) = L(v(t)), R(s) = L(r(t)), etc.), and

$$\underline{B} = \begin{pmatrix} 0 & \\ 0 & \\ (\frac{\sigma_f}{u} s+1) & T_\phi(s) \\ (\frac{\sigma_f}{u} s+1) & T_\delta(s) \end{pmatrix}$$

$(T_\phi(s) = L(t_\phi(t)), T_\delta(s) = L(t_\delta(s))$.

The characteristic function of the system is det(A), a tenth order polynomial in s.

Transfer functions may be easily computed by Cramer's rule. For example,

$$Y_c(s) = \frac{\Phi(s)}{T_\delta(s)} = \frac{\begin{vmatrix} a_{11} & a_{12} & 0 & a_{14} \\ a_{21} & a_{22} & 0 & a_{24} \\ a_{23} & a_{32} & 0 & a_{34} \\ a_{24} & a_{42} & (\frac{\sigma_f}{u} s+1) & a_{44} \end{vmatrix}}{\det(A)} \tag{A.10}$$

The inverse Laplace transform of Equation (A.10) gives the roll angle response, $\phi(t)$, to an impulse of steering torque. Furthermore, letting $s \to j\omega$ in Equation (A.10) yields $Y_c(j\omega)$, the transfer function of the "controlled element" used extensively in Chapters 4-6.

APPENDIX B

SOLUTIONS OF MOTION EQUATIONS

B.1 FLOWCHART, LINEAR ANALYSIS DIGITAL COMPUTER PROGRAMS

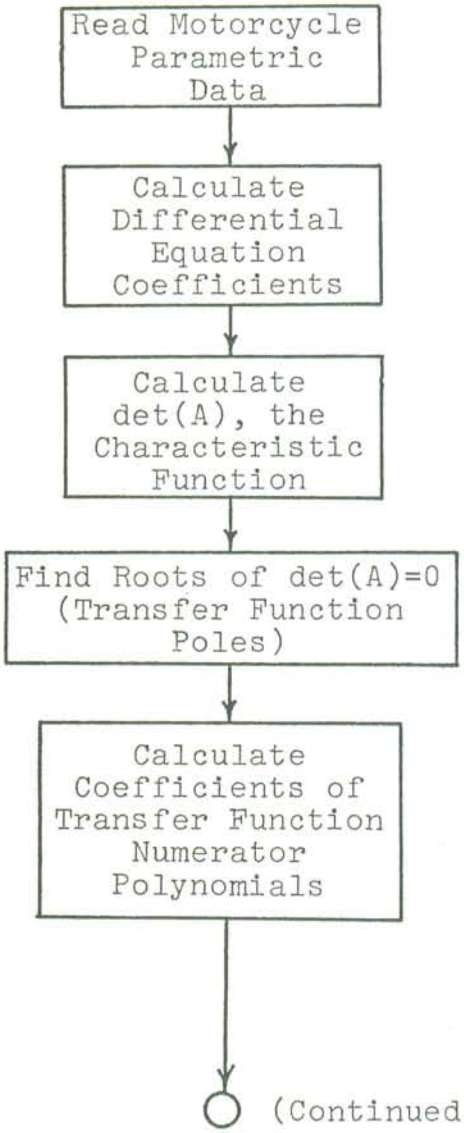

(Continued next page)

Figure B.1 Flowchart

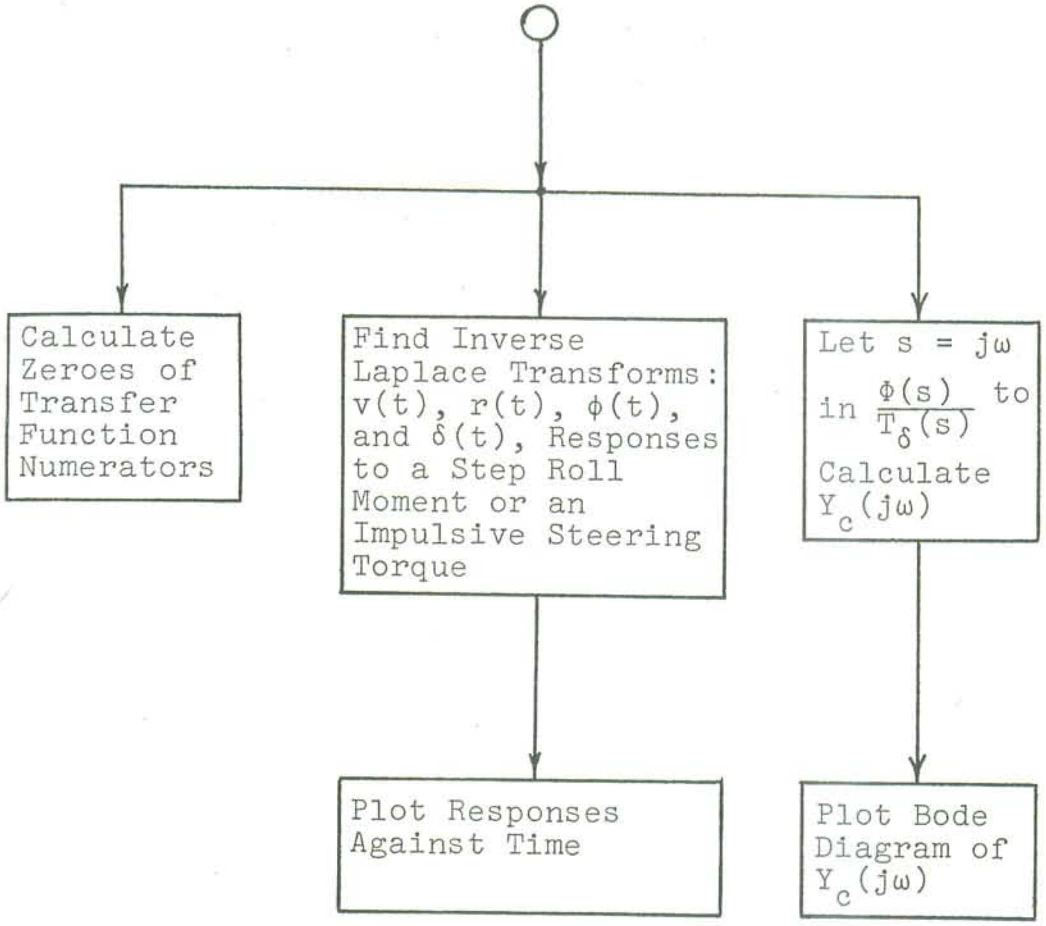

Figure B.1 (Continued)

B.2 ANALOG COMPUTER CIRCUIT

When the differential equation coefficients in Appendix A were calculated from the motorcycle parameter data of Appendix D, it was found that, for at least the speed range of interest, the motorcycle equations of motion, as used in the preparation of Figures 2.4, 2.5 and 3.2-3.5, can be written in the following form:

$$v = a_o r - a_1 \dot{\phi} - a_2 \dot{\delta} - \int (a_3 r - a_4 F_{yf} - a_5 F_{yr}) dt$$

$$r = b_o v + b_1 \dot{\phi} + b_2 \phi - b_3 \dot{\delta} + b_4 \delta$$

$$- \int (-b_5 M_{zf} - b_6 M_{zr} - b_7 r - b_8 F_{yf} + b_9 F_{yr}) dt$$

$$\dot{\phi} = -c_o v + c_1 r - c_2 \dot{\delta} - c_3 \delta - \int (c_4 r - c_5 \phi - c_6 \delta$$

$$+ c_y F_{yf} + c_8 F_{yr} - c_9 t_\phi) dt$$

$$\dot{\delta} = -d_o v - d_1 r - d_2 \dot{\phi} + d_3 \phi - d_4 \delta$$

$$- \int (-d_5 M_{zf} + d_6 r - d_y \phi - d_8 \delta + d_9 F_{yf}$$

$$+ e_o \operatorname{sgn} \dot{\delta} - e_1 t_\delta) dt ,$$

where the constants, a_o, a_1, a_2, ... d_9, e_o, e_1, are all positive.

Figure B.2a shows the implementation of the above equations on the analog computer. Tire lateral forces and aligning moments were simulated (Figure B.2b) directly from the equations following Equation (A.6), Appendix A. In the analog computer simulation of the motorcycle, dimensionalized scaling [52] was used throughout.

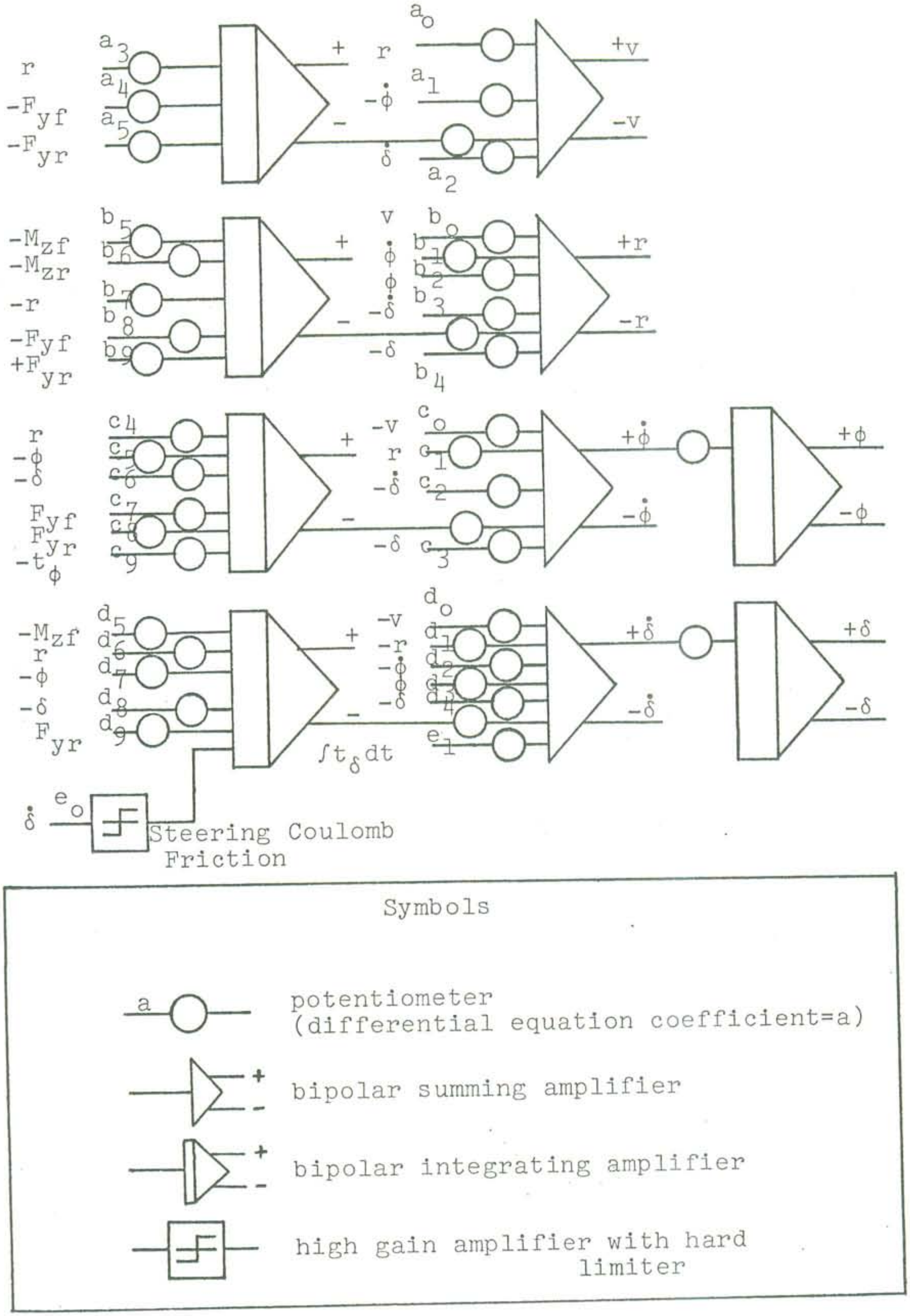

Figure B.2a Analog computer circuit

Front Tire

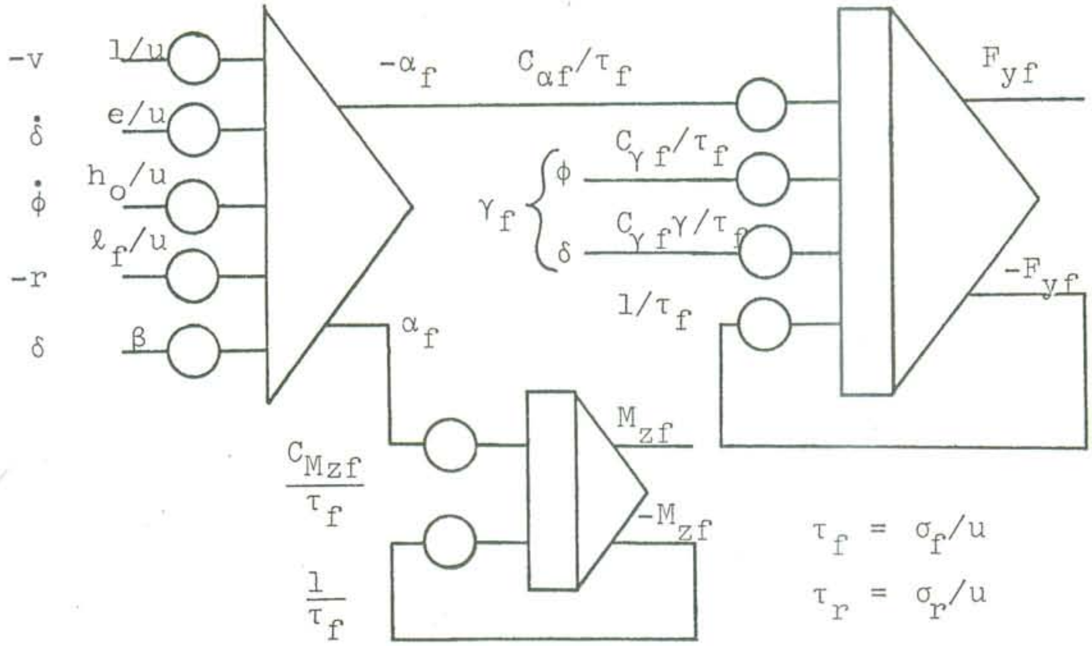

Rear Tire

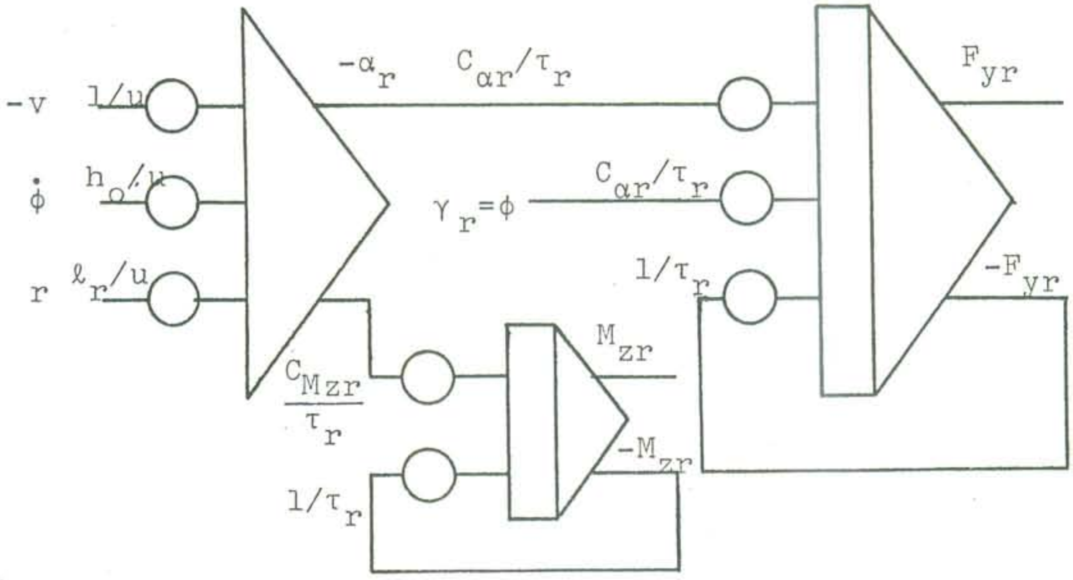

Figure B.2b Simulation of tire lateral force and aligning moment.

APPENDIX C

MEASUREMENT OF VEHICLE PARAMETERS

C.1 MEASUREMENT OF MASSES, CENTER OF GRAVITY LOCATIONS, AND MOMENTS OF INERTIA

The overall vehicle/rider mass and the mass of the front system was determined by simple weighing. Although a second identical vehicle was available for disassembly so that the road vehicle would always be available for tests, total vehicle/rider measurements were made with the road vehicle.

With the single-track vehicle, the rider is a significant part of the total mass and its moments. To measure mass distribution, then, it is necessary to exercise much care to keep the rider's position relative to the vehicle as nearly constant as possible, both during an experiment and from one experiment to another. Because the rider was assumed in the theory to be a rigid body rigidly attached to the rear frame, it is also desirable to restrict his movements during the road tests. It is readily recognized that, even if the rider were encased in a plaster body cast, he would not be completely rigid, and his flexibility is always a source of error. To reduce this error, the motorcycle was fitted with a strong brace (see Fig. C.1) to help the rider maintain his position. While the brace cannot completely restrain the rider, it assists him to intentionally hold his position, a task which is next to impossible without the brace. All total vehicle/rider measurements and road tests were made with the brace attached.

A larger frame was built to hold the motorcycle for linear dimension, center of gravity, and moment of inertia measurements. This is essentially a channel clamped to the frame keeping the tires and suspension compressed as they are on the road. The frame is cross-braced at the top to prevent twisting and has several fittings for the various measurements. (See Figs. C.1 and C.2.) In the following few paragraphs the term "vehicle" refers to the motorcycle and rider mounted in this frame.

Vehicle center of gravity vertical and longitudinal positions were found by resting the vehicle on the edges of two steel angles, one of which loaded a scale to measure the force required for equilibrium. In the case of c.g. vertical position, one angle was positioned directly below the c.g. and the vehicle was then rotated about the pitch (y) axis through angles between ±15°. Taking force measurements for different angles and support positions provided experimental replications. Center of gravity of the front fork, handlebar, and wheel assembly was found by suspending the assembly from two cables and finding their point of intersection.

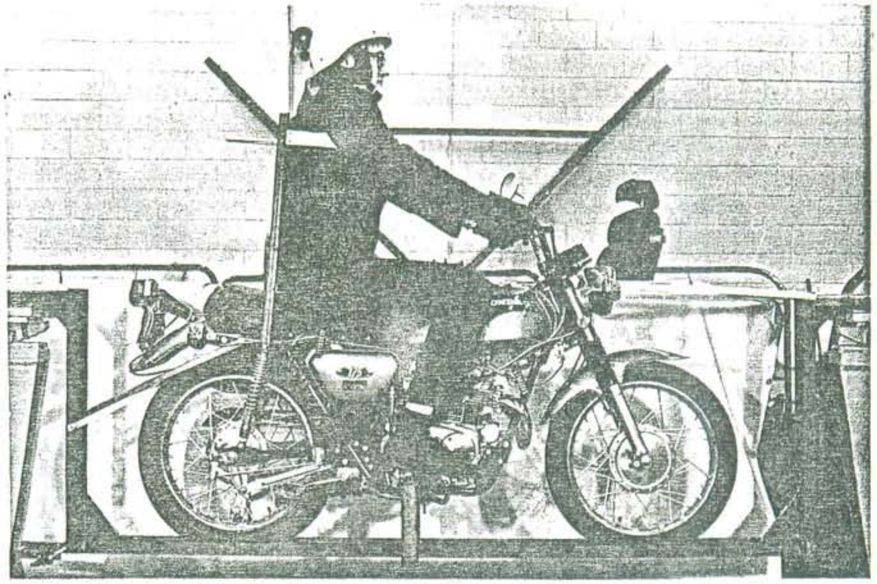

Figure C.1 Measurement of roll moment of inertia, entire vehicle with rider.

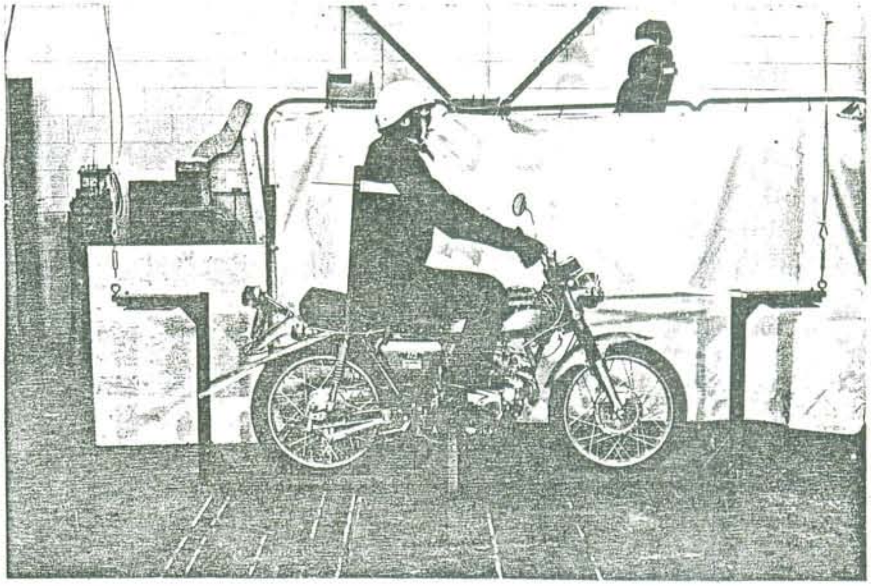

Figure C.2 Measurement of yaw moment of inertia, entire vehicle with rider.

Figure C.1 shows the experimental arrangement for measuring vehicle roll moment of inertia. The vehicle is resting on knife edges at the front and rear. A pair of calibrated coil springs located near the bottom of the frame was needed to ensure oscillatory motion, as the vehicle center of gravity was near the axis of rotation. It is worth noting that rider flexibility had a greater effect on roll measurements than on others; in fact, without the rider restraining brace, only a useless one or two cycles of oscillation would result. With the brace, ten to fifteen cycles were easily obtained. As mentioned before, the brace was used for all total vehicle measurements.

Yaw moment of inertia was found using the arrangement shown in Figure C.2. Here the vehicle is suspended at the front and rear by two cables. The vehicle was caused to oscillate about a vertical axis through its center of gravity.

Vehicle product of inertia was obtained by inclining the roll axis upward 37° from the horizontal. Use of shorter cables allowed the measurement of the vehicle moment of inertia about a vertical axis through the c.g. Use of the values obtained from all three experiments permitted the calculation of the vehicle product of inertia by means of axis rotation relationships.

Moments of inertia of the wheels and front fork-handlebars-wheel assembly were obtained using the torsional pendulum shown in Figure C.3. The front assembly was clamped below the triangle and caused to oscillate about three axes in the assembly, thus permitting calculation of the moments and product of inertia with respect to the x_f and z_f axes. Moments of inertia of engine crankshaft and clutch assembly were obtained from the manufacturer. Moments of inertia of alternator, camshaft and transmission were estimated from geometry. Taking all gear and sprocket ratios (from vehicle shop manual) into account yielded an effective gear-dependent moment of inertia for the engine.

For each moment of inertia measurement, the moment of inertia about the axis of rotation was written as a function of mass, geometry, spring constant and frequency of oscillation, all known quantities. This function was found from a linear differential equation describing the experimental system. The contribution to the moment of inertia due to the frame was subtracted, and the result expressed relative to the appropriate axis system.

C.2 ESTIMATION OF COULOMB FRICTION IN THE STEERING HEAD

As would be expected, since the test vehicle does not have any form of steering damper, the friction level in the steering head is very low. A maximum value was estimated

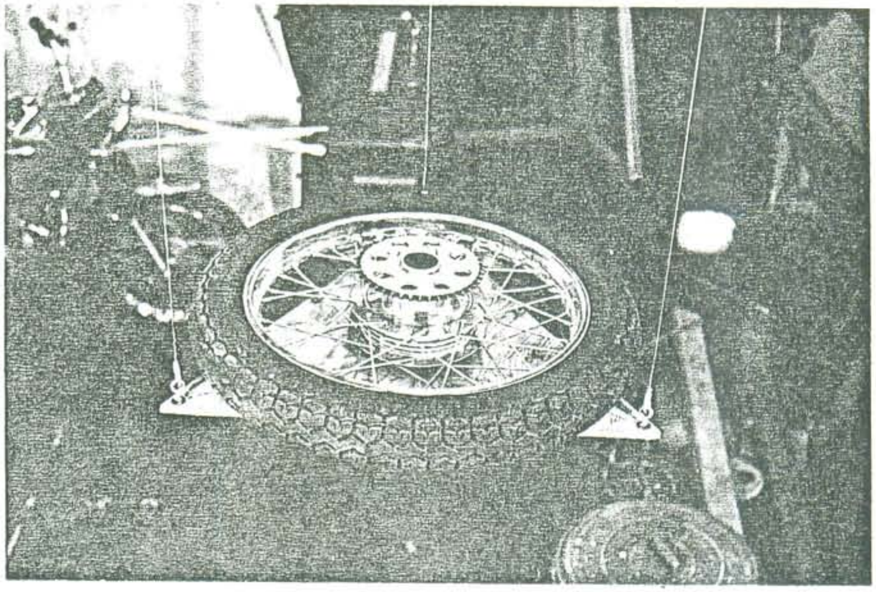

Figure C.3 Torsional pendulum for measurement of moments of inertia of wheels and front frame assembly.

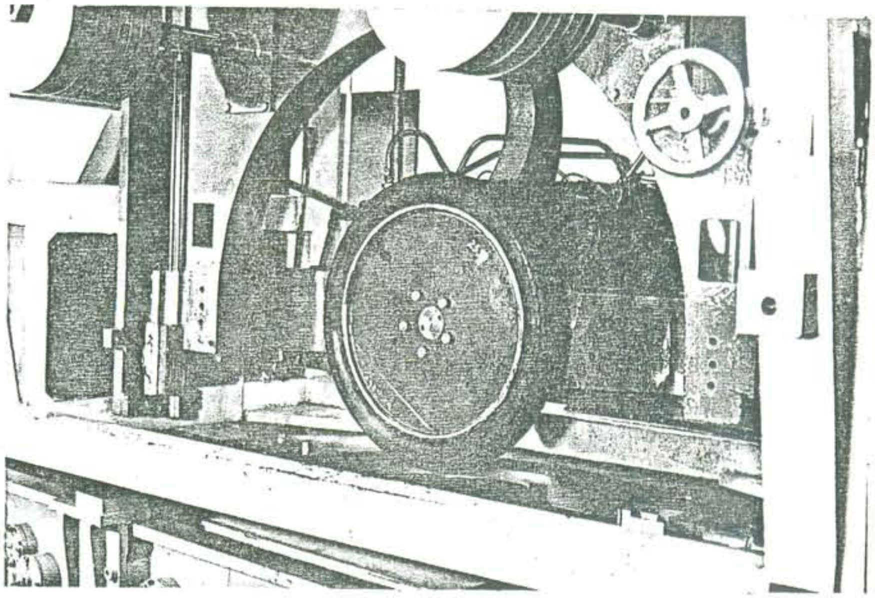

Figure C.4 Motorcycle tire mounted for testing.

in the following way. The front of the vehicle was suspended from the front axle using cables which applied no torque about the steering axis while the steer angle was zero. The vehicle x-axis was kept horizontal and weights were applied to cause the vertical force from the cables to equal the normal operating front wheel load. By means of a small spring scale, a torque was applied about the steering axis and gradually increased until the steering just began to move. The "breakaway" torque (about 1.2 lb-in) was taken to be the maximum coulomb friction that could be in the steering head. Since the effect of this low a level of friction had negligible effect on the computer results, no attempt was made to obtain more accurate values.

C.3 MEASUREMENT OF TIRE PARAMETERS

C.3.1 METHOD OF MEASUREMENT. Tire parameters were measured using the HSRI Flat Bed Tire Tester, which holds the tire against a simulated roadway moving at about 2 feet per second (Fig. C.4). The framework in which the tire is mounted allows the tire to be tested at various vertical loads, slip and inclination angles and is restrained by load cells. Measurement of tire longitudinal force, rolling resistance moment, lateral force, vertical force, overturning moment, and self-aligning torque is possible, and the last four quantities were measured for the tires used on the Honda CL175.

Figures C.5 and C.6 show lateral force as a function of slip inclination angle for the vertical loads existing in the road tests. Self-aligning torque is shown in Figure C.7 as a function of slip angle. Self-aligning torque dependence on inclination angle and overturning moments, due to their low levels, could not be accurately measured. Reference [24] contains some data on self-aligning torque as a function of inclination angle; these measurements were combined with information obtained from the tires tested at HSRI to provide estimates of tire coefficients. Overturning moments arising from slip angles were found to be less than 20 lb-in/degree and had a negligible effect on the analytical results; hence, they were taken to be zero. In Figure C.8, circular tire cross-sections are rotated through an inclination angle of 10° to estimate the amount of lateral motion of the vertical load (center of pressure in the contact patch). This distance, multiplied by the vertical load, approximates the tire overturning moment to a degree consistent with measurements, as shown in Figure C.9.

C.3.2 MEASUREMENT OF TIRE RELAXATION LENGTH. The gradual build-up of tire side force due to a step input of slip angle is shown in Figure C.10. These curves were obtained by loading the tire against the bed with a fixed slip angle and manually cranking the bed to record lateral force versus

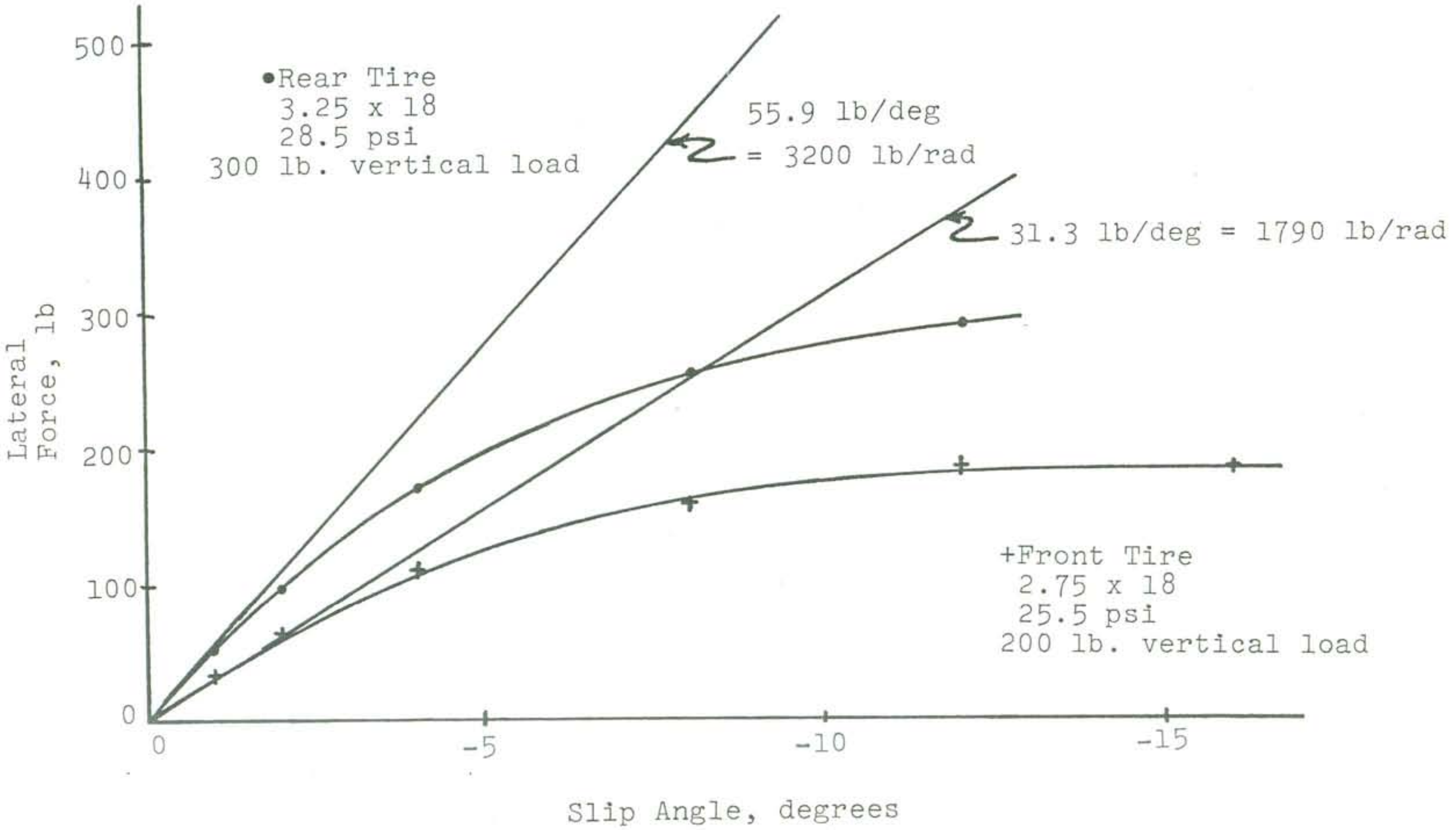

Figure C.5 Measured tire lateral forces as functions of slip angle.

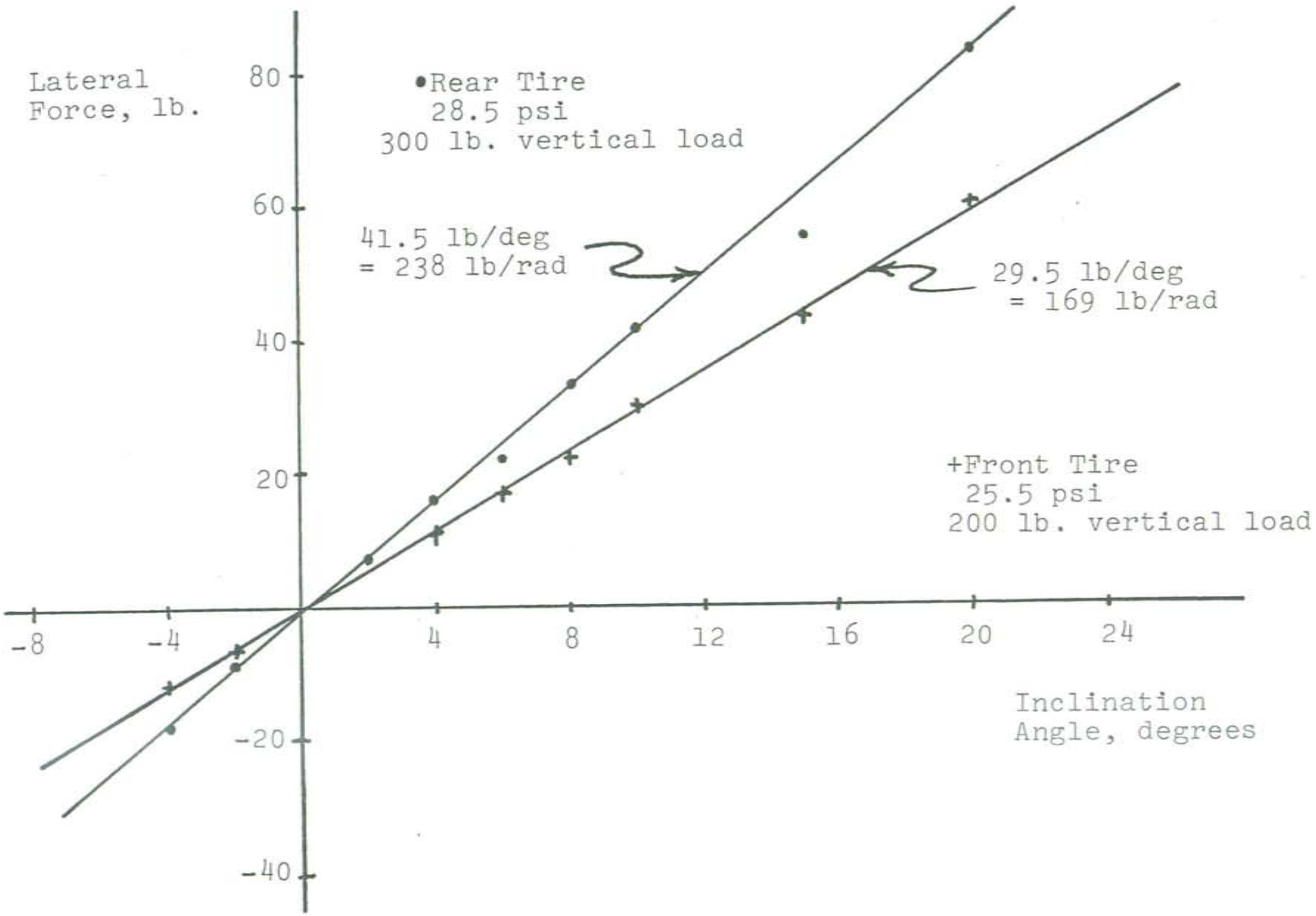

Figure C.6 Measured tire lateral forces as functions of inclination angle.

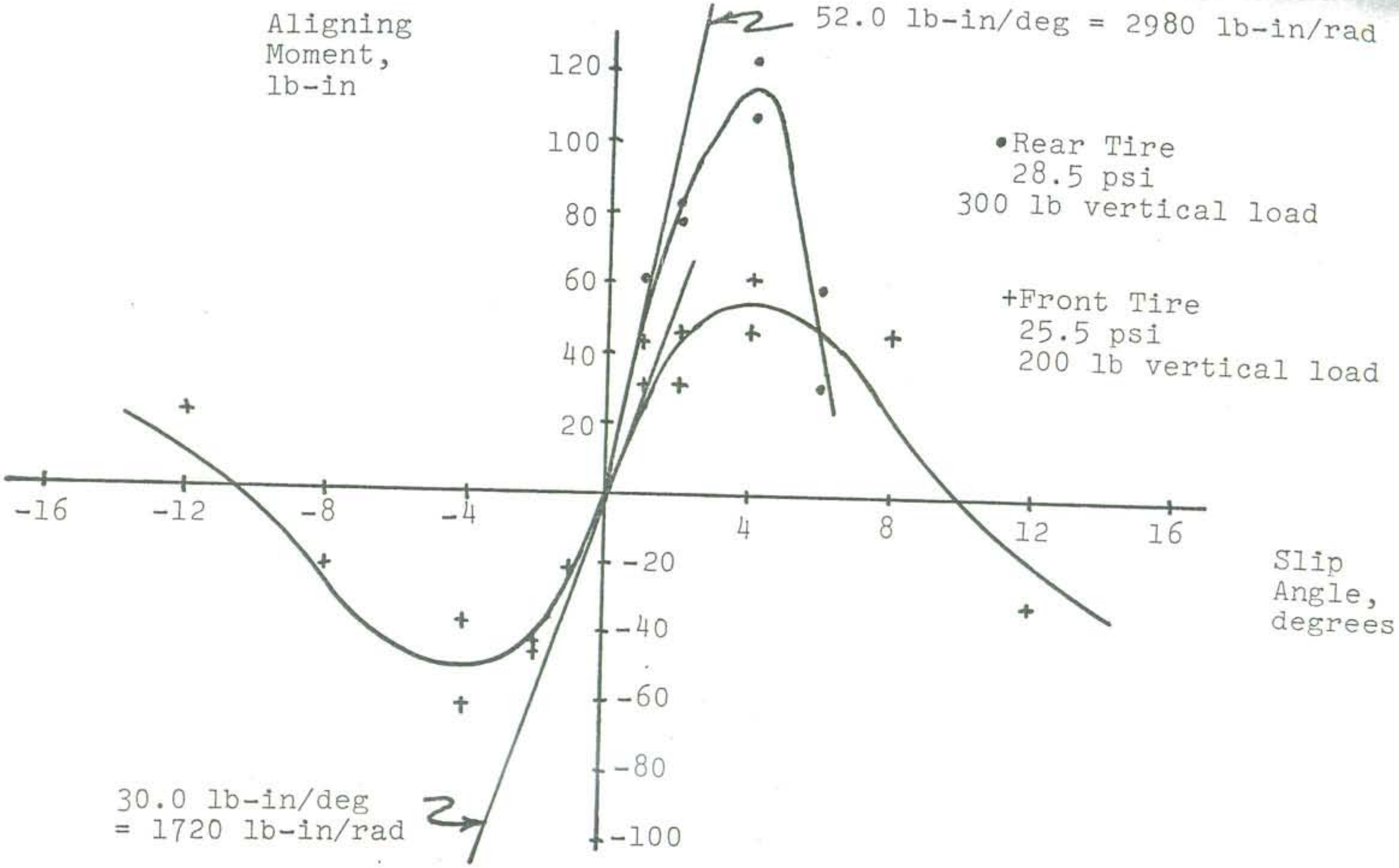

Figure C.7 Measured tire self-aligning moments as functions of slip angle.

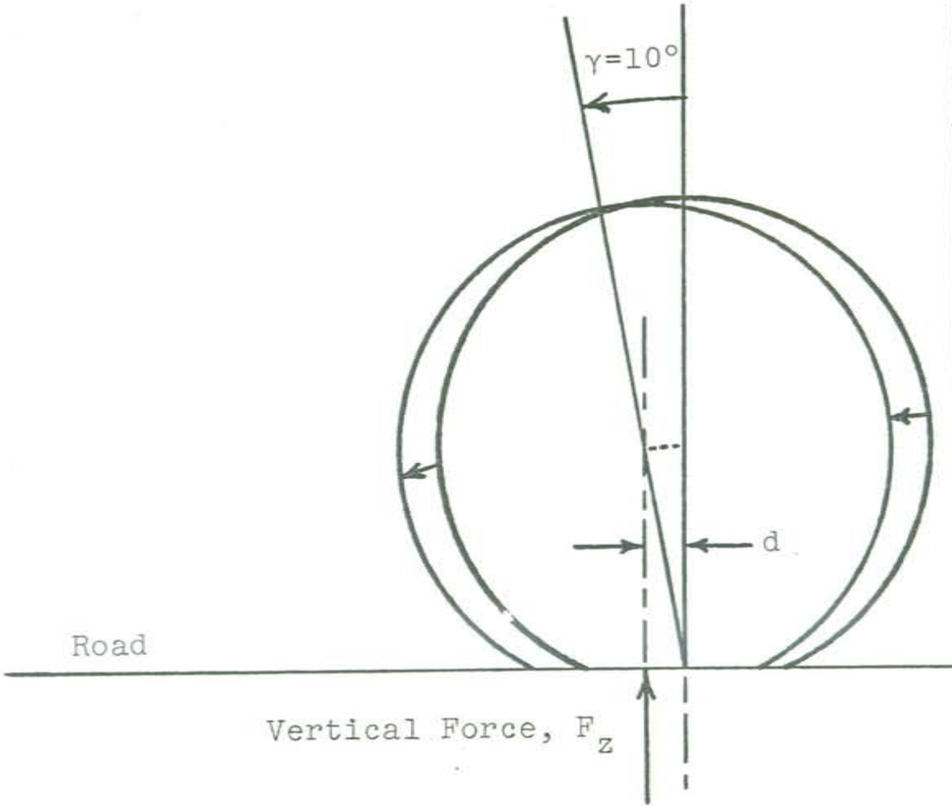

	Front	Rear
Cross-Section Diameter, in.	2.75	3.25
$d(\gamma=10°)$, in.	0.21	0.25
F_z, lb	198	294
$C_{\gamma x} \doteq \frac{F_z d}{10}$, lb-in/deg	4.2	7.35
$C_{\gamma x}$, lb-in/rad	238	421

Figure C.8 Geometrical estimation of tire overturning moment due to inclination angle.

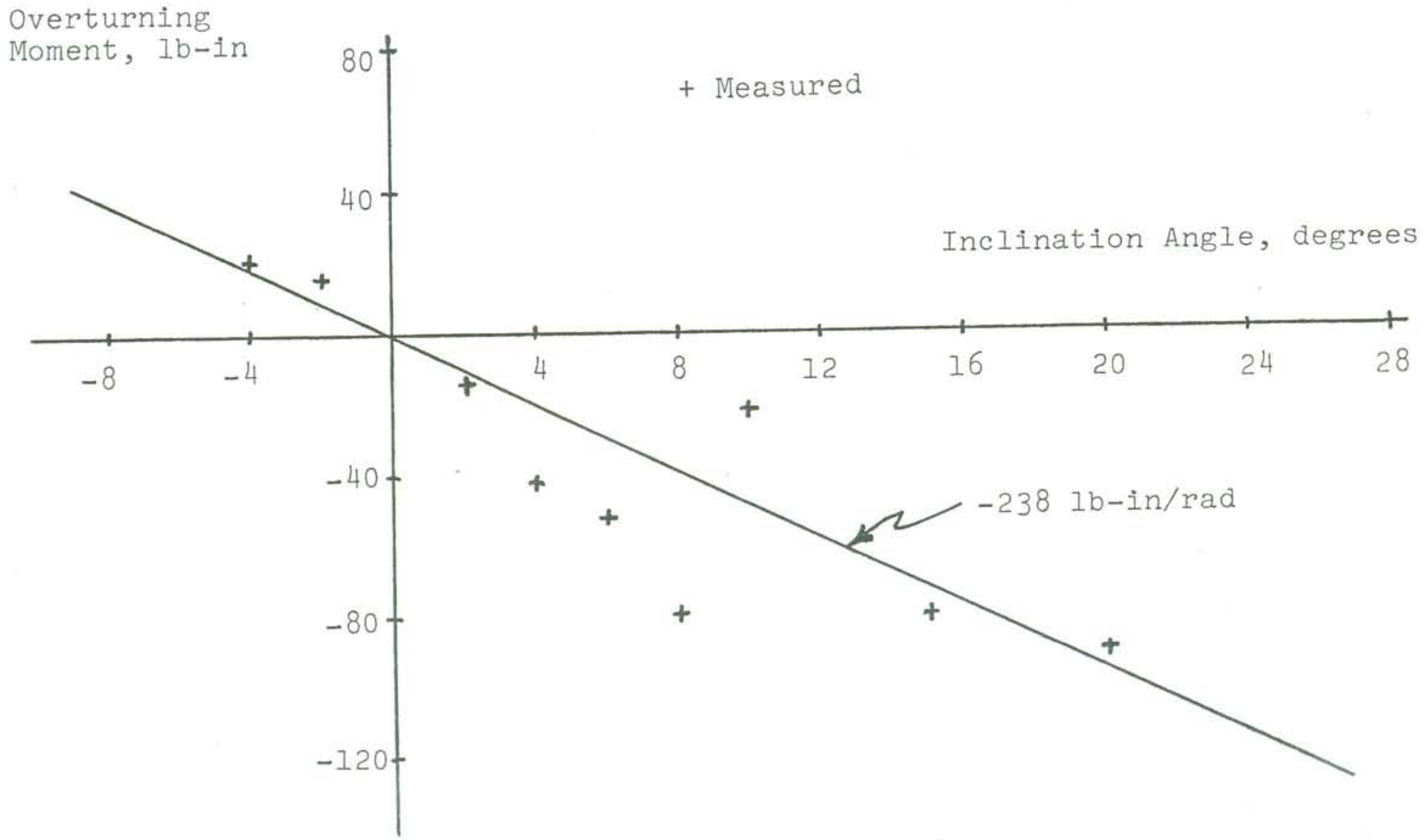

Figure C.9 Measured overturning moments due to inclination angle, front tire.

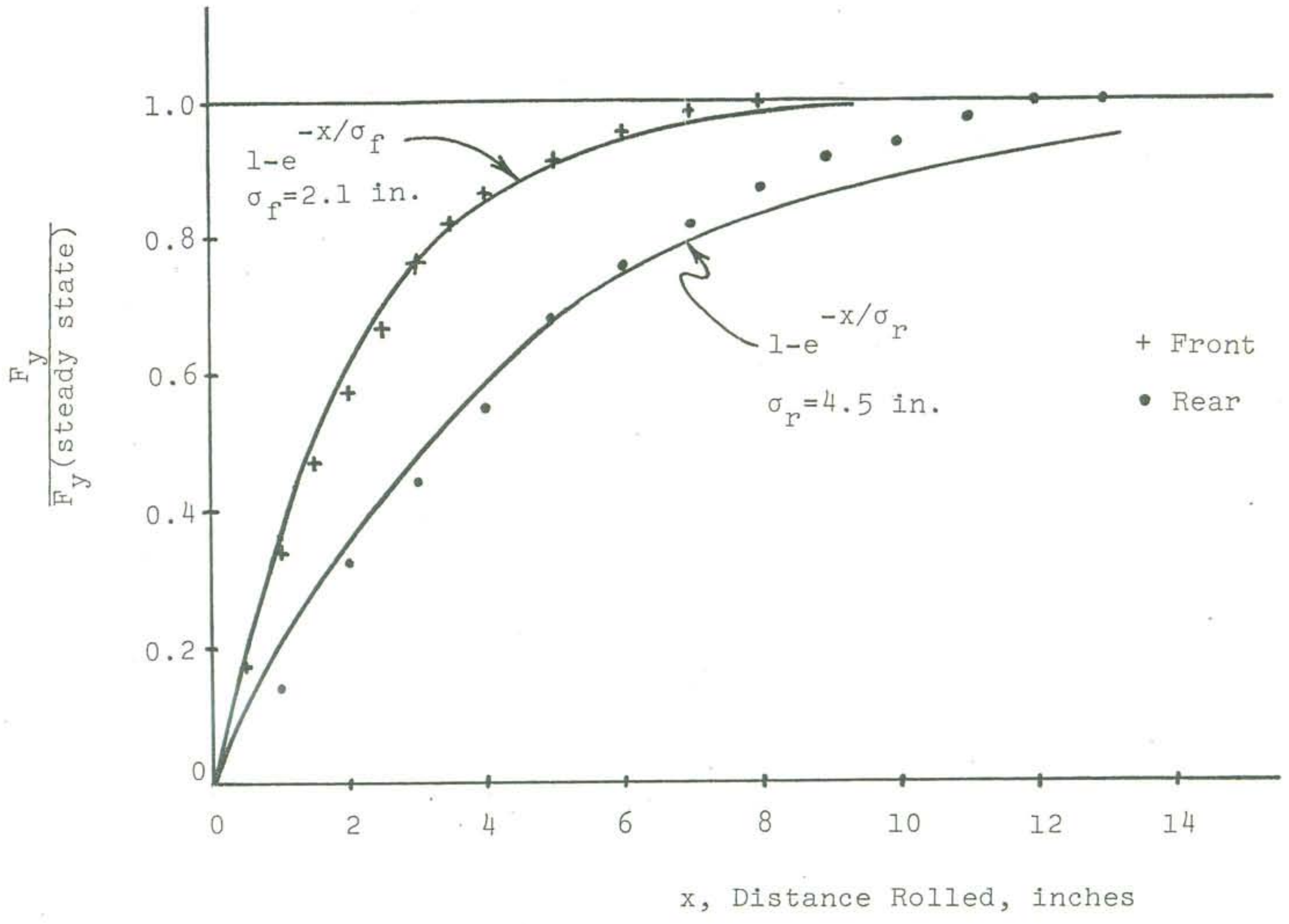

Figure C.10 Tire lateral force response to a step slip angle.

distance rolled (x). The data points were then fitted with a curve of the form $1-e^{-x/\sigma_x}$, where σ_x is the relaxation length for the tire.

It is worth noting that, due to the construction of the test device and the low levels of some of the measurements, it was not possible to observe the build-up of lateral force, self-aligning torque and overturning moment due to a step inclination angle. While it was assumed in the mathematical analysis of the single-track vehicle that this response is identical to that due to a step slip angle, this may not be the case. However, from the computer results, it was found that the forces and moments due to inclination angles influenced only the modes of motion that were insensitive to relaxation length; thus, it was not felt that the validity of the assumption would affect the accuracy of the equations of motion.

Self-aligning torque arising from slip angle was observed to follow the same curve as the lateral force.

APPENDIX D

PARAMETER VALUES FOR TEST VEHICLE

Table D.1 gives the values of measured parameters for the Honda CL 175 with rider, rider restraining brace, full gas tank, and all instrumentation, except the steering torque bar, the effect of which is very small. Numbers in parentheses indicate the values (where changed) after the twelve-pound weight described in Chapter 3 was added to the vehicle. Data for the six-pound weight are not given, but may be calculated by a linear interpolation between the values for no weight and the values for the twelve-pound weight. The root locus plot in Chapter 2 uses the values for the vehicle without the weight.

TABLE D.1

TEST VEHICLE PARAMETER DATA

SYMBOL	VALUE	SYMBOL	VALUE
C_s	0	I_{zt}	800 (867) lb-sec^2-in
$C_{\alpha f}$	1790 lb/rad	I_{xzt}	58 (55.5) lb-sec^2-in
$C_{\alpha r}$	3200 lb/rad	$\bar{I}_{sz}$	3.83 lb-sec^2-in
$C_{\gamma f}$	169 lb/rad	$\bar{I}_{sxz}$	-0.06 lb-sec^2-in
$C_{\gamma r}$	238 lb/rad	$\bar{I}_{fy}$	3.22 lb-sec^2-in
C_{Mxf}	0	$\bar{I}_{ry}$	4.29 lb-sec^2-in
C_{Mxr}	0	K_f	.086 in^{-1}
C_{Mzf}	1720 lb-in/rad	K_r	.0837 in^{-1}
C_{Mzr}	2980 lb-in/rad	m_t	1.278 (1.310) $\frac{\text{lb-sec}^2}{\text{in}}$
$C_{\gamma xf}$	-238 lb-in/rad	m_s	.1386 lb-sec^2/in
$C_{\gamma xr}$	-421 lb-in/rad	C_δ	0.2--1.2 lb-in
$C_{\gamma zf}$	50 lb-in/rad	W_f	-198.5 (-197) lb
$C_{\gamma zr}$	90 lb-in/rad	σ	26^o
e	2.97 in	σ_f	2.1 in
h_o	27.3 in	σ_r	4.5 in
h_s	5.37 in		
H_t	-.60 (-.54) in		
ℓ_f	10.0 in		
ℓ_r	40.3 in		
ℓ_s	4.975 in		
ℓ''_s	2.13 in		
L_t	-20.1 (-20.7) in		
g	386 in/sec^2		
I_{xt}	332 (342) lb-sec^2-in		

Transmission Gear	$\bar{I}_{ey}\alpha$, lb-sec^2
1	.0641
2	.0434
3	.0335
4	.0272
5	.0232

APPENDIX E

INSTRUMENTATION DIAGRAMS, ROLL-STABILIZATION EXPERIMENTS

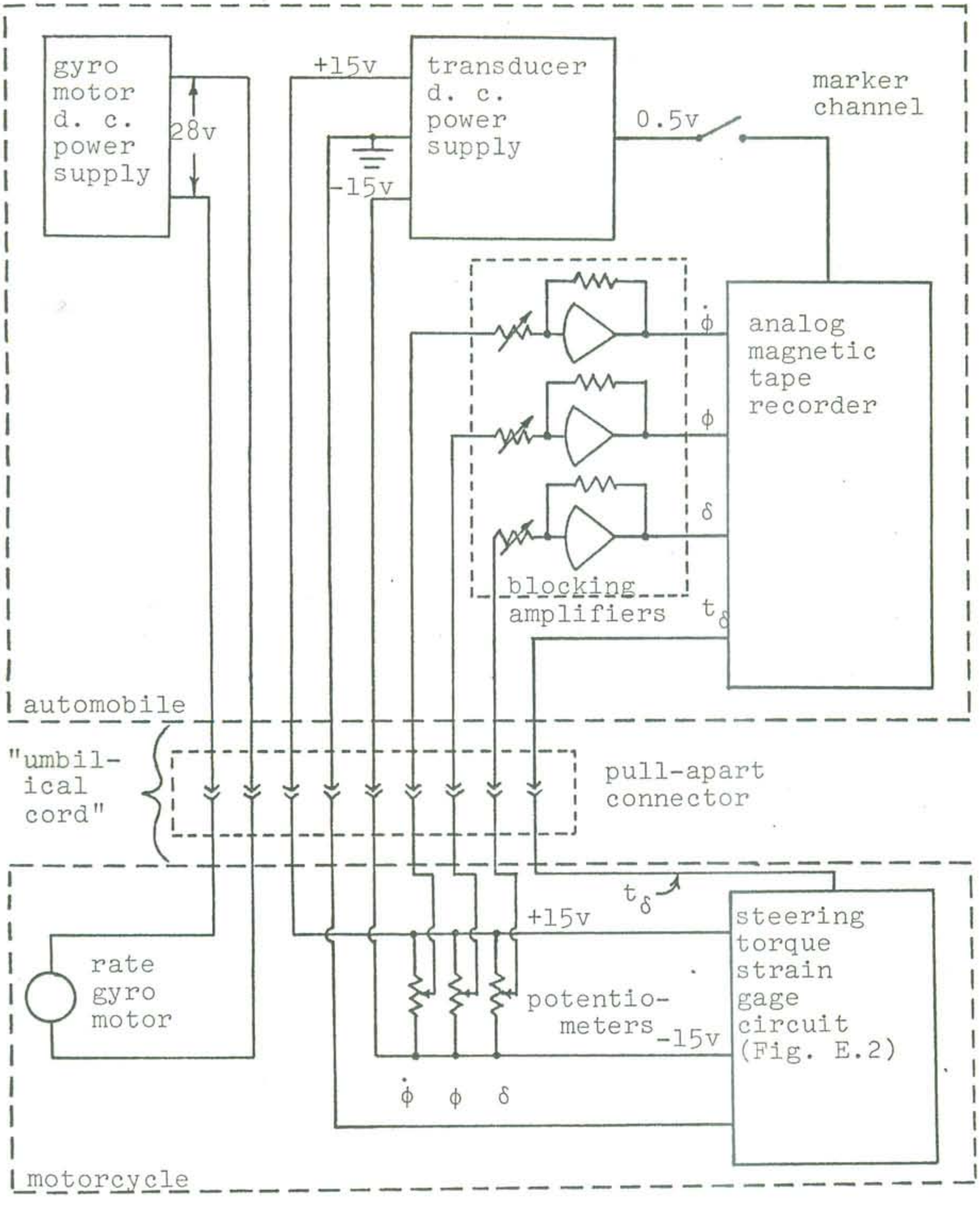

Figure E.1 Instrumentation schematic.

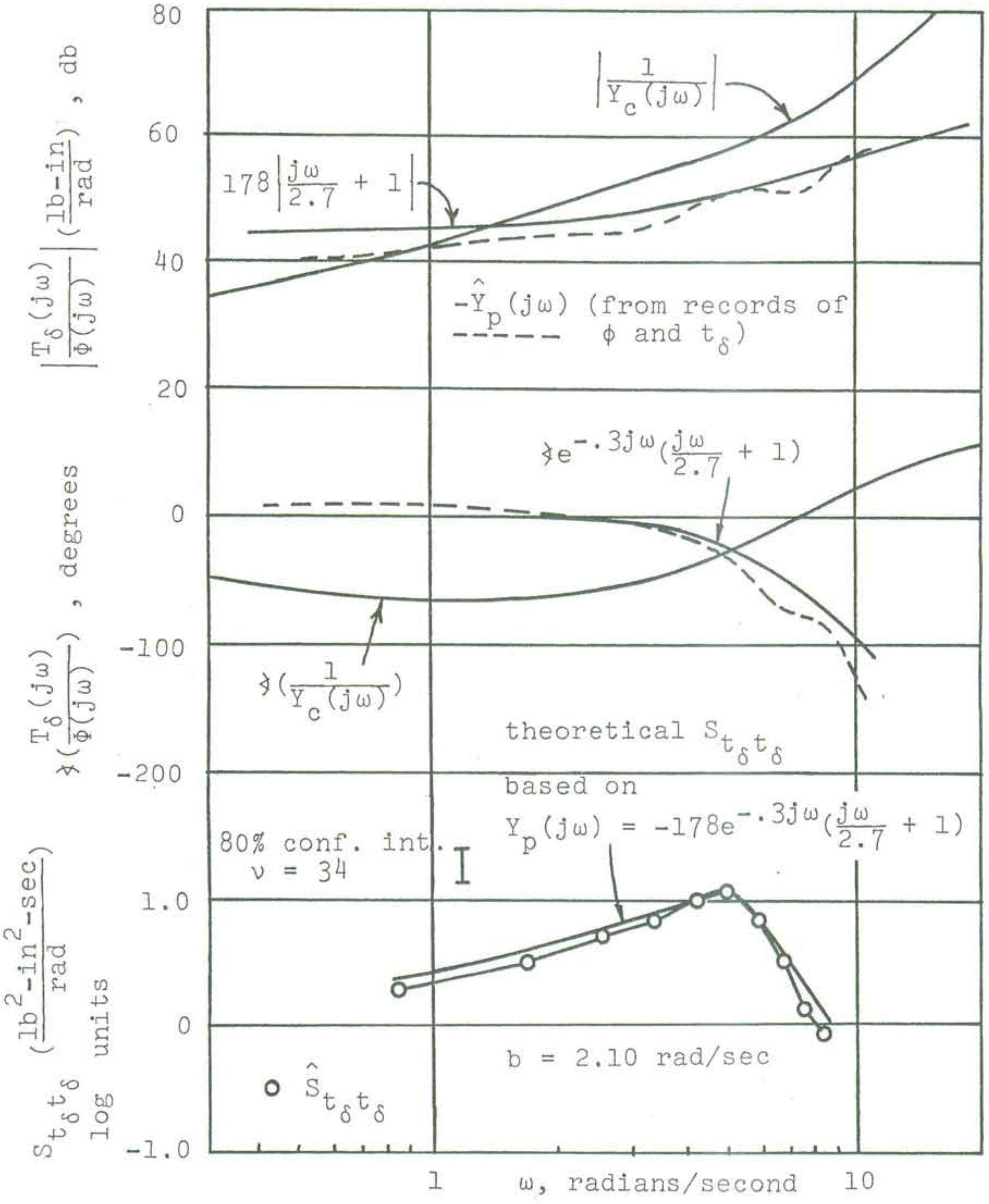

Figure 6.8a Estimation of $Y_p(j\omega)$, 30 mph; Rider A, Day 2; the test in which $Y_p(j\omega)$ evidenced the most lead.

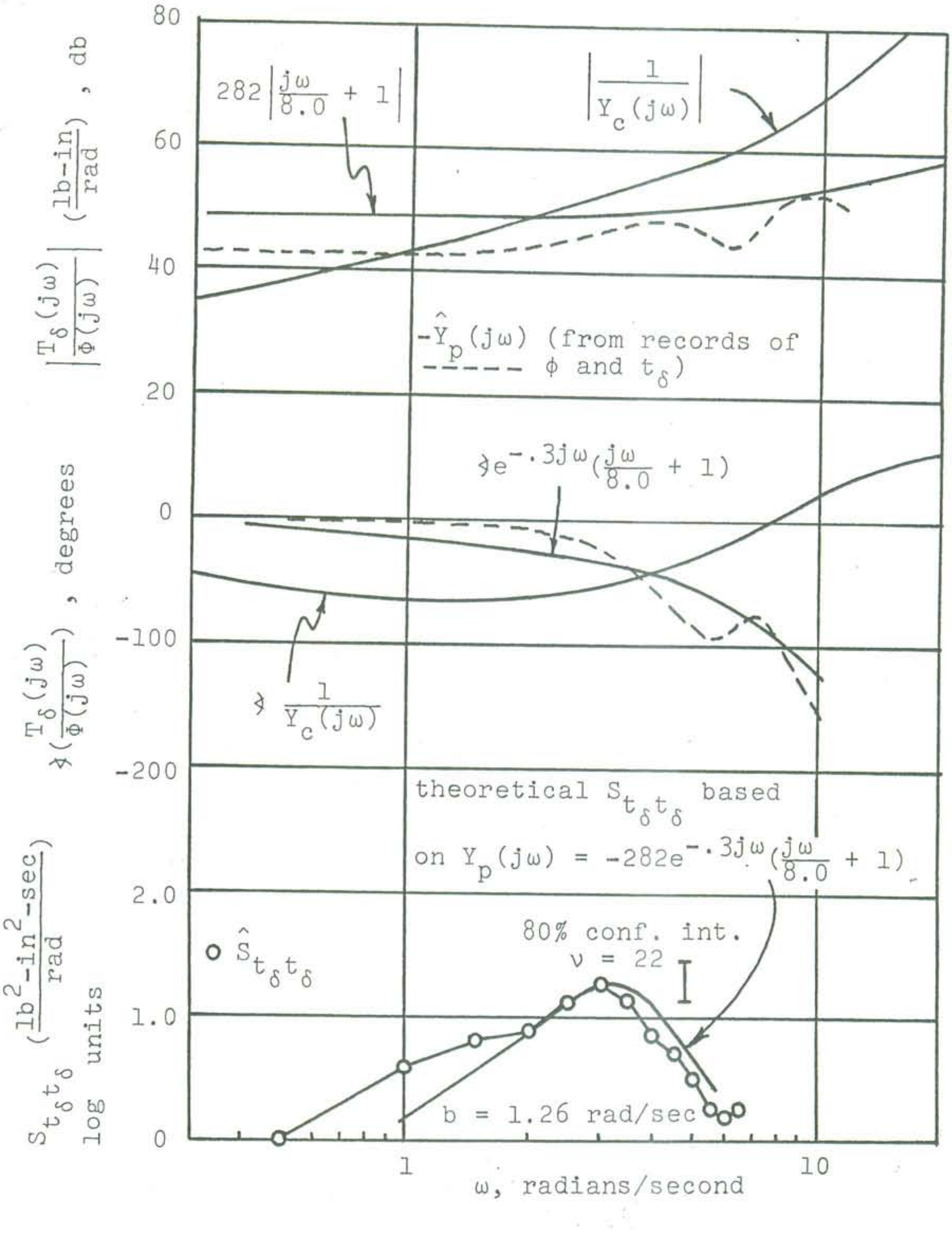

Figure 6.8b Estimation of $Y_p(j\omega)$, 30 mph; Rider A, Day 2.

containing lead equalization.) The $\hat{Y}_p(j\omega)$ Bode diagrams derived from data taken on the second day seemed to contain less bias and a lower level of instability than other sets of calculated results for $\hat{Y}_p(j\omega)$, possibly because the relatively high frequency content of the records obtained on the second day pushed the range of "good" identification to higher frequencies, where bias and instability effects are generally most noticeable.

The transfer function obtained for Rider A using data collected during the second test day was found to be (on the average)

$$\overline{\hat{Y}}_p(j\omega) = - 261 \, e^{-.3j\omega} \, (0.155j\omega + 1)(\frac{\text{lb-in}}{\text{radian}}). \qquad (6.6)$$

The transfer function of the controlled element, as computed from theory, together with the estimates of $Y_p(j\omega)$, yielded an average system phase margin of 48.6°.

The three 15-mph trials performed with Rider A on the first day were obviously not intended to be the basis for a comprehensive study of rider control activities at low speeds. However, the results of these tests do give a fairly good indication of how the rider must change his method of control as speed decreases.

In estimating $Y_p(j\omega)$ from the data collected at 15 mph, it was found that (1) the same results could be obtained regardless of whether roll angle or roll rate was employed in the analysis, and (2) when $\lambda=0$, the estimated transfer function tended toward $-Y_p(j\omega)$ rather than $\frac{1}{Y_c(j\omega)}$. Figure

6.9 shows a sample estimate of $Y_p(j\omega)$, when $\lambda = 0.3$ second. It is immediately seen that $Y_p(j\omega)$ contains a very low frequency lead, the break frequency of which is apparently well below 0.5 radian/second, if it exists at all. For the frequency range of interest here, rate control is implied (a differentiator in Y_p). The phase portion of the Bode diagram also indicates the usual time delay and possibly a lead at relatively high frequency. Hence, a transfer function of the form,

$$Y_p(j\omega) = - K_p j\omega e^{-\tau_p j\omega}(T_\ell j\omega + 1), \quad K_p > 0 \ , \qquad (6.7)$$

was chosen to fit the data. It was possible to fit theoretical t_δ spectra to the experimental t_δ spectra with a system phase margin of about 30°. However, the K_p values necessary to fit the spectra were several decibels lower than the values indicated by the $\hat{Y}_p(j\omega)$ Bode diagrams. Because of this discrepancy, Bode diagrams of $\hat{Y}_p\hat{Y}_c(j\omega)$ were constructed, where $\hat{Y}_c(j\omega)$ is the cross-spectral estimate of $Y_c(j\omega)$ (Section 6.2), and the parameters of $\hat{Y}_p(j\omega)$ were adjusted to give a system phase margin of about 30°. The resulting parameters of $\hat{Y}_p(j\omega)$ were in much better agreement with the values that were predicted from the $\hat{Y}_p(j\omega)$ Bode diagram.

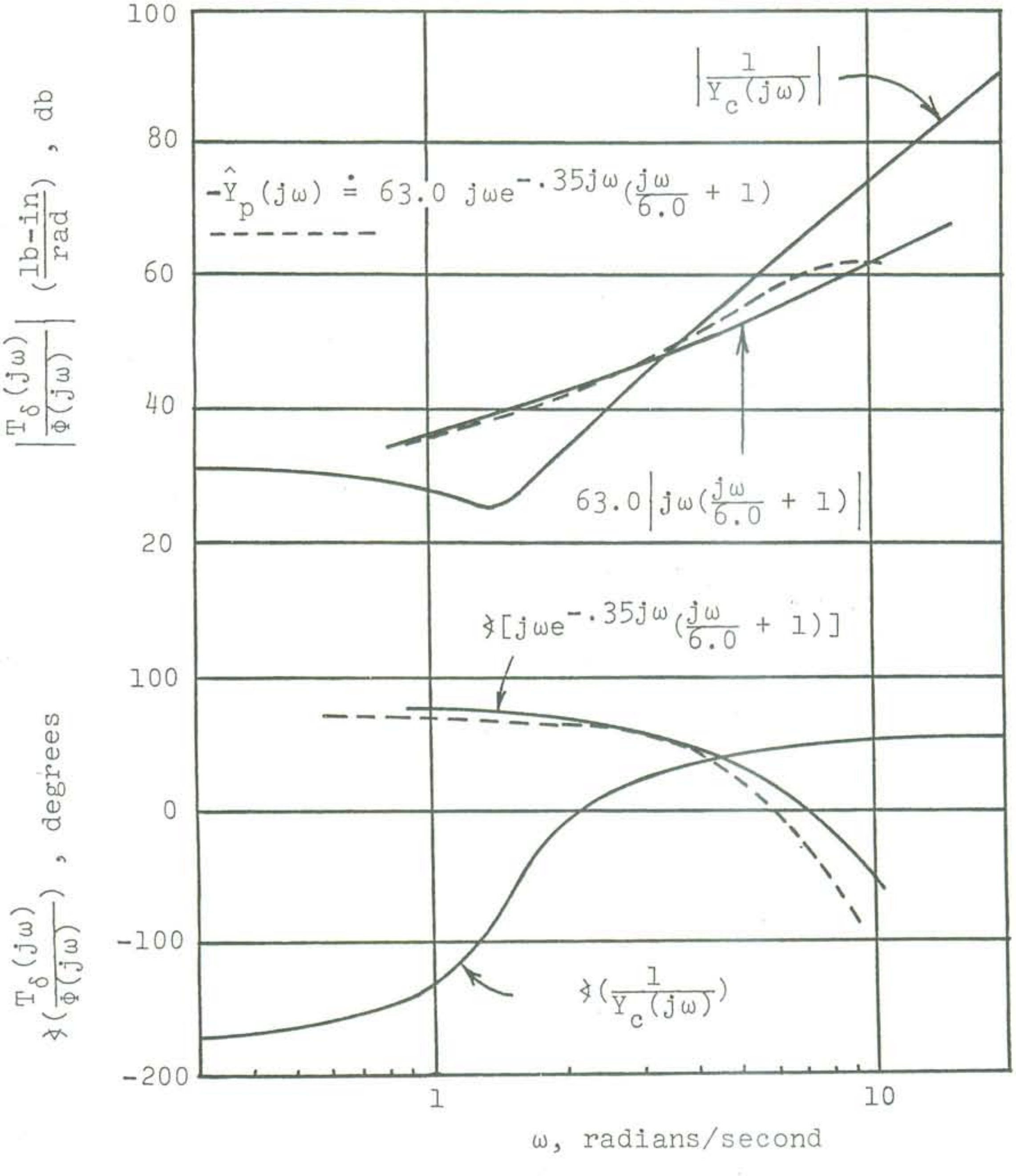

Figure 6.9. Estimation of $Y_p(j\omega)$, 15 mph.

The average transfer function obtained for the rider at 15 mph was

$$\bar{\hat{Y}}_p(j\omega) = - 75.6\ j\omega e^{-.30j\omega}(0.11\ j\omega + 1)\ ,$$

a result that indicates a system phase margin of about 25°, based on the experimental $Y_c(j\omega)$.

The results of the preceding two sets of 30 mph tests and the 15 mph tests are consistent with the "crossover model", used by Weir [16] in his theoretical analysis of the man-motorcycle system.

For example, Figure 6.10 shows Bode diagrams of $\bar{\hat{Y}}_p(j\omega)Y_c(j\omega)$ for the two sets of 30 mph data and of $\bar{\hat{Y}}_p(j\omega)\bar{\hat{Y}}_c(j\omega)$ for the 15 mph tests, $\bar{\hat{Y}}_c(j\omega)$ being the average estimated controlled element for the 15 mph tests. Estimated values of ω_c and τ_e for the crossover model, namely,

$$Y_p(j\omega)Y_c(j\omega) \doteq \frac{\omega_c\ e^{-\tau_e j\omega}}{j\omega}\ ,\ \omega \doteq \omega_c\ ,$$

are shown in Figure 6.10 for each of the three estimates of $Y_p(j\omega)Y_c(j\omega)$.

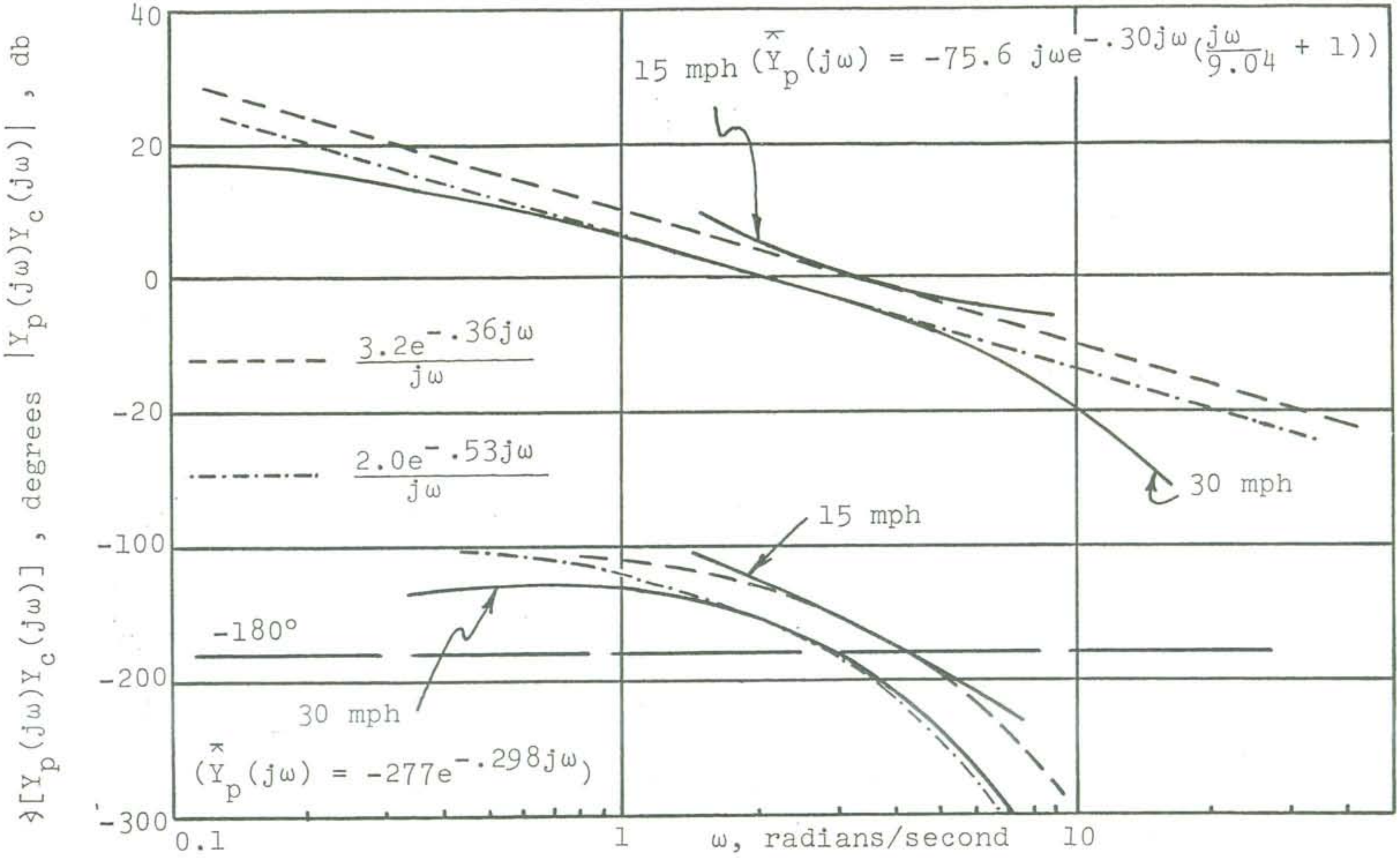

Figure 6.10a Crossover model approximations to $\hat{Y}_p(j\omega)\hat{Y}_c(j\omega)$, 15 mph, and $\hat{Y}_p(j\omega)Y_c(j\omega)$, 30 mph; Rider A, first day.

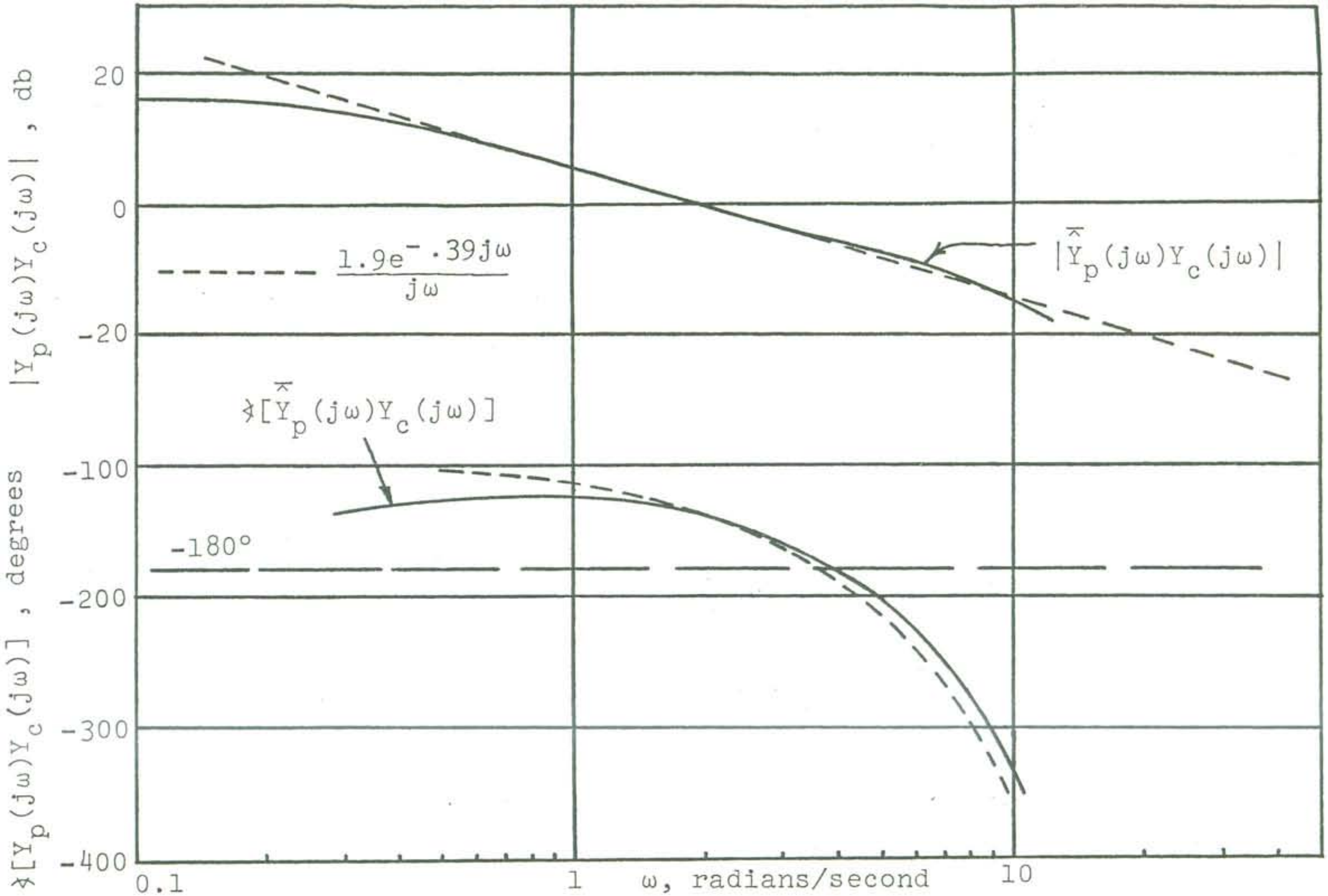

Figure 6.10b Crossover model approximation to $\overset{\wedge}{\bar{Y}}_p(j\omega)Y_c(j\omega)$, 30 mph; Rider A, second day. $\overset{\wedge}{\bar{Y}}_p(j\omega) = -261e^{-.30j\omega}(\frac{j\omega}{6.45} + 1)\ \frac{\text{lb-in}}{\text{radian}}$.

For $Y_p(j\omega)Y_c(j\omega)$ to "fit" the crossover model, it is necessary for the slope of $|Y_p(j\omega)Y_c(j\omega)|$ to be close to -20 db/decade for ω near ω_c, the crossover frequency. This requirement is easily met for moderate and high motorcycle speeds, such as 30 mph, since the slope of $|Y_c(j\omega)|$ is in fact -20 db/decade for a broad range of frequency. Thus, for a suitable choice of K_p, $|Y_p(j\omega)Y_c(j\omega)| = |K_p e^{-\tau_p j\omega} Y_c(j\omega)|$ will have this slope for a wide range of frequencies greater than and less than the crossover frequency of $Y_p(j\omega)Y_c(j\omega)$. As speed decreases, however, the weave mode damped natural frequency decreases, requiring various degrees of lead and rate control on the part of the rider. At 30 mph, it was seen that lead equalization was optional[1]; for 15 mph, both rate control and lead were required. In fact, from consideration of the theoretical $Y_c(j\omega)$ at 15 mph, it would be expected that a rider transfer function closer to the form,

$$Y_p(j\omega) = - K_p e^{-\tau_p j\omega}(j\omega)^2 ,$$

would be required for a crossover frequency greater than the damped natural frequency of the weave mode, since the slope of $|Y_c(j\omega)|$ is -60 db/decade for such a frequency (e.g.,

---

[1] From the point of view of the crossover model, the ideal break frequency of the lead equalization is about 8.5 radians/second. If τ_p for the second day tests is reduced to between 0.25 and .30 second, the average value of $1/T_\ell$ can be made to be 8.5 radians/second. It may be that the rider tends to select this amount of lead on the average.

2 radians/second). However, the experimental $|Y_c(j\omega)|$ slope seems to be less steep (between -60 and -40 db/decade), perhaps due to different locations of the capsize mode break frequency and the damped natural frequency of the weave mode than those locations predicted by the theory. For the experimental $Y_c(j\omega)$, a rider transfer function of the form of Equation (6.7) is sufficient to bring the slope of $|\hat{Y}_p(j\omega)\hat{Y}_c(j\omega)|$ close to -20 db/decade at the crossover frequency.

The constant gain and time delay form of $Y_p(j\omega)$ is a good description of the motorcyclist's method of controlling the roll angle throughout a speed range in which the motorcycle usually operates (speeds greater than, say, 25 mph). This transfer function also lends itself readily to intuitive interpretation. Basically, if the rider wishes to change the roll angle, he applies a steering torque to the handlebars of opposite sign to the direction of the desired change. For example, if the machine is falling to the right ($\phi>0$), the rider applies a positive (right) steering torque, which causes the tires to sideslip and produce positive forces on the vehicle, forces which roll the vehicle in the negative ϕ direction. Although negotiating turns was not studied here, experience [19] has indicated the same behavior at least in a qualitative sense: to enter a right turn, the rider first applies a negative (left) steering torque to "set up" the needed lean to the right. Likewise, leaving the right turn requires a positive (right) torque to zero the roll angle.

6.5 TRANSFER FUNCTIONS FOR OTHER RIDERS

Riders B and C were tested at 30 mph only, on one day per rider. In general, the results of testing these two riders were very similar to each other and were more like the results obtained in the 30 mph tests conducted with Rider A on the first day rather than on the second day.

Specifically, the dominant frequencies in the power spectra of steering torque were relatively low, both for Riders B and C. For Rider B, these frequencies ranged from about 1.5 to 2.5 radians/second. For Rider C, they ranged from about 1.7 to 2.7 radians/second. Also, the t_δ spectra of both riders tended to be more flattened (the peak less pronounced) than those of Rider A.

From Bode diagrams of $\hat{Y}_p(j\omega)$ and the t_δ spectra, it was determined that a constant gain and time delay was a good fit to the transfer functions exhibited by Riders B and C. Sample Bode diagrams of $\hat{Y}_p(j\omega)$ and t_δ spectra are shown in Figures 6.11 and 6.12. As expected, the identification of $Y_p(j\omega)$ tended to be poorer when roll rate was used in the analysis,

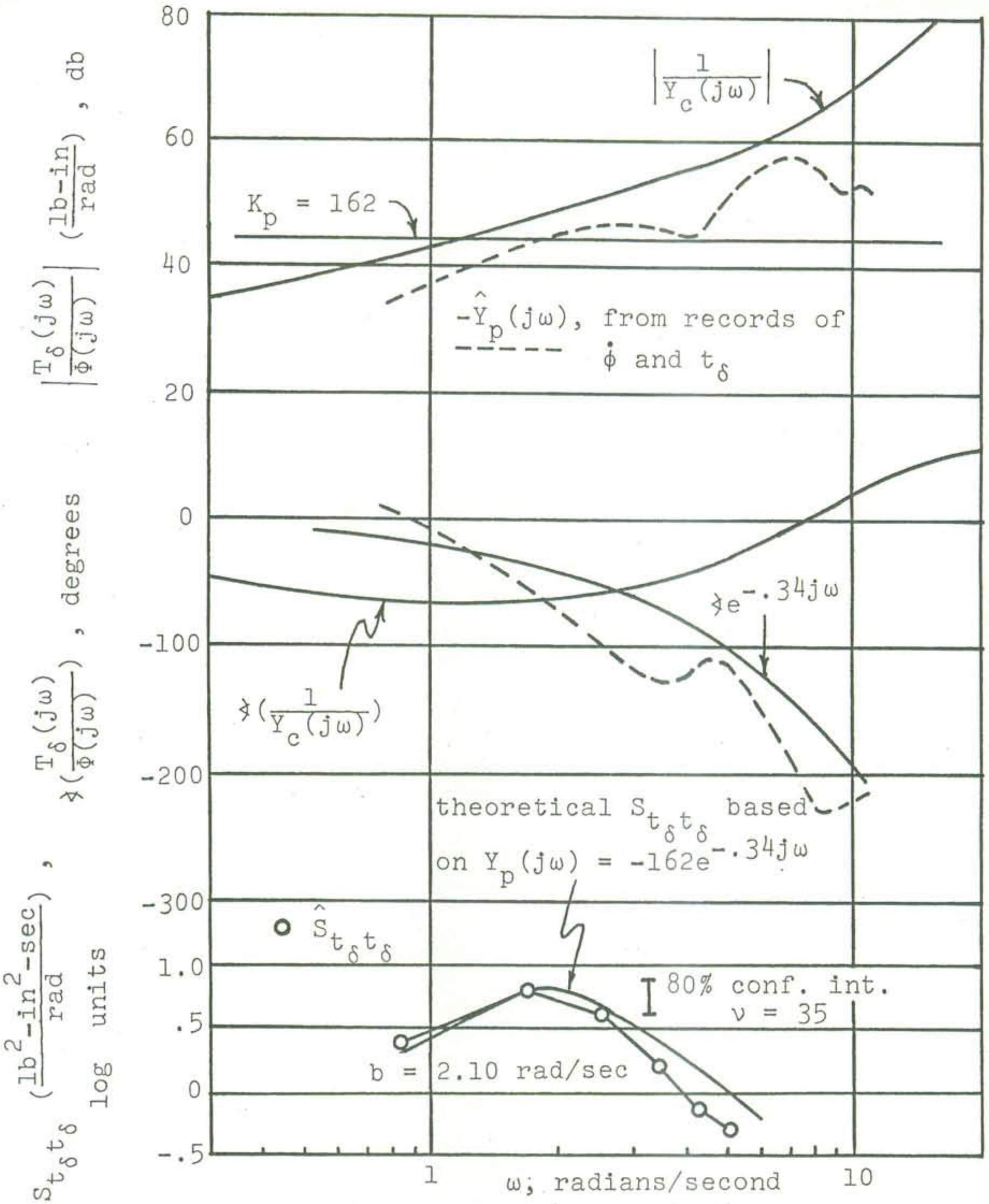

Figure 6.11a Estimation of $Y_p(j\omega)$, 30 mph; Rider B.

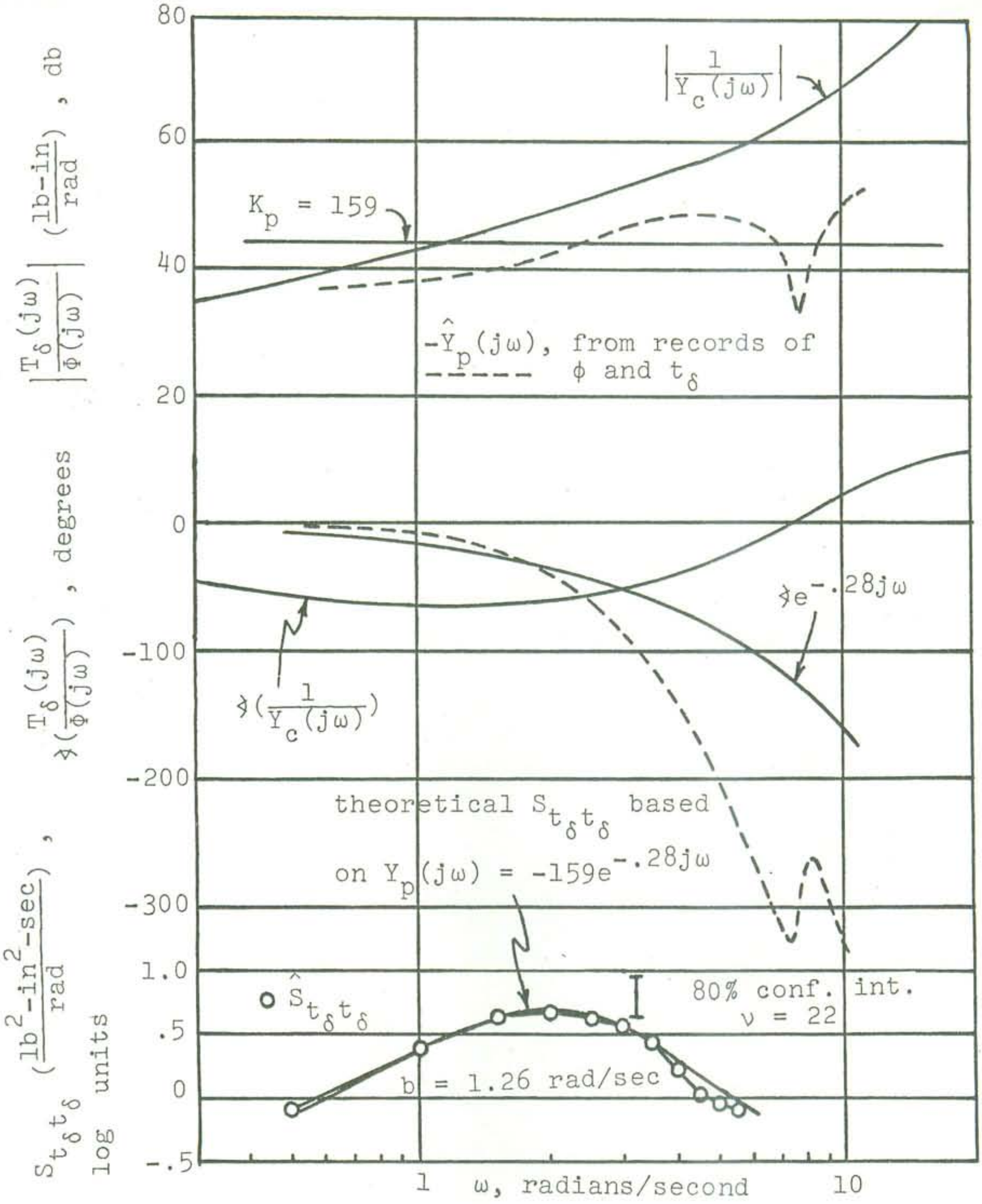

Figure 6.11b Estimation of $Y_p(j\omega)$, 30 mph; Rider B. Extreme example of excessive high frequency phase lag in $\hat{Y}_p(j\omega)$.

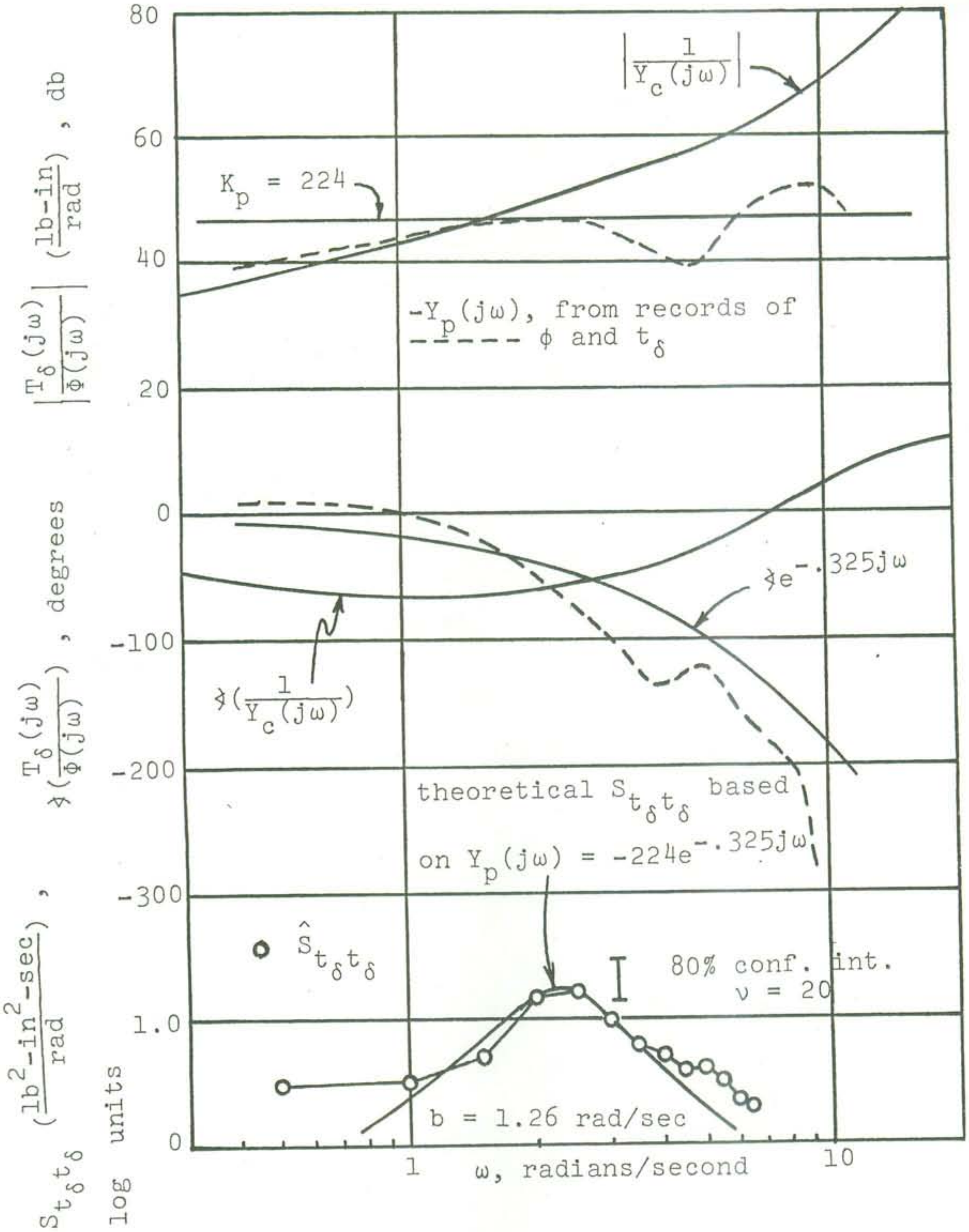

Figure 6.12a Estimation of $Y_p(j\omega)$, 30 mph; Rider C.

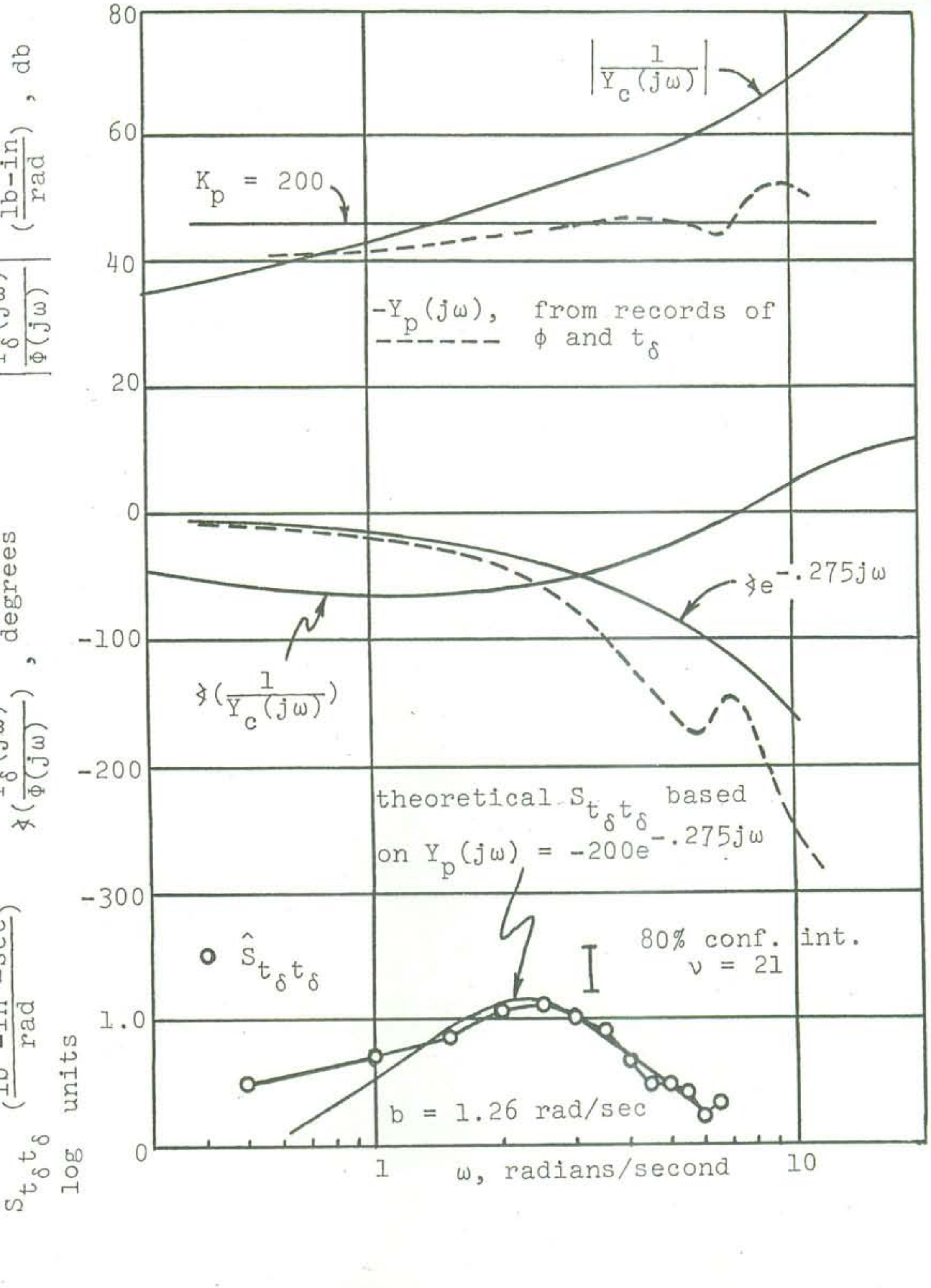

Figure 6.12b Estimation of $Y_p(j\omega)$, 30 mph; Rider C.

rather than roll angle, although this difference was not as great as was noted with respect to data produced by Rider A. The average transfer function obtained for Rider B was

$$\hat{\bar{Y}}_p(j\omega) = - 167\ e^{-.33j\omega} \quad \text{(lb-in/radian).} \qquad (6.8)$$

The mean of the phase margins resulting from the individual $\hat{Y}_p(j\omega)$ estimates for Rider B was 41.4^o. Similarly, the average transfer function exhibited by Rider C was

$$\hat{\bar{Y}}_p(j\omega) = - 206\ e^{-.30j\omega} \quad \text{(lb-in/radian),}$$

and the average phase margin for Rider C was 39.1^o.

The behavior of Rider B differed from that of Riders A and C with respect to the measured levels of steering torque, roll angle, etc. (Table 6.1). Furthermore, Rider B complained about the relative flexibility of the steering torque bar, which did not bother the other riders. Apparently, Rider B tolerated a smaller error level than the other riders. While this error level depended to some extent upon his choice of $Y_p(j\omega)$, it was found to remain much more constant between tests than did $\hat{Y}_p(j\omega)$. Hence, it is felt that Rider B reduced the error level by simply attenuating his remnant.

It is interesting to note that most of Rider B's motorcycle experience was trail riding, while the other riders received their experience on the road. Due to large ground disturbances, trail riding probably requires "tighter" control of the motorcycle than road riding. Hence, Rider B was apparently tending to carry his off-road techniques over to on-road riding.

While system gain margins were not calculated for all of the tests, the gain margins that were calculated give an idea of their relative sizes. The lowest gain margin calculated for the 30 mph tests were about 4 db (Rider A, first day). Rider A, on the second day, and Rider C produced gain margins of about 6 db. Rider B, with gain margins of about 9 db, probably was the most conservative rider, even though his phase margins were lower than those of Rider A on the second day.

Table 6.2 summarizes the rider transfer functions obtained. In this table, the confidence intervals for the means of the $Y_p(j\omega)$ parameters and the phase margins assume that the estimators of those means are unbiased[1]. The variability in transfer function estimates implied by the

---

[1] If X is a random variable and $E(X) = \mu$, then $\overline{x}$ is an unbiased estimator of μ if $E(\overline{x}) = \mu$. ($E(X)$ means "expected value of X".)

TABLE 6.2

SUMMARY OF RIDER TRANSFER FUNCTIONS

	Day of Test	1	1	2	3	4
	Speed, mph	15	30	30	30	30
	Rider	A	A	A	B	C
	Form of $\hat{Y}_p(j\omega)$	$-K_p j\omega e^{-\tau_p j\omega} \cdot (T_\ell j\omega + 1)$	$-K_p e^{-\tau_p j\omega}$	$-K_p e^{-\tau_p j\omega} \cdot (T_\ell j\omega + 1)$	$-K_p e^{-\tau_p j\omega}$	$-K_p e^{-\tau_p j\omega}$
Mean Values of Estimated Quantities	K_p, $\frac{\text{lb-in}}{\text{radian}}$	75.6	277	261	167	206
	τ_p, seconds	0.300	0.298	0.300	0.328	0.299
	$1/T_\ell$ $\frac{\text{radians}}{\text{second}}$	9.04		6.45		
	ϕ_m, degrees	25	28.3	48.6	41.4	39.1
90% Confidence Intervals	K_p, $\frac{\text{lb-in}}{\text{radian}}$	(53.6, 97.6)	(219, 335)	(236, 286)	(152, 182)	(185, 227)
	τ_p, seconds	(.216, .384)	(.260, .336)		(.287, .369)	(.276, .322)
	$1/T_\ell$ $\frac{\text{radians}}{\text{second}}$	(3.37, 11.42)		(5.27, 7.41)		
	ϕ_m, degrees		(15.2, 41.4)	(42.4, 54.8)		(36.7, 41.5)
Parameters for Cross-over Model, Based on Average $\hat{Y}_p(j\omega)$	ω_c, $\frac{\text{radians}}{\text{seconds}}$	3.2	2.0	1.9	1.3	1.5
	τ_e, seconds	0.36	0.53	0.39	0.66	0.58
Average Estimated Linear Coherence	$\bar{\rho}^2$	0.61	0.57	0.335	0.17	0.21

the confidence intervals lumps together (1) actual changes in rider behavior between tests under the same condition, (2) errors in identification and spectral estimation, and (3) errors in curve-fitting.

The confidence intervals were constructed as follows. Let X be a random variable that is measured in an experiment (such as K_p, τ_p, etc.), and let $\mu = E(X)$. If there are n such measurements, x_i, i=1, 2, ...n, the x_i are independent and normally distributed, and $\overline{x} = \frac{1}{n} \sum_{i=1}^{n} x_i$ and $s^2 = \frac{1}{n-1} \sum_{i=1}^{n} (x_i-\overline{x})^2$ are the sample mean and variance, respectively, then it may be shown [50] that $\frac{(\overline{x}-\mu)\sqrt{n}}{s}$ follows a t-distribution with n-1 degrees of freedom. To apply this fact to the motorcycle test results, it is assumed that the x_i are independent. To test for a normal distribution, the x_i and functions of the x_i were plotted on normal probability paper, a straight line indicating normality [49]. The following random variables were found to approximately follow a normal distribution: K_p, τ_p, and $\text{antilog}_{10}(\frac{1}{10T_\ell})$. Phase margin ($\phi_m$) followed a normal distribution except for the Rider B data. When the sample size was only three, it was assumed that K_p, τ_p, $\text{antilog}_{10}(\frac{1}{10T_\ell})$ and ϕ_m were normally distributed.

Usually, when human operator transfer functions are determined experimentally (e.g., [26]), the disturbances *external* to the operator represent the largest excitation to the man-machine system, and nearly all of the operator's output is linearly correlated to his error signal. In the present study, however, where the operator's remnant is the greatest disturbance to the system, it would not be expected that $\hat{\rho}^2$ should approach unity, since a value of one would imply that the remnant was identically zero. Thus, the average values of $\hat{\rho}^2$ shown in Table 6.2 are considerably less than one. In Appendix G, it is seen that an accurate identification of a "rider" transfer function from artificially created data is possible even though the values of ρ^2 are on the order of 0.15.

6.6 REMNANT ESTIMATES

The estimated NMSE ($= 1 - \hat{\rho}^2$, when $\lambda = \tau_p$) indicates the fraction of the total power in a steering torque record (i.e., the area under the t_δ power spectrum) that is remnant. In all the tests performed, the average NMSE is very large, about 0.4 to 0.8. The NMSE tended to be higher for Riders B and C, especially B, and may be a reason why transfer functions for these riders were more difficult to identify.

The remnant spectrum gives an indication of the degree to which bias has been removed from the $Y_p(j\omega)$ estimate. However, the more biased $\overset{\barwedge}{Y}_p(j\omega)$ is, the wider the bandwidth of the estimated remnant is. Hence, observing the autocorrelation function or power spectrum of the estimated remnant does not in practice give a good indication of the degree of bias in $\hat{Y}_p(j\omega)$, but the bias can be qualitatively estimated by comparing the parameter estimates based on the Bode diagrams of $\hat{Y}_p(j\omega)$ with those estimates based on the t_δ spectra.

On the basis of the remnant estimates and subsequent spectral analysis of these estimates, it was found that the power spectrum of $\hat{n}(t)$ was approximately

$$S_{\hat{n}\hat{n}}(\omega) = \frac{\text{Constant}}{25 + \omega^2} , \qquad (6.9)$$

especially when roll rate has been used in the analysis. Some example remnant spectra are shown in Figure 6.13. Only the constant in Equation (6.9) was obviously rider-dependent or speed-dependent. Thus, it appears that with respect to the analog filter applied to the data, the remnant is indeed "white". Since a "white" remnant is ideal from the point of view of removing bias from $\hat{Y}_p(j\omega)$, it is possible that, say, a 10 radians/second filter would have produced better results. On the other hand, permitting higher frequencies in the data degrades the accuracy of the impulse response method. It appears that a study of the effects of data filtering on the use of the time shifting method would be very useful.

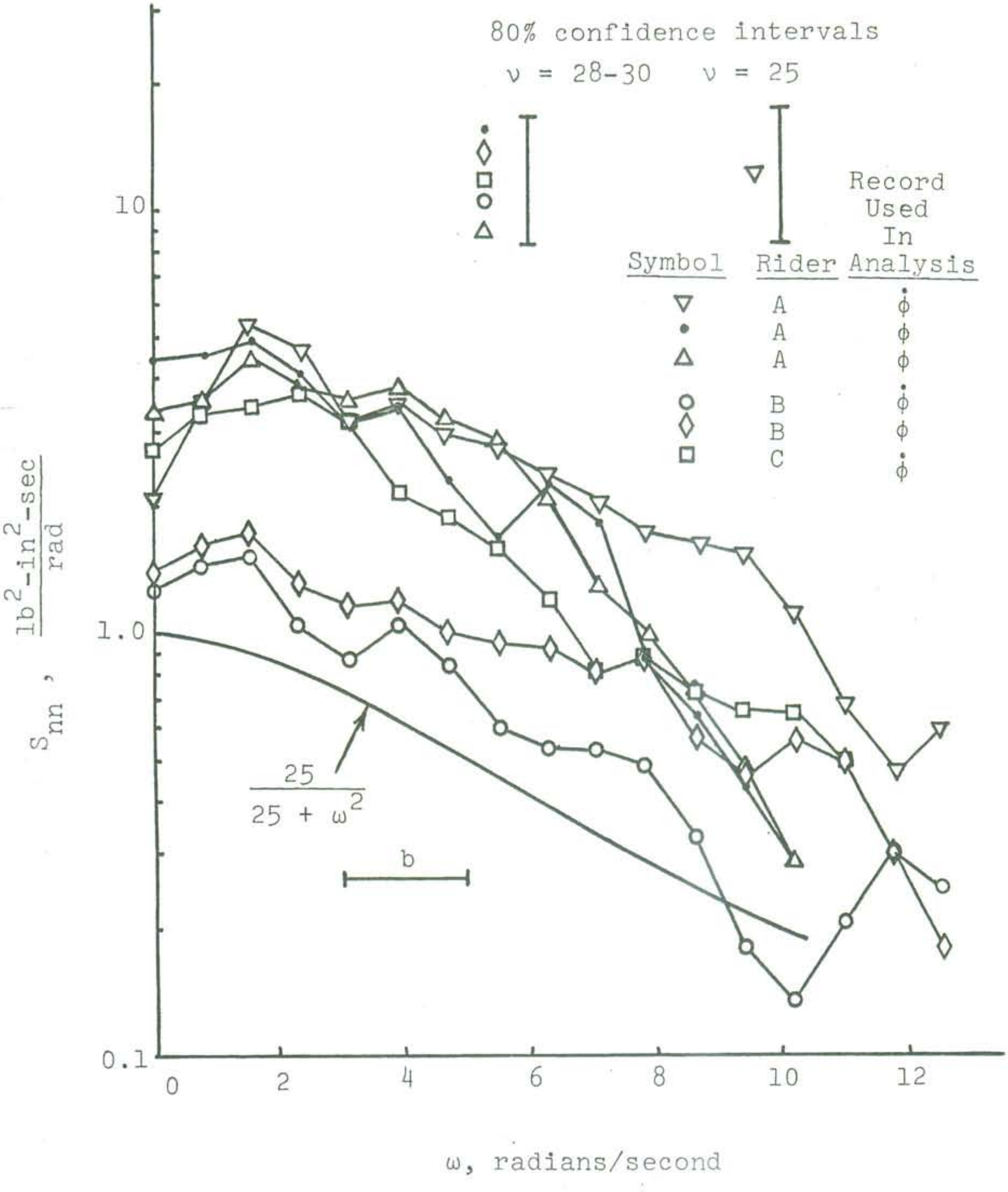

Figure 6.13. Estimated remnant spectra.

7. CONCLUSIONS

The basic objectives of the research described in this dissertation have been to (1) present experimental results and relate them to theoretical studies of both the uncontrolled motorcycle and the man-motorcycle system, and (2) study aspects of the dynamics of the motorcycle which have not been previously investigated.

On the basis of the experimental and theoretical studies of the dynamics of the uncontrolled motorcycle, the following summarizing remarks can be made.

1. The equations of motion derived by Sharp [14] are generally realistic with respect to the weave and capsize modes of motion, except at very low speeds (on the order of 10 mph).

2. These equations of motion do not accurately describe steering wobble motions below about 35 mph. Most likely, a more realistic representation of the dynamic characteristics of the pneumatic tire is needed to produce better agreement between theory and experiment.

3. Experimentally, it was not possible to locate a speed range of complete stability or a speed range in which the damping of the weave mode was near zero. The motorcycle equations of motion, however, predict the existence of such speed ranges in the neighborhood of 15 mph.

4. Inclusion of tire lateral force and aligning moment arising from instantaneous curvature of the path of the contact patch chiefly affects the wobble mode, but gives no significant improvement in the experimental correlation.

5. Tire overturning moments and aligning torques due to tire inclination tend to destabilize and stabilize, respectively, the capsize mode. If both are included in the tire model, the effects almost exactly cancel each other, at least for the motorcycle and tires studied in this investigation.

6. A theoretical evaluation of the relative merits of coulomb friction and viscous steering dampers shows the advantage to be with the latter. The viscous damper does not decrease roll stability, while the coulomb friction damper does. Also, the effectiveness of the coulomb friction damper is dependent upon the magnitude of the steering disturbance, and the effectiveness of the viscous damper is not.

The analysis of roll-stabilization experiments, in which the three experienced riders stabilized the vehicle by applying a steering torque to the handlebars, yielded several important results, which are listed below.

1. During normal operation on a paved road in good condition, the primary source of excitation to the man-motorcycle system is the rider's "remnant". This fact allows accurate identification of the transfer function of the controlled element ($Y_c(j\omega)$) by open-loop cross-spectral

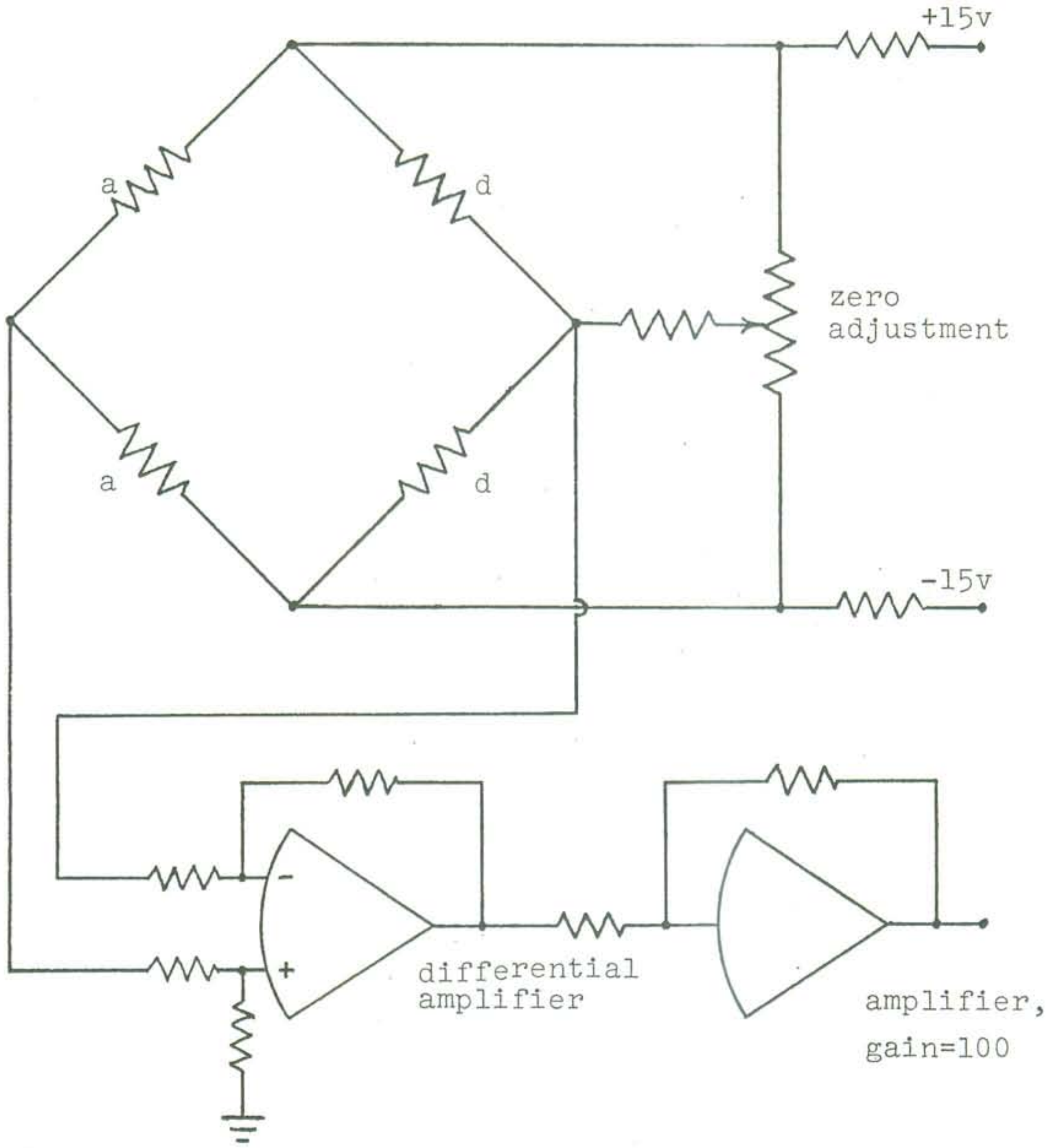

a: active strain gages
d: dummy strain gages (for temperature compensation)

Figure E.2 Strain gage circuit for the measurement of steering torques.

APPENDIX F

IDENTIFICATION OF TRANSFER FUNCTIONS: COMPUTER PROGRAMS

F.1 CROSS-SPECTRAL ANALYSIS

A program prepared by the Statistical Research Laboratory (SRL) of The University of Michigan, based on one of several programs in the "Bimed" series of the University of California, Los Angeles [53], was used for the estimation of auto- and cross-correlation functions, power spectra, cross-spectra, and transfer functions from experimental data.

Let $x'(t)$ and $y'(t)$ be random processes, which are the input and output, respectively, of a linear system, the transfer function of which is $G(j\omega)$. Let $x'(kh)$ and $y'(kh)$, $k=k_o$, k_o+1, ... K, be the sampled version of $x'(t)$ and $y'(t)$, where h is the constant time interval between samples.

The SRL program first removed offset and drift[1] from the data. New time series were defined as follows:

---

[1] In this discussion, a random process $w(t)$ possesses offset if for any t, $E[w(t)] \neq 0$. The random process is said to possess drift or trends if $E[w(t)]$ is a linear function of time.

$$x(kh) = x'(kh) - a_o - a_1 kh,$$

$$y(kh) = y'(kh) - b_o - b_1 kh,$$

where a_o, a_1, b_o and b_1 were determined by performing least squares linear regression analyses on the input and output series.

The quantities of interest were then estimated as follows.

1. Autocovariance function:

$$\hat{C}_{xx}(\ell h) = \frac{1}{K-k_o+1-\ell} \sum_{k=k_o}^{K-\ell} x(kh)x[(k+\ell)h], \quad \ell=0,1,2,\ldots L$$

2. Autocorrelation function:

$$\hat{r}_{xx}(\ell h) = \frac{C_{xx}(\ell h)}{C_{xx}(0)}, \quad \ell=0,1,2,\ldots L$$

3. Cross-covariance function:

$$\left.\begin{aligned} \hat{C}_{xx}(\ell h) &= \frac{1}{K-k_o+1-\ell} \sum_{k=k_o}^{K-\ell} x(kh)y[(k+\ell)h] \\ \hat{C}_{xy}(-\ell h) &= \frac{1}{K-k_o+1-\ell} \sum_{k=k_o}^{K-\ell} x[(k+\ell)h]y(kh) \end{aligned}\right\} \ell=0,1,2,\ldots L$$

4. Cross-correlation function:

$$\hat{r}_{xy}(\ell h) = \frac{\hat{C}_{xy}(\ell h)}{\sqrt{\hat{C}_x(0)\hat{C}_y(0)}}$$

5. Auto-spectrum:

a. Unsmoothed estimate:

$$\hat{S}_{xx}(\tfrac{n\pi}{Lh}) = \frac{2h}{\pi} \sum_{\ell=0}^{L} \varepsilon_\ell \; C_{xx}(\ell h)\cos \frac{n\ell\pi}{L} \text{ , } n=0,1,\ldots L,$$

$$\text{where} \quad \varepsilon_\ell = \begin{cases} 1, & 0 < \ell < L \\ 1/2, & \ell = 0,L \end{cases}$$

b. Spectral estimate as smoothed by "hamming":

$$\bar{\hat{S}}_{xx}(0) = .54 \; S_x(0) + .46 \; S_x(\tfrac{\pi}{Lh})$$

$$\bar{\hat{S}}_{xx}(\tfrac{n\pi}{Lh}) = .23 \; S_x \left[\frac{(n-1)\pi}{Lh}\right] + .54 \; S_x(\tfrac{n\pi}{Lh})$$

$$+ .23 \; S_x \left[\frac{(n+1)\pi}{Lh}\right] \text{ , } \quad 0 < n < L$$

$$\bar{\hat{S}}_{xx}(\tfrac{\pi}{h}) = .54 \; S_x(\tfrac{\pi}{h}) + .46 \; S_x \left[\frac{(L-1)\pi}{Lh}\right]$$

6. Cross-spectrum:

$$S_{xy}(\frac{n\pi}{Lh}) \;=\; L_{xy}(\frac{n\pi}{Lh}) + j\ Q_{xy}(\frac{n\pi}{Lh})$$

where the unsmoothed estimates of the co-spectrum L_{xy} and the quadrature spectrum Q_{xy} were calculated by

$$\hat{L}_{xy}(\frac{n\pi}{Lh}) = \frac{h}{\pi} \sum_{\ell=0}^{L} \varepsilon_{\ell}[C_{xy}(\ell h) + C_{xy}(-\ell h)] \cos \frac{n\ell\pi}{L} ,$$

$$\hat{Q}_{xy}(\frac{n\pi}{Lh}) = \frac{h}{\pi} \sum_{\ell=0}^{L} \varepsilon_{\ell}[C_{xy}(\ell h) - C_{xy}(-\ell h)] \cos \frac{n\ell\pi}{L} ,$$

where the ε_{ℓ} are as previously defined and n=0,1,2,...L. The estimates $\hat{L}_{xy}$ and $\hat{Q}_{xy}$ were then smoothed by "hamming", as is the case of the auto-spectrum, to give the smoothed estimates $\overset{\barwedge}{L}_{xy}$ and $\overset{\barwedge}{Q}_{xy}$.

7. Transfer function:

$$|\hat{G}(\frac{n\pi}{Lh})| = \frac{\sqrt{\overset{\barwedge}{L}_{xy}{}^{2}(\frac{n\pi}{Lh}) + \overset{\barwedge}{Q}_{xy}{}^{2}(\frac{n\pi}{Lh})}}{\overset{\barwedge}{S}_{xx}(\frac{n\pi}{Lh})} , \quad n=0,1,2,\ldots L,$$

$$\measuredangle\ \hat{G}(\frac{n\pi}{Lh}) = -\arg\left[\overset{\barwedge}{L}_{xy}(\frac{n\pi}{Lh}) + j\ \overset{\barwedge}{Q}_{xy}(\frac{n\pi}{Lh})\right] , \quad n=0,1,2,\ldots L,$$

where $|\hat{G}(\frac{n\pi}{Lh})|$ and $\sphericalangle\, \hat{G}(\frac{n\pi}{Lh})$ are the estimated gain and phase, respectively, of the transfer function for the system having x as input and y as output, for the frequency $\omega = \frac{n\pi}{Lh}$ radians/second.

8. Squared Coherence:

$$C^2_{hxy}(\frac{n\pi}{Lh}) = \frac{\hat{\bar{L}}^2_{xy}(\frac{n\pi}{Lh}) + \hat{\bar{Q}}^2_{xy}(\frac{n\pi}{Lh})}{\hat{\bar{S}}_{xx}(\frac{n\pi}{Lh})\ \hat{\bar{S}}_{yy}(\frac{n\pi}{Lh})} , \quad n=0,1,2,\ldots L.$$

To use the spectral analysis program, three important parameters, L, the number of lags, h, the time step, and $T = (K - k_o + 1)h$, the sample record length, must be read into the program. The methods of selection of these parameters is now discussed.

The spectral analysis program restricts the user to a "hamming" spectral window. However, as indicated in [55], the shape of a spectral window is much less important than its bandwidth. Hence, restriction to a "hamming" window is no great handicap.

As discussed in [55], the bandwidth of the spectral window employed in a spectral analysis influences the bias, variance and resolution of the spectral estimator. Greater spectrum detail (resolution of peaks) and less bias can be achieved by the use of a narrow bandwidth. However, a wide bandwidth gives the spectral estimator less variance. In general, selection of the window bandwidth depends upon the nature of the spectrum (degree of smoothness), plus the features of the spectrum which are of interest.

The bandwidth of the "hamming" spectral window is given by [55]

$$b = \frac{1}{\int_{-\infty}^{\infty} w^2(u)du} ,$$

where [56]

$$w(u) = \begin{cases} .54 + .46 \cos \frac{\pi u}{Lh} , & |u| \leq Lh \\ 0 & |u| > Lh . \end{cases}$$

Hence,

$$b = \left[\int_{-Lh}^{Lh} (.54 + .46 \cos \frac{\pi u}{Lh})^2 du\right]^{-1} = \frac{1.256}{Lh} \tag{F.1}$$

Once h has been chosen, the bandwidth b is seen to be determined by the choice of L, the number of lags used in the estimation.

The choice of the time step h is also important in a spectral analysis, and must be chosen with reference to the analog filter which has been applied to the signal before digitizing. The highest frequency (the Nyquist or "folding" frequency) which can be detected from data spaced h seconds apart is 1/2h cycles/second (π/h radians/second). If frequencies higher than 1/2h were present in the original signal after filtering, the higher frequencies would be identified as a frequency less than 1/2h. This is termed "aliasing" of frequencies. To avoid aliasing, it is necessary to choose 1/2h to be larger than any frequencies in the filtered signal having a substantial amplitude. With a first order filter having its break point at 5 radians/second (.796 cycles/second) the amplitude of a filtered spectrum at 2 cycles/second would be about 15% of the amplitude of an unfiltered spectrum at that frequency. A visual inspection of the unfiltered analog road data indicated that the signal amplitudes at frequencies greater than 2 cycles/second were considerably smaller than lower frequency amplitudes. Hence, $h = 0.2$ or 0.25 second was found to be a sufficiently small spacing, for which the Nyquist frequencies are 2.5 and 2.0 cycles/second, respectively.

The number of statistical degrees of freedom associated with a smoothed spectral estimator window is given by [55]

$$\nu = \frac{2T}{\int_{-\infty}^{\infty} w^{2}(u)du} .$$

From Equation (F.1), for a hamming spectral window, this number is

$$\nu = 2.512 \frac{T}{Lh} .$$

To detect a detail of width a in a spectrum, it is shown in [55] that the bandwidth b of the spectral window should be less than a. Also, increasing the record length T decreases the variance of the spectral estimator, which means that peaks in the estimated spectrum are more likely to indicate peaks in the real spectrum, rather than variance in the estimator. From [55], the record length is determined by

$$T = \frac{\nu}{2a} \tag{F.2}$$

In this study, T/Lh is usually about 10, so that $\nu \doteq 25$. From Equation (F.2), a record length of 50 seconds would allow the identification of detail of width 0.25 cycles/second, or 1.57 radians/second. (Road tests were approximately 50-55 seconds in length.) Smaller details could be the result of variance in the estimator.

It is shown in [55] that

$$\frac{\nu \bar{\hat{S}}_{xx}(\omega)}{S_{xx}(\omega)}$$

is a random variable having approximately a chi-square distribution with ν degrees of freedom. This fact can be used in setting up a confidence interval for the spectrum estimate at a particular frequency, using a conventional chi-squared distribution table.

F.2 IMPULSE RESPONSE METHOD

Since no existing computer programs employing the impulse response method of linear, time-invariant system identification were found at The University of Michigan, such a program was written for this study. The necessary equations were taken directly from the literature [38, 39, 44, 57] and are described here.

Consider again the problem of identifying a system, given the random processes $x(t)$ as input and $y(t)$ as output. Let $g(\tau)$ represent the impulse response function of the system, which is assumed to be physically realizable, so that $g(\tau) = 0$ for $\tau < 0$. The processes $x(t)$ and $y(t)$ are then related by the convolution integral

$$y(t) = \int_0^\infty g(\tau)\ x(t-\tau)d\tau \qquad (F.3)$$

Further assume that $g(\tau) = 0$ for $\tau > \tau_M$, that $x(t)$ and $y(t)$ have been sampled at time instants h seconds apart, and that there are K samples per series. A discrete approximation to Equation (F.3) is

$$y(kh) \doteq h \sum_{m=1}^{M} g(mh)\ x\ [(k-m+1)h],\ k=k_o,k_o+1,\ldots K. \tag{F.4}$$

In a practical situation, $x(t)$ and $y(t)$ are transducer voltages which may contain errors due to drift and/or offset. Drift is an instrumentation error, while offset may be caused by instrumentation errors or, in the man/vehicle situation, by operation about a non-zero value, such as when the vehicle is "out of trim". A compensation for drift and offset may be added to Equation (F.4) as follows [38]:

$$y(kh) \doteq b_o + b_1 kh + h \sum_{m=1}^{M} g(mh)x[(k-m+1)h],\ k=k_o,k_o+1,\ldots K. \tag{F.5}$$

It is desired to estimate b_o, b_1, and $g(mh)$, $m=1,2,\ldots M$, from experimental records.

It is easily recognized that Equation (F.5) is of a form which permits estimation of the desired constants by classical linear regression analysis. To do this, let $\hat{q}$ = "estimate of q" , and define

$$\hat{y}(kh) = \hat{b}_o + \hat{b}_1 kh + h \sum_{m=1}^{M} \hat{g}(mh)x(k-m+1), \; k=k_o,k_o+1,\ldots K. \tag{F.6}$$

It is desired to minimize the error function

$$\hat{\varepsilon}^2 = \sum_{k=1}^{K} [y(kh) - \hat{y}(kh)]^2 \tag{F.7}$$

In vector-matrix form the standard formulation for estimation of the desired constants is [38, 44]

$$\underline{g}' = (X^T X)^{-1} X^T \underline{y} ,$$

where

$$\underline{g}' = \begin{pmatrix} b_o \\ b_1 \\ g(h) \\ g(2h) \\ \vdots \\ g(mh) \end{pmatrix} \qquad \underline{y} = \begin{pmatrix} y(k_o h) \\ y[(k_o+1)h] \\ y[(k_o+2)h] \\ \vdots \\ y(kh) \end{pmatrix}$$

$$X = h \begin{pmatrix} 1/h & 1/h & \cdots & 1/h \\ k_o & k_o+1 & \cdots & K \\ x(k_o h) & x[(k_o+1)h] & \cdots & x(kh) \\ x[(k_o-1)h] & x(k_o h) & \cdots & x[(k-1)h] \\ \vdots & & & \\ x[(k_o-m)h] & & \cdots & x[(k-m)h] \end{pmatrix}$$

The terms for bias and drift correction in the above matrices were not shown in References [38] and [44], but these terms were readily added to the formulations in those references by including the independent variables 1 and kh, in addition to x[(k-m+1)h], m=1,2,...M.

After an estimate $\hat{g}(mh)$, m=1,2,...M, of the impulse response function is found by the above method, the frequency domain representation of the system transfer function, can be calculated by the following approximation of the Fourier transform [38]:

$$\hat{G}(j\omega) = h \sum_{m=1}^{M} \hat{g}(mh) e^{-(m-1)hj\omega} \quad .$$

Given the original input x(kh), the output of the system having the estimated transfer function is found from Equation (F.5). The normalized mean squared error, defined as

$$\text{NMSE} = \frac{\hat{\varepsilon}^2}{\sum\limits_{k=k_o}^{K} y^2(kh)} ,$$

is a measure of the degree with which the output y(kh) differs from the estimated output $\hat{y}(kh)$. The larger the NMSE is, the poorer the estimated transfer function "explains" the relationship between x(kh) and y(kh).

F.3 THE TIME SHIFTING METHOD

Application of the time shifting method to the identification of rider transfer functions involves the application of the impulse response method to the rider's assumed input and output, after the input has been delayed by an amount λ relative to the output. In practice, the impulse response method was applied after the output series had been shifted by an inverse time delay; that is, the shifted series $t'_\delta(kh) = t_\delta(kh + \lambda)$, where $t_\delta(kh)$ was the original output series. By shifting the output rather than the input, the analysis could be performed for a number of values of λ without needing to invert the (X^TX) matrix for each value, thus saving a considerable amount of computation time.

Shifting the output series and applying the impulse response method yields the discrete impulse response function estimate, $\hat{g}_m(\ell h)$, $\ell=1,2,\ldots M$, and the transfer function $\hat{Y}_m(j\omega)$. The estimate of the rider's transfer function is then $\hat{Y}_p(j\omega) = e^{-\lambda j\omega}\,\hat{Y}_m(j\omega)$, which may be calculated directly from $\hat{g}_m(\ell h)$ by

$$\hat{Y}_p(j\omega) = e^{-\lambda j\omega}\, h \sum_{\ell=1}^{M} \hat{g}_m(\ell h) e^{-(\ell-1)hj\omega} \quad .$$

In applying the Wingrove-Edwards and impulse response methods to the identification of rider transfer functions from experimental data, h was chosen to be 0.1 second, and M was usually 15.

APPENDIX G

IDENTIFICATION OF KNOWN TRANSFER FUNCTIONS

G.1 CREATION OF ARTIFICIAL TEST DATA

To test the validity of the methods employed in analyzing the steady-state behavior of the motorcycle and rider, and to better understand the limitations of the methods, known transfer functions were identified by means of the impulse response and cross-spectral analysis computer programs described in Appendix F. The test data were created in digital form as follows: a subroutine generated a series of random numbers $Z(kh)$, where $k=1, N$ $(N > 500)$, and h was taken to be 0.1 second. For any k, the random variable $Z(kh)$ was normally distributed with a mean of zero and a standard deviation of 500. A second series of numbers $n_t(kh)$ was calculated using the equation

$$n_t(kh) = \alpha_1 \; n_t[(k-1)h] + Z(kh), \; 1 \leq k \leq N, \; \alpha_1 = 0.3.$$

The series $n_t(kh)$ is known as a discrete first order autoregressive series [55]. The theoretical autocorrelation function of $n_t(kh)$ is

$$r_{n_t n_t}(k'h) = \alpha_1^{|k'|},\ k'=0,\ \pm 1,\ \pm 2,\ \ldots,$$

and is shown graphically in Figure G.1.

The series $n_t(kh)$ was assumed to be the digitized representation of a ficticious continuous signal $n_t(t)$, which was assumed to disturb the ficticious continuous system shown in Figure G.2, in which figure Fourier transform representations of the various signals and transfer functions are given. Note that this test system is of the same general form as the system assumed to represent the rider/cycle roll stabilization task. The signal $n_t(t)$ is analogous to the rider's remnant $n(t)$, as are $c(t)$ to steer torque, $t_\delta(t)$, $e(t)$ to the negative of roll angle, $-\phi(t)$, $G(j\omega)$ to the rider transfer function $Y_p(j\omega)$, and $H(j\omega)$ to the motorcycle transfer function $Y_c(j\omega)$. Analogous to the case of the rider/cycle system, the entire excitation of the test system was assumed to arise from the "remnant" $n_t(t)$, with other excitations $i(t)$ being identically zero.

More specifically, two systems of the general form of Figure G.2 were employed to test the data processing procedures. For each system, the open-loop transfer function was given by

$$G(j\omega)H(j\omega) = \frac{e^{-j\tau\omega}}{j\omega},$$

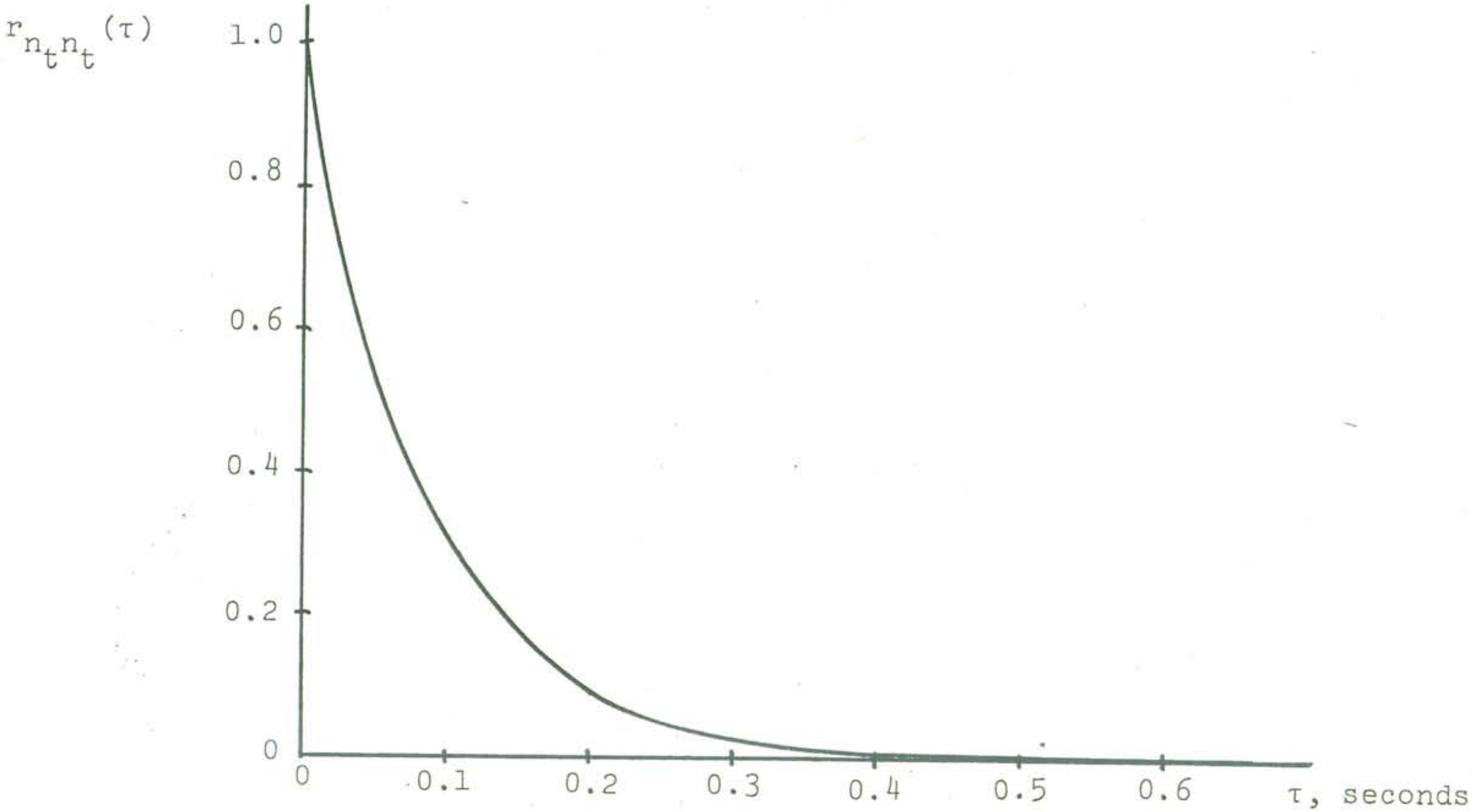

Figure G.1 Theoretical autocorrelation function of the artificial test remnant, $\alpha_1=0.3$ (discrete points connected with a smooth curve).

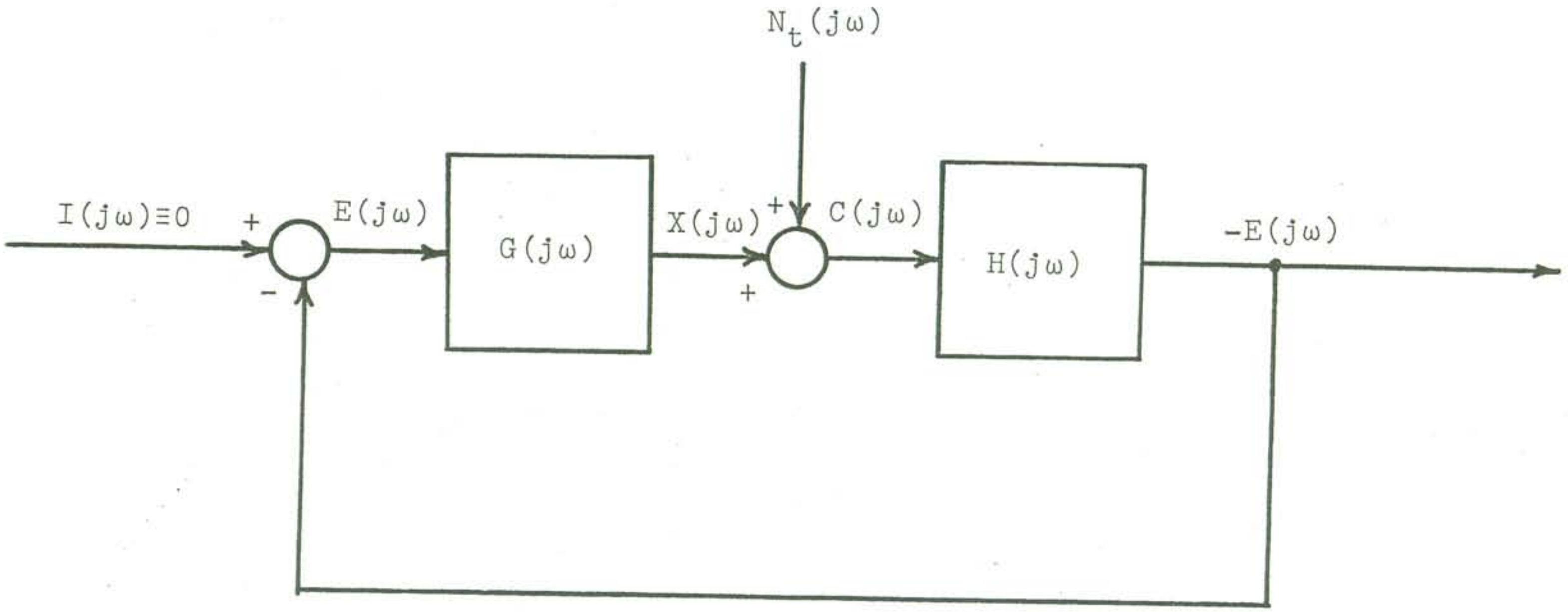

Figure G.2 Control system representation of the artificial test data.

or a "crossover model" with a crossover frequency of 1 radian/second. This form of open-loop transfer function was chosen because of its similarity to the form anticipated to represent the open-loop transfer function of the rider/cycle system. The transfer functions $G_1(j\omega)$ and $H_1(j\omega)$ for the first system were chosen to be

$$G_1(j\omega) = e^{-.4j\omega}, \text{ and } H_1(j\omega) = \frac{1}{j\omega} .$$

To allow the identification of a more complex "rider" $(G(j\omega))$, a second set of data was prepared for which it was assumed that

$$G_2(j\omega) = \frac{e^{-.3j\omega}}{j\omega}, \text{ and } H_2(j\omega) = 1.$$

Given $n_t(kh)$, the discrete versions of $x(t)$, $c(t)$, and $e(t)$ were calculated with the use of a trapezoid-rule approximation to integration. For the first system, the following equations were used:

$$x(kh) = c(kh) = e(kh) = 0, \; 1 \leq k \leq 4$$

$$\left.\begin{aligned} x(kh) &= e[(k-4)h] \\ c(kh) &= n(kh) + x(kh) \\ e(kh) &= e[(k-1)h] - \frac{h}{2}\{c[(k-1)h] + c(kh)\} \end{aligned}\right\} \; 5 \leq k \leq N$$

For the second system, the following equations were used:

$$x(kh) = c(kh) = e(kh) = 0, \quad 1 \leq k \leq 4$$

$$\left.\begin{aligned} x(kh) &= x[(k-1)h] + \frac{h}{2}\{e[(k-4)h] + e[(k-3)h]\} \\ c(kh) &= n(kh) + x(kh) \\ e(kh) &= -c(kh) \end{aligned}\right\} \quad 5 \leq k \leq N$$

Note that it was necessary to set the first four data points to zero to ensure the definition of terms like $e[(k-4)h]$, etc. When the data was read into the impulse response or spectral analysis computer program, the first few values of k for which $x(kh)$, $c(kh)$ or $e(kh)$ were zero were omitted. The value of N was adjusted to give a total record length of 50 seconds (500 data points) after the "start-up" data points had been removed.

G.2 IDENTIFICATION OF TRANSFER FUNCTIONS FROM INPUT-OUTPUT RECORDS

Given digitized records of the steady-state input and output of a linear transfer function, both the cross-spectral and impulse response methods can be easily applied to identify the transfer function. For this identification, no time shifting of the input relative to the output is needed (λ=0).

For the first data set investigated ($G(j\omega) = e^{-.4j\omega}$ and $H(j\omega) = 1/j\omega$), the half-power bandwidths of $n_t(kh)$ and $c(kh)$ (about 2.5 cps) were considerably larger than those of $e(kh)$ and $x(kh)$ (about 0.5 cps), due to the attenuation of amplitude at frequencies greater than 1 radian/second by the integrator $H(j\omega)$. To avoid aliasing of frequencies, the time increment used in the spectral analysis was small enough to accommodate the signals with the largest bandwidth. Thus a step of 0.1 second was used. The number of lags, L, was taken to be 50. Estimation of transfer functions using cross-spectral methods was not found to be very sensitive to the value of L, at least for values of L from 5 to 15% of the total number of data points.

For the impulse response method, the time step was also chosen to be 0.1 second. The impulse response function was estimated for ten, fifteen and twenty time instants ($M = 10, 15, 20$).

The most striking difference between the cross-spectral and impulse response methods is that the accuracy of the spectral method is independent of the particular transfer function being identified, while the accuracy of the impulse response method is very much transfer function sensitive. This sensitivity is clearly demonstrated in Figure G.3, in which the results of applying the impulse response method to

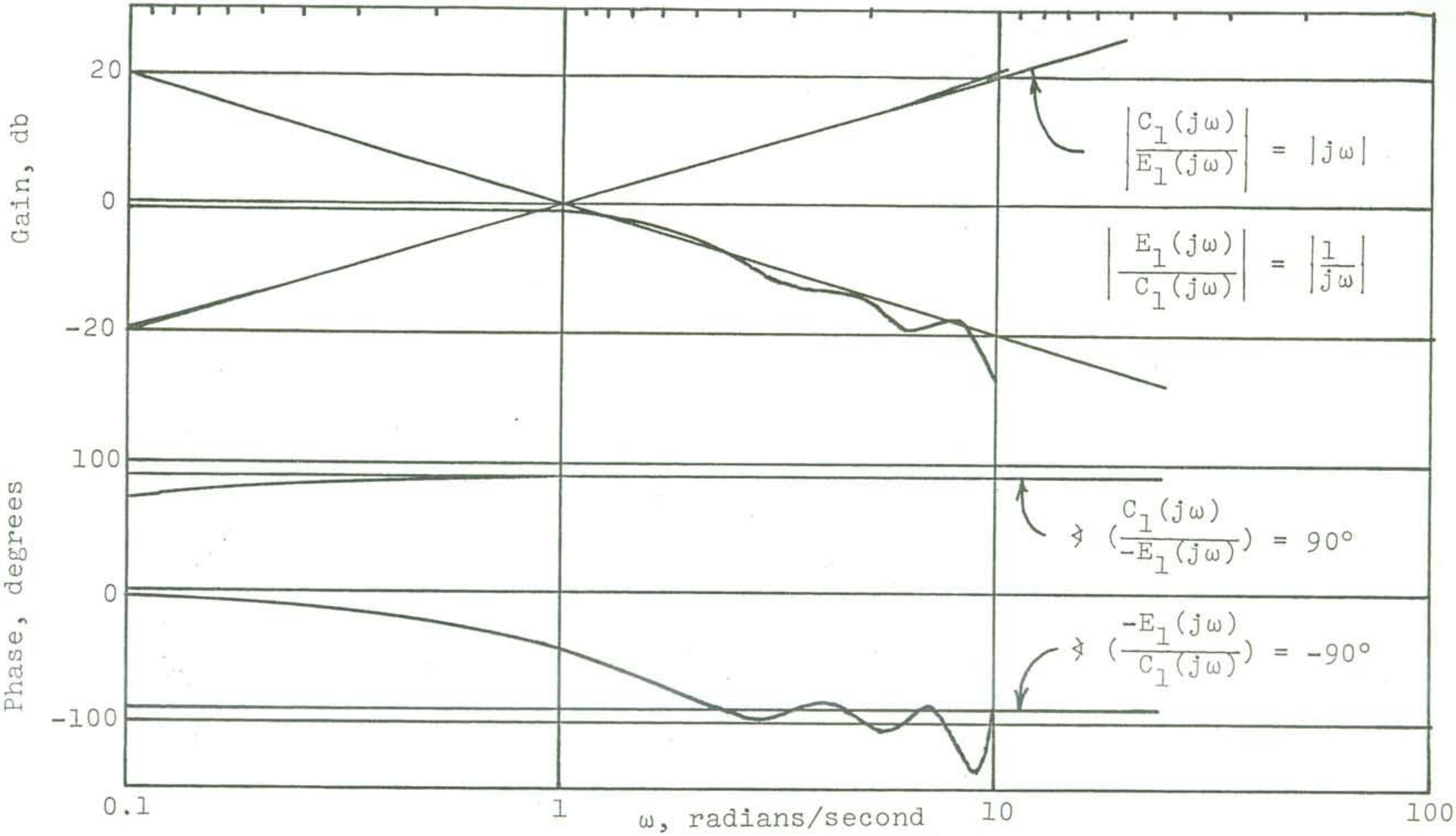

Figure G.3 Identification of a differentiator and an integrator with the impulse response method ($M=20$, $\lambda=0$).

the integrator, $H_1(j\omega) = 1/j\omega$, and the differentiator, $1/H_1(j\omega)$, are shown. To identify $H_1(j\omega)$, c(kh) and -e(kh) were taken to be the input and output, respectively, and to identify $1/H_1(j\omega)$, -e(kh) was used as input and c(kh) was the output. Note that the impulse response method is able to identify a differentiator considerably more accurately than it can identify an integrator. Also, in Figure G.4 it is shown that the impulse response method can very accurately identify a pure time delay. The gain and phase of the pure time delay were identified with accuracy to at least three significant digits.

It is not difficult to understand the reasons that the accuracy of the impulse response method is system-dependent. Basically, the accuracy of the method depends upon the degree to which the discrete system output at time kh can be approximated by a weighted sum of the values of the digitized input a time kh and a finite number of previous time instants. The output at time kh of a pure time delay of $k_o h$ seconds can be exactly predicted by applying a weight of 1 to the input at time $(k-k_o)h$ and a weight of 0 to the input at any other time instant. However, for an integrator, the impulse response of which is a step function (a constant for all $t>0$), the output at time kh depends on all values of the input at times previous to and including kh. The impulse response method attempts to

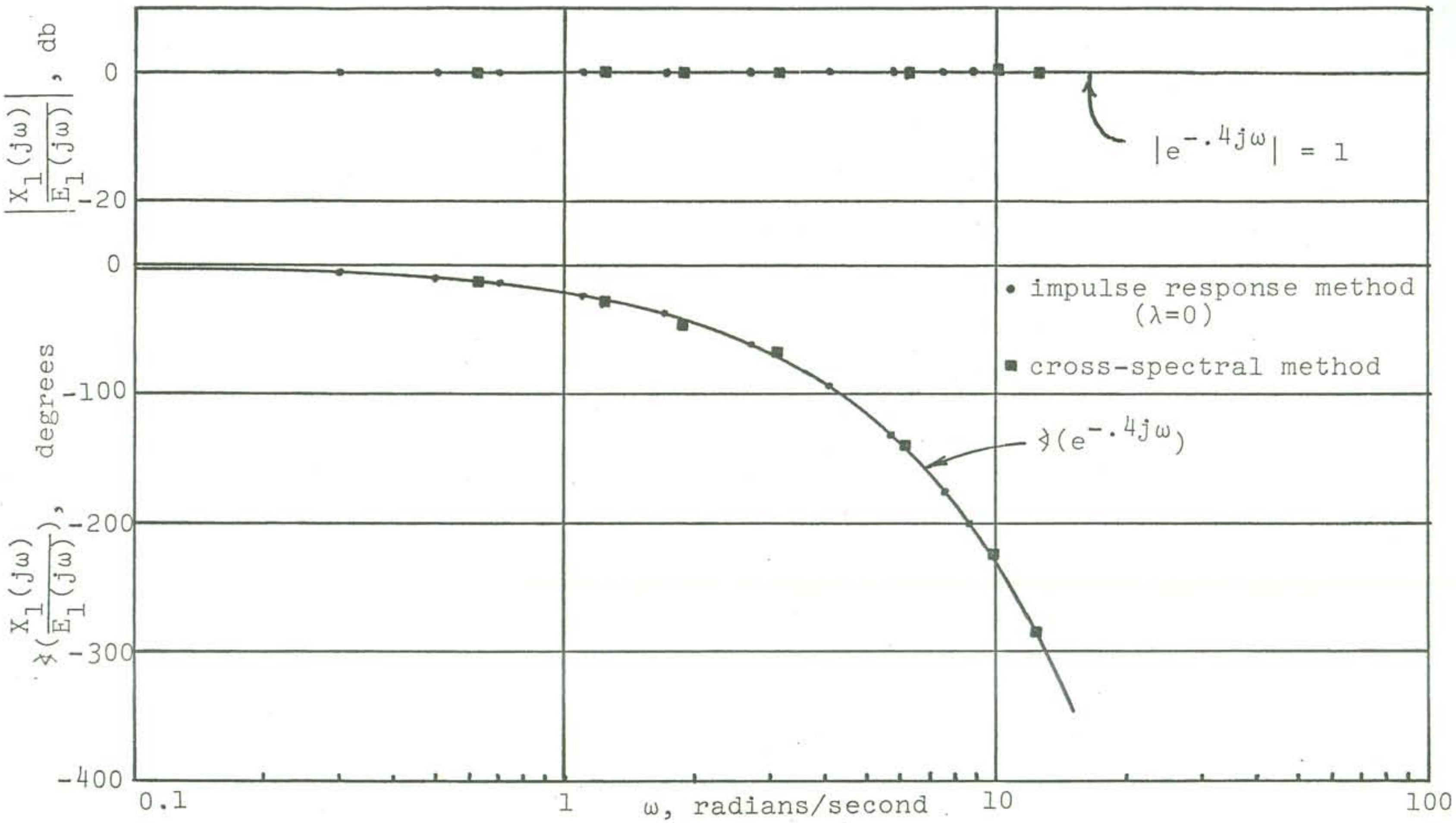

Figure G.4 Identification of a pure time delay.

approximate this impulse response function by a truncated estimate, and the approximation reduces the accuracy of the transfer function identification, especially at low frequencies. It would be expected that the accuracy of the method in identifying transfer functions having impulse response functions which do not decay to zero would be improved by increasing the truncation number, M.

Figure G.5 shows the identification of a more complex transfer function, $e^{-.3j\omega}/j\omega$, actually the product of two types of transfer functions previously identified. The impulse response function corresponding to $e^{-.3j\omega}/j\omega$ does not decay to zero as time increases without bound; thus, the impulse response method does not give accurate results. However, increasing the value of M from 10 to 20 does, in fact, significantly improve the accuracy of the identification.

G.3 IDENTIFICATION OF G(jω) WHEN x(kh) IS NOT KNOWN

The data obtained from actual road experiments differ from the artificial test data in that, for the rider/cycle system, the time series analogous to x(kh) is not known. In order to identify the rider's transfer function, then, the method outlined in the text and Appendix F (the Wingrove-Edwards or time shifting method) must be used in conjunction with the impulse response method. (Cross-spectral methods cannot be used.)

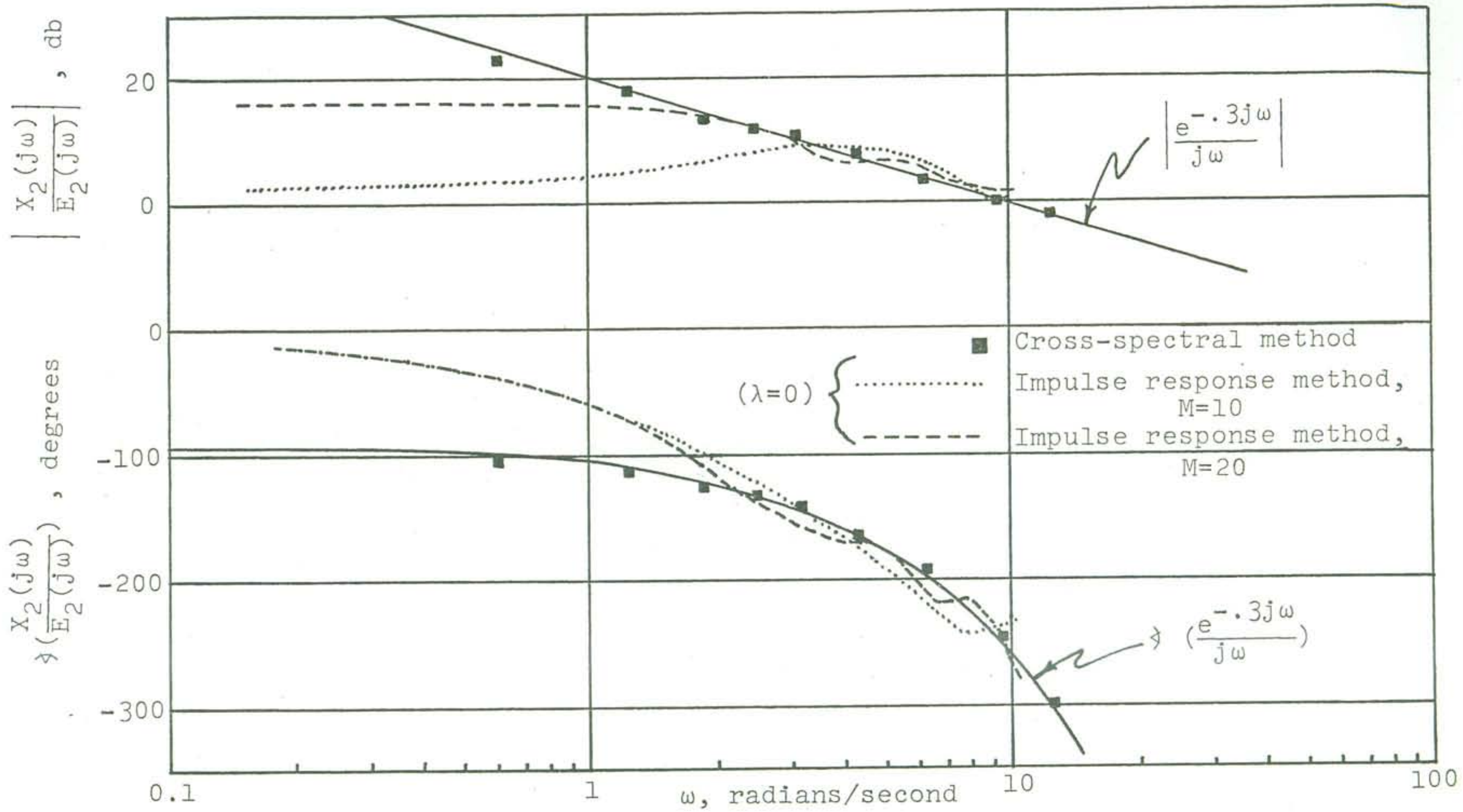

Figure G.5 Identification of $e^{-.3j\omega}/j\omega$.

The results of applying the Wingrove-Edwards technique and the impulse response method to both sets of artificial test data are shown in Figures G.6 and G.7. To produce these results, the "rider's" input e(kh), delayed in time by an amount λ, was treated as the input series in the impulse response analysis, while c(kh) was taken to be the output series. The result was a transfer function $\hat{G}'(j\omega)$ relating $e(kh-\lambda)$ to c(kh). The estimated "rider" transfer function was then taken to be $\hat{G}(j\omega) = e^{-\lambda j\omega} \hat{G}'(j\omega)$. For $\lambda=0$, $\hat{G}(j\omega) \doteq -1/H(j\omega)$. In Figure G.6, the "rider" transfer function is $G_1(j\omega) = e^{-.4j\omega}$, while the "controlled element" is $H_1(j\omega) = 1/j\omega$. Identification of $G_1(j\omega)$ is seen to be more accurate than the identification shown in Figure G.7, in which the "rider" transfer function is $G_2(j\omega) = e^{-.3j\omega}/j\omega$, and the "controlled element" is $H_2(j\omega) = 1$. Thus, Figures G.6 and G.7 present evidence that rider identification using the Wingrove-Edwards technique and the impulse response method is sensitive to the actual transfer function being identified in the same way that the accuracy of the impulse response method alone is system dependent. Also, identification of the rider transfer function when x(kh) is unknown is seen to be not much less accurate than when x(kh) is known. Thus, it appears that the errors in identifying the rider transfer function when x(kh) is unknown are to a large extent

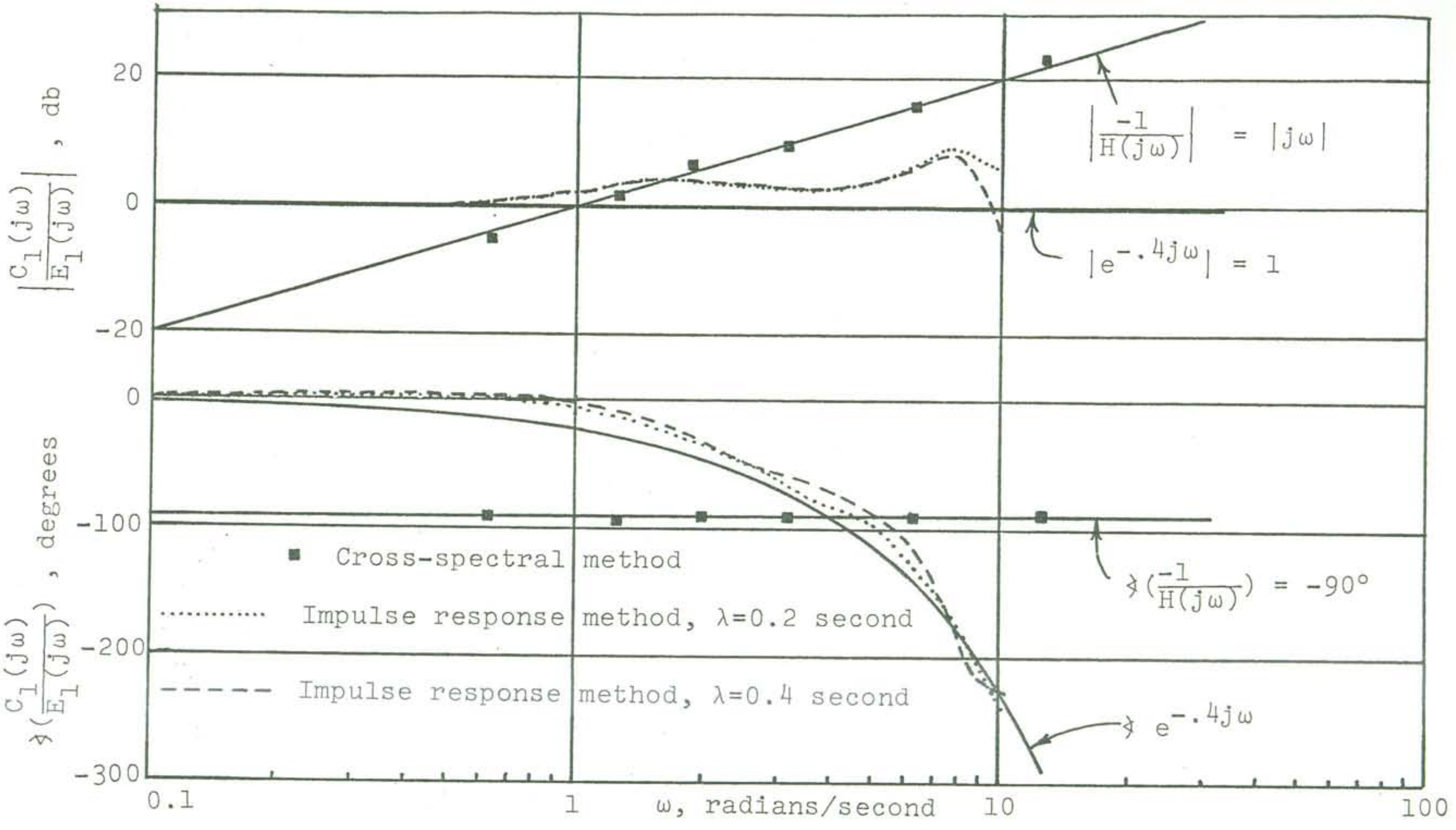

Figure G.6 Identification of "rider" transfer function, $G(j\omega) = G_1(j\omega) = e^{-.4j\omega}$.

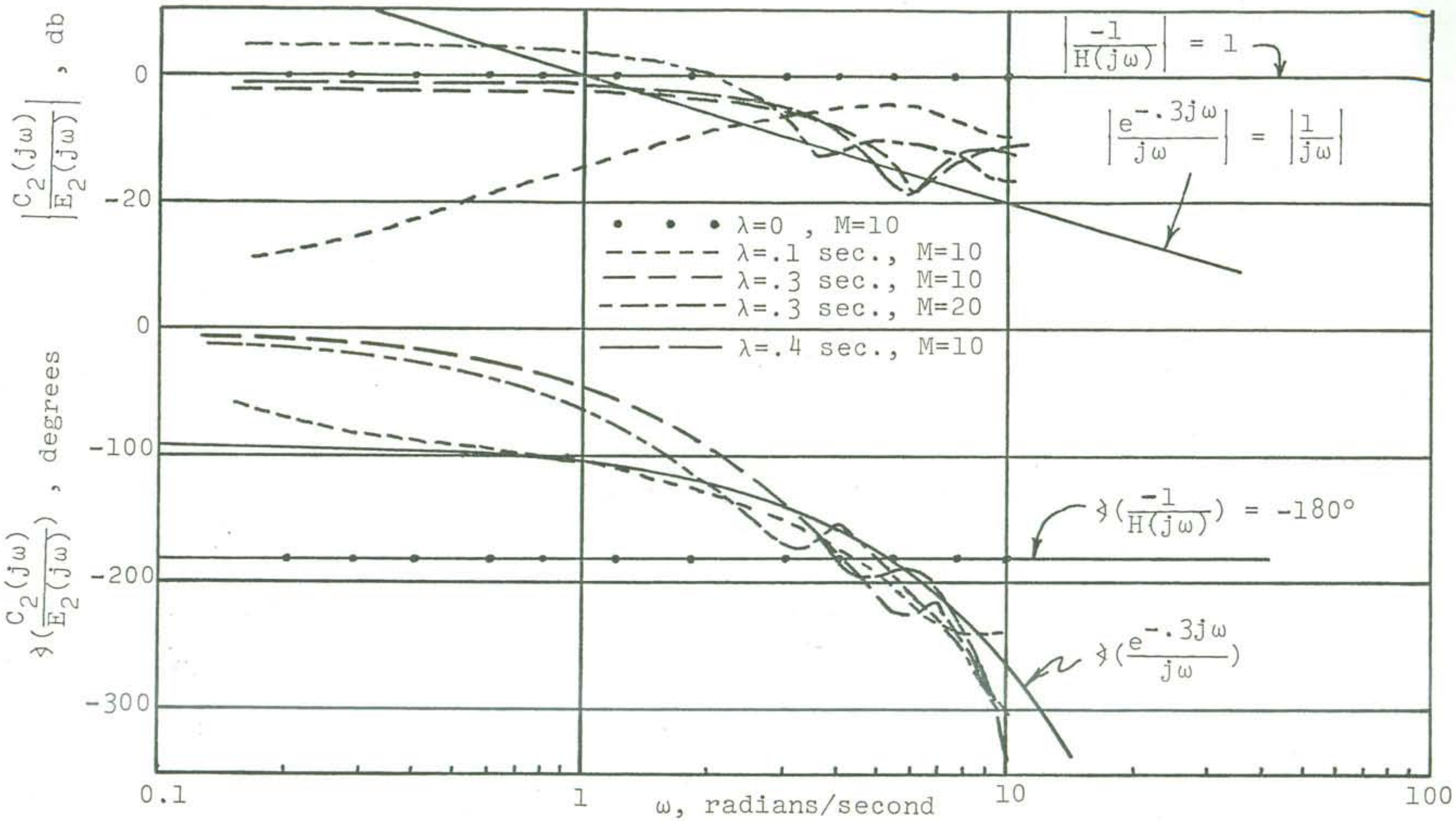

Figure G.7 Identification of a "rider" transfer function, $G(j\omega) = G_2(j\omega) = e^{-.3j\omega}/j\omega$ (impulse response method).

due to the limitations of the impulse response method and not due to the additional complication of employing the Wingrove-Edwards technique.

Once an impulse response function, $\hat{g}(mh)$, $m=1,2,\ldots M$, has been estimated for the "rider" transfer function, the unknown quantity $x(kh)$ may be estimated by

$$\hat{x}(kh) = \sum_{m=1}^{M} \hat{g}(mh)e[(k-m+1)h].$$

The series

$$\hat{r}_{\varepsilon}(kh) = c(kh) - \hat{x}(kh)$$

is an estimate $\hat{n}_t(kh)$ of the "remnant" $n_t(kh)$ when $\lambda = \tau$, the time delay of the "rider". The autocorrelation function, $r_{n_t n_t}(\tau)$, of the remnant, $n_t(t)$, was estimated (for integer multiplies of the time step h) from the series $n_t(kh)$ and $\hat{n}_t(kh)$, the latter series being estimated from both sets of artificial data (Fig. G.8). Both estimates are close to the theoretical autocorrelation function, although the estimate based upon $n_t(kh)$ shows more scatter for larger values of τ than do the estimates based upon either $\hat{n}_t(kh)$ series. If this scatter is not due to errors in estimating the autocorrelation function, it would indicate that the identification of $G_1(j\omega)$ and $G_2(j\omega)$ through use of the Wingrove-Edwards

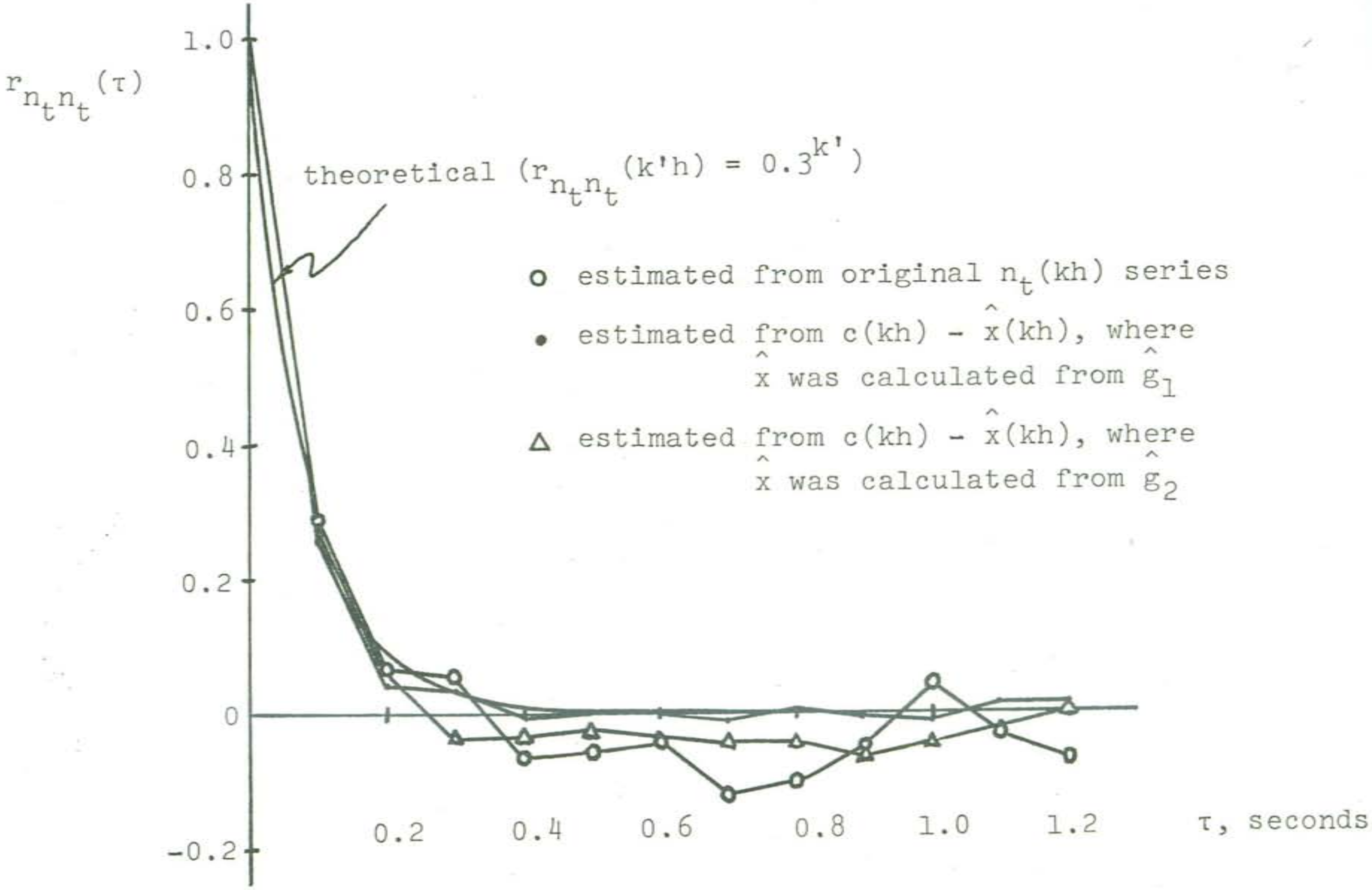

Figure G.8 Identification of $r_{n_t n_t}(\tau)$.

technique would have been more accurate if the autocorrelation function of $n_t(kh)$ had been closer to the desired theoretical function shown in Figure G.1.

The quantity

$$\sum_{k=11}^{510} \hat{r}_{\varepsilon}(kh)/\sum_{k=11}^{510} c^2(kh) ,$$

termed the "normalized mean squared error" (NMSE), is shown in Figure G.9 as a function of λ. The NMSE is a measure of the degree with which c(kh) is correlated with e(kh) by a linear transfer function. Thus, the NMSE is very small when $\lambda=0$, since e(kh) and c(kh) are highly correlated via $-1/H(j\omega)$. As λ increases, the NMSE increases rapidly. There exist ranges of λ, which ranges depend upon the form of $G(j\omega)$, for which the NMSE is not very sensitive to the value of λ, and it was found that the corresponding transfer function estimates for λ in these ranges were also nearly independent of λ. For $\lambda > \tau$, the NMSE again increases. The large values of the NMSE do not indicate that $G(j\omega)$ has been poorly identified; rather, they indicate that c(kh) is approximately the same series as n(kh). Due to the attenuation of the integrator for frequencies greater than 1 radian/second, the amplitudes of x(kh) are considerably smaller than those of n(kh). Hence, $c(kh) = n(kh) + x(kh) \doteq n(kh)$.

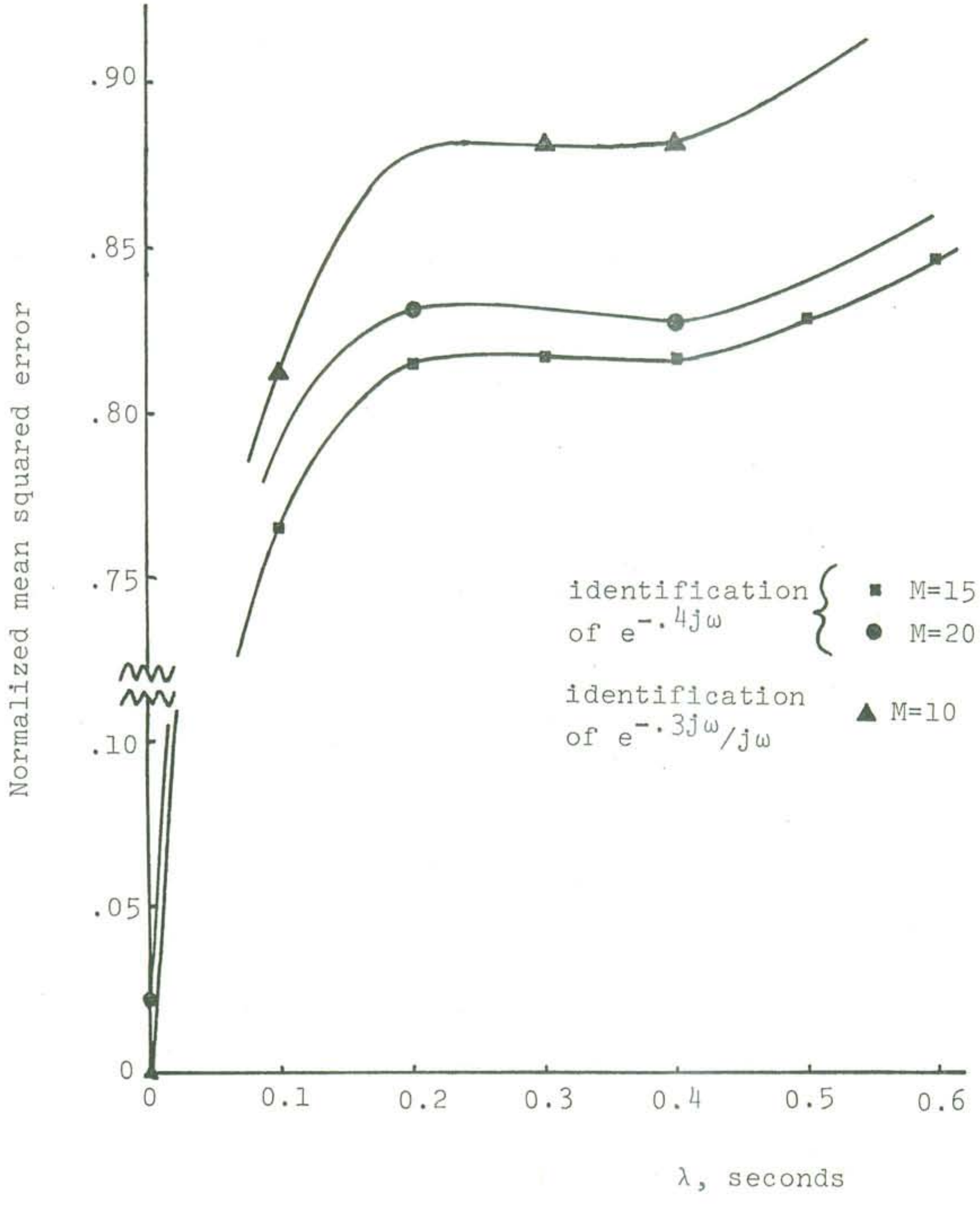

Figure G.9 Normalized mean squared error as a function of λ; artificial test data.

G.4 IDENTIFICATION FROM DATA CONTAINING OFFSET AND DRIFT

The actual experimental data further differed from the artificial test data in that the former could contain offset and/or drift[1]. The artificial test data contained such low levels of offset and drift that no correction was used in the impulse response program for the results shown in Sections G.2 and G.3.

The method of minimizing the effect of offset and drift in the impulse response computer program was tested in the following manner. First, the artificial test data with $G(j\omega) = G_3(j\omega) = e^{-.3j\omega}$ and $H(j\omega) = H_1(j\omega) = 1/j\omega$, were modified somewhat arbitrarily to include offset and drift by defining new series as follows:

$$e_m(kh) = e(kh) + 100 - .5\ k,$$

$$c_m(kh) = c(kh) + 250 - .65\ k.$$

Series $e_m(kh)$ and $c_m(kh)$ are analogous to the output of transducers employed in the road tests, which output may be the desired quantities (voltages proportional to roll angle, steering torque, etc.) corrupted by offset and drift. Next,

---

[1] Appendix F discusses offset and drift and the method in which their effect is minimized.

with $e_m(kh)$ and $c_m(kh)$ as transfer function input and output, respectively, the impulse response analysis, including the Wingrove-Edwards technique, was performed. Figure G.10 shows the results of including an offset and drift correction versus the results of not including such a correction, for $\lambda=0$ and $\lambda=0.3$ second. Note that the offset and drift, when not compensated for, tend to reduce the accuracy of the estimate of $-1/H_1(j\omega)$ ($\lambda=0$) for low frequencies, while not having significant influence upon the estimate for $G_3(j\omega)$ ($\lambda=0.3$ second).

G.5 IDENTIFICATION OF "RIDER" TRANSFER FUNCTIONS WHEN THE REMNANT BANDWIDTH IS SMALL

Figure G.11 shows the theoretical autocorrelation functions of $n_t(kh)$ when $\alpha_1 = 0.8$. For a "rider" time delay τ of 0.4 seconds, it can be seen that there is an appreciable bias error in identifying the "rider" transfer function when the closed-loop system is excited by this remnant.

An identification of $G(j\omega)$ is shown in Figure G.12, with $\lambda = 0.4$, and

$$G(j\omega) = G_4(j\omega) = 1.5\ e^{-.4j\omega}$$

and

$$H(j\omega) = H_1(j\omega) = 1/j\omega.$$

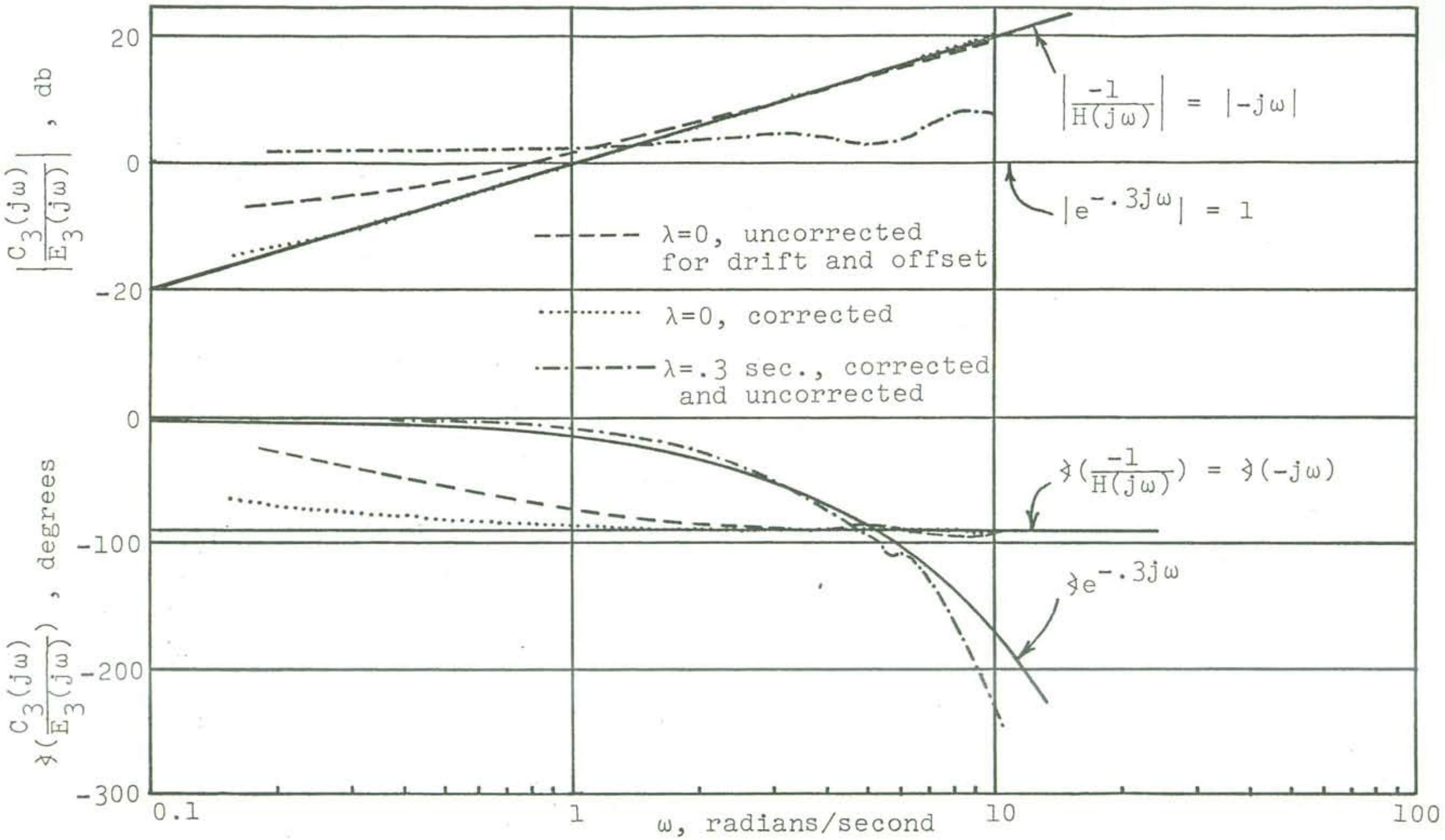

Figure G.10 Correcting for offset and drift in the data records (impulse response method, M=10).

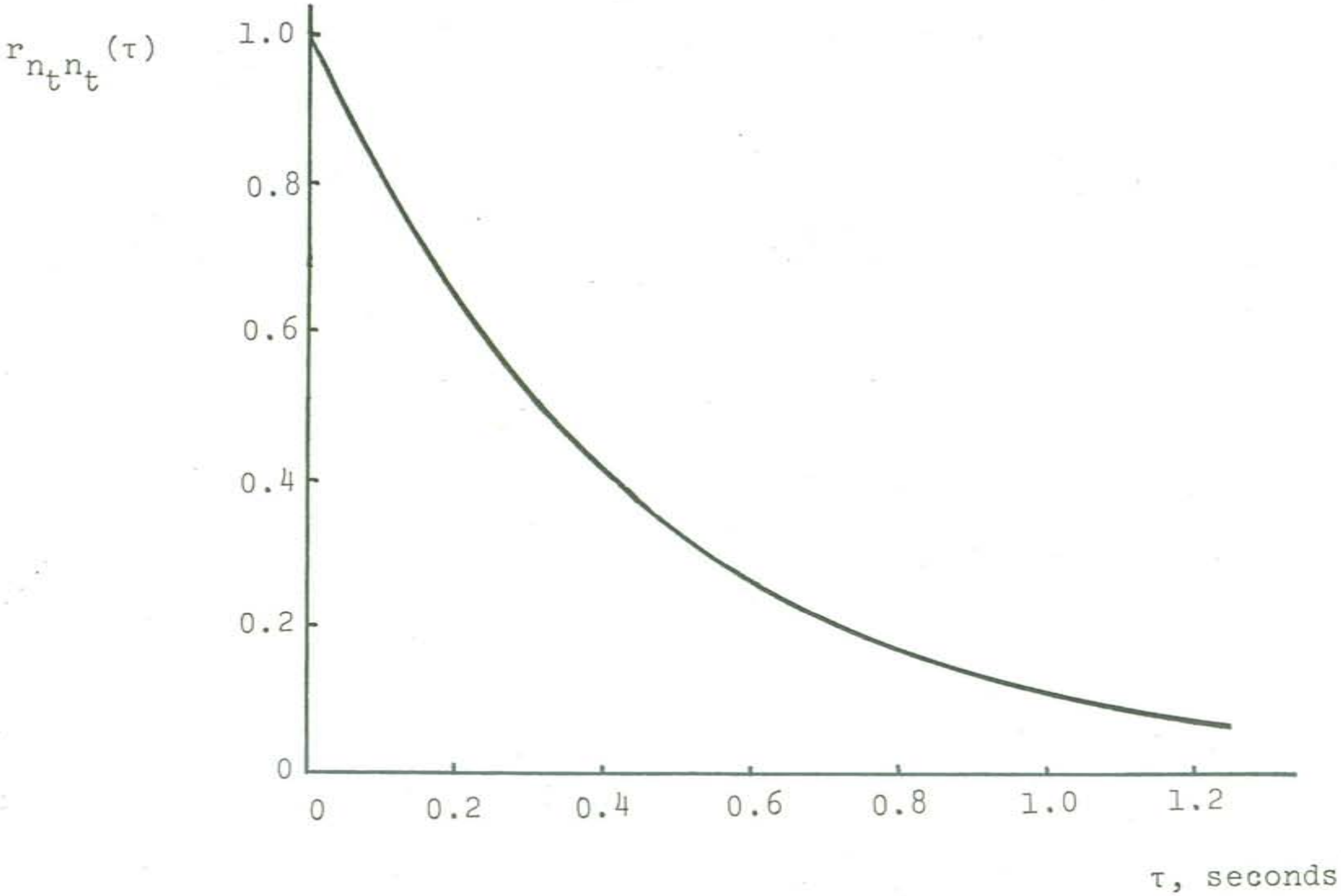

Figure G.11 Theoretical autocorrelation function of the artificial test remnant, α_1=0.8 (discrete points connected with a smooth curve).

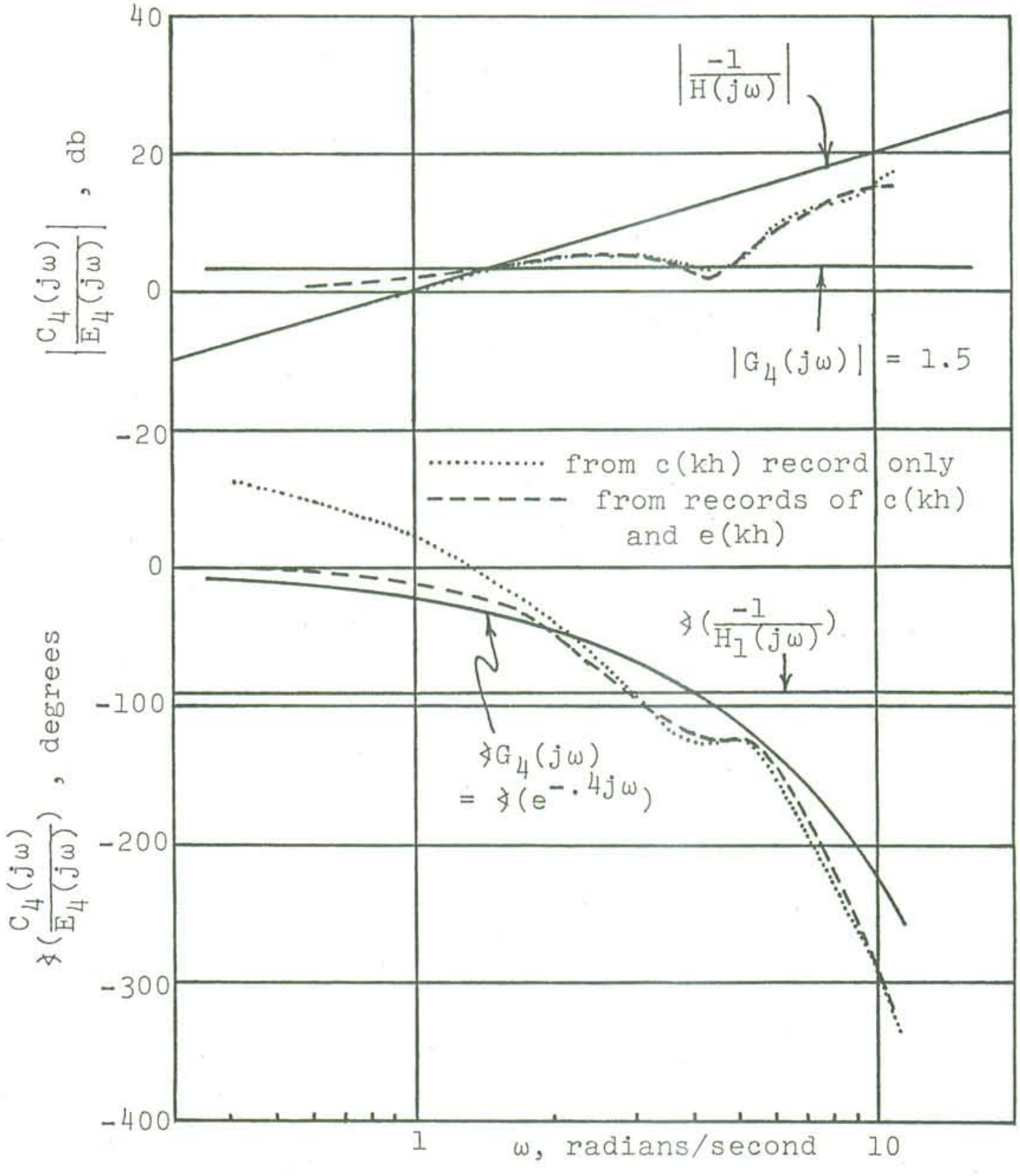

Figure G.12 Identification of "rider" transfer function (α_1=0.8, λ=0.4 sec.).

Two identifications are shown. One was prepared in the usual manner, using $e(kh)$ as transfer function input and $c(kh)$ as output. The other was calculated in a manner analogous to the analysis of road test data using the roll rate record; that is, $G(j\omega)/j\omega$ was first identified (using the series $-c(kh)$ and $c(kh)$ and subsequently multiplied by $j\omega$ to estimate $G(j\omega)$).

In Figure G.12, notice how the $|G(j\omega)|$ estimates are "pulled" toward $|\frac{1}{H(j\omega)}|$, particularly at the high and low frequencies. The phase of $G(j\omega)$ is underestimated at high frequencies and overestimated at low frequencies. Instabilities, which occur in both estimates of $G(j\omega)$, tend to bring the estimated gain and phase graphs closer to their correct values in the 4-6 rad/sec range. For frequencies greater than 6 rad/sec, however, the estimated gain and phase diverge from the true gain and phase. Notice also that the identifications in which $G(j\omega)$ was estimated directly and in which $G(j\omega)/j\omega$ was estimated first have about the same accuracy, except at low frequencies, which difference is a result of constraints inherent in the impulse response method.

The remnant $n_t(kh)$ was estimated from the results of these identifications. Spectral analysis of $\hat{n}_t(kh)$ for several values of λ indicated that the bandwidth of $\hat{n}_t(kh)$, while decreasing with increasing λ, was always greater than the actual bandwidth of $n_t(t)$. Further, there was no local minimum of the NMSE with respect to λ, for $\lambda = \tau_p$, as was the case (Fig. G.9) when $n_t(kh)$ was closer to "white" noise. Rather, an increase in λ always increased the NMSE.

If new data is created, using the same $n_t(kh)$ ($\alpha_1 = 0.8$), but decreasing τ, more bias will result. Figure G.13 shows such an identification, for $\lambda = 0.1$ and 0.2, where

$$G(j\omega) = G_5(j\omega) = 5\ e^{-0.1j\omega}$$

and

$$H(j\omega) = H_1(j\omega) = 1/j\omega\ .$$

Notice that $|\hat{G}(j\omega)|$ shows less "pulling" toward $|-\frac{1}{H(j\omega)}|$ and that $\hat{G}(j\omega)$ appears to be a constant gain and a pure time delay. However, the estimated values of gain and delay are considerably in error, gain being underestimated and the delay being overestimated. Increasing λ from 0.1 to 0.2 did not affect the accuracy significantly, and the estimator displayed more variance or instability.

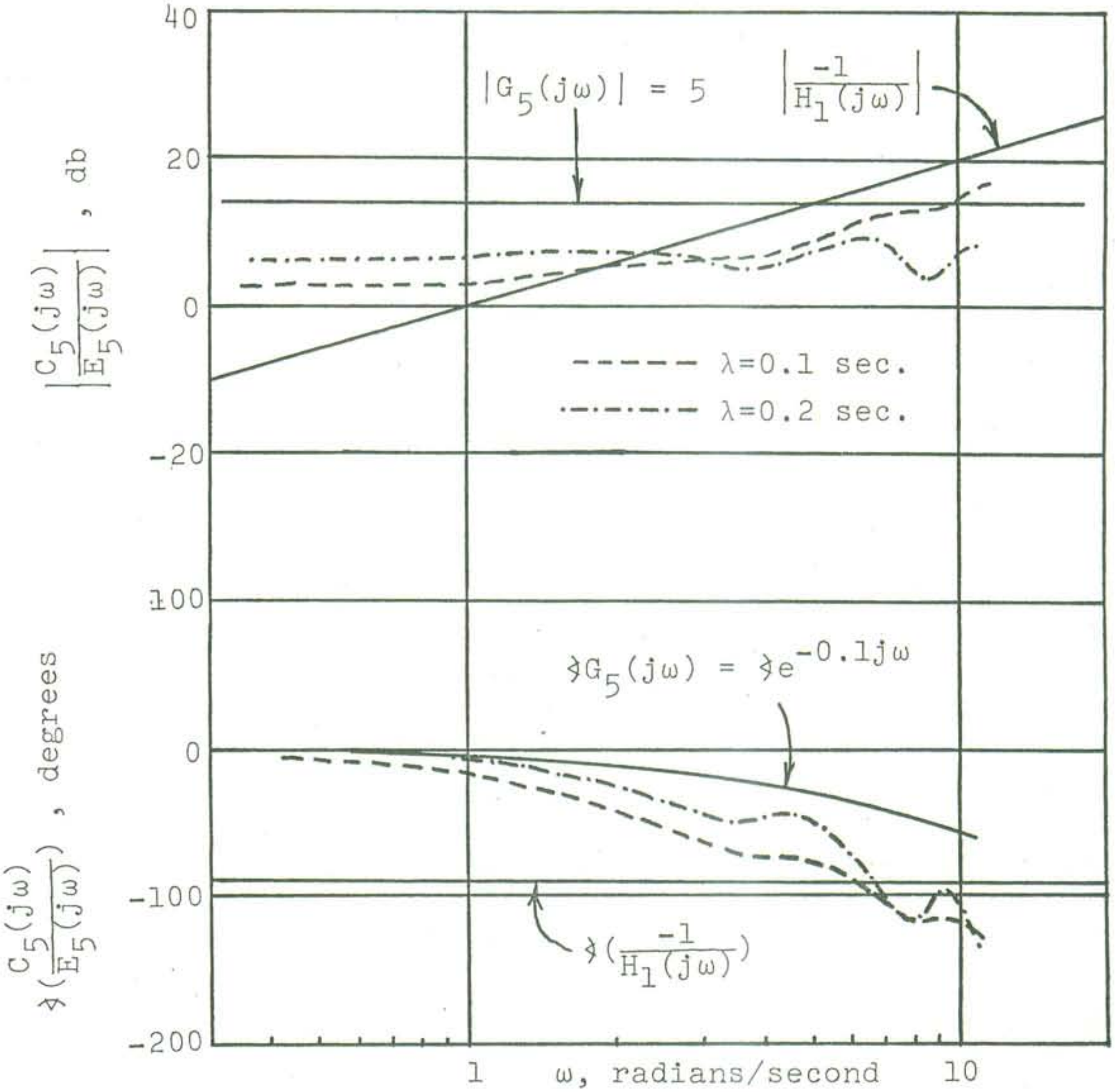

Figure G.13 Identification of "rider" transfer function (α_1=0.8).